WestVirginiaUniversity
THE RESEARCH REPOSITORY @ WVU

Graduate Theses, Dissertations, and Problem Reports

2007

Dissolution and diffusion characteristics of 316L stainless steel in molten zinc containing variable concentrations of aluminum

Mark A. Bright
West Virginia University

Follow this and additional works at: https://researchrepository.wvu.edu/etd

Recommended Citation

Bright, Mark A., "Dissolution and diffusion characteristics of 316L stainless steel in molten zinc containing variable concentrations of aluminum" (2007). *Graduate Theses, Dissertations, and Problem Reports*. 2763.
https://researchrepository.wvu.edu/etd/2763

This Dissertation is protected by copyright and/or related rights. It has been brought to you by the The Research Repository @ WVU with permission from the rights-holder(s). You are free to use this Dissertation in any way that is permitted by the copyright and related rights legislation that applies to your use. For other uses you must obtain permission from the rights-holder(s) directly, unless additional rights are indicated by a Creative Commons license in the record and/ or on the work itself. This Dissertation has been accepted for inclusion in WVU Graduate Theses, Dissertations, and Problem Reports collection by an authorized administrator of The Research Repository @ WVU. For more information, please contact researchrepository@mail.wvu.edu.

Dissolution and Diffusion Characteristics of 316L Stainless Steel in Molten Zinc Containing Variable Concentrations of Aluminum

By

Mark A. Bright

Dissertation

Submitted to the
College of Engineering and Mineral Resources
West Virginia University

In Partial Fulfillment of the Requirements for the
Degree of

Doctor of Philosophy
in
Mechanical Engineering

Ever Barbero, Ph.D., Chair and Advisor
Frank Goodwin, D.Sc.
Xingbo Liu, Ph.D.
Eung Cho, Ph.D.
Nick Wu, Ph.D.

Department of Mechanical and Aerospace Engineering

Morgantown, West Virginia
2007

Keywords: Zinc, Galvanizing, Stainless Steel, Dissolution, Diffusion
Copyright 2007 Mark A. Bright

Abstract

Dissolution and Diffusion Characteristics of 316L Stainless Steel in Molten Zinc Containing Variable Concentrations of Aluminum

Mark A. Bright

Molten metal corrosion of pot hardware materials in continuous galvanizing lines is an important factor in maintaining high productivity at steel sheet mills around the world. A complete understanding of the mechanisms which impact the corrosion properties of structural metals submerged in industrial molten zinc baths has not been achieved. Acquisition of deeper knowledge in this field is very difficult because of the numerous variables involved with the zinc environment. As an example, the aluminum content that is employed varies from near 0% aluminum in general (batch) galvanizing pots to around 0.14wt% Al for high-grade automotive sheet steels and again to aluminum levels exceeding 0.2wt% for various construction-grade steels. Moreover, it is widely experienced that the molten metal corrosivity of these small changes in aluminum concentration can have a pronounced impact on the life of submerged galvanizing hardware.

One aspect of understanding the molten zinc corrosion characteristics is determining the solubility of structural hardware metals as a function of changes in aluminum content in the liquid zinc. Hence, an array of tests was performed to measure the actual corrosion loss of 316L stainless steel samples after immersion in molten zinc with aluminum concentrations ranging from about 0% to 1wt% Al. In general, these tests indicated that the corrosion rate of 316L was quite high for pure zinc (0% Al) then decreased drastically at increasing aluminum levels between 0% and about 0.14wt% to a rather minimal corrosion rate beyond 0.14% aluminum, maintaining a low dissolution rate beyond 1% Al. The significance of 0.14wt% Al has been defined by not only the microanalysis of the reaction mechanisms on test samples but also by industry-accepted phase diagrams and previously published research.

Based on the results and procedures characterized by this investigation, it may be possible to further understand the reaction mechanisms and detailed corrosion features of other alloys utilized in industrial galvanizing operations, such as cobalt-based and iron-based superalloys. Furthermore, recognizing the significance of the phase transformations in the region of 0.14wt% aluminum on these advanced alloys may promote more focused research in this economically important aluminum regime.

Acknowledgements

In this long and arduous journey, numerous individuals provided endless support and contributed tremendously to the realization of this project. First, I would like to thank Richard Chandler and Metaullics Systems Co. L.P. for providing, not only the financial support to this effort, but also for having the vision and confidence to permit me to pursue this endeavor. Additionally at Metaullics, thanks to Greg Becherer for his steadfast encouragement and positive reinforcing personality. His support was crucial to the completion of this project. Also, I want to thank Robert Grodeck, Nathan Deem and Frank Beznoska for their assistance in running and preparing corrosion test samples and helping whenever I asked.

I want to thank Dr. Ever Barbero and the members of my doctoral review committee for providing insight and guidance through this process, but especially Dr. Xingbo Liu who's numerous conversations and teachings gave me both a deeper knowledge of fundamental metallurgy and a stronger focus on the objective of doctoral research in general. Additionally from WVU, I would like to thank Jing Xu for openly sharing her wealth of knowledge and selflessly giving her time to help me. I also greatly appreciate the cooperation of Liviu Magean, Steve Carpenter and Adrienne Macleod in the WVU Chemical Engineering Analytical Laboratory for their assistance in performing the SEM/EDS analyses contained herein.

An exceptional thanks to my family. To my parents for their continual encouragement towards any project I undertake, but especially to my mother, Rebecca Leonard, whose drive and determination have always been an inspiration to me. To my other parents, David and Linda Carson (Wendy's father and mother), for always caring

and being there to help and support us in anyway that they could. And a very special thanks to my wife, Wendy. Without her encouragement, confidence and sacrifices, I could never have undertaken such a daunting task. She has been the foundation for this entire project.

And finally, my endless gratitude goes to Jorge Morando. He not only provided the technical premise for this research, but more importantly his tenacious inspiration and "never accept the status quo" attitude have given me the drive and motivation to continually push myself to be better and achieve more than I ever imagined I could.

And for everyone else who helped me, motivated me and inspired me throughout my life and career, I thank you.

Table of Contents

List of Figures

Page:

Page:

Page:

Page:

Page:

Page:

Page:

List of Tables

Page:

Chapter 1: Introduction

In the U.S., the total production of steel is approximately 100 million tons per year and it has been reported that over 30% of this tonnage is generated in the form of zinc-coated (galvanized) sheet for enhanced environmental corrosion resistance. However, with ever increasing costs of production, the expense of adding a zinc coating to a steel substrate now accounts for over 30% of the total manufacturing cost of the galvanized sheet. Thus, maintaining efficient, productive galvanizing facilities is becoming increasingly critical, and one of the primary focus areas for reducing maintenance downtime is the equipment in and around the molten zinc galvanizing pot.

Degradation of zinc bath hardware in continuous galvanizing operations is a significant contributor to excessive maintenance expenses and costly production downtime. Numerous projects, including a pair of U.S. Department of Energy-sponsored Projects at West Virginia University and Oak Ridge National Laboratory, have been aimed at testing, ranking, and recommending new materials to extend pot equipment campaigns and minimize lost production. However, few projects have taken an expanded scope and discovered what actually causes the failure of this molten zinc submerged industrial equipment. With the knowledge and lab equipment developed at WVU as a result of the DOE Projects and in conjunction with the on-going research from these projects, it could be possible to begin to understand and predict these inherent material failure mechanisms.

1.1 Definitions

Dissolution (units: g/hr or mg/cm^2/hr)

Dissolution is the process by which a solid, gas, or liquid is dispersed homogeneously in a gas, solid, or, especially a liquid. With regards to molten metals, dissolution indicates a mass transfer from a solid object to the liquid metal phase where the solid is immersed.

Diffusion (units: μm/hr)

Diffusion is the process whereby particles of liquids, gases, or solids intermingle as the result of their spontaneous movement caused by thermal agitation and move from a region of higher to one of lower concentration. For the cases presented herein, diffusion refers to the mass transfer of liquid phase constituents into the surface of a solid object.

Corrosion

Corrosion is a state of deterioration in metals caused by oxidation or chemical reaction due to thermal, electrical or environmental activation. The term corrosion may provide a general description of degradation when the exact nature of the metallurgical reaction is not known. In this work, the term corrosion is used to denote the process of combined diffusion, dissolution and other effects such as chemical reactions which are further described and quantified herein.

1.2 Overview

It is widely accepted that most metals will dissolve quickly when immersed in either pure zinc or pure aluminum baths at typical industrial operating temperatures. However, actual field performance has shown that standard metal alloys can survive for an appreciable amount of time in a typical molten zinc-aluminum alloy bath used in industrial galvanizing operations. Thus, a logical thought process would indicate that a minimum dissolution rate in zinc may be obtained at a given aluminum concentration somewhere between 0% and 100% Al. (see Figure 1-1) This critical aluminum concentration could even vary for different metal alloy substrates as well.

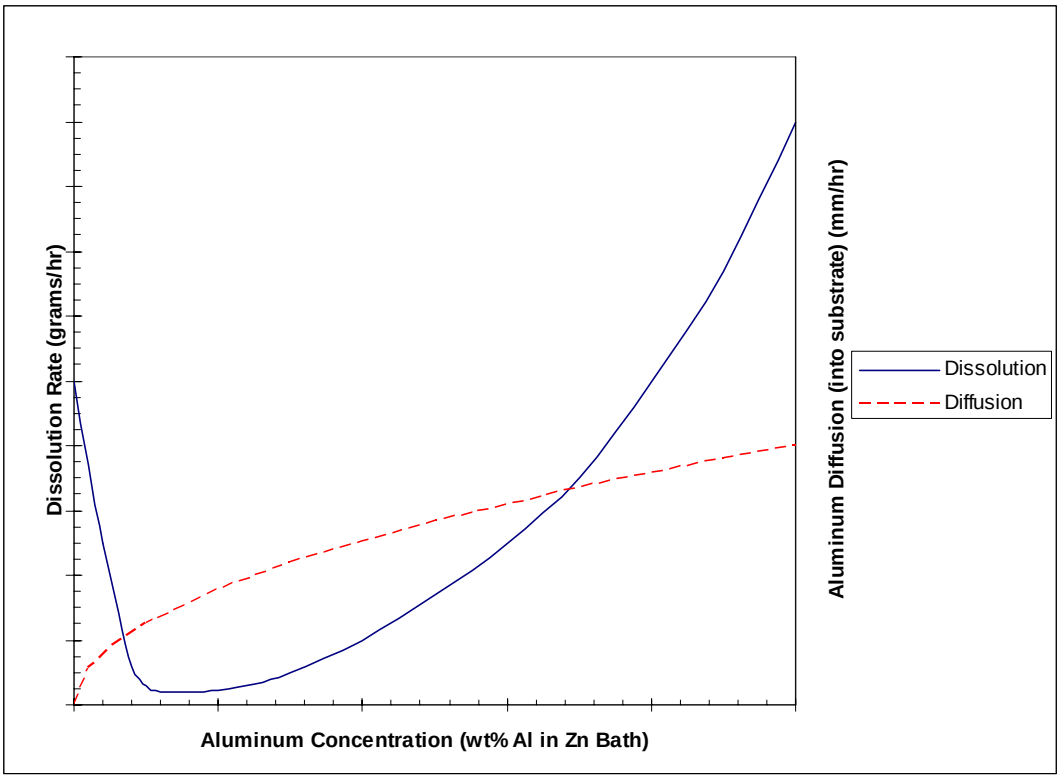

Figure 1-1: Hypothetical Dissolution and Diffusion Characteristics of a Metallic Sample in Molten Zn/Al Bath

In addition, it has been recently proposed [Refs. 47, 50, 52] that aluminum and zinc diffusion into the surface of bulk metal alloys may have a significant impact on the operating life of the industrial components. Thus, it could be assumed that aluminum

diffusion rate into the metal would be similarly impacted by the concentration of aluminum in the zinc bath (as a result of aluminum activity and/or chemical reaction), but with the aluminum diffusion rate equal to zero at 0% aluminum and increasing henceforth. (see Figure 1-1)

Extensive dissolution testing and some preliminary diffusion analysis have been performed previously for various metallic alloy materials for fixed zinc bath parameter such as aluminum concentration or bath temperature. In 1955, Hodge reviewed the dissolution rates of various metals in a pure zinc bath. Much later, Brunnock, et al. (1990's) detailed the reactions of numerous metallic substrates in a zinc + 0.135% aluminum bath (480°C), and similarly, Sikka, et al. (2001-2005) identified the dissolution rate in zinc + 0.16% aluminum (465°C) of an array of alloys. Ghuman and Goldstein (1971) researched the effects of varying the temperature from 450°C to 700°C and the aluminum content from 0% to 10%, but only as they related to the short-time coating reaction on an iron substrate. Recently, Zhang (2002-2004) started to look at the aluminum diffusion effects of several cobalt-based alloys in a zinc + 0.12% aluminum bath at 460°C (in conjunction with wear and erosion characteristics). Numerous researchers have also investigated similar molten zinc dissolution projects.

Although these tests were effective one-dimensional investigations (with respect to the bath chemistry) and provided significant contributions to the knowledge of galvanizing hardware research, most industrial systems are not only dynamic operations but also may vary from the bath chemistries maintained in these tests. Thus, multidimensional tests should be reviewed incorporating aluminum concentration and bath temperature as primary independent variables.

1.3 Research Objective

In accordance with the need for further research into the effects of bath chemistry on pot hardware, the current investigation explores a series of experiments to generate the molten zinc dissolution characteristics and associated substrate reaction mechanisms of 316L stainless steel at increasing aluminum concentrations in the zinc bath. (316L stainless is the most common structural material employed for galvanizing bath hardware.)

The first activity of this project reviewed previous research ventures in the area of corrosion effects on metals in liquid zinc. In addition, phase diagrams of the responsible alloy systems were studied to understand the intermetallic compounds that may be encountered in this study. Next, a series of laboratory corrosion experiments were undertaken to physically investigate the actual dissolution rates of 316L stainless steel in molten zinc at increasing aluminum concentrations. Subsequent data analysis of the dissolution responses was further supported by investigating the interface reactions between the zinc/aluminum bath and the surface of the substrate using advanced SEM/EDS analysis techniques.

It is the anticipation that the research effort will provide another piece to the puzzle of molten metal corrosion in liquid zinc. Enhanced comprehension of the dissolution and diffusion characteristics of standard galvanizing bath hardware materials could provide a major breakthrough to the understanding of operating life issues and subsequent minimization of equipment downtime on steel coating production lines.

Chapter 2: Commercial Alloy Research

Zinc has been used as a corrosion protectant for carbon steel for over a century. Correspondingly, the need for long-life hardware in the manufacturing of zinc-coated galvanized steel has existed over the same duration with the major factor in galvanizing hardware endurance being the appropriate selection of materials for construction. In 1914, James Davies [Ref. 1] noted the following in his book Galvanized Iron: Its Manufacture and Uses, one of the first published works on galvanizing. "The duration of the galvanizing [hardware] varies considerably, and sometimes leads to disputes between the maker of the [hardware] and the galvanizer. One of the chief essentials to the duration of the [hardware] is the quality of the iron or steel of which it is constructed." And similarly, "The endurance of the rolls in the bath also depends on the quality of the iron used, which should be of the best hammered scrap forgings."

Over the past 93 years much has changed in the manufacture of galvanized steels from substantial automation integration to the utilization of high-tech materials for these extreme environments. However, just as it was in Davies' time, the alloys used for the immersed galvanizing hardware are the primary factor in maintaining a resilient galvanizing operation.

In spite of the long-known fact that galvanizing hardware materials are the key feature in minimizing galvanizing production stoppages, minimal dedicated research has been executed in an effort to obtain a complete understanding of the failure mechanisms encountered by submerging galvanizing hardware materials in molten zinc alloys. It has only been in the past ten years that a major emphasis has been placed on understanding metallic reactions in zinc, as they relate to the manufacture of coated steels.

The first published report of a concerted investigation into reactions of galvanizing hardware materials in zinc baths was undertaken in the early 1950's at Battelle Memorial Institute in Columbus, Ohio by Hodge, et al. [Ref. 2] . In the study they explored the baseline dynamic corrosion of numerous metallic samples (rods and plates) rotating (at 12rpm) in a bath of 99.99% ("SHG") zinc (at 440°C and 700°C) for 50 hours (see Table 2-1). As outlined in Figure 2-1, several materials were completely consumed during the 50 hour test at 440°C, including pure cobalt and titanium, and similarly 310 stainless was 95% dissolved after 50 hours. Meanwhile, numerous samples (tungsten, molybdenum, silicon, and other alloys) portrayed only minimal dissolution. The common characteristic among many of the low solubility samples was high levels of molybdenum and/or tungsten.

Table 2-1: Approximate Compositions of Alloys (wt%) Tested by Hodge, et al. [Ref. 2]

	Approx. composition:
446 Stainless:	Fe + 27% Cr
310 Stainless:	Fe + 26%Cr + 20%Ni
Hastelloy B:	Ni + 33% Mo + 7% Fe
Hastelloy C:	Ni + 20% Mo + 7% Fe + 18% Cr + 6% W
Stellite 21:	Co + 27% Cr + 6% Mo + 2% Ni + 1% Fe
Colmonoy 6:	66% Ni + 17% Cr + 4% B + Fe, Si, C
Colmonoy WRC 100 :	Fe + 20% W + 16% Cr + 3.5% B

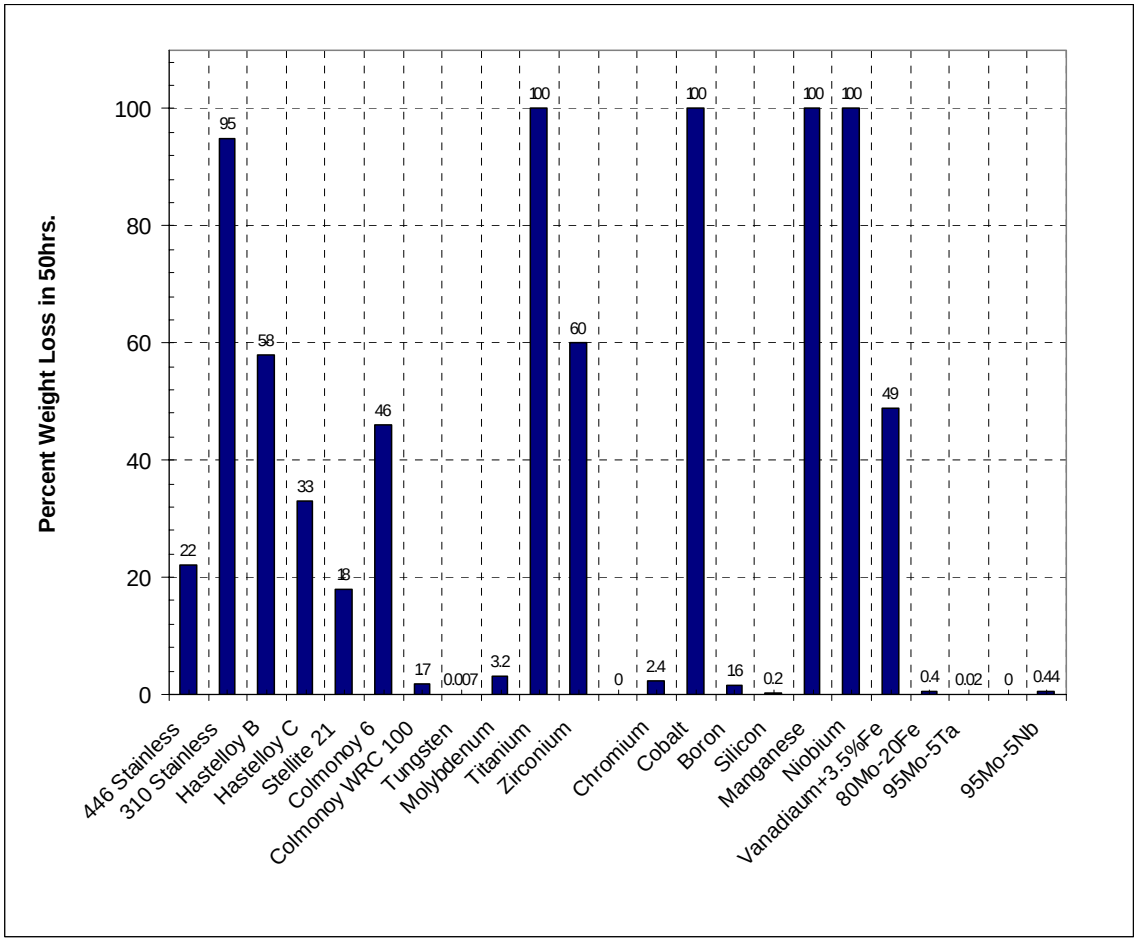

Figure 2-1: Results of Dynamic Corrosion Tests (12 rpm) for 50 Hours in 99.99% Pure Zinc at 440°C [reproduced from Ref. 2]

Moreover, the comparative dissolution rate for several samples can be identified in Figure 2-2 when the temperature was increased from 440°C to 700°C. As a result of the drastic temperature increase, dissolution reactions accelerated tremendously. The dissolution rate of tungsten increased by almost 600% but still remained negligible, while molybdenum and Colmonoy WRC 100 each had analogous increases in corrosion (3.7X and 7X, respectively). Alternatively, after only indicating 2.4% weight loss at 440°C, the chromium sample was completely consumed at 700°C in less than 50 hours. (This severe increase in corrosion rate brings into question the validity of the results at 440°C.)

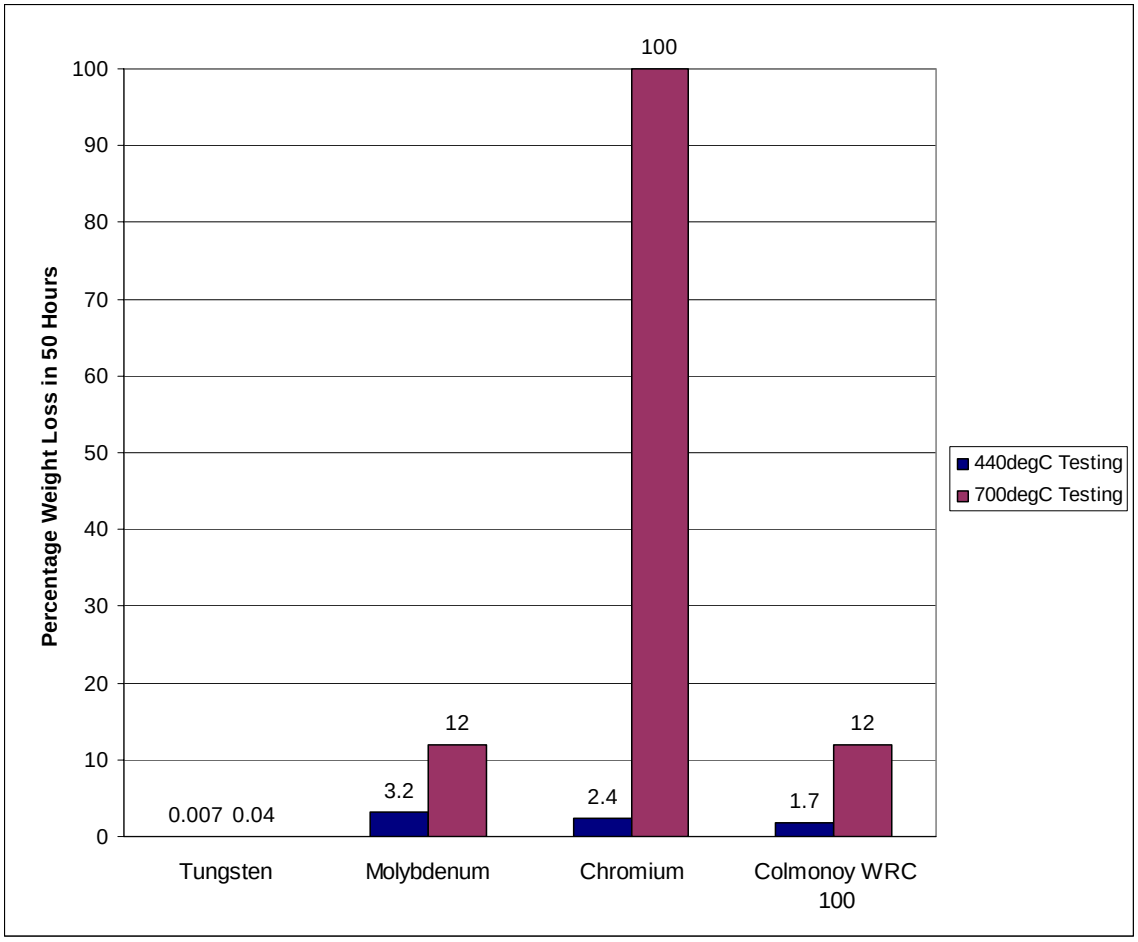

Figure 2-2: Comparison of 440°C and 700°C Dynamic Corrosion Tests (12 rpm) for 50 Hours in 99.99% Pure Zinc [reproduced from Ref. 2]

Next, Hodge, et al. reviewed the better performing alloys in more detail, using 1010 carbon steel as a baseline for comparison. Extrapolating the actual weight loss to an annual average, the superior dissolution performance of refractory metals, such as tungsten and molybdenum (and their alloys), in a pure zinc bath are shown in Figure 2-3. Comparatively, iron alloys containing high levels of W or Mo still performed poorly demonstrating the high reactivity of Fe in pure zinc.

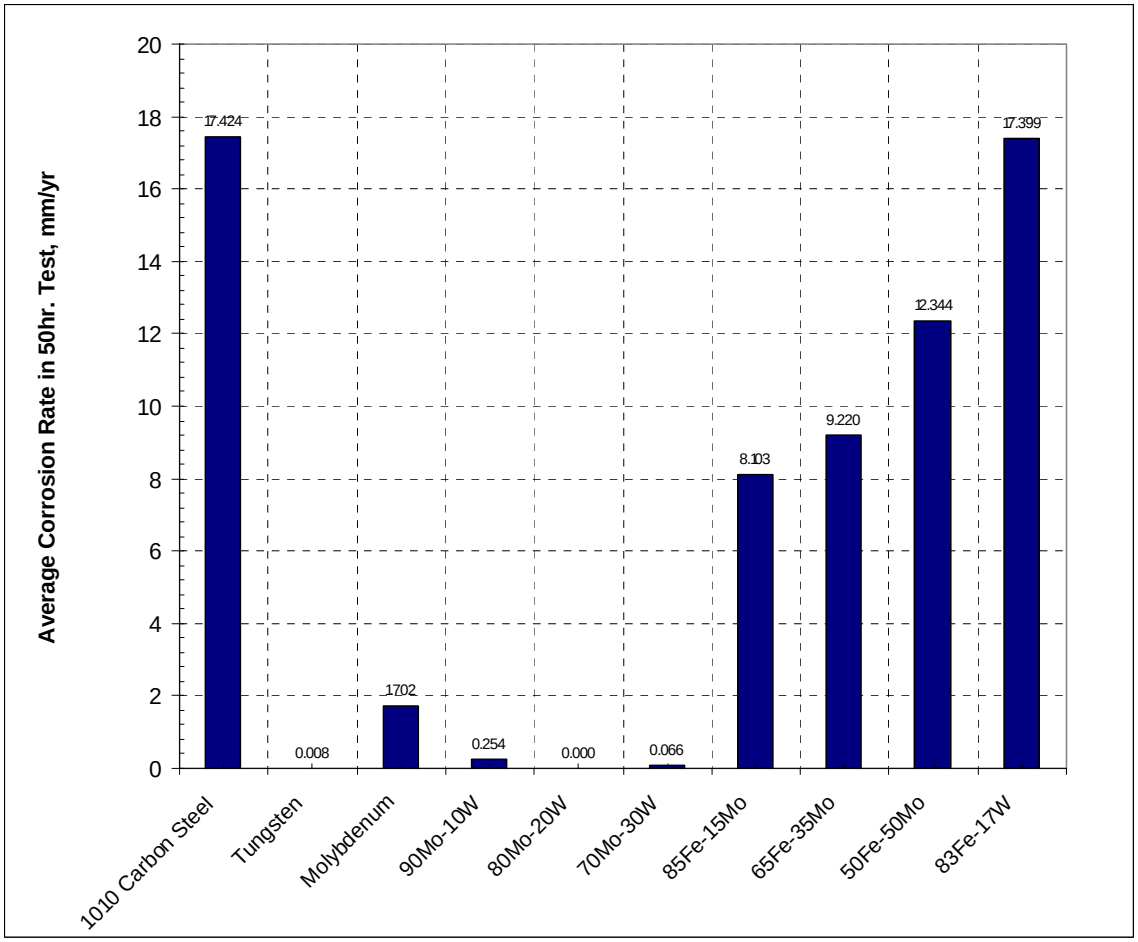

Figure 2-3: Annualized Results of "Top Performers" from Dynamic Corrosion Tests (12 rpm) for 50 Hours in 99.99% Pure Zinc at 440°C [reproduced from Ref. 2]

In contrast, several discrepancies should be noted in the work done by Hodge, et al. First, although each test was conducted with the same mechanical configuration and bath parameters, the individual samples were of varying sizes, including rod, sheet, and even foil. This variability in sample geometry not only skews the amount of wetted surface area, but questions the calculation of percentage weight loss as a result of differing starting weight and analogous mass transfer to the molten bath. Next, it is difficult to extrapolate from a 50 hour test to corrosion rate units in millimeters per year. During each 50 hour test it is not clear whether the bath achieved a steady-state saturation

point which could limit further solubility or if the degradation would continue linearly for extended time periods. Finally, very little information was provided concerning the precise chemistry of the metallic samples, specifically the carbon content. (Perhaps it was not available at that time?) Overall, Hodge, et al. provided a general "snapshot" of the possible rankings of the zinc corrosion rates for several pure metals and conventional alloys. As a result, this work has furnished the starting point for all subsequent zinc hardware corrosion research studies for the past fifty years.

Following this work by Hodge, et al., metals suppliers began to recognize the potential for equipping galvanizing facilities with more advanced materials for their coating hardware. In the 1960's, Climax Molybdenum Company began promoting an alloy of molybdenum with 30wt% tungsten for its superior performance in industrial molten zinc environments, specifically in pure zinc applications [Ref. 3]. Previously (even before Hodge's research), Climax had marketed ferrous alloys with additions of molybdenum for use in zinc die casting machines [Ref. 4], but these alloys would not provide extensive hardware life in rigorous pure zinc applications, such as molten metal pumps. Burman, et al. noted [Ref. 5] that "zinc die casting alloys contain aluminum that markedly reduces the corrosive attack of zinc upon the more common iron or steel components."

Consequently, Burman, et al. initiated field trials of Mo-30wt%W components in the pure zinc baths at two zinc smelting operations. "Because previous experience had demonstrated that static tests may be an unreliable indicator of the corrosion resistance of any material to flowing zinc, a series of exploratory dynamic tests were carried out simulating the vigorous mechanical action encountered by a rotating [molten metal]

pump impeller. [Ref. 5]" For the first trial, a 14mm thick plate of Mo-30W (length and width dimensions not given) was attached to a shaft and rotated at 228 revolutions per minute. The sample was removed intermittently and the thickness at the edge of the plate was measured. Also, the temperature was increased step-wise at each interval from 488°C ultimately to 600°C. The relatively minor degradation of the sample over the duration of the test is shown in Figure 2-4. Only 4.3% of the thickness was lost subsequent to (over) 2000 hours of immersion.

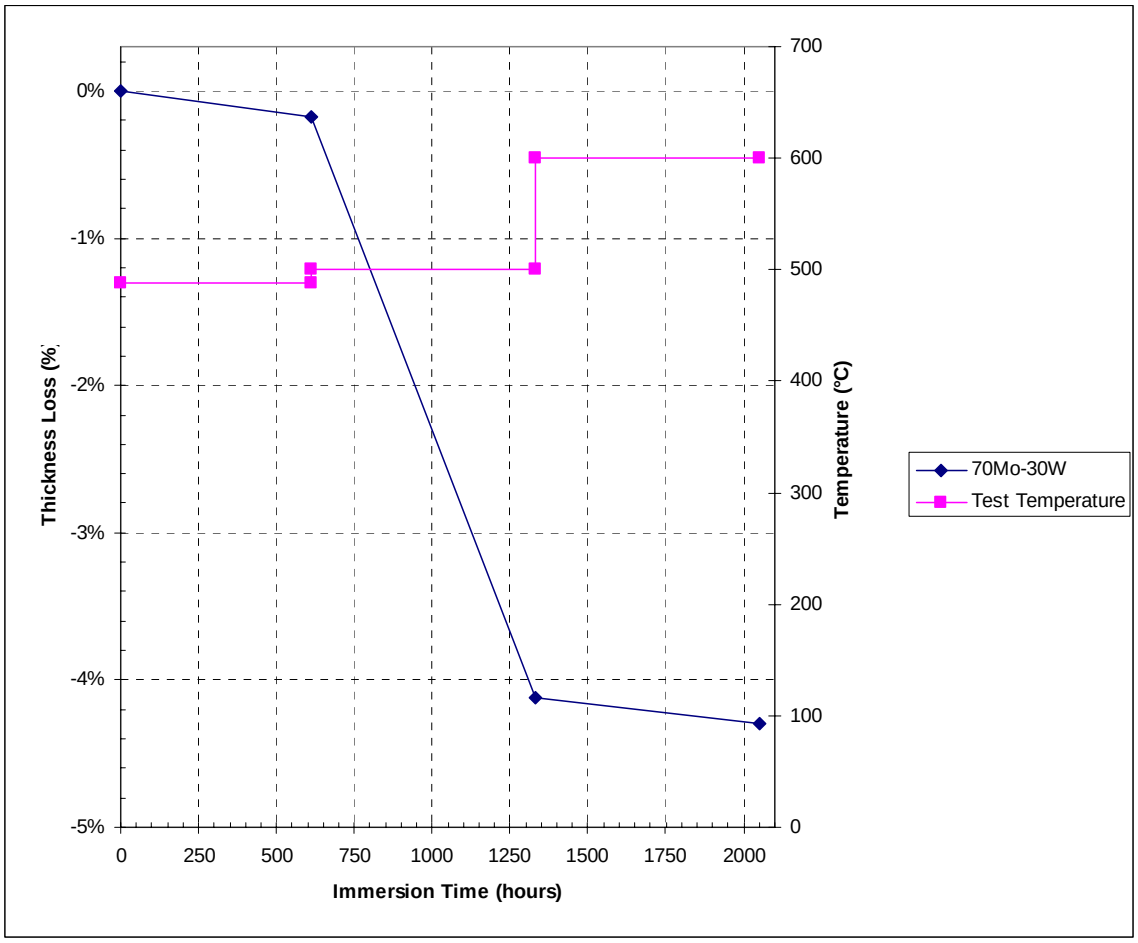

Figure 2-4: Degradation of 70%Mo + 30%W Alloy in Pure Zinc at Increasing Temperatures from 488°C to 600°C. [reproduced from Ref. 3]

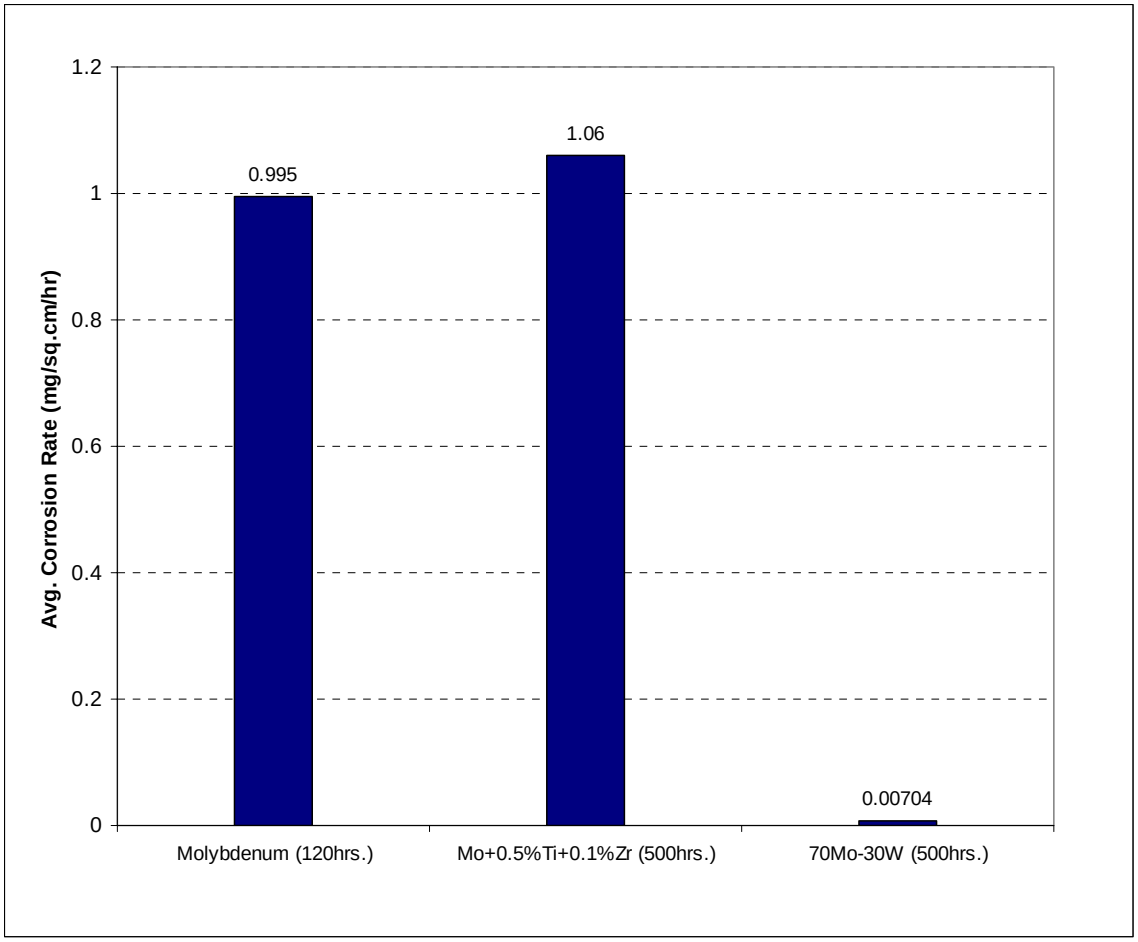

Figure 2-5: Corrosion Results of Three Molybdenum Alloys in Flowing (0.05m/s) Pure Zinc at 520°C for 500 Hours [reproduced from Ref. 3]

Concurrently, Burman, et al. tested three different molybdenum alloys in a bath of flowing (0.05m/s velocity) pure zinc at 520°C. In Figure 2-5 it is observed that the Mo-30wt%W sample had excellent corrosion resistance over the 500 hours of testing. Thus, from these basic tests it is recognized that an alloy of molybdenum with 30wt% tungsten can provide exceptional life for mechanical hardware applications in pure zinc environments. However, it should also be identified that 70Mo-30W castings have a phenomenal cost and should be used sparingly with careful consideration for overall economics.

In the same manner yet thirty years later, Schwarzkopf Technologies Corporation [Ref. 6] , one of the leading suppliers of refractory metal components, provided corrosion data relating to the performance of several molybdenum-tungsten alloys in pure zinc.

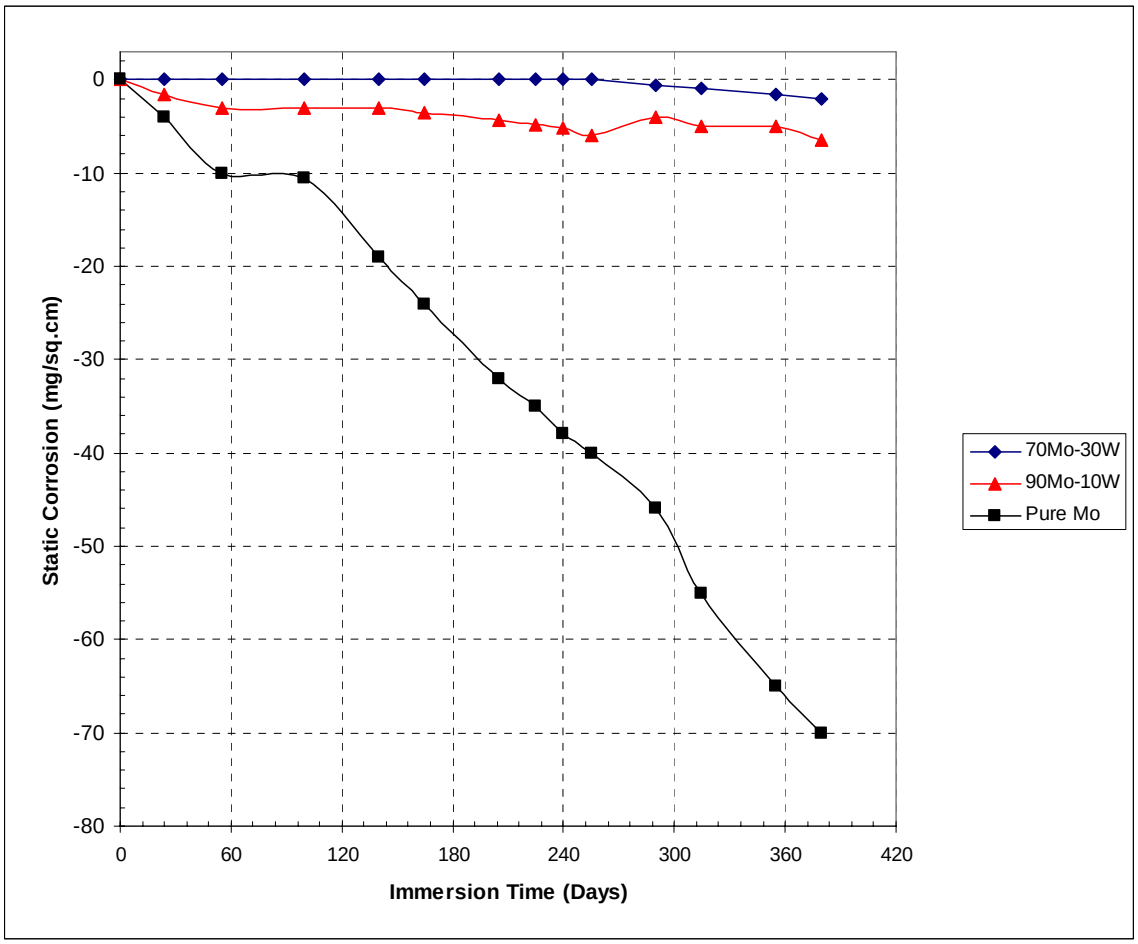

Figure 2-6: Static Corrosion of Several Molybdenum Alloys in Pure Zinc at 455°C [reproduced from Ref. 6]

As indicated in Figure 2-6, although pure molybdenum metal had a steady rate of dissolution in a pure zinc bath (at 455°C), alloying additions of tungsten greatly reduced the corrosion degradation. In fact, molybdenum with addition of 30wt% tungsten had no decay after 8 months in service. Thus, since it is known that pure tungsten has no solubility in liquid zinc at 455°C [Ref. 7], it can be assumed that, by alloying

molybdenum with only 30wt% tungsten, nearly the minimal reactivity of pure tungsten can be achieved (for reasonable operating durations). Molybdenum-30% Tungsten alloy also has excellent strength at elevated temperatures. However, 70Mo-30W is very brittle and can easily fracture under impact. Thus, when combined with the exorbitant cost constraints, the use of this material for industrial galvanizing applications has been somewhat limited and careful considerations must be made when specifying its use.

Meanwhile several other new alloys have been purported by their manufacturers to possess superior corrosion resistance in various molten zinc environments. In 1982 Wakita and Sakonooka received a patent for a new alloy which portrayed greater resistance to molten zinc attack [Ref. 8]. They claimed that their new Fe-Co-Cr-Ni alloy would have good zinc corrosion resistance and adequate hardness to resist mechanical wear in order to provide longer life to galvanizing pot hardware while being less expensive than standard hardware materials such as Stellite 6.

Table 2-2: Compositions of Alloys Tested (wt%) for Zinc Corrosion Resistance [Ref. 8]

element	Wakita, et. al.	Control Alloy	HH stainless	Stellite 6	Low-Carbon Steel	Haynes 25
C	0.93	1	0.4	1.2	0.05	0.05
Si	0.80	0.8	0.8	1.5	0.2	0.6
Mn	0.80	0.8	0.8	0	0.4	0
Ni	13.64	17.6	14	1.5	0	10
Cr	15.18	18	23	28	0	20
Mo	5.45	3.62	0	0	0	0
W	1.23	1.54	0	5	0	15
Ta	0.48	0.6	0	0	0	0
Co	22.55	19.8	0	60.8	0	51.35
Zr	0.07	0	0	0	0	0
B	0.00	0	0	0	0	0
Nb	2.64	1.84	0	0	0	0
Fe	36.24	34.4	61	2	99.35	3
-Hv-	170.64	149.4	127	370	-	-

- Vickers hardness at 500°C

The chemical composition of the alloy developed by Wakita and Sakonooka (in addition to a similar "control alloy") is outlined in Table 2-2. Four other commercial alloys are also noted for reference. According to the patent publication, Wakita and Sakonooka [Ref. 8] performed a series of dynamic zinc corrosion experiments on these alloys. For two different temperatures (470°C and 520°C) each sample (12mm diameter x 35mm long) was rotated on a circle (70mm diameter) in the molten zinc bath at 230rpm for 25 hours. The results of these corrosion trials are outlined in Figure 2-7 . (Note: No corrosion results were listed for Stellite 6 at 520°C)

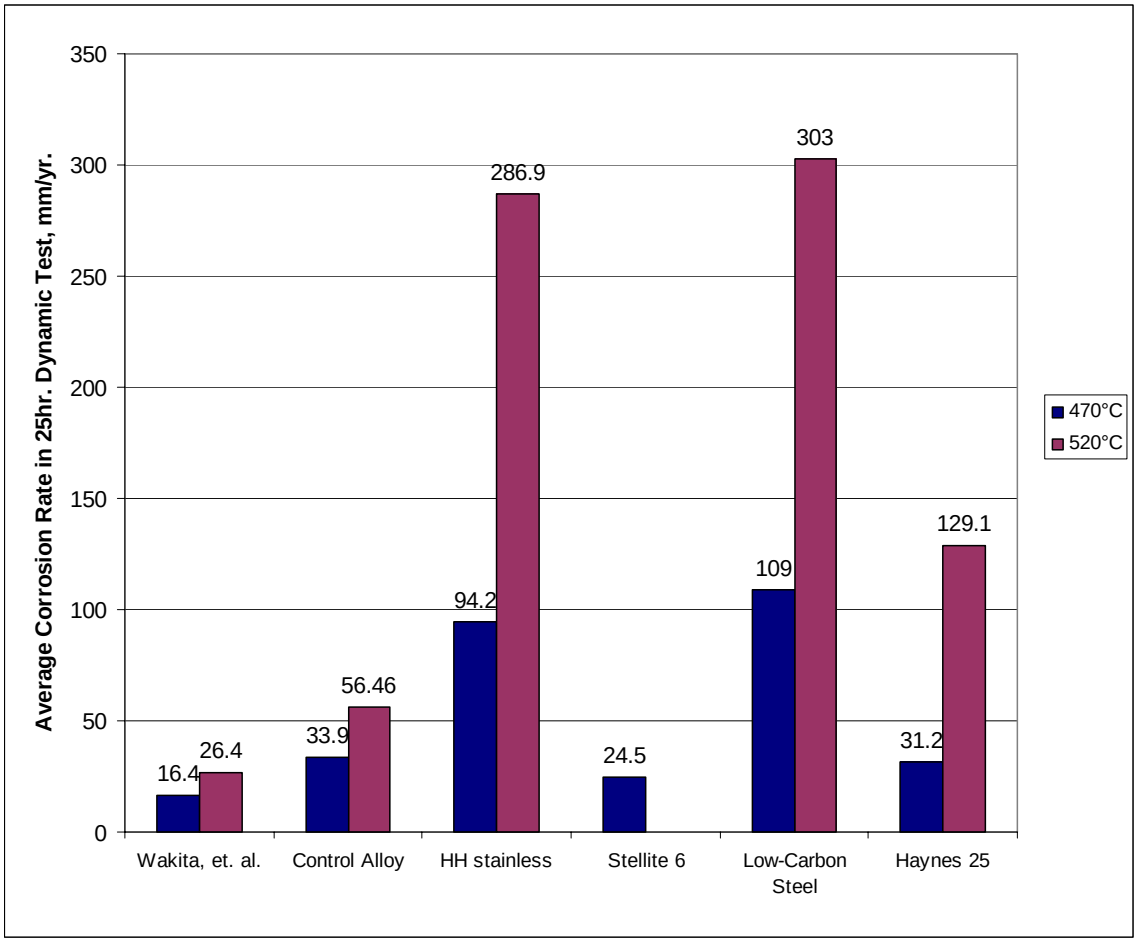

Figure 2-7: Dynamic Corrosion (230 rpm) of Several Alloys in Molten Zinc at 470°C and 520°C after 25 Hours [reproduced from Ref. 8]

As predicted, the new alloy developed by Wakita and Sakonooka [Ref. 8] did have superior corrosion resistance to Stellite 6 (16.4mm/yr vs. 24.5mm/yr at 470°C, respectively) and they noted that an alloy "desirably" should have an "average depth of corrosion less than 20.0 mm/year when it is immersed in fluid molten zinc having a conventional operating temperature (450° to 470°C)".

Reviewing these results, several observations can be made. First, it is difficult to extrapolate to a corrosion rate unit of millimeters per year from only a 25 hour test. It is not wise to assume that the corrosion rate will continue at a linear proportionality. Next, although the chemical identification of the sample alloys was very thorough, the exact chemical nature of the molten zinc bath was not described, even though it is widely known that the zinc bath composition can have a major impact on the reactivity in this type of corrosion experiment. In conjunction, it was noted that the samples were rotated at 230rpm on a 70mm circle, but nothing was defined as to any means for preventing oxidation or air-ingestion at this rapid sample speed.

Finally, the corrosion improvement of the new alloy over Stellite 6 is only about a 30% improvement and no evidence was provided for comparison at alternative temperatures. Additionally, comparing the hardness values listed in Table 2-2 , the new alloy has less than half of the hot hardness level of conventional Stellite 6, which is typically a material used for zinc-submerged bearings on continuous galvanizing lines where wear-resistance is extremely important. No justification was identified for a minimum hardness requirement. Thus, it cannot be stated with certainty that the new alloy is an adequate replacement for Stellite 6 over a complete range of operating parameters. Analogously, if the new alloy is intended to be utilized as a submerged roll

material, 316L stainless steel (the industry standard) should have been tested as a baseline comparison. However, with the elevated alloying content of this new material, it would not be directly cost competitive with 316L stainless, which is manufactured in large quantities.

Similarly, in 1998 Handa, et al. [Ref. 9] patented a concept for making stainless steel more corrosion resistant to a molten zinc bath. They claimed that by adding 0.35wt% to 0.75wt% nitrogen to a ferrous stainless alloy that the zinc attack could be significantly reduced. The impact of elevated nitrogen levels in stainless steel alloys with various levels of chromium can be observed in Figure 2-8. Handa, et al. performed numerous corrosion experiments in a bath of Zn + 55wt%Al at 600°C. Each specimen was machined to 50mm wide x 20mm thick x 300mm long then immersed in the molten bath for 336 hours. After removal, the "decrease (mm) in thickness of one side of each of the specimens was determined to evaluate the corrosion resistance of the alloy steel".

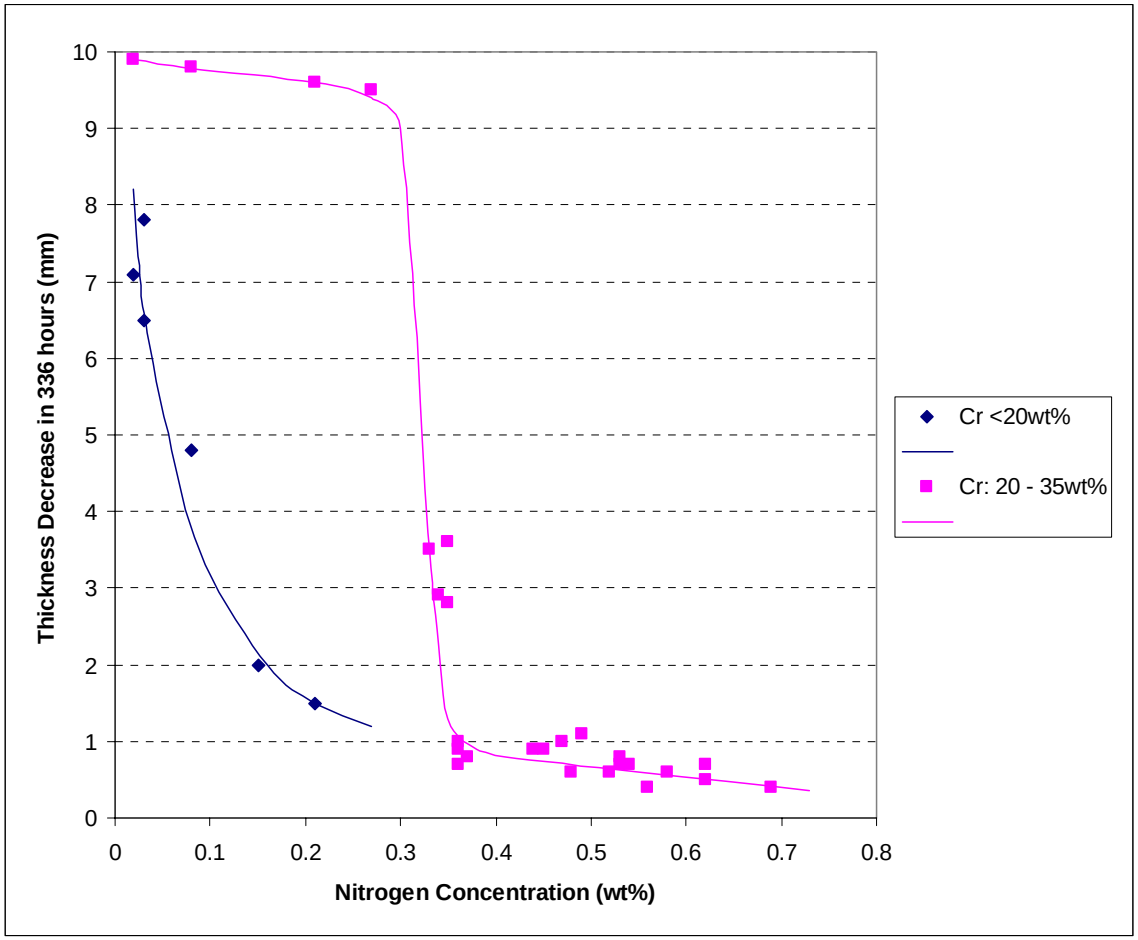

Figure 2-8: Comparative Effect of Nitrogen Level in High-Chromium Stainless Steels following Immersion in Zn-55Al Bath at 600°C for 336 Hours [reproduced from Ref. 9]

Table 2-3: Compositions of Alloys Tested (wt%) for Corrosion Resistance in Liquid Zn-55%Al [Ref. 9]

element	Handa, et. al.	316L stainless	~'Handa' (but lower N, W, C)
C	0.12	0.03	0.06
Si	1.06	0.68	0.98
Mn	1.66	1.27	1.72
Ni	13.80	12.02	14.00
Cr	25.19	17.10	25.40
Mo	0.94	2.08	0.94
W	1.54	0.00	0.25
N	0.51	0.03	0.17
Fe	55.19	66.79	56.49

Among the significant alloys tested (Table 2-3), the results by Handa, et al. (Figure 2-9) indicate that the new high-nitrogen alloy provides a significant improvement in dissolution resistance in a Zn + 55wt%Al bath as compared to conventional 316L stainless steel. No further results were provided to define the performance of this alloy in baths other than zinc-55% aluminum.

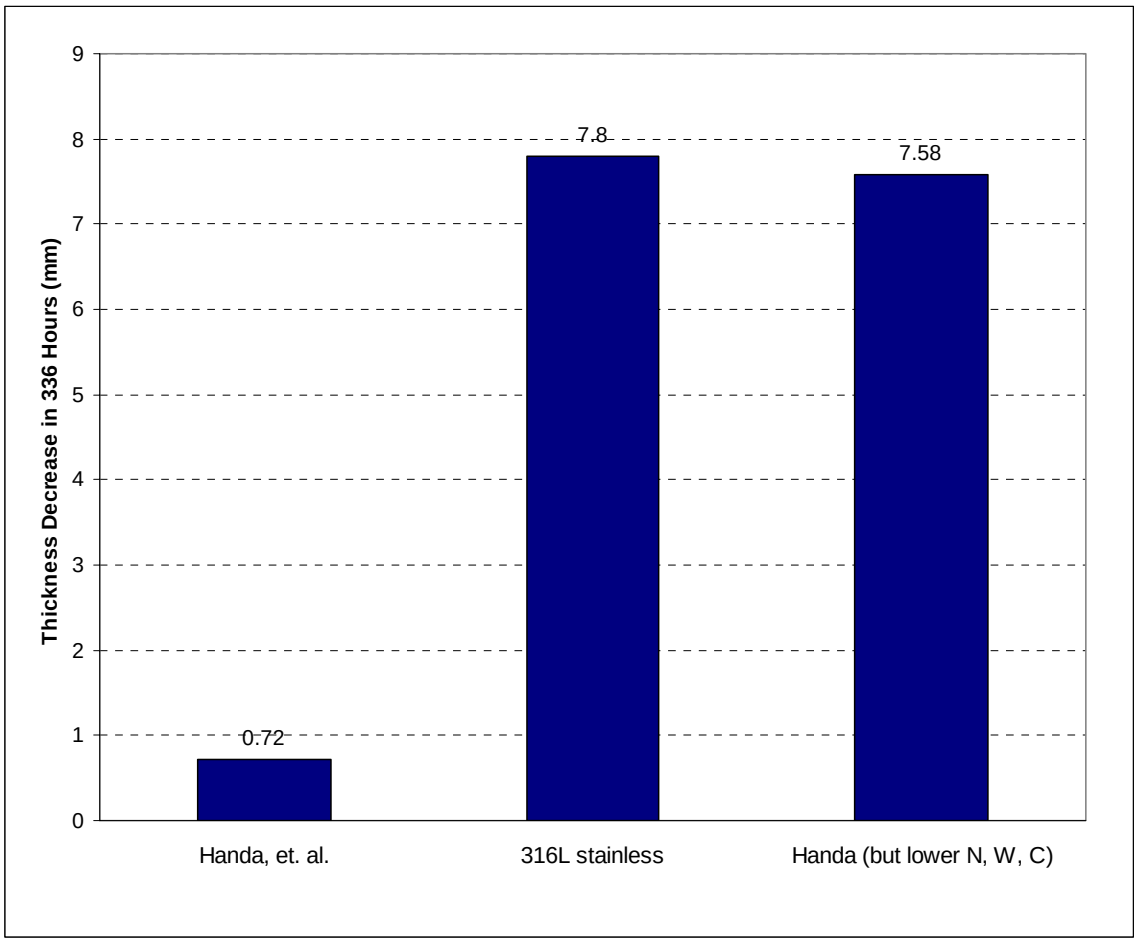

Figure 2-9: Corrosion Performance of Three Alloys after Testing in a Molten Zn-55%Al Bath at 600°C for 336 Hours [reproduced from Ref. 9]

However, five years prior to the publication of the patent by Handa, et al., literature was released indicating that the zinc corrosion resistance of stainless steel is improved with only 0.2wt% nitrogen content. In 1993, Rolled Alloys Inc. of

Temperance, Michigan performed a series of experiments [Ref. 10] to compare the reactivity of various alloys in molten zinc. A laboratory test program was initiated to compare the corrosion resistance of a limited group of metal alloys [Table 2-4] in a pot of molten zinc [Table 2-5] at 454°C.

Table 2-4: Compositions of Ferrous Alloys Tested (wt%) for Corrosion Resistance in Molten Zinc [Ref. 10]

Alloys	C	Ni	Co	Cr	Mo	W	Si	N	Fe	Others:
Haynes 556	0.1	20.0	18.0	22.0	2.5	2.5	-	0.20	34.1	0.6Ta, 0.02 Zr, 0.02 La
AL-6XN	0.03	25.5	-	22.0	7.0	-	1.0	0.25	41.5	2.0 Mn, 0.75 Cu
Carbon Steel	0.08	-	-	-	-	-	0.25	-	99.2	0.45 Mn
446 Stainless	0.02	-	-	25.0	-	-	-	0.25	74.7	
309 Stainless	0.1	13.5	-	23.0	-	-	-	-	63.4	
316 Stainless	0.08	12.0	-	17.0	2.5	-	-	-	68.4	

Table 2-5: Zinc Bath Composition for Corrosion Tests Performed by Rolled Alloys Inc. [Ref. 10]

	wt%
Zn	97.20
Al	0.437
Fe	0.051
Pb	1.254
Cu	0.263
Sn	0.437
Cd	0.150

From the results of these brief trials (Figure 2-10), they realized that AL-6XN (a super-austenitic stainless steel with high nitrogen content) provided dissolution resistance in zinc comparable with Haynes 556, but at a lower material cost. On the other hand, the testing also indicated (Figure 2-10) that carbon steel (0.08% C) displayed a lower susceptibility to zinc corrosion than 316 stainless (the standard industrial hardware material), which does not seem logical. The bath composition (Table 2-5) contained an elevated aluminum level (0.437wt%) and an extremely high lead content (1.254wt%). These elemental thresholds are not exactly representative of typical continuous galvanizing lines which usually operate at less than 0.2wt% aluminum, 0.03wt% iron and

virtually no lead (due to health and environmental considerations). Thus, these inconsistencies in the trial zinc bath could have produced conclusions that may or may not be representative when scaled up to production environments. Nevertheless, the results provide legitimate support to continue testing AL-6XN and other high nitrogen alloys as potential materials for galvanizing bath hardware.

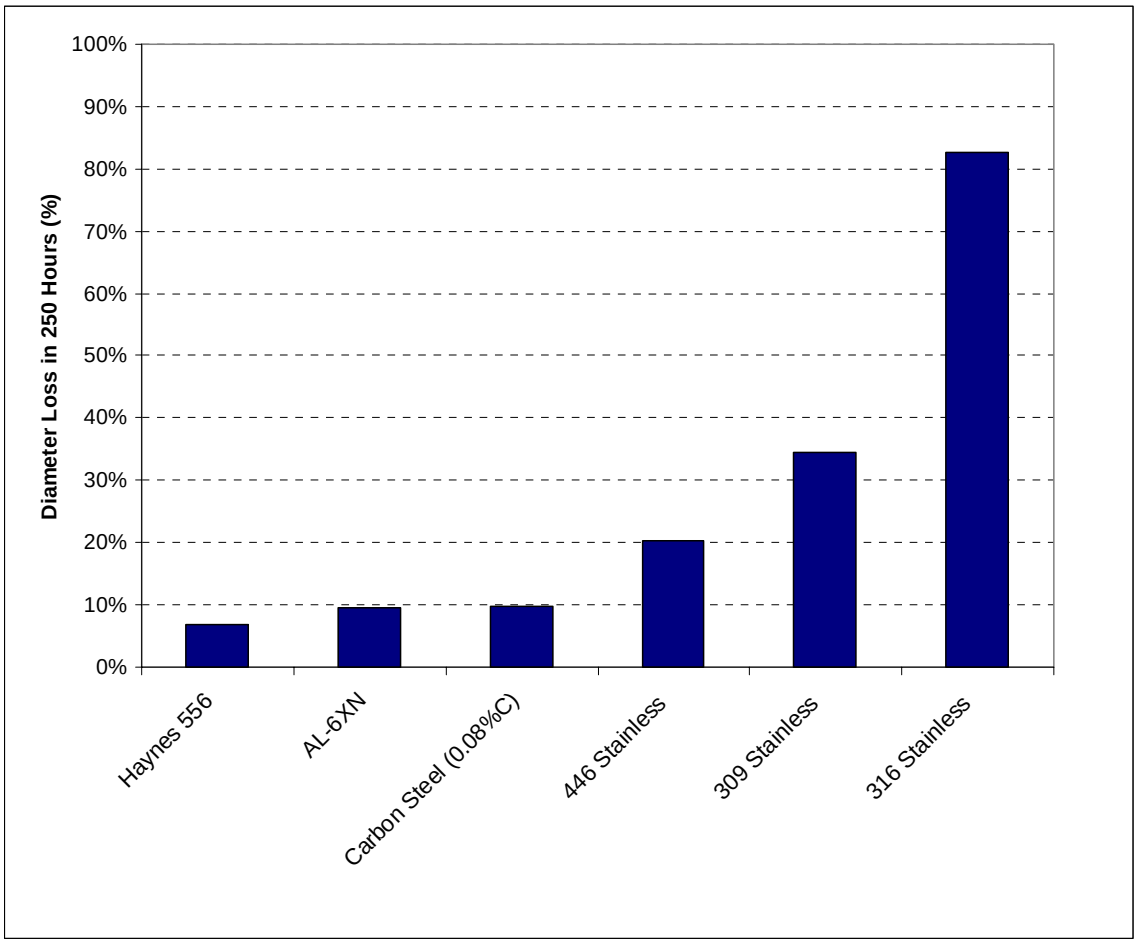

Figure 2-10: Results of Corrosion Tests in Molten Zn-0.44%Al at 454°C for 250 Hours [reproduced from Ref. 10]

Since Rolled Alloys is a distributor of heat and corrosion resistant alloys, the impetus for this zinc corrosion study was to determine if Rolled Alloys already possessed a cost competitive material with performance similar to Haynes 556 in industrial

galvanizing baths. From these results it was determined that AL-6XN was able to fill that role. In those regards, previous testing had already been performed on Haynes 556 alloy.

Haynes International Inc. is "a world leader as the premier inventor, developer, producer and solution provider in the supply of quality high performance nickel- and cobalt-based alloys" [Ref. 11]. In 1993, Haynes International published a technical bulletin describing the zinc corrosion resistance of Haynes 556 alloy [Ref. 12]. In this report Antony & Srivastava defined the necessary properties for an alloy to be effectively utilized in galvanizing hardware. Primarily, the metal must "possess adequate mechanical strength at temperature and resistance to corrosion from molten zinc". "Additionally, the alloy must be resistant to embrittlement and associated cracking, and be metallurgically stable so it can be repaired by either welding or mechanical working." [Ref. 12]

Haynes 556 alloy was developed to have a good combination of strength, fabricability, weldability and resistance to molten zinc. Antony & Srivastava performed a series of experiments to evaluate the dissolution characteristics of Haynes 556 alloy in zinc galvanizing baths. On a laboratory basis, a series of alloys (Table 2-6) were immersed for 50 hours in a bath of pure zinc at 455°C. Observing Figure 2-11, the results show that the Haynes 556 had the best zinc resistance of the alloys tested and outperformed 304 stainless by over 8 times.

Table 2-6: Compositions of Alloys Tested (wt%) for Corrosion Properties in Zinc [Ref. 12]

Alloys	C	Ni	Co	Cr	Mo	W	Si	N	Fe	Others:
Carbon Steel	0.2	-	-	-	-	-	0.25	-	99.1	0.45 Mn
304 Stainless	0.08	9.5	-	19.0	-	-	-	-	71.4	
309 Stainless	0.1	13.5	-	23.0	-	-	-	-	63.4	
316 Stainless	0.08	12.0	-	17.0	2.5	-	-	-	68.4	
330 Stainless	0.05	35.0	-	19.0	-	-	1.7	0.17	44.1	
446 Stainless	0.02	-	-	25.0	-	-	-	0.25	74.7	
Haynes 25	0.1	10.0	51.9	20.0	-	15.0	-	-	3.0	
Haynes 188	0.1	22.0	38.9	22.0	-	14.0	-	-	3.0	0.04 La
Haynes 556	0.1	20.0	18.0	22.0	2.5	2.5	-	0.20	34.1	0.6Ta, 0.02 Zr, 0.02 La
Alloy 800H	0.05	32.5	-	21.0	-	-	-	-	45.7	0.4 Al, 0.4 Ti

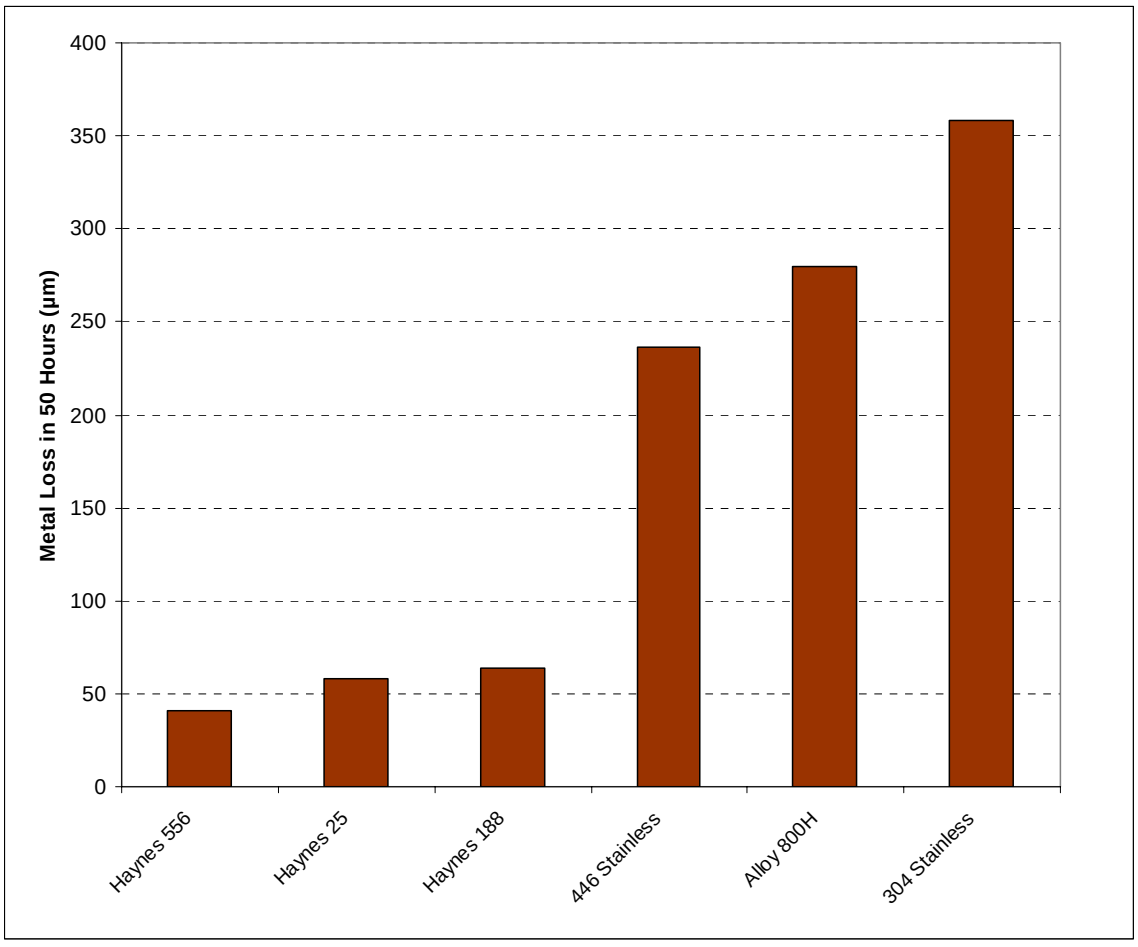

Figure 2-11: Results of Corrosion Testing in Pure Zinc at 455°C for 50 Hours [reproduced from Ref. 12]

Next, Antony & Srivastava submitted test samples to two different industrial galvanizing lines for immersion in actual zinc pots. The first trial consisted of running 4 different alloy samples (see Table 2-6) for 152 hours and 2500 hours concurrently in a bath of molten zinc with 0.10-0.12% aluminum (plus saturated iron). The results of the 152 and 2500 hour tests are displayed in Figure 2-12. It should be noted that extensive cracking was present in both the Haynes 25 and 316 stainless samples after 152 hours. Antony & Srivastava commented that this cracking was probably due to liquid metal embrittlement and could be very detrimental to the mechanical properties of an actual component in this condition.

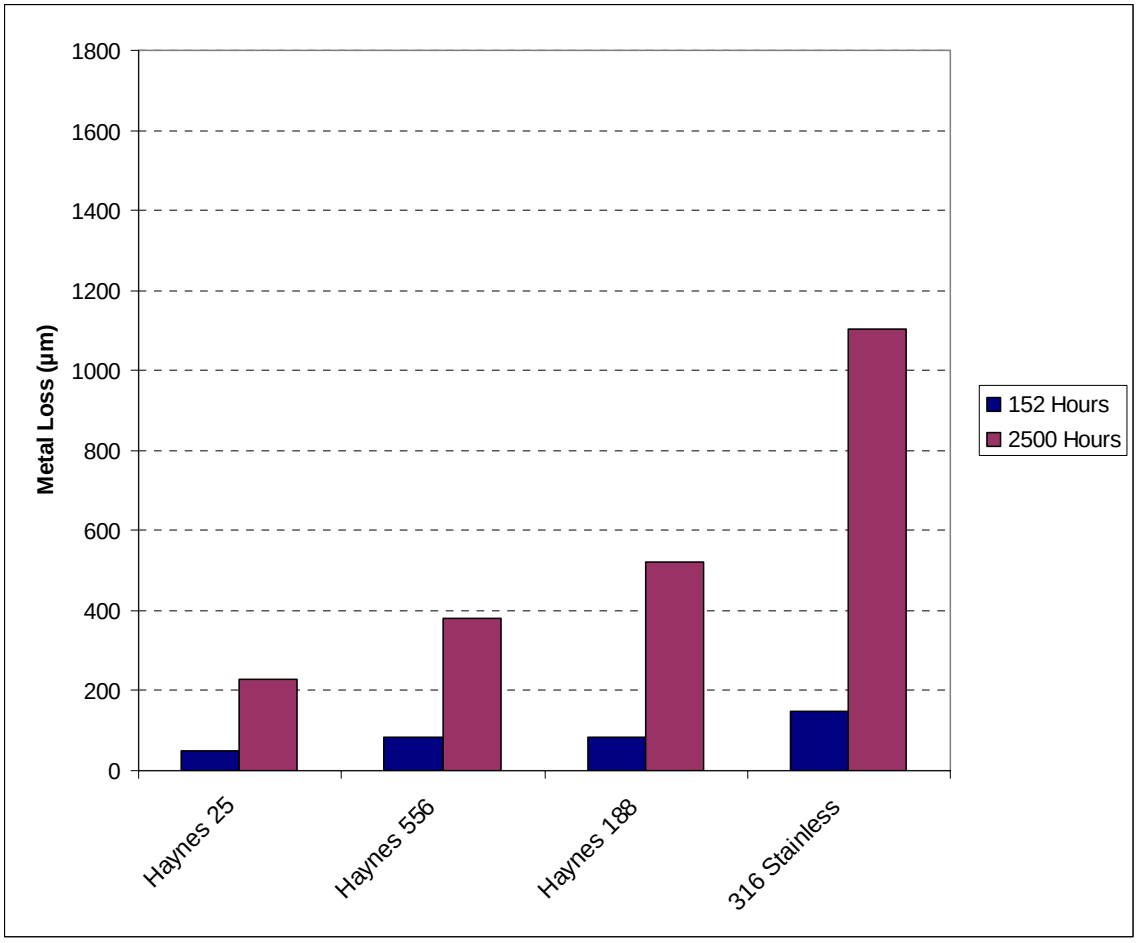

Figure 2-12: Performance of Alloys Immersed in an Industrial Galvanizing Pot (Zn-0.12%Al) for either 152 Hours or 2500 Hours [reproduced from Ref. 12]

By further analyzing Figures 2-11 and 2-12, it may also be recognized that Haynes 25 had significantly better corrosion properties than Haynes 188 in the 0.10-0.12% aluminum bath while being nearly equivalent in the pure zinc bath. It was seen from Table 2-6 that the two alloys are very similar except that Haynes 25 (10%Ni, 52%Co) has substantially lower nickel and higher cobalt than Haynes 188 (22%Ni, 39%Co), thus substantiating the high solubility of nickel in liquid aluminum.

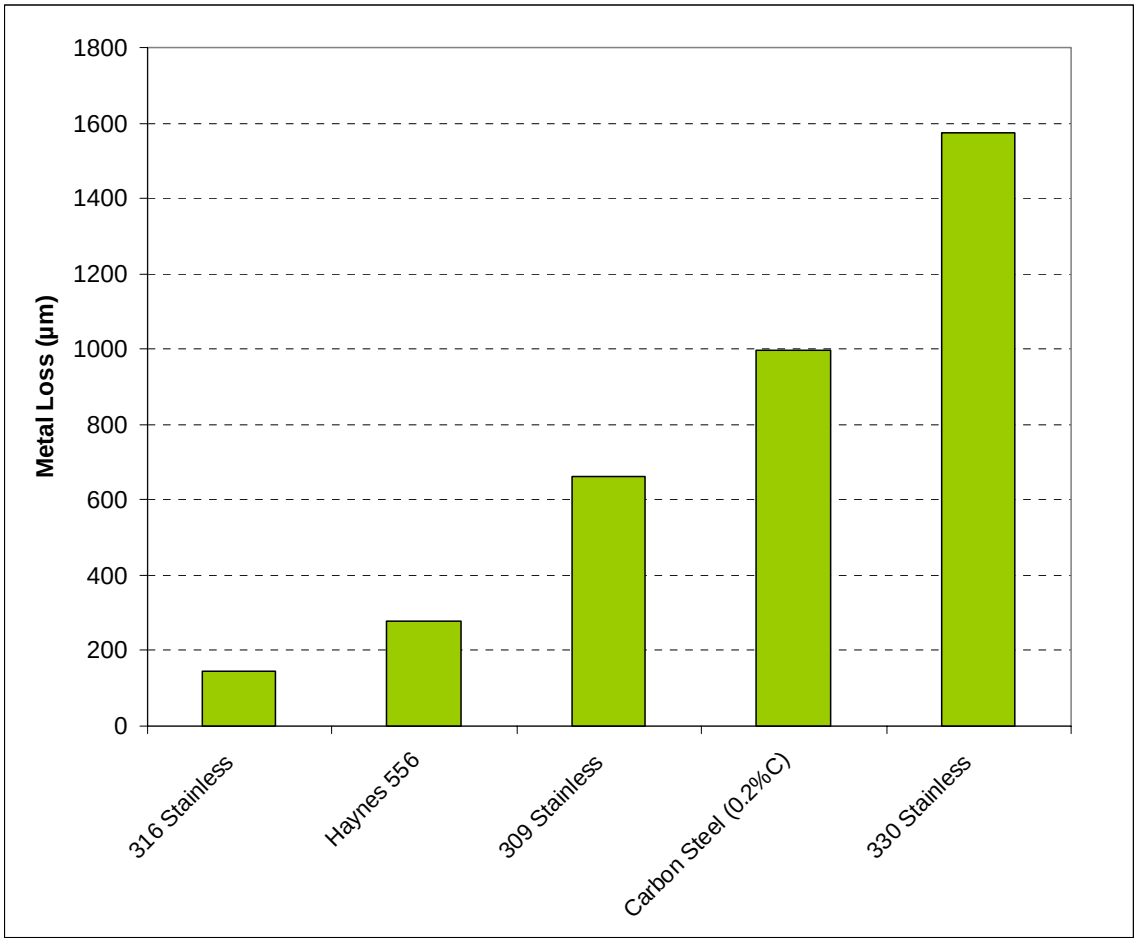

Figure 2-13: Performance of Alloys Immersed in an Industrial Galvanizing Pot at 455°C for 652 Hours [reproduced from Ref. 12]

In the second field trial, Antony & Srivastava immersed another series of samples [see Table 2-6] in a different continuous galvanizing line at 455°C for 652 hours. (Bath chemistry was not noted.) As indicated in Figure 2-13, 316 stainless had the best corrosion resistance among the five samples in this trial, including Haynes 556. However, Antony & Srivastava again commented that 316 stainless had a significant amount of cracking as opposed to Haynes 556 and thus "it is believed 556 alloy is the best choice".

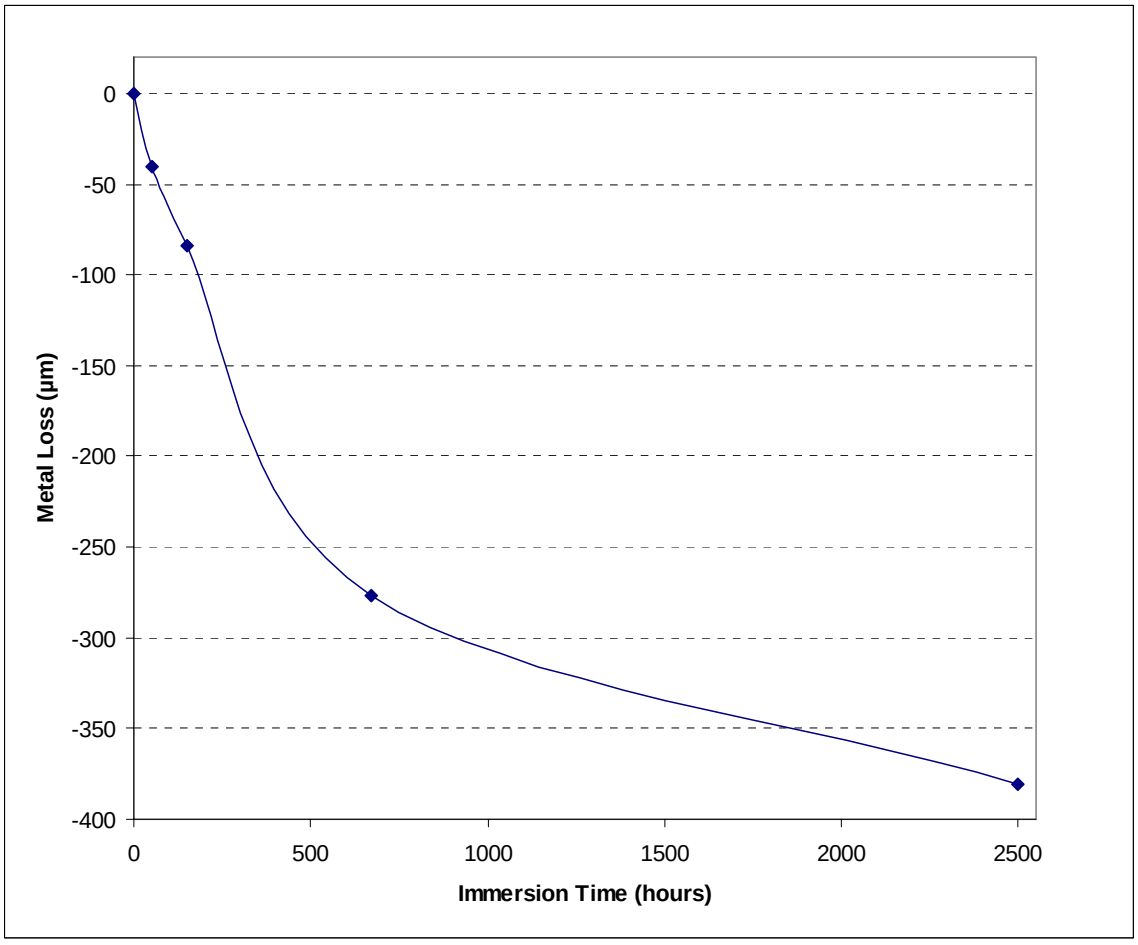

Figure 2-14: Compilation of all Corrosion Tests for Haynes 556 Showing Corrosion Trend as a Function of Time [reproduced from Ref. 12]

From the three different molten zinc corrosion trials, it is apparent that Haynes 556 alloy has an adequate level of corrosion resistance. The consistent trend of corrosion rate across all time intervals is shown in Figure 2-14. However, it should be pointed out that each of the three trials were in different chemistry galvanizing baths: Trial #1 (lab trial) was in pure zinc (0% Al); Trial #2 was in zinc with 0.10-0.12% aluminum; Trial #3 was unknown, but in all likelihood the aluminum content was greater than 0.12%Al since that is a rather low aluminum concentration for a typical continuous galvanizing bath. This variability probably defines the inconsistencies in the 316 stainless corrosion results, but, regardless, the degradation of the Haynes 556 samples followed an expected trendline.

In another study that reviewed cobalt-rich alloys, Wang, et al. [Refs. 13 & 14] published the results of a series of experiments that investigated the solubility aspects in liquid zinc of a specific Co-Cr-W cast alloy (Table 2-7). Not only did they study the static corrosion in a typical galvanizing zinc bath, but they also looked at the dynamic corrosion rate as well as the corrosive wear degradation. (Note: The results of their wear testing will not be reviewed at this time.)

Table 2-7: Composition of Co-Cr-W Alloy [Ref. 13 & 14]

element	wt%
Cr	28.0
W	9.8
Fe	9.1
Si	1.3
Mn	0.6
C	0.44
Co	50.8

For the static and dynamic solubility experiments, Wang, et al. melted a pot of liquid zinc (supplied by BaoSteel Co. Ltd.) with a composition of 0.12-0.20wt%Al, 0.03-0.12wt%Pb

and Zn balance. "The static corrosion sample of [the Co-Cr-W] alloy was prepared to be a size of 20mm x 10mm x 10mm." "The dynamic corrosion specimen was ring-shaped with a size of 50mm in internal diameter, 70mm in outer diameter, and 10mm in thickness." "Static immersion tests were conducted in little alumina crucibles that were filled with small zinc ingots," which were maintained at 465°C in a crucible furnace. Samples were immersed for varying time periods up to 720 hours and the weight loss as a function of time was plotted.

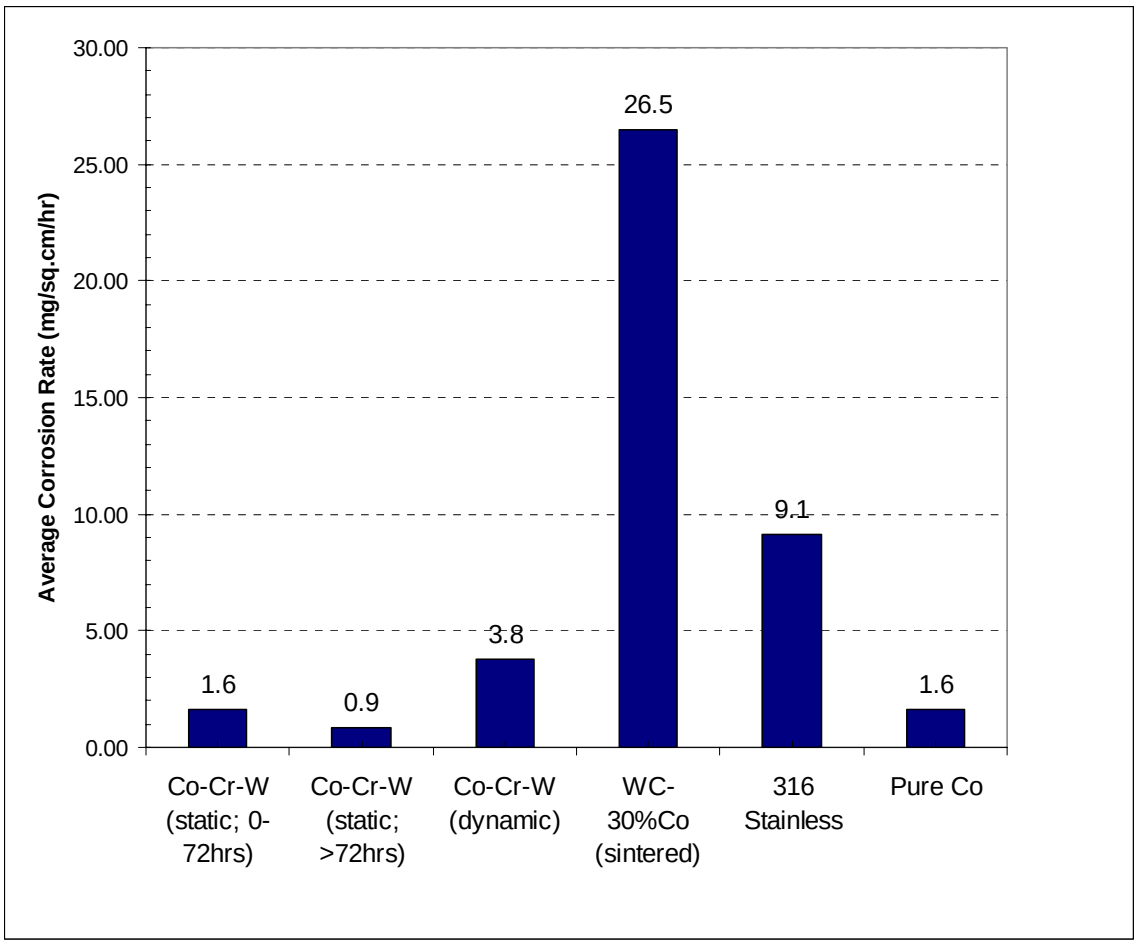

Figure 2-15: Static Corrosion Results of Several Alloys in Zn-(0.12%-0.2%)Al Bath at 465°C for 720 Hours [reproduced from Ref. 14]

The average (static) corrosion rates of several materials are outlined in Figure 2-15, included is the Co-Cr-W alloy under three different conditions (dynamic, static-short time

& static-long time), after 720 hours of static immersion in liquid zinc. (Note: The specific aluminum concentration was not defined for these tests only a range, 0.12 – 0.20wt%Al.) It was observed that the static corrosion rate for the Co-Cr-W alloy was nearly two-times higher for the initial 72 hours of immersion then subsequent to that time. Additionally, under dynamic conditions the Co-Cr-W Alloy showed about a 240% increase in corrosion rate versus the maximum corrosion rate under static conditions. Interestingly, however, the average corrosion rate for pure cobalt (over 720 hours) was the same as the initial rate (0 to 72 hours) for the Co-Cr-W alloy. This indicates that the alloying elements in the Co-Cr-W alloy create a passivation effect, limiting additional corrosion. On the other hand, the sample of sintered WC-Co alloy (with 30wt% Co) displayed a significantly higher static corrosion rate than any of the other samples tested. This high corrosion level is curious in the fact that WC-Co plasma spray coatings on 316L stainless steel are typically employed in industrial galvanizing applications to inhibit corrosive reactions. (Is it possible that the WC-Co coating and 316L stainless steel work in tandem to create a mutually beneficial anti-corrosion effect?)

In general, Wang, et al. found that "the corrosion of the Co-Cr-W cast alloy in liquid zinc is characterized as alloying (of Co-Zn and Fe-Zn) and dissolution (of Cr and W atoms) from Co-base γ phase [matrix] into liquid zinc." Then, the $M_{23}C_6$, M_7C_3 and M_6C carbides in the Co-Cr-W were "easily broken from the corroded surface during the corrosion process." Furthermore, "the static corrosion of the Co-Cr-W alloy [was defined by] preferential corrosion in eutectic groups and uniform corrosion of Co-base γ phase [matrix]," where the eutectic groups were determined to be 42.5%Cr, 37.3%W, 17.3%Co and 2.8%Fe. (It was intriguing that Wang, et al. failed to comment on any reactionary

effects of the aluminum content in the zinc bath.) From the analysis it was "determined that Fe is the easiest element in this alloy to be dissolved in liquid zinc, [which] indicates that [a] higher Fe content will make this alloy have a higher corrosion rate." Meanwhile, "the dynamic corrosion of this alloy is characterized as a frequent break of the corroded surface layer and preferential corrosion in grain boundaries, as well as alloying and dissolution corrosion."

Most recently, Deloro-Stellite, Inc., a leading supplier of materials for galvanizing hardware applications, has taken a significantly more technical approach to alloy development for liquid zinc applications. In 2005 Yao, et al. [Ref. 15] published the experimental results from the development of a new cobalt-based alloy, Tribaloy T-401. The goal of the project was to maintain the superior molten zinc corrosion resistance of T-800, but improve the ductility and impact resistance to approach that of conventional Stellite-6. By adjusting the Cr, Mo, Si and C contents (Table 2-8) the microstructure and strengthening phases were modified such that "the alloy transfers to hypoeutectic (T-401) from a hypereutectic (T-800 & T-400), that is, the primary phase changes to Co-rich solid solution from the Laves intermetallic compounds (Co_3Mo_2Si and/or CoMoSi)".

Table 2-8: Compositions of some Cobalt-based Alloys (wt%) supplied by Deloro-Stellite, Inc. [Ref. 15]

element	T-400	T-401	Stellite 6	T-800
Co	60.30	60.50	58.1	49.5
Cr	8.50	16.00	29.0	18.0
Mo	28.50	16.00	0.8	28.0
Si	2.60	1.20	1.4	3.4
C	0.1	0.3	1.2	0.1
Ni	-	-	2.0	1.0
Fe	-	-	2.0	-
W	-	-	4.5	-
Mn	-	-	1.0	-

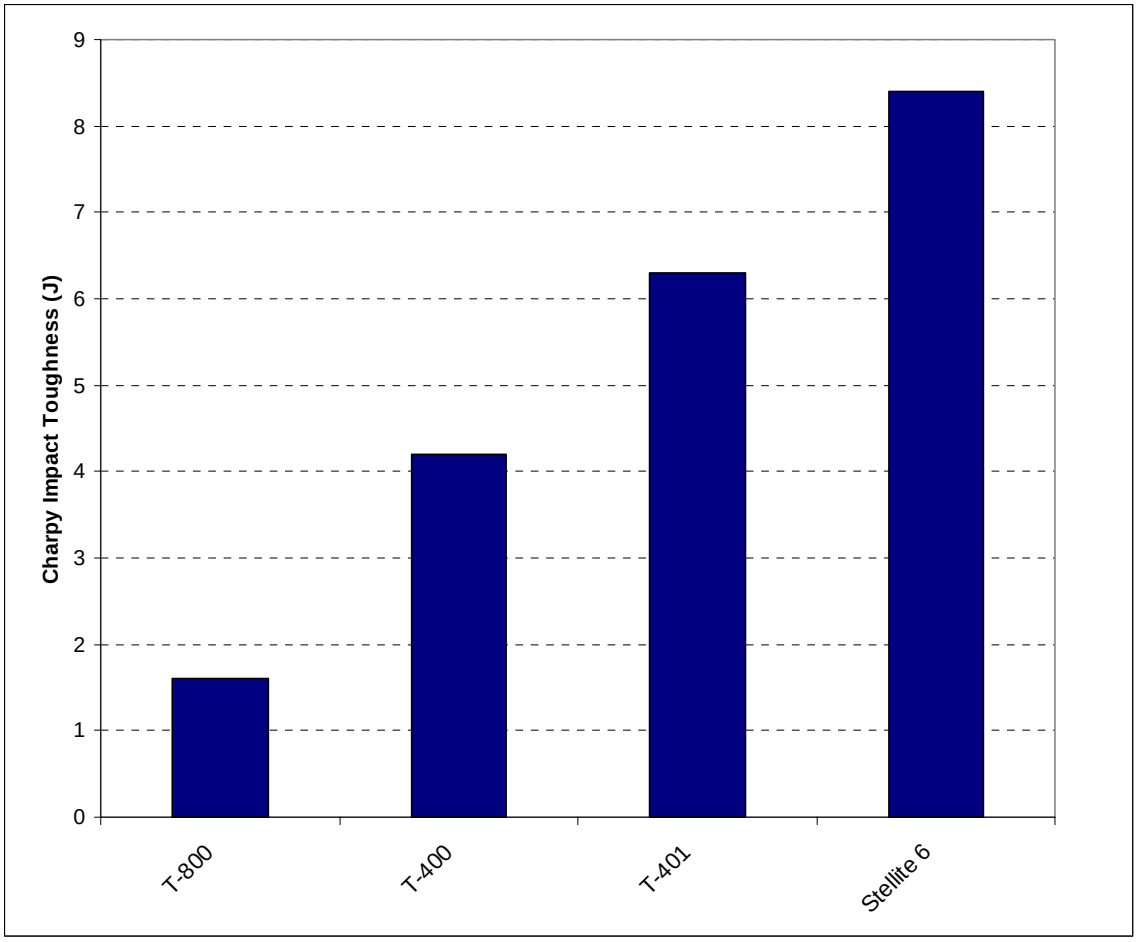

Figure 2-16: Bulk Ductility by Unnotched Charpy Impact Testing at Room Temperature [reproduced from Ref. 15]

With the alloying modifications, Tribaloy T-401 was in fact able to achieve a significant increase in impact toughness (Figure 2-16) over T-800, nearly reaching the toughness of Stellite-6. However, these results are for room temperature measurements, and may not necessarily be proportionally representative to the ductility at 460°C operating in molten zinc. It has been previously shown by Deloro-Stellite [Ref. 16] that the mechanical properties of various cobalt-based alloys behave differently with temperature. As an example, the bulk hardness (Vickers VHN) does not degrade consistently at increasing temperatures for the five different cobalt alloys displayed in

Figure 2-17. Thus, it may not be accurate to state that the ranking of room temperature toughness will be relatively proportional at elevated temperatures.

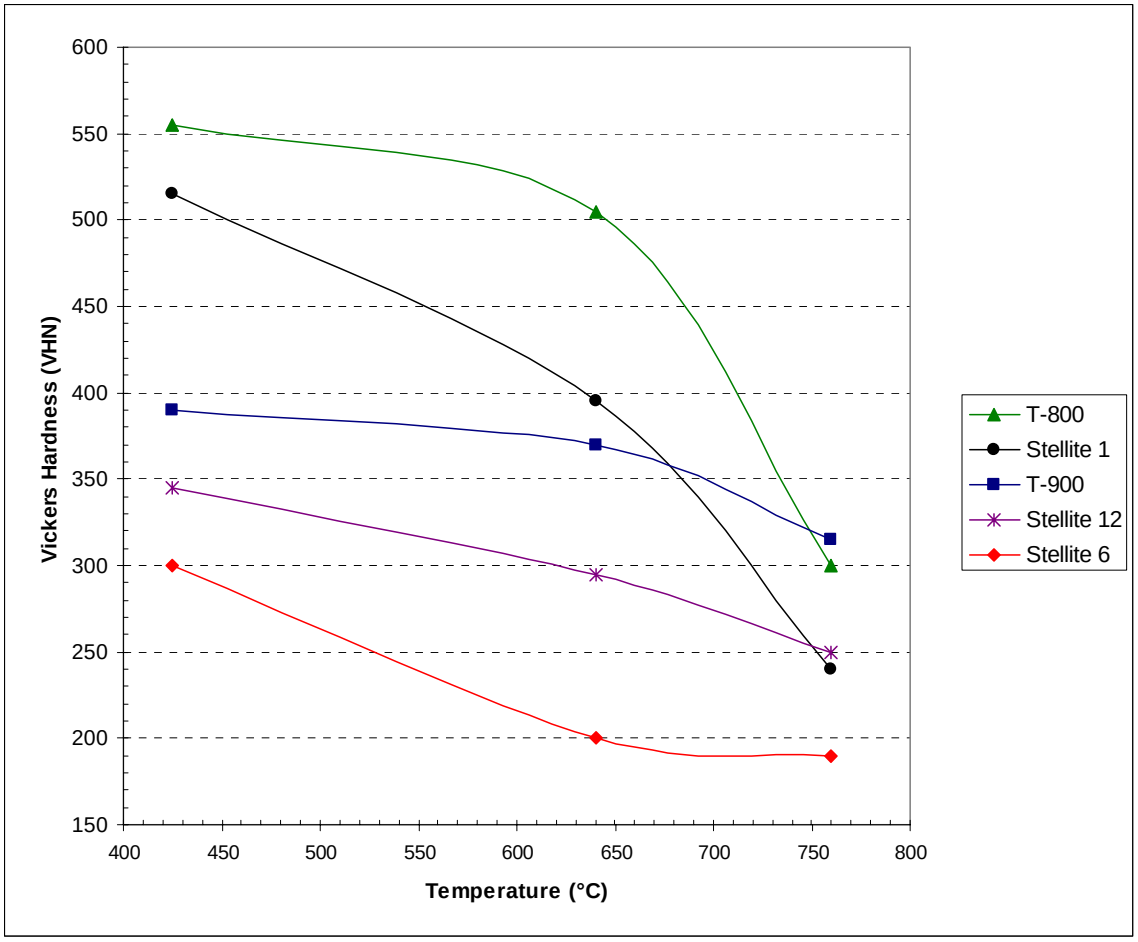

Figure 2-17: Effect of Temperature on Hardness of Several Cobalt-based Alloys [reproduced from Ref. 16]

Looking at the degradation characteristics in zinc, specimens of each of the four alloys studied by Yao, et al. were immersed in a bath of molten zinc with 0.22wt% aluminum (and saturated iron) at 470°C with samples being retrieved at various time intervals (1, 4, 24 and 168 hours). After the test, samples were sectioned and the intermetallic reaction layer of each was measured. The change in reaction layer thickness over time for each of the samples is displayed in Figure 2-18. After one week immersion,

the T-401 sample possessed over a 40% thinner reaction layer than Stellite 6 and almost 30% less than T-800. Yao, et al. indicated that the Mo-rich phases in the Tribaloy alloys resisted attack by the molten Zn-Al bath much better than the cobalt eutectic regions in the Stellite 6.

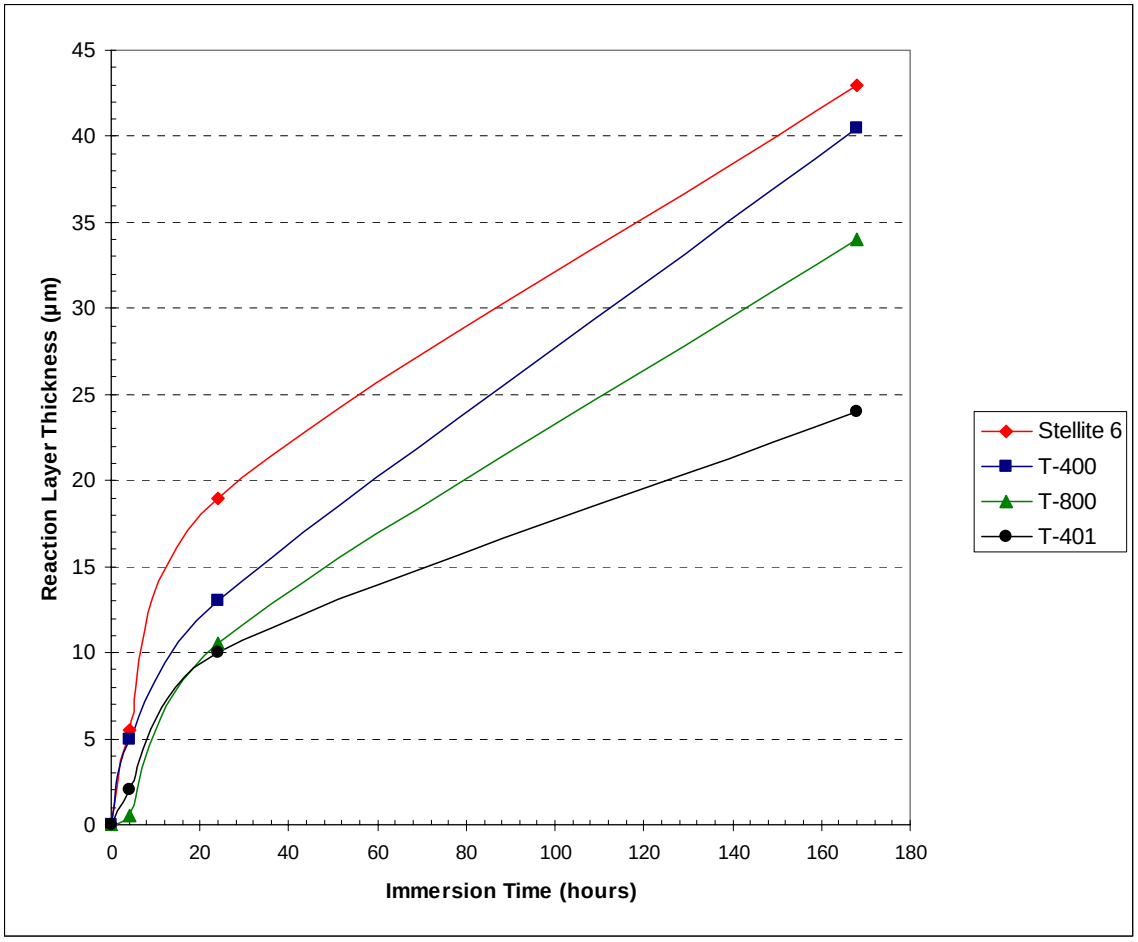

Figure 2-18: Reaction Layer Formation after Immersion in Liquid Zn-0.22%Al at 470°C for 1 Week [reproduced from Ref. 15]

Yao, et al. noted that "a rate equation, $D^2=Kt$, describes the experimental results very well, where D is the thickness of the reaction layer, t the dipping time, and K is the rate constant." "The growth kinetics of the reaction layers in the alloys has revealed that the

reactions are diffusion controlled." However, identifying the diffusion-controlled kinetics may not fully define the corrosion resistance of an alloy in a liquid Zn-Al bath. Previous research has not yet thoroughly defined that the rate of change of the reaction layer thickness is directly proportional to the solubility of a metal alloy in a molten galvanizing bath. Diffusion is important, but it is not the whole picture.

Chapter 3: Investigating Corrosion Mechanisms

As indicated by Yao, et al., performing dissolution testing in molten zinc and then measuring the weight loss over a given duration does not provide a complete indication as to the mechanisms that produce the degradation of materials in a galvanizing environment. Therefore, more in-depth analyses must be employed if a better understanding of the metallurgical failure progression of galvanizing pot hardware materials is to be accomplished. As with Yao, et al., several investigations have been carried out which employed controlled molten zinc environments.

In 1971, Ghuman and Goldstein of Lehigh University [Ref. 17] published the results of a series of laboratory experiments that examined the effects of aluminum content, immersion time and bath temperature on the galvanizability of pure iron sheets. The goal of the study was to "attempt to determine which, if any, of the inhibition mechanisms proposed, control the galvanizing process when aluminum additions are made to galvanizing baths". These trials were some of the earliest published data that reviewed the iron-zinc reaction response from increasing the aluminum content in the zinc bath. For each test, Ghuman and Goldstein prepared a bath of molten zinc with a predetermined aluminum concentration (and saturated with iron) at a specified temperature and immersed small samples (50mm x 25mm x 0.4mm thick) of "Decarburized Armco Iron Sheet" (<0.002% carbon). After a given (short) time duration, the samples were removed and the cross-sections analyzed using X-ray diffraction and photo-micrographs.

As outlined in Table 3-1, the coating reactions were reviewed from samples at various bath aluminum levels for time intervals up to one hour. As would be expected,

the 0% aluminum bath created a coating containing the three conventional Fe/Zn phases [$\Gamma(=Fe_3Zn_{10})$, $\delta(=FeZn_7)$ and $\xi(=FeZn_{13})$] which thickened over time. It was not until about 0.25% aluminum was reached that an aluminum-rich coating was observed. (Note: No data was presented between 0.09% Al and 0.25% Al in order to help define the exact transition point.) At 0.25% aluminum, the structure of the coating changed over time, starting with a "primary inhibiting phase" (23wt% Fe, 13wt% Al, 64wt% Zn) and converting to a higher-aluminum "secondary phase" (approx. 34wt% Fe, 27wt% Al, 39wt% Zn). Subsequently at 1% aluminum, intermetallic reactions with the iron surface were delayed briefly immediately after immersion with this inhibition period lengthening with increases in aluminum content. In conjunction, the aluminum content of the intermetallics within the coating increased with elevated aluminum levels.

Table 3-1: Coating Reactions of Iron Sheets (0.002%C) Immersed in Liquid Zinc Baths with Varying Levels of Aluminum [reproduced from Ref. 17]

Immersion Time (sec)	**0% Aluminum**	**0.09% Aluminum**	**0.25% Aluminum**
3		Similar to 0%AL; Fully developed (~8μm)	"Primary inhibiting phase" formed (~2μm)
5	Fully Developed Layers of conventional Fe/Zn Phases [Γ, δ & ξ] (~14μm thk.)		same structure as 3 sec.
10			same structure as 3 sec.
30			primary phase with small (~4μm) outbursts of "secondary inhibiting phase"
60			more outbursts of "secondary phase" (up to ~8μm)
120			Full layer of "secondary phase" across entire surface (~10μm) with Fe_2Al_5 structure at outer portions
320			Full "secondary phase" layer (~13μm) with detached particles in Fe_2Al_5 in the outer surface phase of $FeZn_7$
1800			
3600	Same layers as 5sec., but thicker (~200μm thk.)		

Immersion Time (sec)	**1% Aluminum**	**3% Aluminum**	**5-10% Aluminum**
3		similar to 1% Aluminum tests	No reaction at short immersion times
5	Mostly zinc coating with thin layer (<1μm) "primary phase" on iron surface		
10	Similar to 3 sec., but with outbursts of "secondary phase" (up to 7μm)		
30			
60			
120			
320	Similar to 0.25%AL at 320sec., but with nodules of Fe_2Al_5 on iron surface		For immersion times exceeding 640sec., full layer of $FeAl_3$ forms and thickens with time.
1800	Fully Developed Layers of conventional Fe/Zn Phases, but with Fe_2Al_5 particles embedded		
3600			

Along the same lines, increasing the bath temperature at equivalent aluminum concentrations [Table 3-2] caused the intermetallic layers to grow more rapidly, but maintained similar structures. Ghuman and Goldstein noted that "one important effect of higher bath temperatures is to increase breakdown inhibition by accelerating the process of transformation of primary inhibiting phase through a secondary inhibiting phase to a more stable structure which is isomorphous with Fe_2Al_5." Additionally, "the effect of higher bath temperature is to favor the growth of Fe/Zn phases."

Table 3-2: Temperature Effect on Coating Reactions of Iron Sheets (0.002%C) Immersed in Liquid Zn-Al Baths [reproduced from Ref. 17]

Immersion Time (sec)	**1% Aluminum at 450°C**	**1% Aluminum at 525°C**	**1% Aluminum at 590°C**
5	Mostly zinc coating with thin layer (<1μm) "primary phase" Fe/Zn on iron surface	Simultaneous growth of Fe/Zn phases [Γ, δ] covering 75% of surface (~9μm thk.)	Similar to 525°C, but with over 95% surface coverage (~7μm thk.)

Immersion Time (sec)	**5-10% Aluminum at 450°C**	**5-10% Aluminum at 525°C & 560°C**	**5-10% Aluminum at 590°C**
640	For immersion times exceeding 640sec., full layer of $FeAl_3$ forms and thickens with time.	$FeAl_3$ layer was considerably thicker and more compact containing more aluminum and less zinc.	$FeAl_3$ layer increased slightly in aluminum and decreased in zinc while growing thicker.

The promotion of Fe_2Al_5 growth at elevated temperatures may be further observed in Figure 3-1 . When the bath temperature was raised to 600°C, Γ(=Fe_3Zn_{10}) and δ(=$FeZn_7$) layers formed quickly and stabilized. Then, the η(=Fe_2Zn_5) layer developed and continued to grow at an increasing rate with higher aluminum. It should be noted, that at temperatures exceeding 600°C, "a 0.4mm thick specimen was completely consumed by reaction in less than 20 minutes," making it impossible to run long duration tests at higher temperatures.

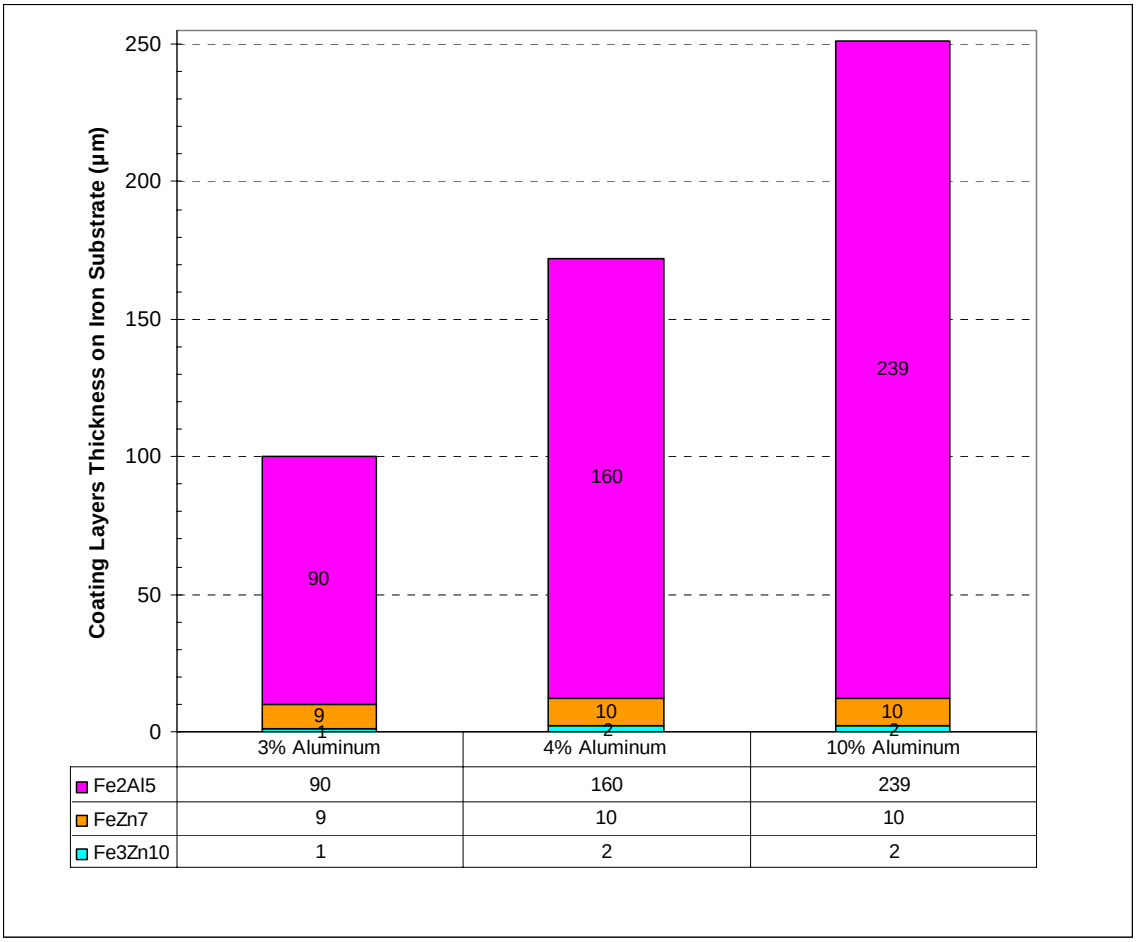

Figure 3-1: Zinc Coating Structure on Iron Sheets (0.002%C) at Increasing Aluminum Content after 10 seconds Immersion at 600°C [reproduced from Ref. 17]

From these experiments several interesting observations can be made which relate to corrosion in molten zinc. First, with additions of aluminum content to the bath (at constant temperature), the solubility of the iron sheet decreased and concurrently minimized formation of intermetallic build-up on the iron surface. Ghuman and Goldstein concluded that "aluminum additions to the zinc bath inhibit the reaction between solid iron and liquid zinc in the normal galvanizing process." The inhibition reaction was found to be applicable to temperatures up to 600°C but at a decreasing rate.

Subsequently, another research project was undertaken to explore the galvanizing response when varying levels of silicon were added to the iron substrate metal. In the

early 1980's, Uchiyama, et al. [Ref. 18] studied the effects of galvanizing in pure zinc, while varying the silicon level (from 0 to 2.84wt% Si) in binary Fe-Si alloys. The compositions of the seven different substrate alloys that were examined in their research are outlined in Table 3-3. From this list it is apparent that Uchiyama, et al. did an excellent job in controlling the consistency of the extraneous elements in the samples.

Table 3-3: Compositions of Iron Substrates (wt%) with Varying Levels of Silicon [Ref. 18]

wt%	C	Si	Mn	P	S	Cu	Ni	Cr	Al	Fe
Fe-0.10SI	-	0.10	0.04	0.003	0.007	0.02	0.02	0.02	0.002	99.79
Fe-0.25Si	-	0.25	0.04	0.005	0.007	0.02	0.02	0.02	-	99.64
Fe-0.73Si	-	0.73	0.04	0.004	0.006	0.02	0.02	0.01	-	99.17
Fe-0.97Si	-	0.97	0.04	0.004	0.006	0.02	0.02	0.01	0.011	98.92
Fe-1.15Si	-	1.15	0.04	0.004	0.006	0.02	0.02	0.01	-	98.75
Fe-1.84Si	-	1.84	0.04	0.003	0.006	0.02	0.02	0.00	0.005	98.07
Fe-2.84Si	0.01	2.84	0.04	0.003	0.004	0.02	0.02	-	0.006	97.06

Small plates (25mm x 20mm x 2mm thk.) of each of the compositions were produced for this testing. Each sample was then placed in a bath of pure molten zinc at a given temperature (from 440°C to 600°C) for 600 seconds (i.e. 10 minutes). Upon removal from the zinc bath, each specimen was sectioned for microstructural analysis. It should be noted that the size of the zinc pot along with the initial concentration of iron in the zinc were not precisely defined. Additionally, it was not clear whether or not each sample was immersed independently or collectively for a given temperature setting. Moreover, with the lack of carbon in the substrate and a zinc bath void of any aluminum or saturated iron, the actual direct industrial application of these experimental results is limited. Irrespective, several conclusions can be made from their research efforts.

The change in resultant coating thickness at various temperatures for increasing silicon levels in Fe-Si binary alloys may be observed in Figure 3-2. From this graph, it is

observed that the maximum coating thickness (1.25mm) occurs at Fe-1.15%Si at 500°C. Similarly, most temperatures developed a maximum coating at approximately Fe-1.15%Si. Meanwhile, at temperatures exceeding 560°C minimal coating expanded on the surface of the substrate, regardless of silicon concentration. However, at lower temperatures (440°C to 520°C) an inflated coating thickness also resulted at around Fe-0.10%Si. One interesting observation is the high magnitude of the coating thickness. Remember, the original thickness of the sample was only 2mm, but the maximum coating thickness observed was 1.25mm…on one side. Thus, the full size of this sample upon removal from the zinc bath was 4.5mm thick!

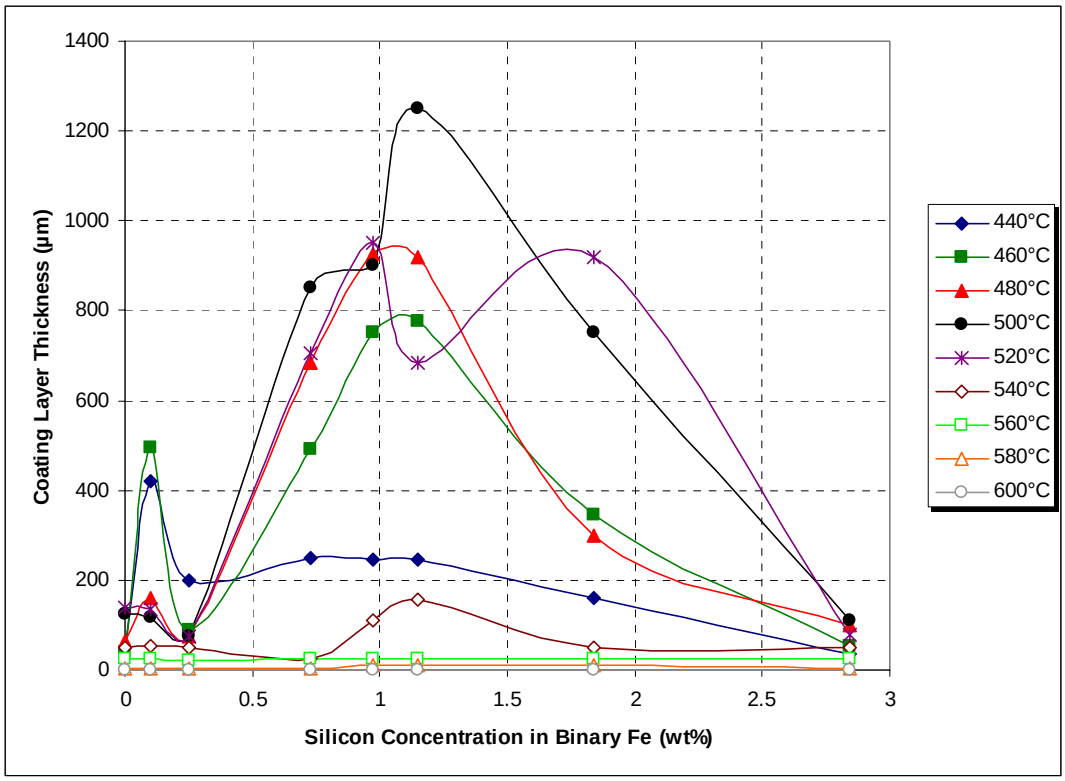

Figure 3-2: Effect on Galvanized Coating Layer of Silicon Concentration in the Iron Substrate [reproduced from Ref. 18]

If the coating structure at Fe-0.10%Si is investigated in more depth (Figure 3-3), three different phases are observed at varying levels for increasing temperatures. At lower temperatures the ξ-phase is prevalent giving way to the δ_1-phase at higher temperatures. At the same time, η-phase particles were observed near the surface of the δ_1-phase at temperatures from 500°C to 540°C. It should be noted that the chemical compositions of each of this phases were not defined by Uchiyama, et al. in this report.

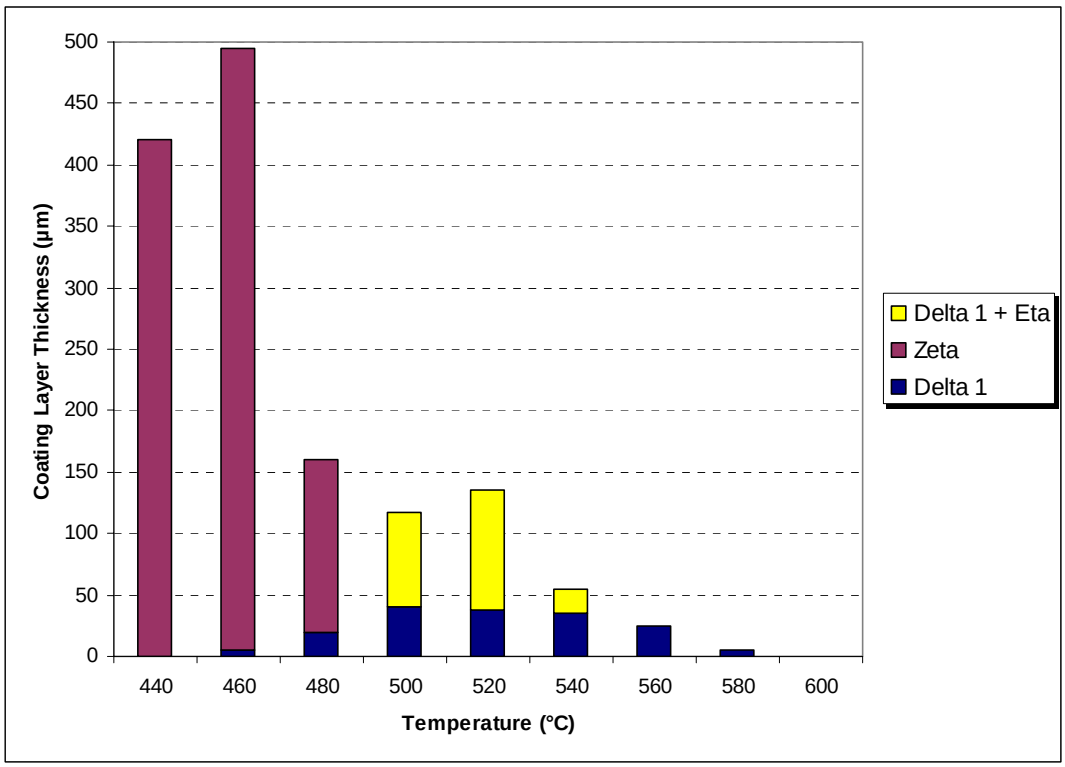

Figure 3-3: Galvanized Coating Structure Due to Increasing Temperature in a Fe-0.10%Si Substrate [reproduced from Ref. 18]

In a similar manner, the effect of temperature and silicon content on zinc solubility of the substrate material can be examined. From Figure 3-4, Fe-1.15%Si has the highest corrosion rate with a peak of 21mg/cm^2 at 520°C. However, the corrosion

rate dropped at subsequent higher temperatures and then all substrates became linear and nearly equivalent at temperatures above 560°C. It is interesting that the alloy with the highest corrosion rate was also the alloy developing the highest coating thickness. (As a reminder, each of these tests was only run for 10 minutes. Thus, the long-term corrosion aspects may vary.)

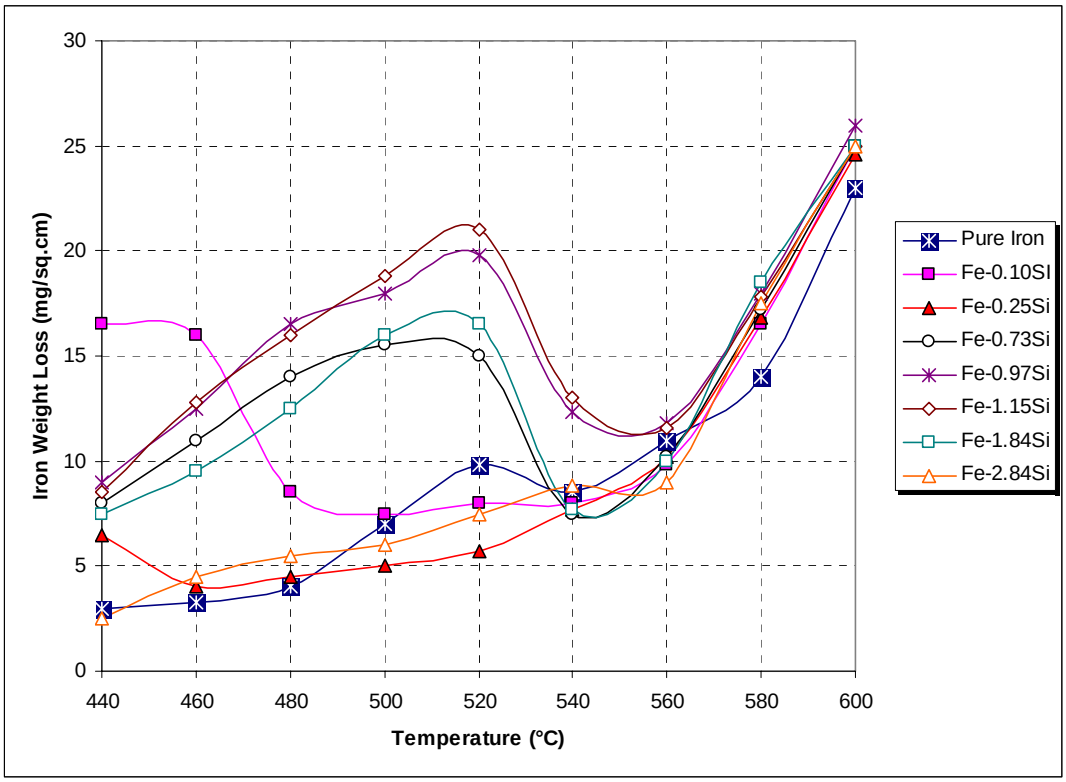

Figure 3-4: Dissolution Characteristics of Fe-Si Substrates in Pure Zinc (for 10 Minutes) at Increasing Temperatures [reproduced from Ref. 18]

Furthermore, in their paper, Uchiyama, et al. identified the "Iron Weight Loss" from the substrate (Figure 3-4), but they also measured the resultant accumulation of "Iron in the Zinc Bath". Hence, if the quantity of "Iron in the Zinc Bath" is subtracted from "Iron Weight Loss" it defines the "Iron Concentration in the Coating" (i.e. if the

iron is no longer part of the substrate, but it does not enter the bath, then it must be in the coating). As displayed in Figure 3-5, the Fe-concentration in the coating drops to almost 0% for all alloy substrates at temperatures exceeding 560°C. However, from the very low overall coating thicknesses at those temperatures (Figure 3-2), it can be concluded that pure dissolution is occurring at temperatures above 560°C. Additionally, the low-Si (0% & 0.25%) and high-Si (2.84%) alloys displayed low-Fe levels in the coating regardless of temperature. But, once again, low coating thicknesses at these points are noted in Figure 3-2, so it can be assumed that pure dissolution occurs for low and high silicon levels. (It is unclear why Fe-0.10%Si had a high-Fe level in the coating at less than 460°C. It does not follow any of the other trends.)

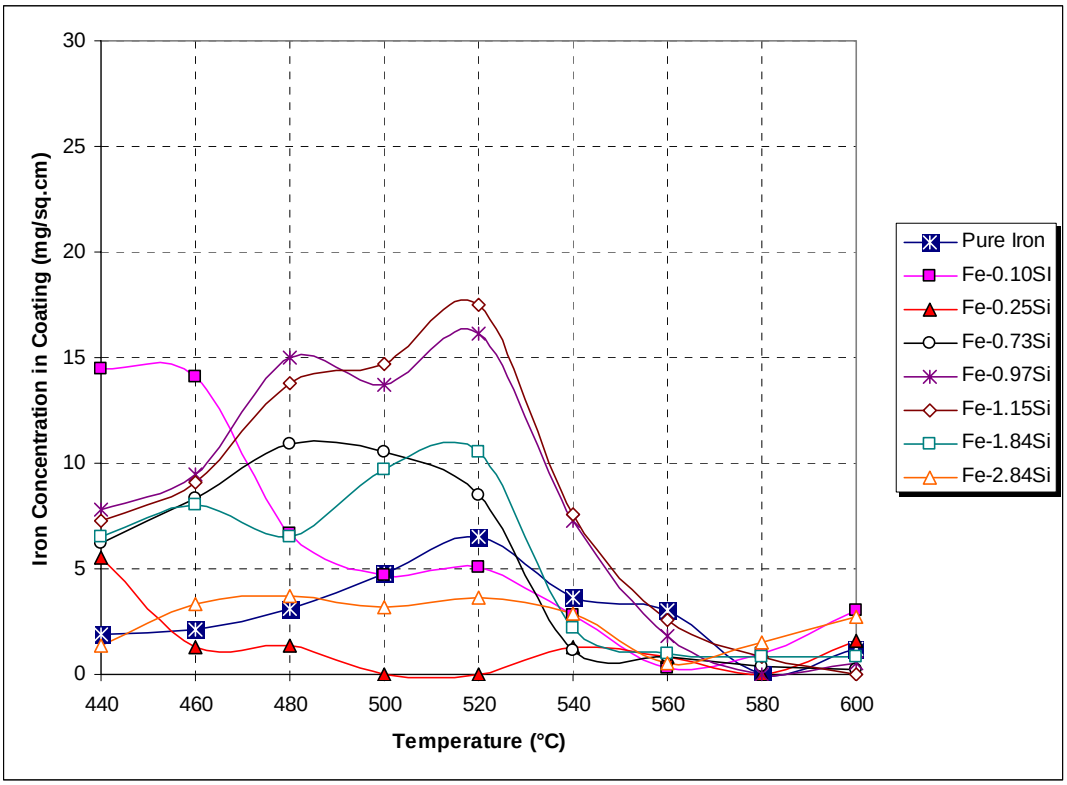

Figure 3-5: Concentration of Iron in the Coating as a Result of Dissolving Fe-Si Substrates not Diffusing into the Zinc Bath [reproduced from Ref. 18]

Overall, it was realized that, by increasing the silicon content in the iron substrate (up to about 2wt%Si), a significant increase in the corrosive zinc solubility of the iron alloy substrate was observed at typical galvanizing temperatures (< 500°C). Also, the galvanized coating thickness was maximized at these silicon levels. Conversely, at very high temperatures (> 560°C) the ensuing coating thicknesses diminished and the consequential dissolution of the substrate became exponentially advanced. From the research by Uchiyama, et al., a better understanding of the coating formation and solubility of high-silicon ferrous alloys was obtained. With the increasing use of silicon steels as a galvanized substrate, their research was one of the initial efforts to understand Zn-Si-Fe reactions.

Later, in 1988 Selverian, et al. [Ref. 19] published the results of a study observing the static corrosion reactions of iron sheet (0.002%C) in high-aluminum zinc baths. Three different zinc baths (45%Al-55%Zn, 55%Al-45%Zn and 75%Al-25%Zn) were tested at varying temperatures between 570°C and 655°C. The size of the iron sheets tested was 50mm x 50mm x 0.65mm thick and the bath contained 1000cm^3 of molten zinc alloy.

Selverian, et al. noted that "the reaction between the iron panel and the Al-Zn bath was very severe and in all cases the iron panel was totally consumed by the bath in less than two minutes" and, as indicated in Figure 3-6, the samples immersed in 75Al-25Zn bath were completely dissolved in less that 60 seconds. Selverian, et al. went on to describe an exothermic reaction between the iron sheet and the bath that raised the surface temperature of the samples. They also described possible diffusion mechanisms in the iron-aluminum dissolution.

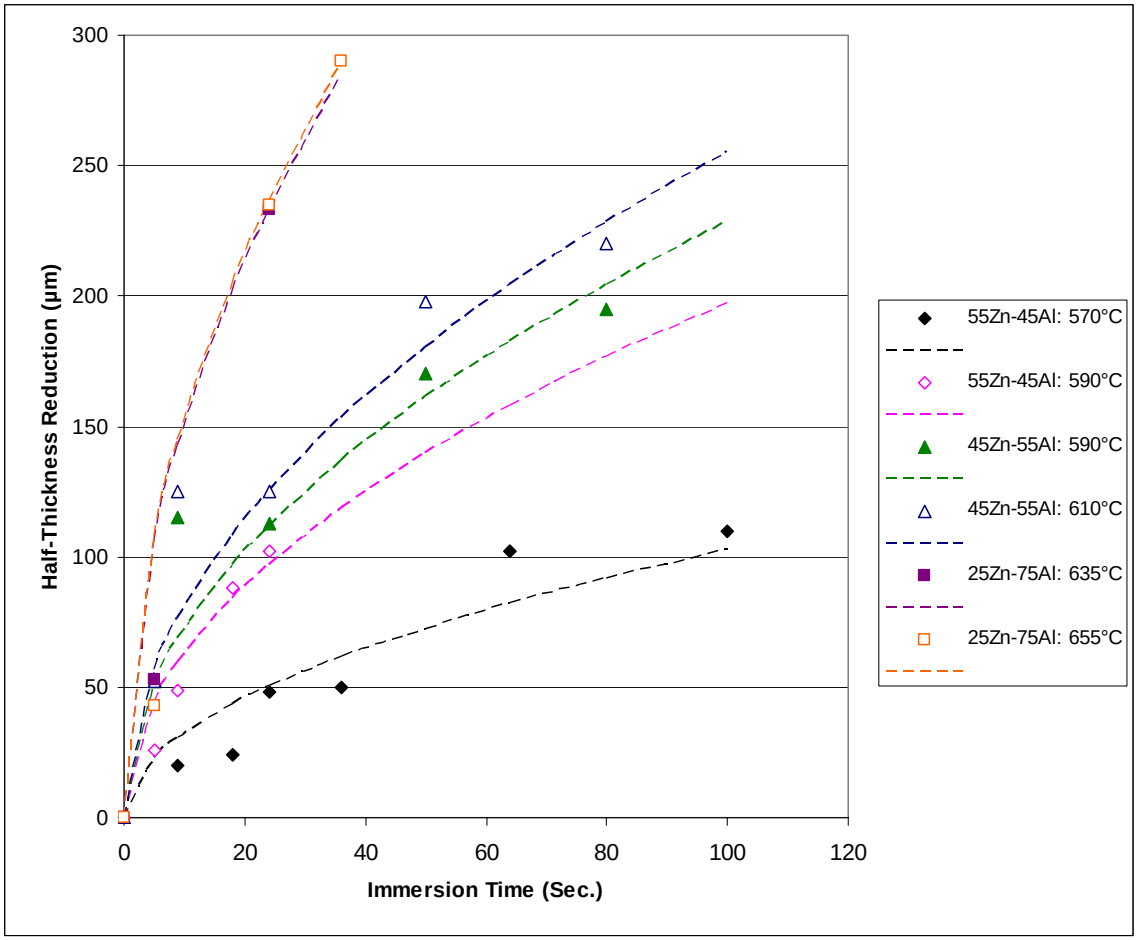

Figure 3-6: Static Corrosion (Wall Thickness Loss) of Iron Sheet (0.002%C) in High-Aluminum Galvanizing Baths [reproduced from Ref. 19]

The experimental results obtained by Selverian, et al. are displayed in Figure 3-6. ("Half-Thickness Reduction" refers to the dissolution from one side of the iron sample simulating a single-plane reaction between the substrate and the bath.) In its unalloyed state, the iron sheets dissolved very quickly in the high-aluminum baths. As expected, the corrosion rates accelerated with either increasing temperature or aluminum content. The corrosion rate inflation from 45Al-55Zn to 55Al-45Zn at 590°C was analogous to the corrosion change of 55Al-45Zn from 590°C to 610°C, thus, indicating that increasing the aluminum content has a similar effect to increasing temperature. However, the reactivity of 45Al-55Zn increased much more significantly over a 20°C span from 570°C to 590°C,

implying that the impact of temperature is exponential and could possess a critical point above which the bath corrosion accelerates rapidly.

Now, in the three previously noted research efforts by Ghuman, Uchiyama and Selverian, the common thread was the iron substrates (or modified-Fe) used, where the general terms of each project was geared towards developing a better understanding of zinc-iron reactions from the perspective of coated steel sheet. However, with regards to identifying the effects of zinc exposure on galvanizing hardware, the aforementioned articles are quite relevant in that the ideal pot hardware material is one that is NOT easily galvanized. Hence, if research can determine how to make a substrate *easier* to galvanize then it provides insight on how to develop *non-galvanizable* materials for submerged production hardware.

As a starting point, it is important to understand the response of aluminum in the galvanizing bath. Ghuman and Selverian both noted the severe change in reactivity as a result of varying levels of aluminum in the zinc. Thus, a comprehension of the dissolution characteristics of materials in pure aluminum should be reviewed.

In the late 1980's Tunca, et al. [Refs. 20 & 21] performed an extensive array of experiments and analytical calculations aimed at identifying the diffusion parameters of pure molybdenum, niobium and chromium substrates immersed in pure molten aluminum. They arranged a test apparatus by which 12.7mm diameter discs of each material were rotated at 200rpm in a 150g bath of (99.999%) liquid aluminum at specified temperatures under a vacuum (to avoid oxidation of the aluminum). At each temperature (from 725°C to 915°C) a 1.0g sample of the bath was taken to observe saturation of the solute material. Similarly, at specified time intervals (from 1 to 180

minutes) the discs samples were removed to observe the aluminum diffusion layer penetrating into the substrate.

First, the saturation concentration was determined for the three metals at each of the respective temperatures (Figure 3-7). Not surprisingly, these values follow equivalently to the liquidus line of the aluminum-rich corner of the Al-(Cr, Mo, Nb) phase diagrams (Figures 3-8, 3-9, 3-10, respectively). All three metal samples exhibited increasing saturation levels at rising temperatures with chromium having advanced solubility, niobium having low solubility in liquid aluminum and molybdenum possessing a solubility level about halfway between the other two metals.

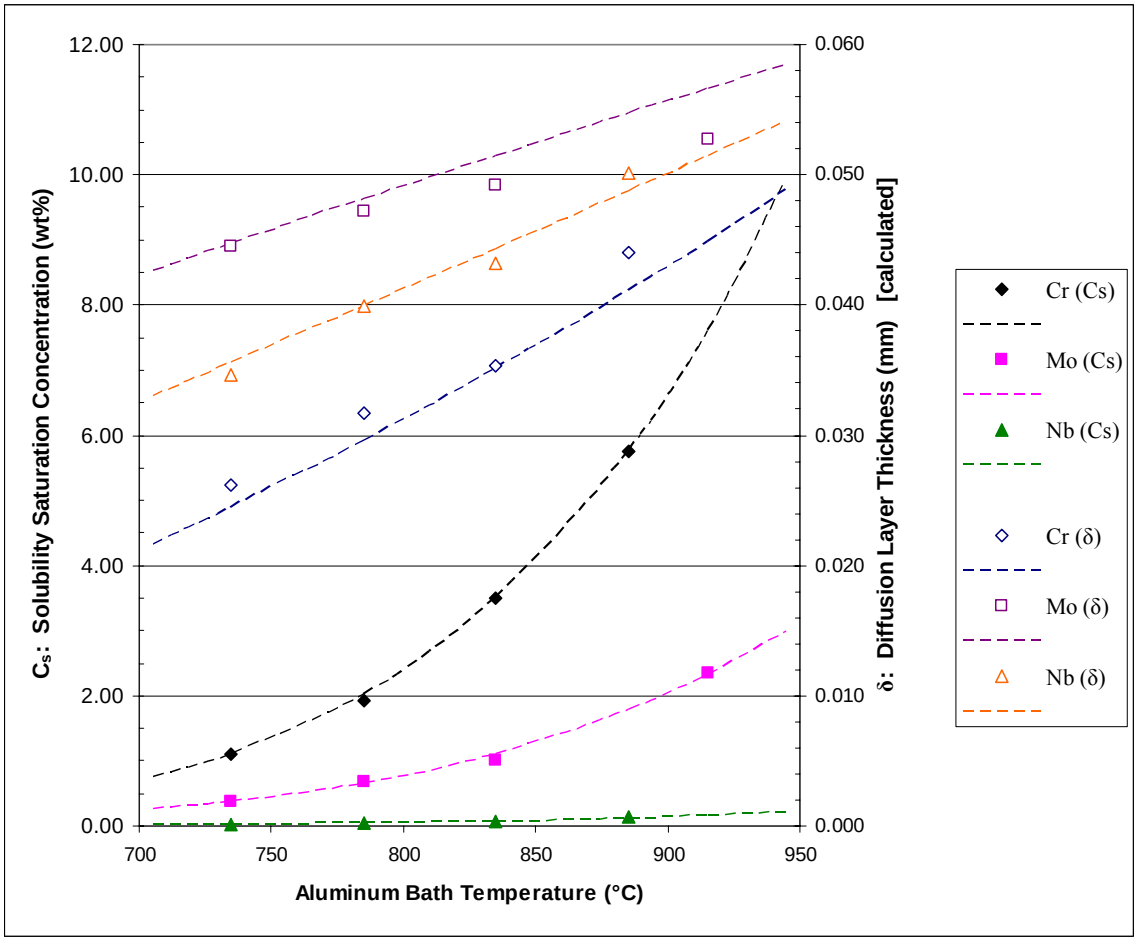

Figure 3-7: Dissolution and Diffusion Characteristics of Pure Solid Metals in Molten Aluminum [reproduced from Refs. 20 & 21]

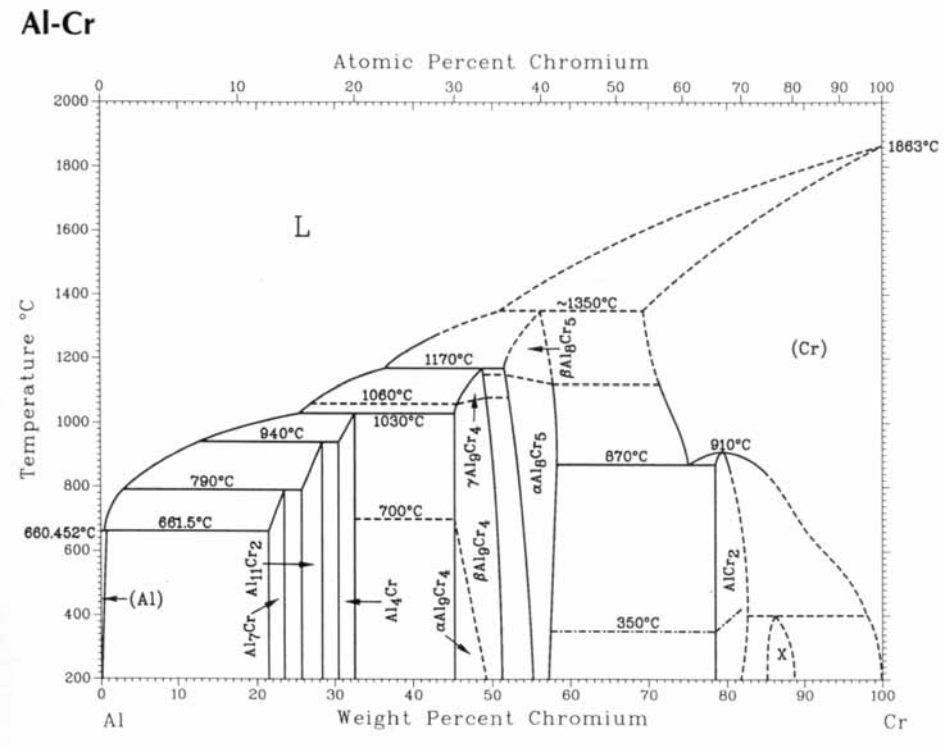

Figure 3-8: Aluminum-Chromium Binary Phase Diagram
[Ref. 7, reprinted with permission from ASM International,
All rights reserved, www.asminternational.org]

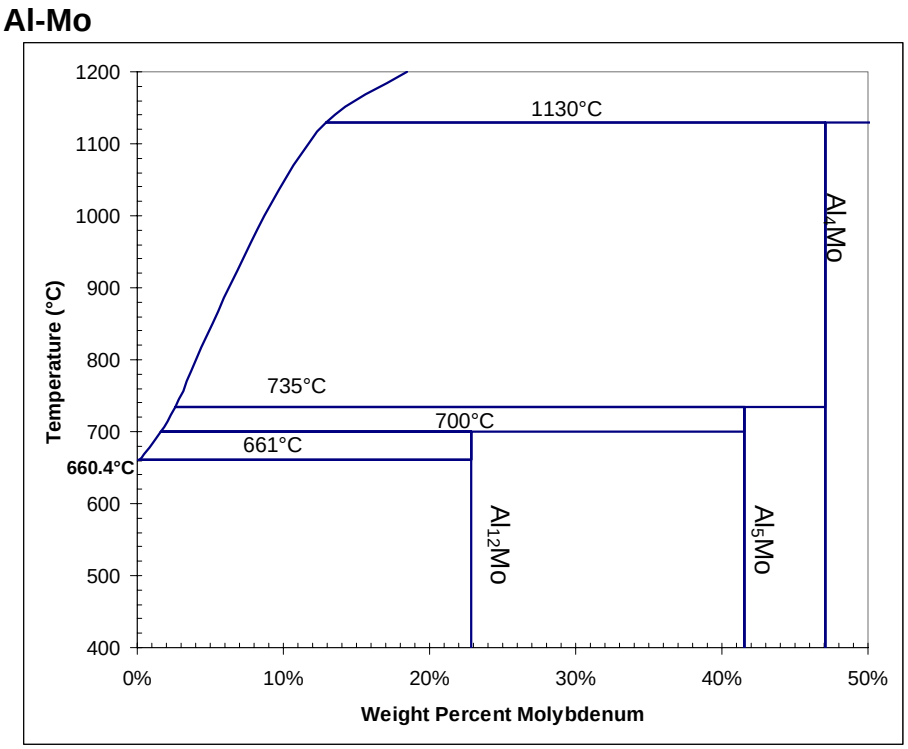

Figure 3-9: Aluminum-Molybdenum Binary Phase Diagram (Al-rich corner)
[reproduced from Ref. 26]

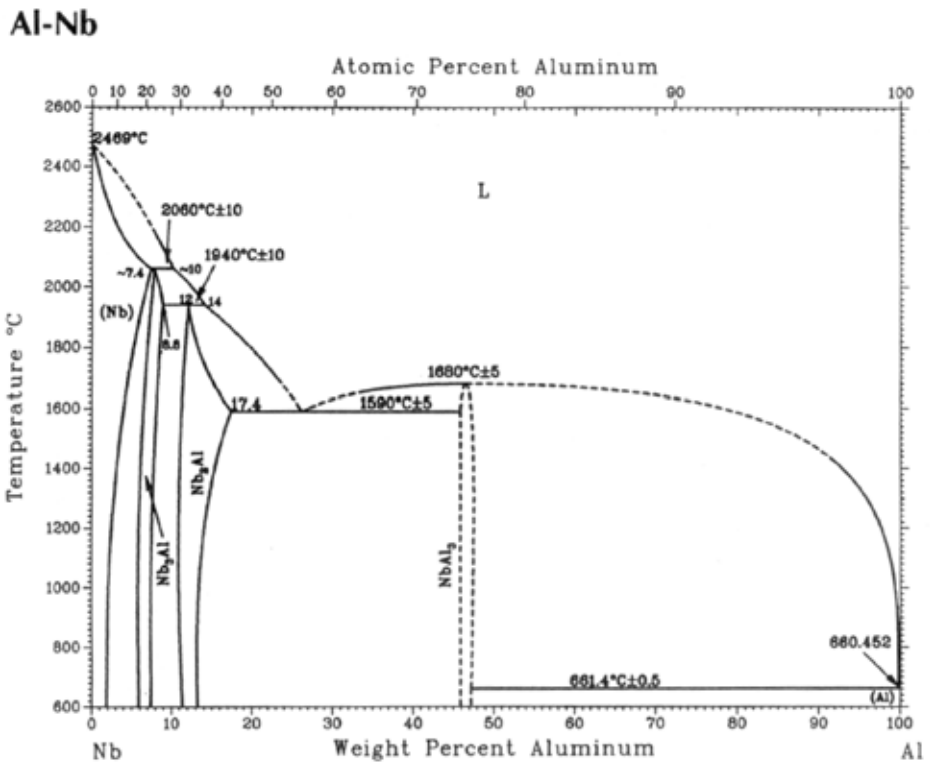

Figure 3-10: Aluminum-Niobium Binary Phase Diagram
[Ref. 7, reprinted with permission from ASM International,
All rights reserved, www.asminternational.org]

Tunca, et al. noted that "the dissolution of a solid metal in a molten metal is described by the Nernst-Shchukarev equation and may be written:

$$dC/dt = K \cdot A/V \cdot (C_s - C)$$

where C is the instantaneous concentration of the dissolved metal in the melt (wt%), C_s is the saturation concentration (wt%), K is the dissolution rate constant (m/s), A is the surface area of the disc sample (m^2), and V is the volume of the melt (m^3)". By integrating with initial conditions: $C = 0$ at $t = 0$, an exponential trend (with respect to time) may be observed for the concentration of the dissolved metal in the melt.

$$\ln[C_s / (C_s - C)] = K (A \cdot t/V)$$

Furthermore, Tunca, et al. similarly presented theoretical Arrhenius equations to calculate the dissolution rate constants, K (in m/s):

$$K = K° \exp(-E_K/R \cdot T)$$

And the diffusion coefficients, D (in m^2/s), of a metal ion in molten aluminum:

$$D = D° \exp(-E_D/R \cdot T)$$

where E_K and E_D are the activation energies for the dissolution and diffusion rates, respectively and $K°$ and $D°$ are frequency constants.

Additionally, Tunca, et al. stated that the thickness of the boundary diffusion layer may be defined according to the Nernst theory as:

$$\delta = D / K$$

As a result, the calculation of the diffusion thickness is portrayed in Figure 3-7 based on the experimental determination of dissolution rate constants, K, and the diffusion coefficients, D by Tunca, et al. Thus, from Figure 3-7, it is observed that molybdenum had the highest diffusion penetration in molten aluminum followed by niobium then chromium. Conversely, chromium had the greatest rate of diffusion acceleration at increasing temperatures.

Tunca, et al. performed a thorough analysis of the theoretical equations necessary to define both the concentration change of a molten bath over time and the diffusion aspects of a substrate metal exposed to molten aluminum. These theoretical calculations were then supported with in-depth laboratory experimentation. However, the level of detail was to such an elevated magnitude that it diluted the excellent results that were being presented.

In a similar manner at around the same time, Dybkov [Ref. 22] investigated the reactions of 18Cr-10Ni stainless steel (Table 3-4) in molten aluminum baths. He ran extensive testing utilizing cylindrical specimens (11.28mm diameter) with single plane (1 cm^2) exposure to a specified bath composition of liquid aluminum (approx. 11cm^3). Two different baths were used. The first was (99.995%) pure aluminum and the other was 99.3%Al, 0.24%Fe, 0.3%Si, 0.003%Cr, 0.005%Ni and 0.1%Zn. Samples were rotated in the bath for a designated time and removed for microscopy analysis. Bath samples were also taken during the immersion testing.

Table 3-4: Composition of 18Cr-10Ni Stainless Steel Alloy [Ref. 22]

element	wt%
Fe	68.7
Cr	18.0
Ni	10.5
Cr	0.08
Mn	1.2
Ti	0.58
Si	0.64
Cu	0.22
P	0.032
S	0.003

In order to describe the dissolution kinetics of a solid metal into a liquid metal bath, Dybkov noted the following equations (analogous to Tunca, et al.):

$$dc/dt = k \cdot S/v \cdot (c_s - c)$$

"where c is the concentration of the dissolved metal in the bulk of the melt (kg/m^3), t is the time (sec), c_s is the saturation concentration (kg/m^3), k is the dissolution rate constant (m/s), S is the solid specimen surface area (m^2), and v is the melt volume (m^3)".

If the initial concentration of the solute in the melt is c_o, then by integrating with initial conditions: $c = 0$ at $t = 0$ the dissolution equation may be written as:

$$\ln[(C_s - C_o) / (C_s - C)] = k\,(S \cdot t/v)$$

This equation has been known to hold true for the dissolution of pure (or low alloyed) iron, but "the stainless steel investigated in this work contained totally about 30% alloying elements and impurities", so it was important to experimentally verify the applicability of this dissolution kinetics equation for "such a relatively complex material".

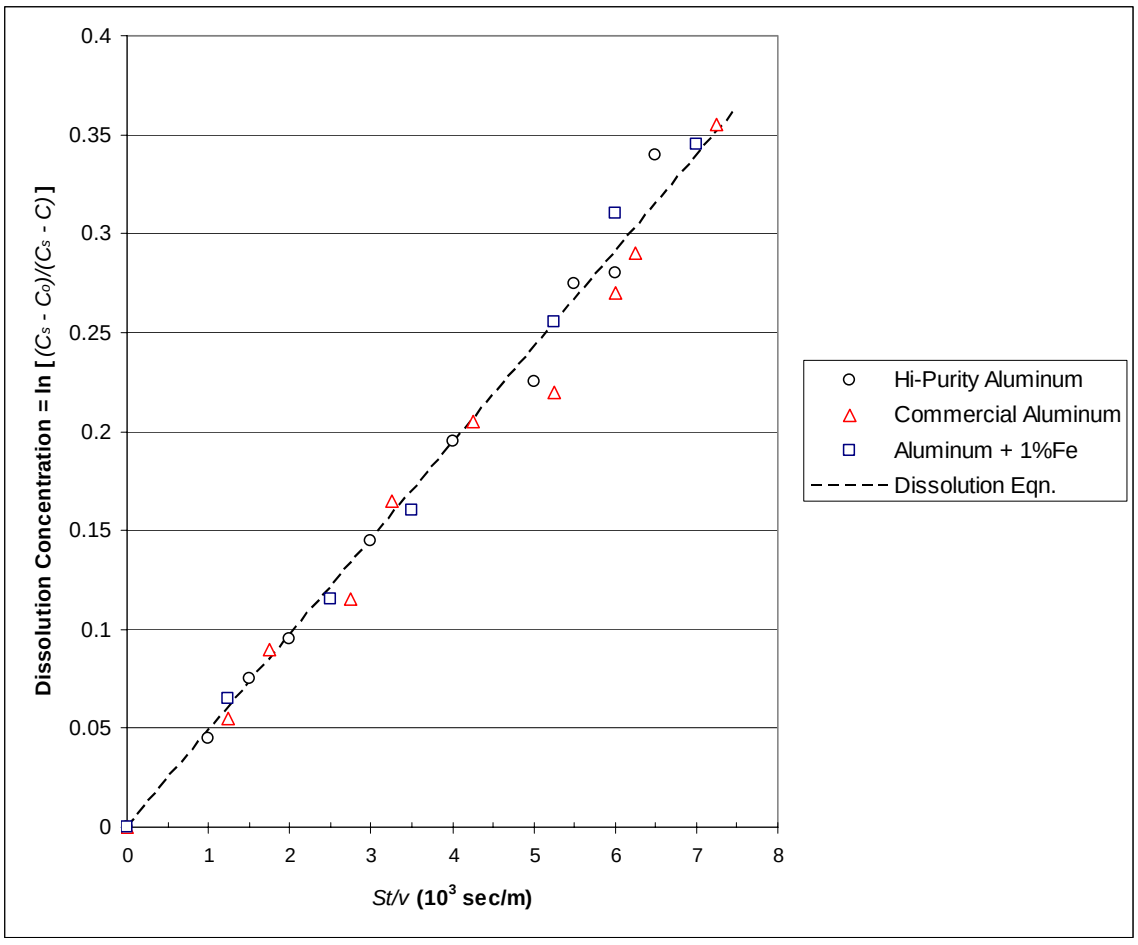

Figure 3-11: Comparison of Molten Aluminum Experimental Data to Theoretical Dissolution Equation [reproduced from Ref. 22]

Hence, the experimental data (Figure 3-11) of three different aluminum baths (high-purity aluminum, commercially-pure aluminum and aluminum containing 1% dissolved

iron) at 700°C with a sample rotational speed of 23rpm explicitly portrays that the dissolution equations noted previously do, in fact, hold true for dissolution of 18Cr-10Ni stainless steel in molten aluminum.

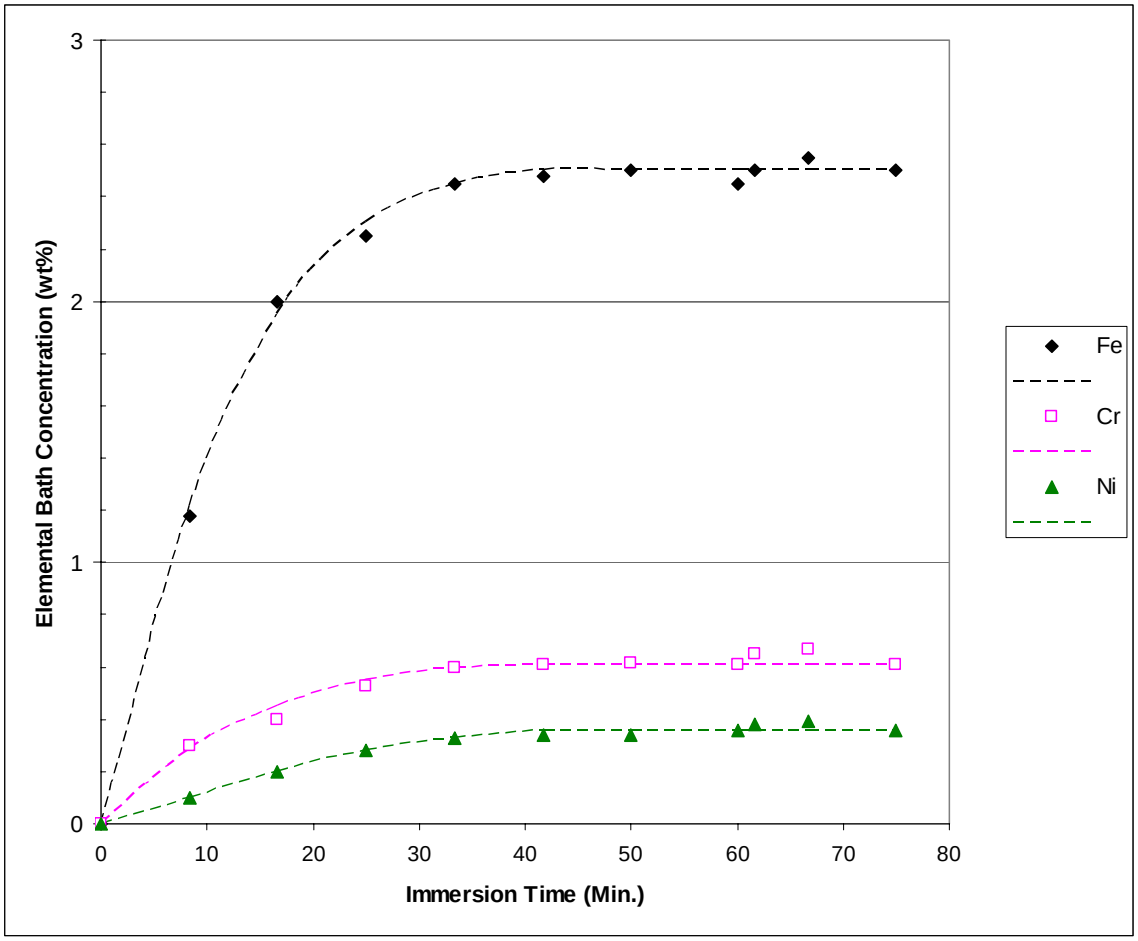

Figure 3-12: Elemental Solubility Limits of 18Cr-10Ni Stainless Steel in Pure Aluminum at 700°C [reproduced from Ref. 22]

Continuing, Dybkov investigated the aluminum solubility limits of the primary constituents in the 18Cr-10Ni stainless steel (specifically, Fe, Cr & Ni) in order to not only have a baseline for dissolution relations of this material in aluminum but also to compare the combined solubility limits to those of (*M*+Al) binary systems. The experimental results of dissolution studies of 18Cr-10Ni stainless steel samples (rotating

at 52rpm) in a high-purity aluminum bath at 700°C (Figure 3-12) identify that the saturation limits of each of the components were reached in under 40 minutes.

However, if the experimental saturation concentrations for the iron, chromium and nickel from the immersion test of 18Cr-10Ni stainless steel are compared with published saturation limits of the analogous binary systems (Al-Fe, Al-Cr, Al-Ni) (Figures 3-13, 3-8, 3-14, respectively) an interesting discrepancy is observed (Figure 3-15). The solubility limit of iron in the aluminum bath was nearly the same for both the binary and experimental features, but the chromium and (especially) the nickel saturation concentrations were much lower in the presence of the iron saturation than just in their respective binary systems alone. Additionally, this experimental divergence became even more substantial at greater elevated temperatures.

Thus, Dybkov identified the degradation process of 18Cr-10Ni stainless steel in molten aluminum to be a non-selective (uniform) dissolution and noted the following: "In its lattice the iron, chromium and nickel atoms are connected together by metallic bonds of nearly equal strength because those elements are neighbors in the Periodic Table. Therefore, it [is] supposed that the iron and chromium atoms, being major constituents of the steel, will not 'permit' the nickel atoms to leave its lattice at a rate which exceeds their own rates of transition into liquid aluminum. From this viewpoint all the elements should pass into the melt in those ratios in which they are present in the steel."

Al-Fe

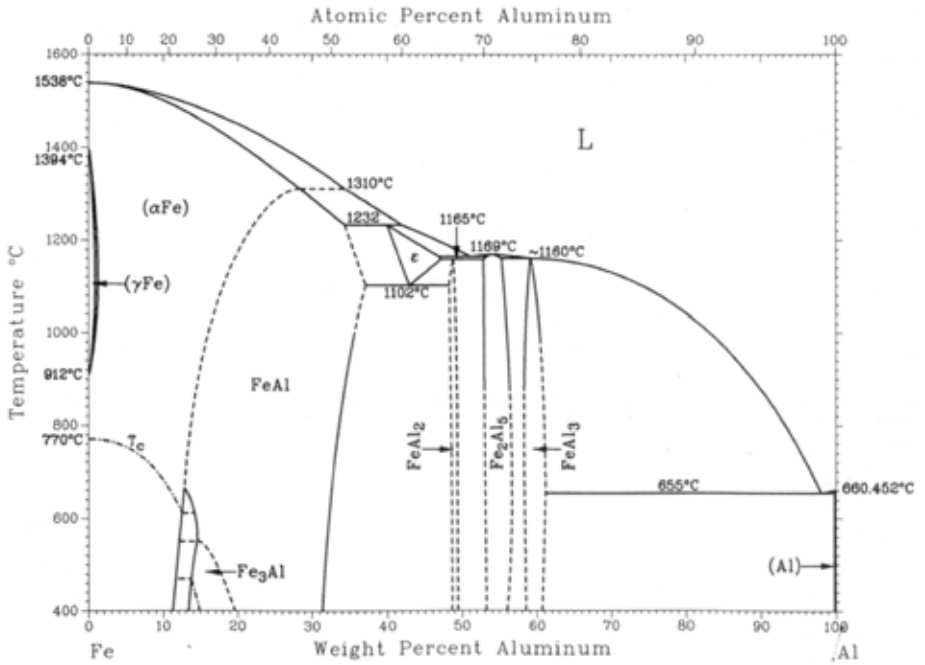

Figure 3-13: Aluminum-Iron Binary Phase Diagram
[Ref. 7, reprinted with permission from ASM International,
All rights reserved, www.asminternational.org]

Al-Ni

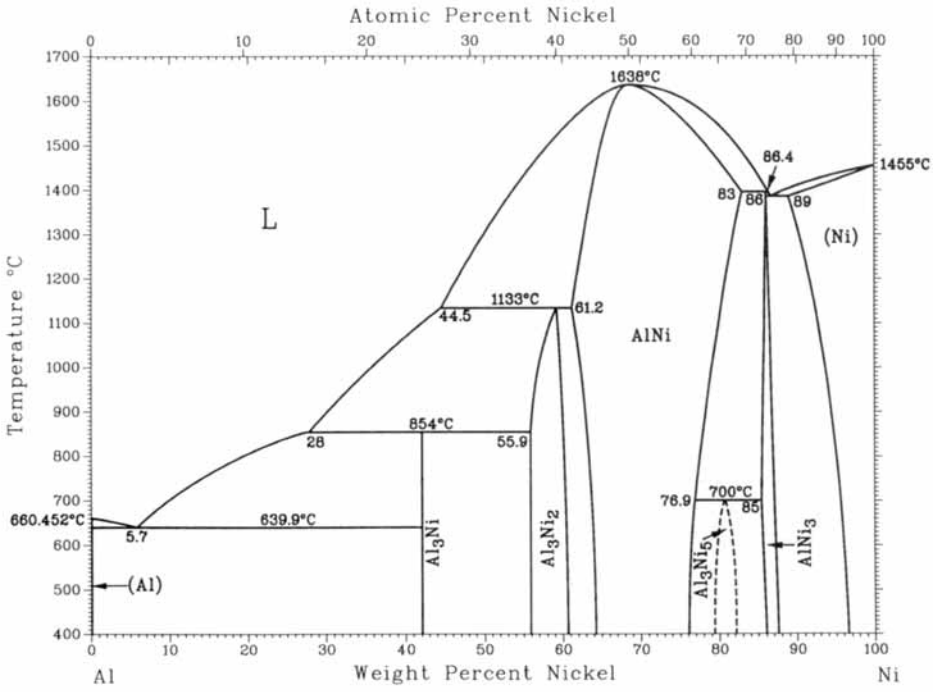

Figure 3-14: Aluminum-Nickel Binary Phase Diagram
[Ref. 7, reprinted with permission from ASM International,
All rights reserved, www.asminternational.org]

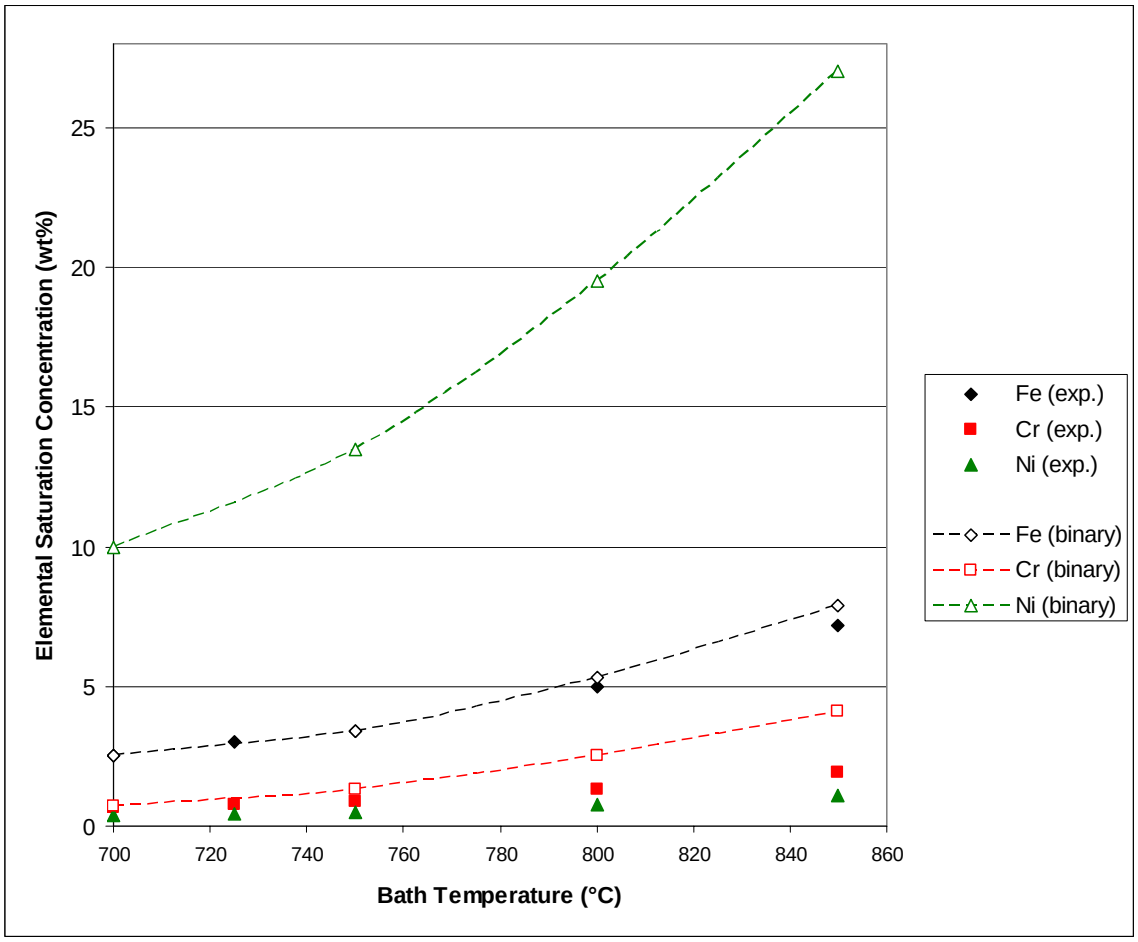

Figure 3-15: Comparison of Elemental Saturation Levels in Binary Aluminum Alloys Versus 18Cr-10Ni-Fe Dissolved in Aluminum (at 700°C) [reproduced from Ref. 22]

In addition to studying the solubility characteristics of 18Cr-10Ni stainless steel in molten aluminum, Dybkov also investigated the analogous adhesive reaction aspects of the aluminum on the surface of the ferrous material. A bath of liquid aluminum with 2.5% iron at 700°C was prepared for this portion of the research. It was claimed that "because the melt had been saturated with respect to the steel constituents, no dissolution of the steel could clearly occur during the run at this [constant] temperature". Each test stainless sample was immersed for up to 3600 seconds in the aforementioned bath. Subsequently, the samples were sectioned to observe the reaction layers on the surface.

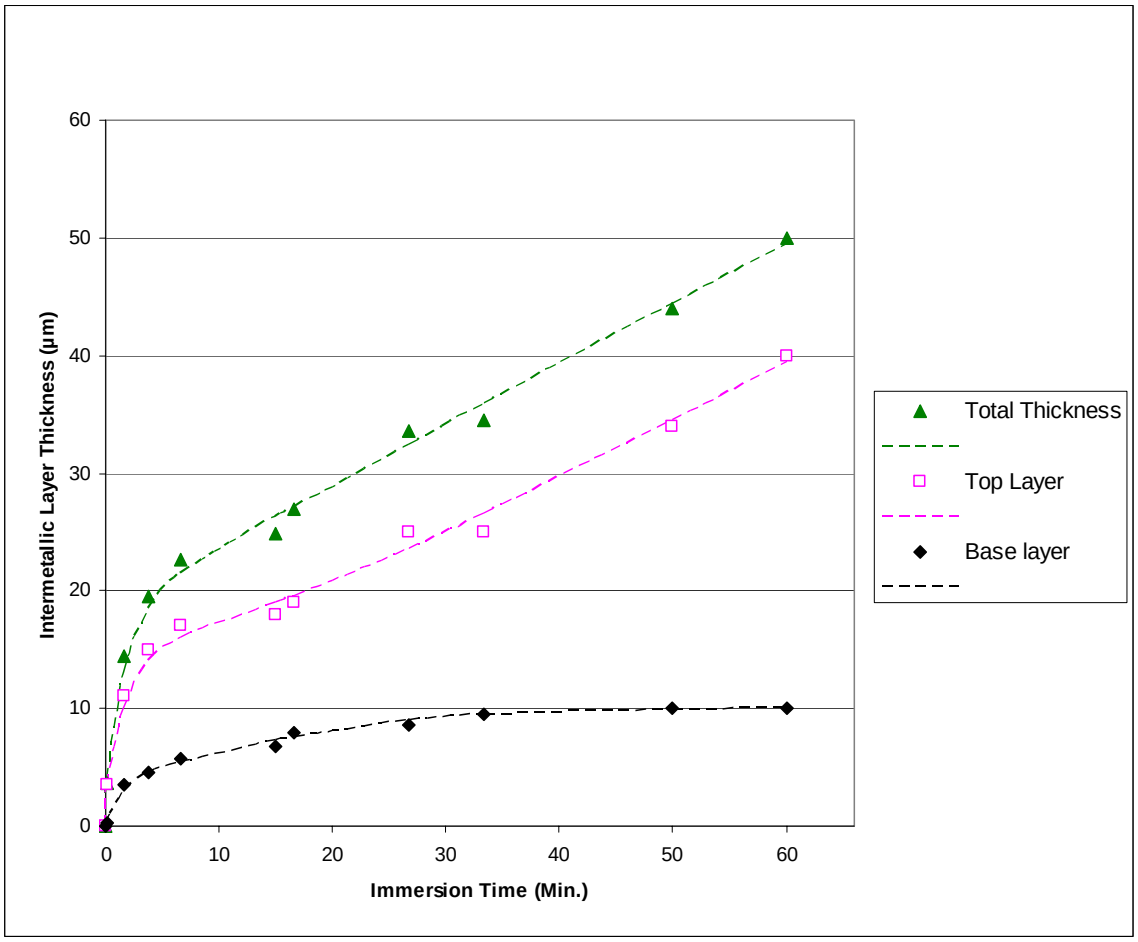

Figure 3-16: Reaction Layer Build-up on 18Cr-10Ni-Fe Immersed in 2.5%Fe Saturated Aluminum Bath (at 700°C) [reproduced from Ref. 22]

Two intermetallic layers were found on the surface of the stainless steel with their thicknesses increasing as a function of time. From this Figure 2-31 it is observed that the intermetallic layer closest to the substrate material ("Base Layer") appears to reach a steady-state thickness (10µm) in less than 45 minutes. Conversely, the layer adjacent to the liquid aluminum ("Top Layer") continued to expand for the duration of this test (40µm after 60 minutes). It is not clear from these results if the "Top Layer" would have eventually reached a constant thickness at extended time durations. Moreover, both

layers began to form almost immediately after immersion indicating the highly reactive nature this ferrous alloy in liquid aluminum.

Dybkov described the layer adjacent to the stainless steel substrate ("Base Layer") as having a compact structure while the outer layer ("Top Layer") was more porous. Through electron probe microanalysis he also defined the chemical characteristics of each of the layers. The "Base Layer" possessed a (Fe, Cr, Ni) $_2Al_5$ identity and the "Top Layer" a (Fe, Cr, Ni)Al_3 configuration, which are analogous to typical common dross particles (Fe_2Al_5 and $FeAl_3$, respectively) found in Al/Fe baths. Dybkov noted that "While a few elements diffuse from the steel bulk across the ["Base Layer"], it is the slowest diffusing element (probably iron) that plays a decisive role in determining the overall layer-growth rate."

From these studies, Dybkov defined a previously unreported interdependence of the constituents of a highly-alloyed structural ferrous material (18Cr-10Ni stainless steel) when subjected to the diffusion-driven, high dissolution rate environment of a molten aluminum bath. Considerable mutual influence on the dissolution rates of iron, chromium and nickel in the base metal was discovered, ascertaining that the diffusion rate of iron into liquid aluminum provided the controlling factor and the other two elements followed at rates proportional to their concentration levels in the solute material.

Subsequently, in 1993 Sundqvist and Hogmark [Ref. 23] published the results of a series of experiments which investigated the dissolution corrosion aspects of tool steels employed in pressure dies for aluminum die casting. They reviewed the reaction mechanisms on samples of H-13 tool steel immersed in A380.0 (high-silicon) aluminum casting alloy at 730°C, as well as the reactions on dynamic samples (50rpm) of H-13 at

increasing temperatures from 690°C to 760°C. (The chemical compositions of H-13 tool steel and A380 aluminum alloy are outlined in Table 3-5).

Table 3-5: Compositions (wt%) of H-13 Test Material and A380 Aluminum Bath [Ref. 23]

element	H-13 Tool Steel
Fe	90.72
Cr	5.30
Mo	1.30
V	0.90
C	0.38
Si	1.00
Mn	0.40

element	A380.0 Aluminum
Al	86
Si	8.5
Cu	3.5
Fe	2

The results of the static immersion tests of H-13 tool steel in A380 aluminum are displayed in Figure 3-17. This graph indicates a very rapid development of iron-aluminide intermetallic layers on the surface with a decline in rate of formation after subsequent time duration.

Similarly, by describing the intermetallic layer formation (Figure 3-18) on the dynamic samples of H-13 tool steel rotating at 50 rpm in the A380 aluminum at increasing temperatures for 500 seconds, it was identified that elevating the temperature had a response analogous to the extended time in the static tests. It may also be noted that, by comparing Figures 3-17 and 3-18 at 730°C for 500 seconds, the intermetallic layer formation was nearly identical for the static and dynamic samples at this one data point.

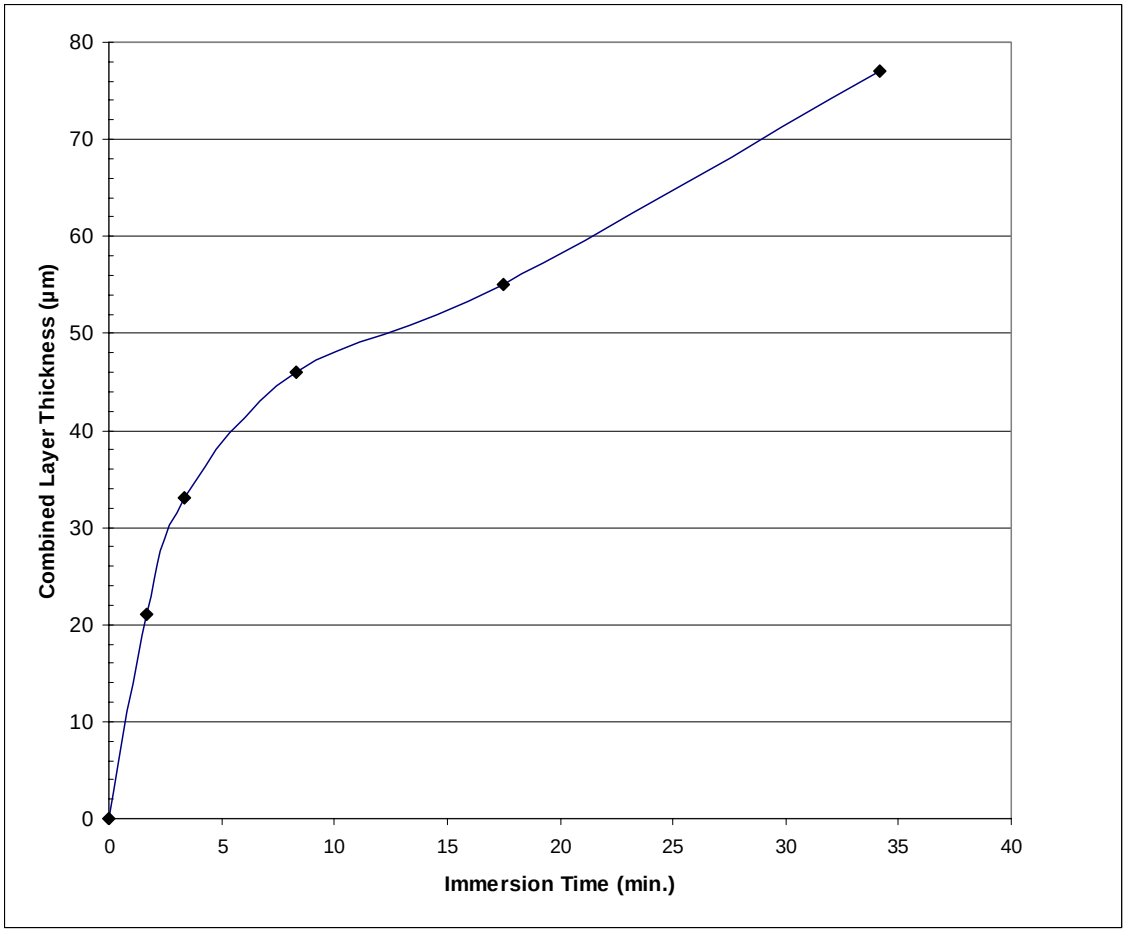

Figure 3-17: Surface Build-up on H-13 Tool Steel after Static Immersion in A380 Molten Aluminum at 730°C [reproduced from Ref. 23]

Due to the relative short time duration of these tests minimal dissolution of the H-13 tool steel substrate was observed. Moreover, it is difficult to predict the intermetallic reactions at extended exposure from these limited results. In general, Sundqvist and Hogmark did a good job in identifying the reactions of H-13 with molten aluminum immediately after immersion, but these results may not be relevant for long-term exposure.

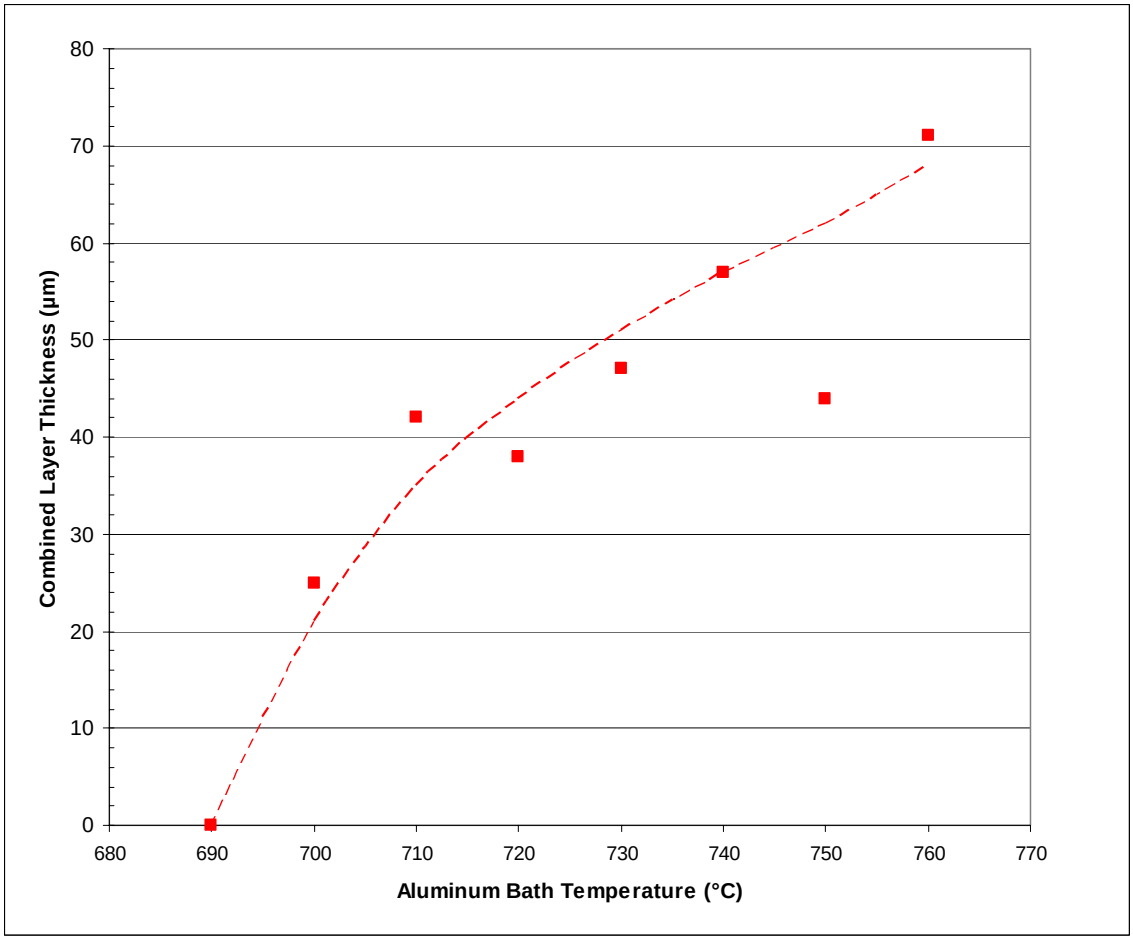

Figure 3-18: Surface Build-up on H-13 Tool Steel after Dynamic Testing (50rpm for 8.3 minutes) in A380 Molten Aluminum at 730°C [reproduced from Ref. 23]

Continuing to look at dynamic reactions in molten aluminum, in 1996, Batchelor, et al. [Ref. 24] performed a series of experiments to compare the erosion-corrosion wear aspects of metallic samples rotating in a bath of molten aluminum with and without suspended alumina particles. For reference to the current research, only the data relating to dynamic corrosion in the clean aluminum bath (no alumina particles) will be reviewed.

Batchelor, et al. utilized 6.3mm diameter pins of 304 stainless steel and low-alloy titanium [Table 3-6], rotating in a bath of A356.0 aluminum alloy at 800°C, and measured the reduction of cross-section at a constant location for given time intervals.

Table 3-6: Compositions (wt%) of Stainless Steel and Titanium Corrosion Samples, and A356 Aluminum Bath [Ref. 24]

AISI 304 Stainless Steel	
Fe	68.85
Cr	18.00
Ni	10.00
C	0.08
Mn	2.00
Si	1.00
S	0.03
P	0.05
	wt%

ASTM Grade 2 Titanium	
Ti	99.31
N	0.03
C	0.10
H	0.02
F	0.30
O	0.25
	wt%

A356.0 Aluminum	
Al	92.05
Si	7.00
Mg	0.35
Cu	0.20
Zn	0.10
Mn	0.10
Fe	0.20
	wt%

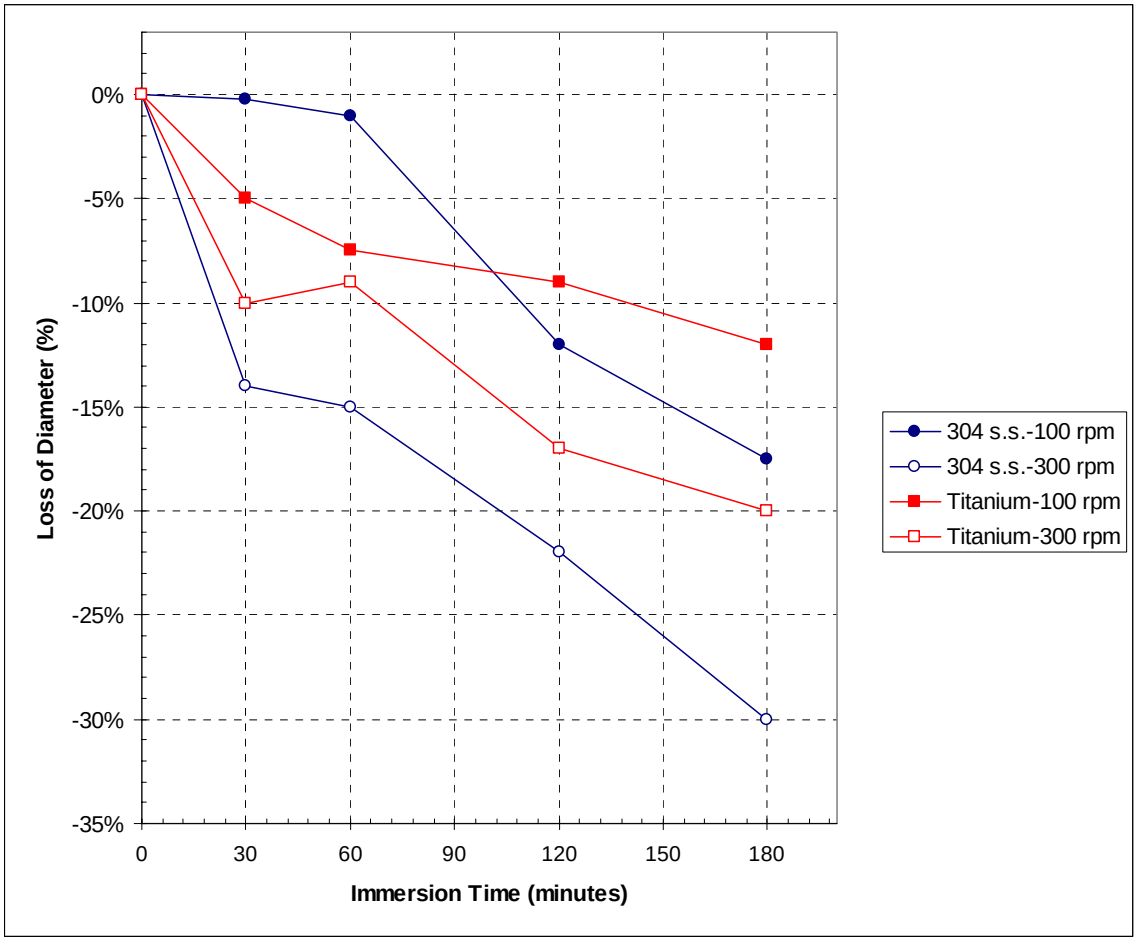

Figure 3-19: Dynamic Corrosion in A356 Aluminum Bath at 800°C [reproduced from Ref. 24]

With data for rotational speeds of 100 rpm and 300 rpm, 304 stainless had a much higher dissolution rate (>30%) than titanium in molten aluminum (Figure 3-19). Similarly, accelerating the surface velocity of the flowing liquid metal (i.e. from 100 rpm to 300 rpm rotation) greatly enhanced the relative dissolution rate (>80% increase) of both metal samples.

Batchelor, et al. proceeded by stating that the 304 stainless samples quickly developed a thick intermetallic layer (> 30μm after 3 hours) on the surface when submerged in molten aluminum at 800°C. However, they did not provide a chemical analysis describing the nature of this intermetallic layer. Moreover, the erosion of the base metal was a result of detachment of portions of this intermetallic layer. Conversely, only a small transition zone (~3μm after 3 hours) was observed on the titanium sample. Batchelor, et al. theorized that the high solubility of nickel (18%) in molten aluminum at 800°C, compared to only titanium (1% solubility), was the probable source of the higher dissolution rate of the 304 stainless sample. Additionally, the authors noted that addition of 10wt% alumina particles to the aluminum bath had little impact on the rate of degradation of the samples, commenting that the particle velocity was probably not high enough (<1 m/s) to do significant erosive damage. Thus, solubility of the metal in the bath was the primary driving mechanism.

And then, in 1998, Tsipas, et al. [Ref. 25] published the results of a brief series of corrosion experiments in both molten zinc and molten aluminum. Sample discs (40mm diameter x 3mm thick) were machined from plain carbon steel (0.2% C) and a high-alloy steel (20% Cr + 1% Mo). [Note: no indication was made as to the carbon content in the high-alloy steel.] Carbon steel specimens were then tested in both liquid zinc and liquid

aluminum, while the high-alloy steel was only tested in liquid zinc. As outlined in Figure 3-20, Tsipas, et al. described a significant increase in the degradation of the high-alloy steel versus carbon steel when exposed to molten zinc at 500°C. Conversely, the carbon steel had appreciably less corrosion in molten aluminum (630°C) than in zinc (500°C).

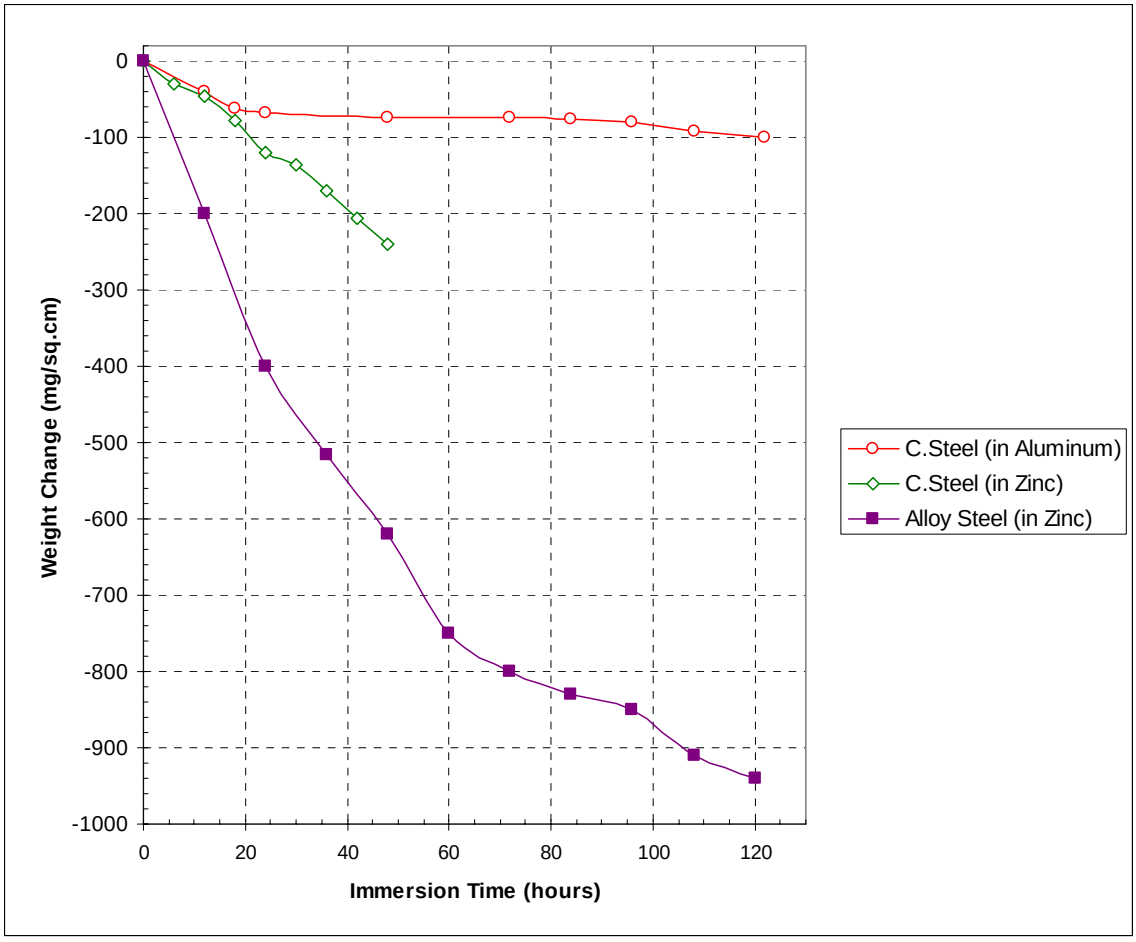

Figure 3-20: Corrosion Data in Molten Aluminum (at 630°C) and Zinc (at 500°C) [reproduced from Ref. 25]

On the other hand, several discrepancies in these results should be noted. First, the bath temperature of the aluminum was listed as 630°C, but the liquidus temperature of pure molten aluminum is 660°C. Thus, this experiment did not utilize pure aluminum, but rather some hypoeutectic alloy with a reduced melting point. Since the actual bath

aluminum alloy composition was not depicted, it is difficult to make conclusions related to the reactivity of carbon steel in this unknown environment. Similarly, the bath composition of the liquid zinc was not listed.

Furthermore, the mass and surface area of a new 40mm diameter x 3mm thick sample are calculated to be about 30g and 36cm^2, respectively, which results in a total possible weight change of less than 850mg/cm^2. However, the high-alloy steel corrosion results show two data points exceeding 900mg/cm^2, but the sample should have been completely dissolved in the zinc at that point. This inconsistency brings into question how the corrosion loss was actually measured and recorded, questioning the validity of all the data. In general the results in this report should be used for ranking comparison of the contained specimens, but probably cannot be extrapolated for analysis to other research projects and outside data.

In another endeavor that investigated the corrosion mechanisms of molten zinc and aluminum, Jorge Morando of Alphatech Inc. performed an array of experiments [Refs. 26-29], as depicted in a series of patents for alloys resistant to molten zinc and aluminum attack, to study the reactions of various ferrous alloys in molten aluminum and zinc/aluminum baths. Then more recently, he investigated alloy substrate reactions in molten magnesium melts [Ref. 30]. In the former work, Morando identified the need for more durable materials to be utilized in pot hardware of continuous galvanizing lines (instead of the widely-used 316L stainless steel). He defined a series of requirements that would be necessary to maximize operational longevity of the materials in galvanizing bath hardware.

1. *Low solubility in molten zinc/aluminum melts.* Morando noted that the minimum "amount of radial loss due to molten metal dissolution" for the submerged bath rolls should not exceed 1.0μm per hour (i.e. thickness loss).
2. *Low adhesion (non-wettable) to zinc/iron and zinc/iron/aluminum dross.* "[Adhesion] plays the main role in the bonding of solid-liquid state metals."
3. *High surface hardness (HRc>40).* "Abrasive wear contributes to nearly half of the loss of the roll life in metalizing applications."
4. *Dimensional stability at operating temperatures (for straightness and roundness up to 700°C).* Excessive distortion in rotating mechanical equipment may cause significant vibration or abnormal wear leading to unplanned maintenance.
5. *Thermal shock resistance.* "The roll should be capable of withstanding a thermal shock of no less than 250°C when going from air into the molten metal."
6. *Good impact and notch resistance strength.*
7. *Easily manufacturable (casting, machining, etc.) by standard procedures.*
8. *Economic viability.*

In regards to solubility and adhesion, Morando commented that, "the joining of dissimilar metals in a solid-liquid state is governed by their physico-chemical properties and by the interaction between them" and in the case of galvanizing pot hardware, "a strong metallic bond between the atoms of the coating metal and the roll material occurs in the wetting process." However, with respect to the zinc melts in discussion, "formation,

interdiffusion and dissolution of intermetallics [may] have a significant effect on the bonding properties of the intermetallic layers being formed."

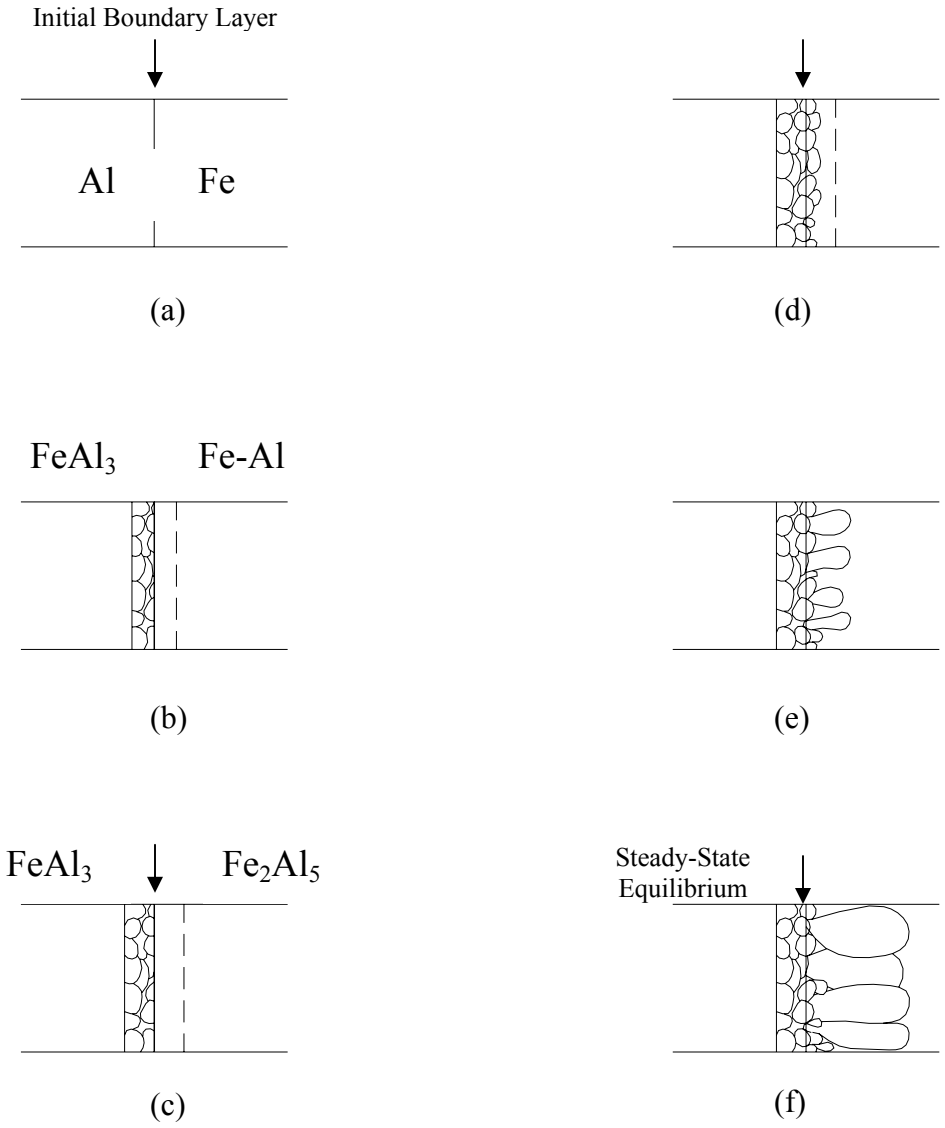

Figure 3-21: Stages of Diffusion Reaction between Liquid Zn/Al and an Iron-based Substrate [reproduced from Ref. 26]

Through theoretical findings and experimental justification, Morando recognized that "the attack on a solid metal by [liquid] zinc and zinc/aluminum alloys is a topochemical reaction in which a two-stage formation of strong bonds between atoms of the two materials is a characteristic feature." In the initial stage, physical contact

between the liquid (Zn/Al) and solid (Fe) create an "electro-static interaction" of the surface atoms promoting adhesion [Figure 3-21: (a) and (b)]. In the second stage, quantum processes between the surface electrons impart a chemical interaction which induces the completion of a strong bond [Figure 3-21: (b) and (c)]. Furthermore, "zinc/aluminum alloys are so active that adhesion and diffusion into steel is achieved in the presence of a passive film of iron oxides, as long as the oxide layer is no thicker than 0.01μm [note dotted line in Figures 3-21: (b), (c) and (d)]." Subsequent diffusion of Zn/Al atoms into the Fe substrate induced the formation and growth of intermetallic layers at the liquid-solid contact zone [Figure 3-21: (d), (e) and (f)].

This diffusion reaction may be further described by observing the example of an iron-carbon binary alloy immersed in a bath of molten aluminum (Figure 3-22). As defined previously, a surface reaction occurs between the liquid (Al) and solid (Fe-C) and eventually aluminum atoms begin to diffuse into the substrate surface. However, as Morando notes, "aluminum decreases the solubility of carbon in liquid and solid iron, [so] carbon is forced out from the solid solution of iron during formation of the intermediate layer [Figure 3-22: (f, pt.2)] and an area rich in carbon [Figure 3-22: (f, pt.3)] develops immediately in front of the diffusion zone." This accumulation of carbon at the diffusion front "retards the dissolution of iron by acting like a barrier to the aluminum diffusion progress."

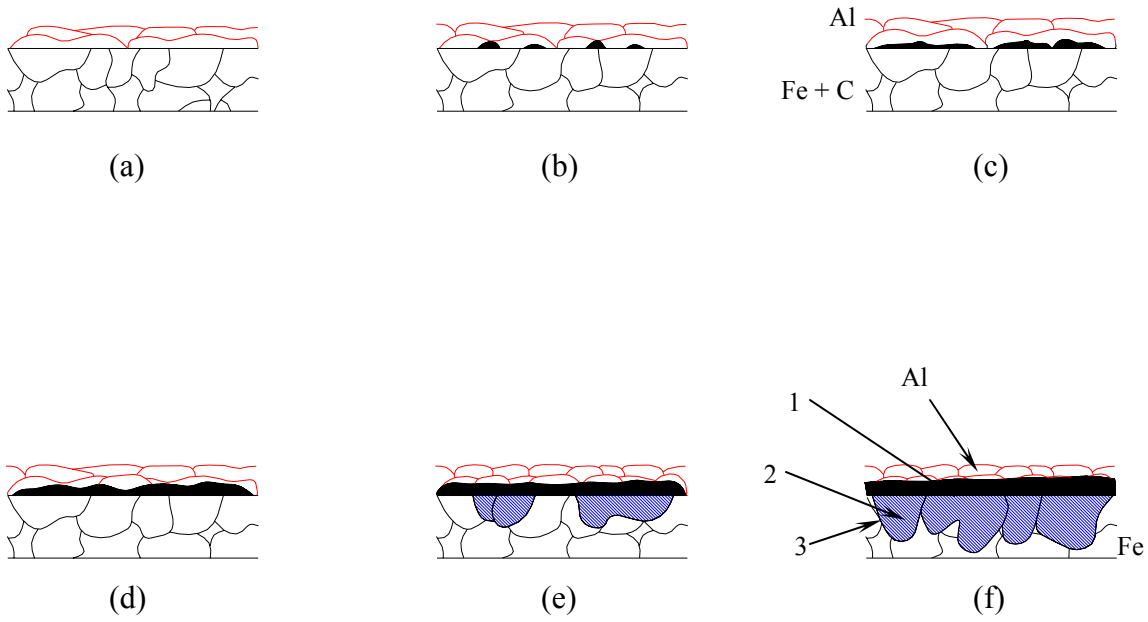

Figure 3-22: Theoretical Diffusion Reaction of Fe-C Alloy Immersed in Molten Aluminum [reproduced from Ref. 26]

In support of these concepts, Morando performed a series of experiments where specific binary ferrous alloys of incremental alloying additions were immersed in a bath of molten aluminum and the resultant intermetallic layers observed. (Since aluminum is the more aggressive activation component in Zn/Al/Fe baths, pure aluminum was tested independently to understand its constituent effect.) Binary Fe alloys of C, Mn, Mo, Ni and Cr were each produced at varying concentrations. After two weeks immersion (at two different temperatures, 750°C and 850°C), each sample was removed and sectioned in order to measure the depth of the diffusion penetration.

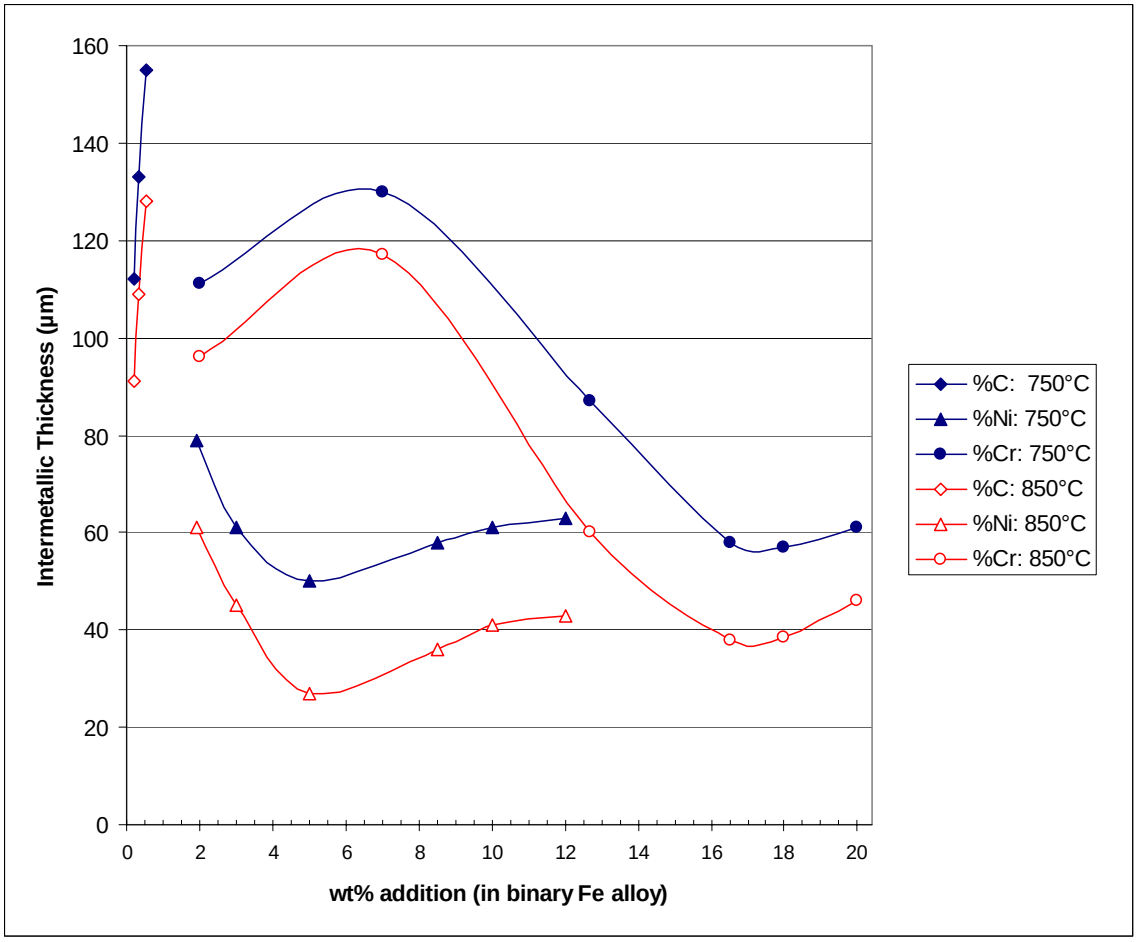

Figure 3-23: Intermetallic Diffusion Reaction Between Molten Aluminum and Binary Fe-C, Fe-Ni and Fe-Ni Alloys [reproduced from Ref. 26]

As displayed in Figure 3-23, the infiltration of the intermetallic diffusion reaction into alloys of Fe-C, Fe-Ni and Fe-Cr shows consistent trends at both 750°C and 850°C bath temperatures. For all three of these substrate alloys, the higher temperature provided less diffusion penetration. (However, it is not clear if this is actually a result of surface dissolution degrading the original thickness of the material.) Furthermore, while the Fe-C alloy displayed a constant diffusion increase at only minor carbon concentration enhancements, the Fe-Ni and Fe-Cr alloys provided maxima and minima intermetallic thickness locations. It is curious however that Fe-Cr indicated a point (Fe-7%Cr) of maximum thickness at nearly the same concentration (Fe-5%Ni) where Fe-Ni showed the

minimum diffusion reaction. Nevertheless, both Fe-Ni and Fe-Cr achieved relatively low diffusion thicknesses at higher alloy concentrations.

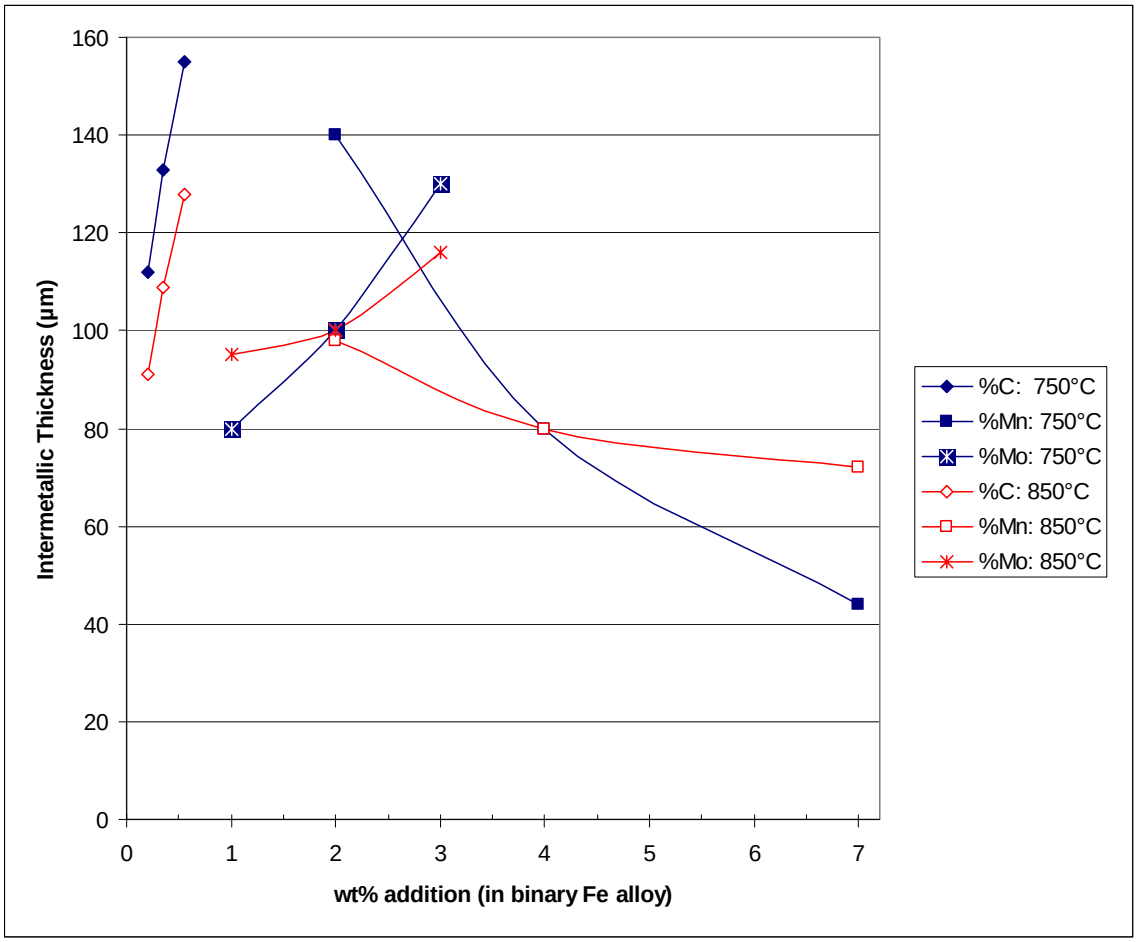

Figure 3-24: Intermetallic Diffusion Reaction Between Molten Aluminum and Binary Fe-C, Fe-Mo and Fe-Mn Alloys [reproduced from Ref. 26]

Next, as presented in Figure 3-24, the reactions between the aluminum bath and alloys of Fe-Mo and Fe-Mn can be characterized. (The previously noted results of Fe-C are also repeated for clarity.) The first attribute that can be established from Figure 3-24 is that, contrary to Figure 3-23, the increase in temperature from 750°C to 850°C does not provide a consistent response for enhanced alloy concentrations in Fe-Mn and Fe-Mo. For this Fe-Mn alloy, enrichment of the Mn concentration provided a decrease in the

reaction thickness, but an increase in the temperature at these higher concentrations promoted intermetallic formation. Conversely, a higher alloying content in Fe-Mo advanced the diffusion depth, but subsequent temperature inflation suppressed the intermetallic penetration.

As a result of these experiments as well as an in-depth understanding of the relevant zinc and aluminum phase diagrams, Morando concluded that in order for a metallic alloy to resist attack from zinc/aluminum melts it should meet numerous requirements [Refs. 26 - 28]. Among these requirements, Morando stated that "the intermetallic layer thickness formed during molten zinc/aluminum immersion at steady-state conditions should not be less that 120μm." Hence, as described in Figures 3-23 and 3-24, increases in C and Mo with decreases in Mn as well as narrowly controlled concentrations of Cr and Ni appear to promote an adequate intermetallic thickness. Furthermore, Morando "strongly suggests that the work of adhesion of metals and transition metal alloys decreases with increases in the surface hardness and a reduction of surface energy of the adhesion resistant alloy" as a consequence of increased concentrations of low surface energy carbides present at the substrate surface.

Through his patented formulation process, Morando devised an iron-based, high-carbide-content superalloy (named "AT101") with potentially high corrosion resistance in zinc/aluminum melts. As verification, several experiments were performed utilizing actual galvanizing pot hardware (rolls) in industrial applications. The resultant change in material thickness (i.e. roll radial material loss) was recorded for several materials at increasing bath aluminum concentrations (and temperatures).

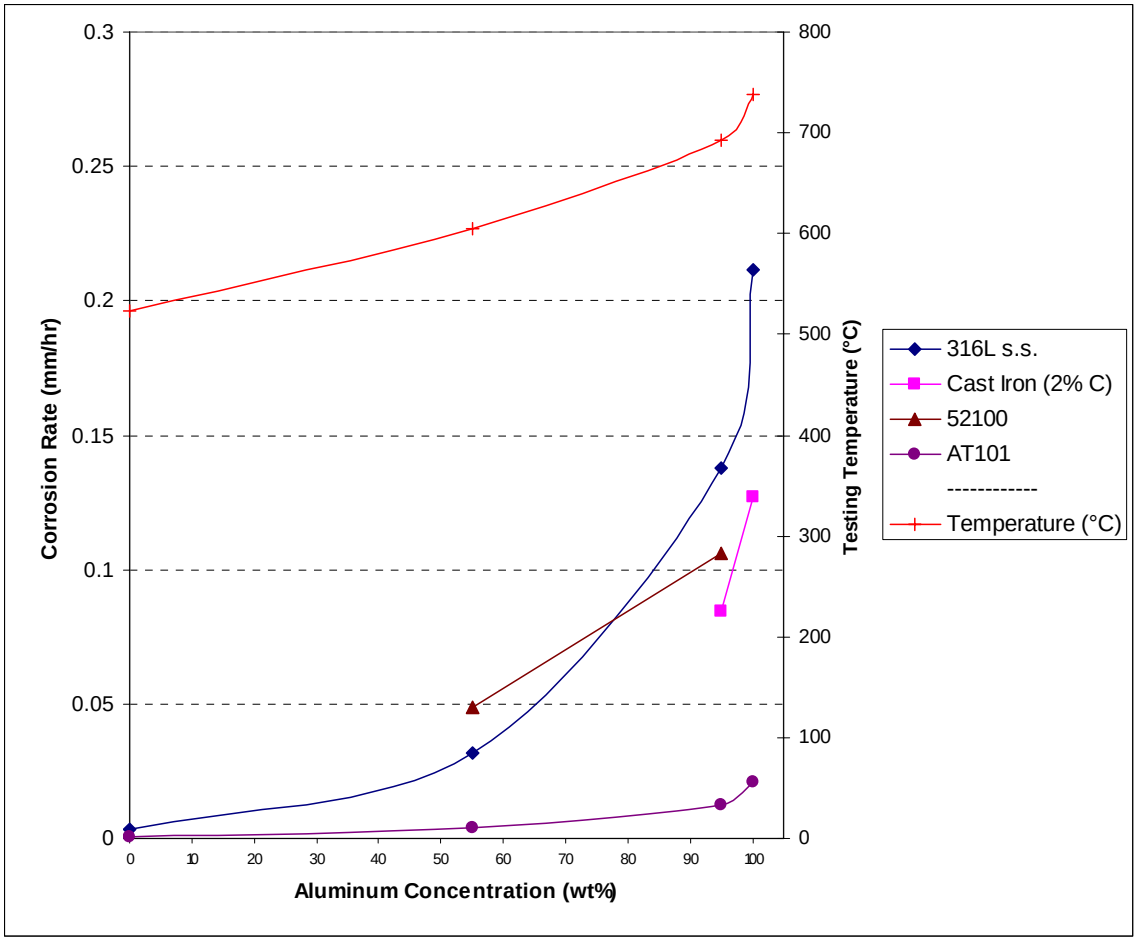

Figure 3-25: Corrosion Rates of Several Ferrous Alloys in galvanizing Baths with Varying Aluminum Concentrations [reproduced from Ref. 26]

As shown in Figure 3-25, the three standard reference alloys (316L stainless, cast iron and AISI 52100; see Table 3-7) exhibited rapidly accelerating degradation at elevated aluminum concentrations. However, the patented AT101 alloy portrayed very low solubility and decay at all aluminum concentrations, even in an industrial aluminizing bath (with "100%Al" + saturated iron).

Table 3-7: Compositions (wt%) of Test Samples [Ref. 26]

element	AISI 52100	Cast Iron (typ.)	AT101
C	1.00	3.50	2.2
Cr	1.45	0.40	18
Mn	0.35	0.70	1
P	0.03	0.12	-
S	0.03	0.15	-
Si	0.23	2.10	-
Cu	-	0.30	-
Mo	-	0.10	4
Ni	-	0.15	-
Co	-	-	15
V	-	-	3
W	-	-	10
Fe	96.92	92.48	46.80

As a result of these investigations by Morando, a better understanding of the reactions between molten aluminum and solid ferrous alloys was determined, especially with regards to the intermetallic diffusion layer formation. By utilizing the techniques outlined by Morando, alloys with high resistance to zinc/aluminum attack may be developed. As Morando stated, "By formulating a material based on the restraints of the selected criteria, the mass transfer rate is reduced with the increase in complexity of the intermetallic layer and with a decrease in the bonding strength of the diffusion layer, as a consequence of the minimization of matrix exposure and reduction of exposed area."

Chapter 4: Focused Research Efforts

Meanwhile, the 1990's marked the beginning of a period of concentrated research endeavors aimed at understanding degradation of galvanizing pot hardware materials. The first of these projects was sponsored by British Steel Strip Products of Port Talbot, U.K. (now known as Corus Steel Group) and was the most extensive investigation into galvanizing pot hardware materials up to that point. [Refs. 31 – 34]

Brunnock, et al. performed a broad range of studies on numerous ferrous materials, maintaining 316L stainless steel as the consistent baseline. Not only did they research the effects of silicon and chromium contents on static dissolution, but also the protection effects of various coatings in static and dynamic conditions. Additionally, they initiated research into a reaction called "supermeniscus intermetallic climb" [Ref. 33], which refers to a capillary-type reaction between the liquid zinc and the stainless steel causing the stainless sample to expand in size at locations above the zinc bath. For the relevance of the current research, only the results of zinc dissolution reactions with ferrous alloys (and only standard coatings) will be reviewed at this time.

Brunnock, et al. established a standard experimental apparatus (Figure 4-1) for testing various metal samples. Cylindrical bars (150mm long x 15mm dia.) were suspended in an enclosed crucible furnace containing 30kg of liquid zinc at test temperatures of 455°C and 480°C. The bath composition was commenced at 0.135% aluminum, 0.03% iron and 99.83% zinc. The compositions of the substrate test alloys are provided in Table 4-1.

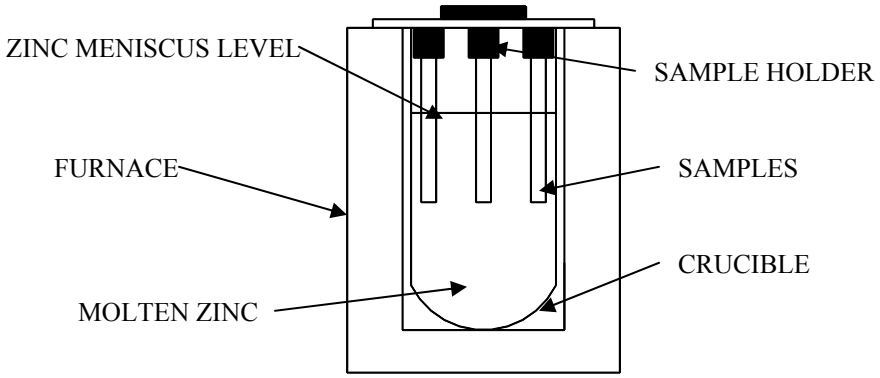

Figure 4-1: Static Immersion Test Apparatus
[image reproduced from Refs. 31 – 34]

Table 4-1: Compositions (wt%) of Test Samples [Refs. 31 – 34]

element	Low Carbon Steel	410 s.s.	430 s.s.	304 s.s.	316L s.s.
Cr	-	11.9	17	17.8	16.6
Ni	-	-	-	10.5	11.2
Mo	-	-	-	-	2.12
C	0.2	0.08	0.08	0.06	0.03
Mn	0.15	1	0.5	1.5	1.64
Si	0.25	0.5	0.5	0.5	0.5
Fe	99.4	86.52	81.92	69.64	67.91

As a basic overview, Brunnock, et al. mapped the static corrosion degradation (percentage weight loss after 120 hours) of typical test alloys and several thicknesses of a plasma spray coating of tungsten-carbide in a cobalt binder. (This is a standard corrosion resistant coating used in industrial galvanizing operations.) Outlined in Figure 4-2, they classified that 316L stainless had significantly more corrosion resistance than either carbon steel or 410 stainless, but was nearly identical to 304 stainless. Also, the tungsten-carbide coatings further reduced the corrosion attack. Surprisingly, when tungsten-carbide was applied to the carbon steel, the zinc-corrosion was nearly abated, making it actually better than the 316L with an equivalent coating. This difference could

possibly be a result of the difference in thermal expansion. Carbon steel would have thermal expansion characteristics closer to that of the tungsten-carbide coating than would the 316L stainless. At elevated temperatures the higher thermal expansion could cause the coating to crack allowing zinc to penetrate to the substrate. Brunnock, et al. found no significant change in the percentage weight loss when the bath temperature was raised to 480°C for a subsequent test.

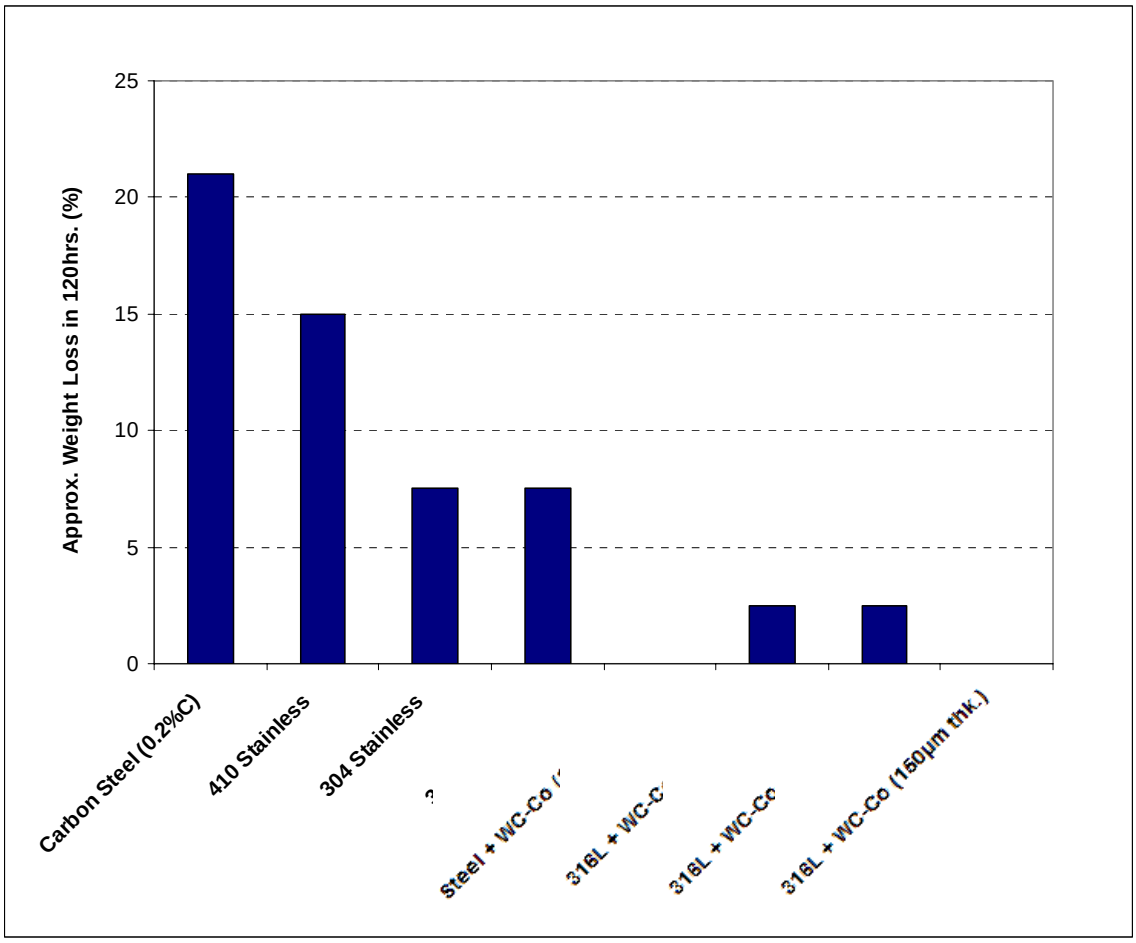

Figure 4-2: Static Corrosion Results in Zn-0.135%Al (0.03%Fe) Bath at 455°C for 120 hours [reproduced from Ref. 32]

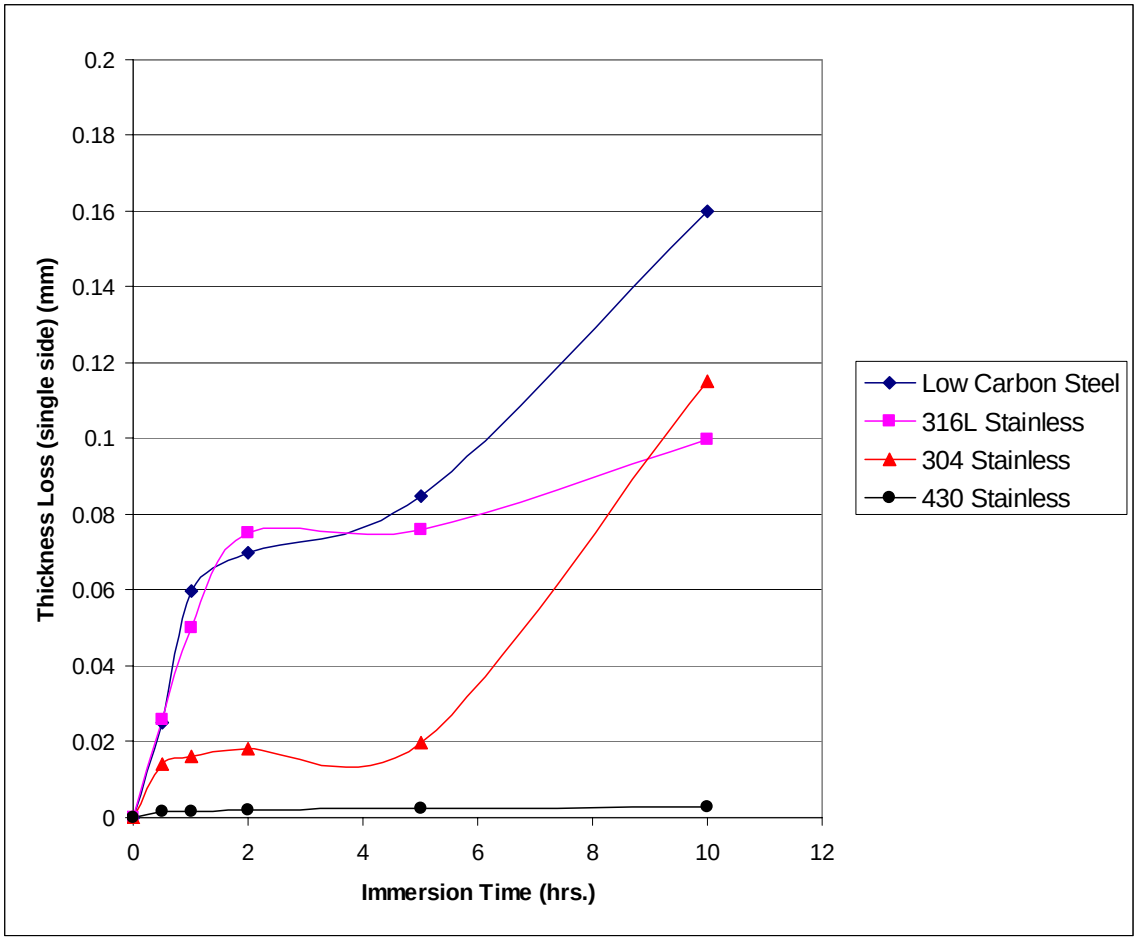

Figure 4-3: Static Corrosion Rates in Zn-0.135%Al (0.03%Fe) Bath at 480°C [reproduced from Ref. 31]

Looking at the static corrosion aspects in more depth, the dissolution responses of four different alloys are indicated in Figure 4-3 for the initial ten hours of immersion with the bath at 480°C. For the first 5 hours the corrosion of the carbon steel and 316L stainless samples were quite rapid and nearly identical, but the losses from the 304 and 430 stainless samples were rather low. During the latter stages of these results, the carbon steel continued to decay very rapidly while the 316L stainless seemed to passivate. The 304 stainless also accelerated its loss and had virtually the same total loss as 316L after 10 hours. On the other hand, the 430 stainless sample showed negligible

corrosion over the entire duration of this brief test which does not seem to correspond well with the 410 stainless results of the 120 hour long-term trial (Figure 4-2).

Next, Brunnock, et al. [Ref. 34] studied the effects of varying the alloying content in 316L stainless steel. Preliminarily, several samples of 316L stainless were produced with increasing levels of silicon content. Corrosion tests were performed in the standard Zn-0.135%Al bath for 24 hours at 480°C. The results of these tests (Figure 4-4) point toward several interesting trends.

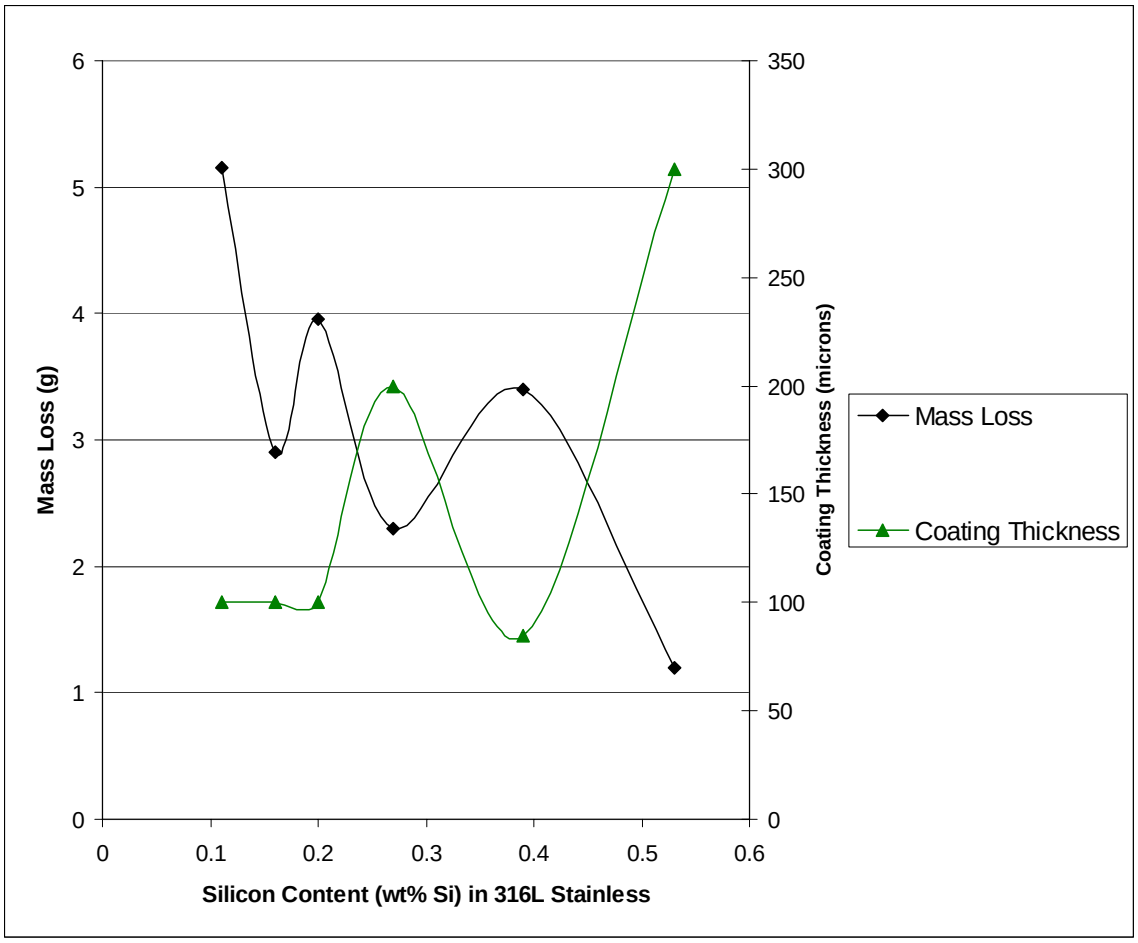

Figure 4-4: Static Corrosion Rates of Si-Modified 316L Stainless after 120 hours in Zn-0.135%Al (0.03%Fe) Bath at 480°C [reproduced from Ref. 34]

First, it is apparent that as the silicon level was increased (up to 0.53wt% Si) the corrosion rate decreased. Additionally, it seems as if the corrosion loss of the sample was inversely proportional to thickness of the intermetallic layer buildup on the sample. However, several issues are not necessarily clear from this data. Since this was only a 24 hour test, would the observed trends have continued for longer time durations? Similarly, since silicon readily dissolves into aluminum, would these results be applicable at higher bath aluminum levels? In conjunction, is there a maximum threshold (for a given bath aluminum concentration) of increased silicon level providing a further reduced corrosion rate?

Along those same lines, Brunnock, et al. investigated [Ref. 34] the corrosion response (120 hours at 480°C) of "316L stainless" (0.03% C) with increasing levels of chromium and nickel. They also compared the effects of these alloys in an "as-rolled" state and with subsequent solution annealing (1050°C for 1 hour). With the intermediate peaks in the curves of Figure 4-5, it appears as if the corrosion of these stainless alloys may be easily influenced by the chromium and have specific "ideal" levels of desirable chromium content. Additionally, the results show that the annealed samples, in general, had lower corrosion than the as-rolled pieces. Based on this data, it is possible that the varying chromium levels and the effects of annealing provided alternating levels of "sensitization" within the grains of the stainless alloys. Sensitization refers to the chromium depletion at grain boundaries when it forms chromium carbide ($Cr_{23}C_6$). The inhomogeneous chemistry then enhances the susceptibility of corrosion. As observed, the chromium carbides can easily be dissolved with the proper annealing procedures.

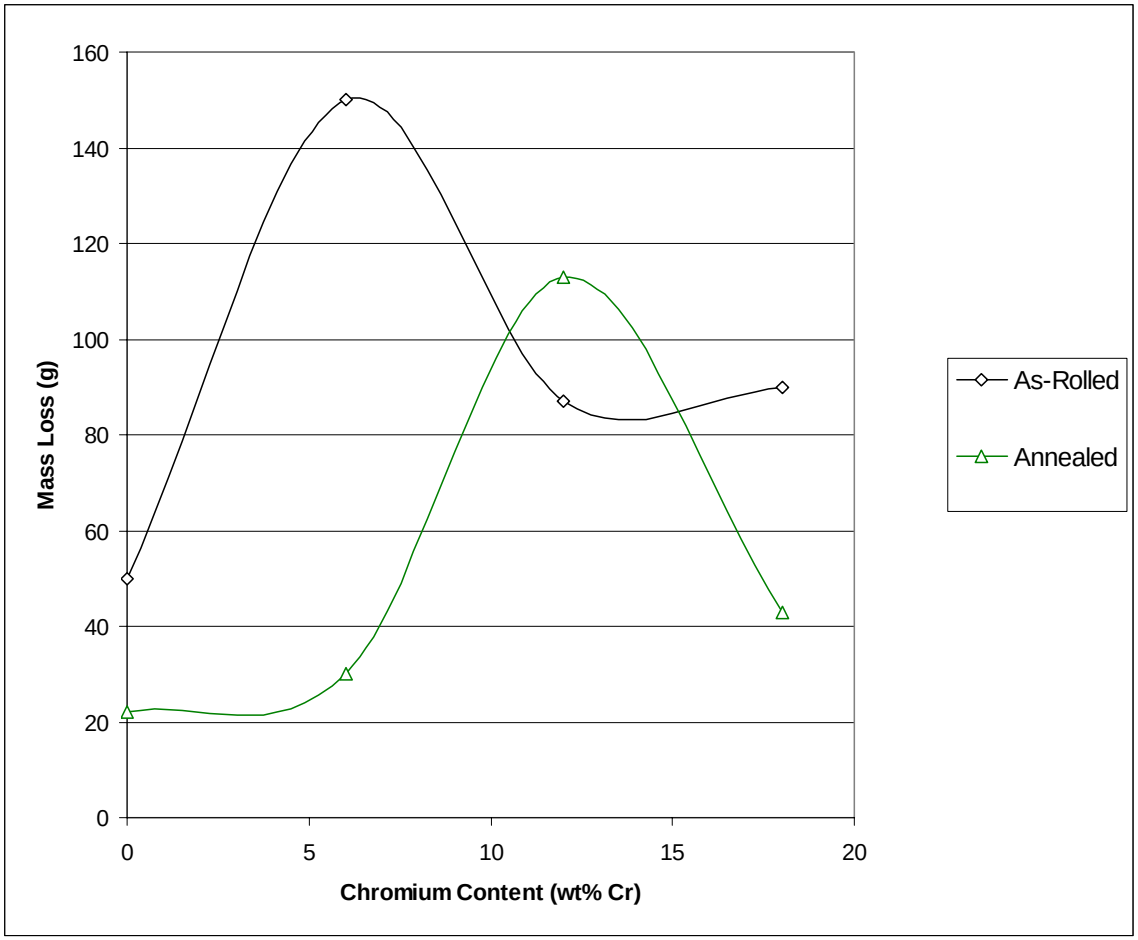

Figure 4-5: Static Corrosion Rates of Cr-Modified 316L Stainless after 120 hours in Zn-0.135%Al (0.03%Fe) Bath at 480°C [reproduced from Ref. 34]

Finally, Brunnock, et al. briefly researched [Ref. 34] the impact of nickel content on the zinc-dissolution of stainless steel with 18% chromium (0.03% C, 0.5% Si). As Figure 4-6 demonstrates, increases of nickel (up to 9wt%) greatly reduced (by over 50%) the dissolution loss. However, as with the testing of variable silicon content, is there a maximum ideal ceiling (for a given bath aluminum concentration) of increased nickel level providing a further reduced corrosion rate? And similarly, since nickel readily dissolves into aluminum, would these results be applicable at higher bath aluminum levels?

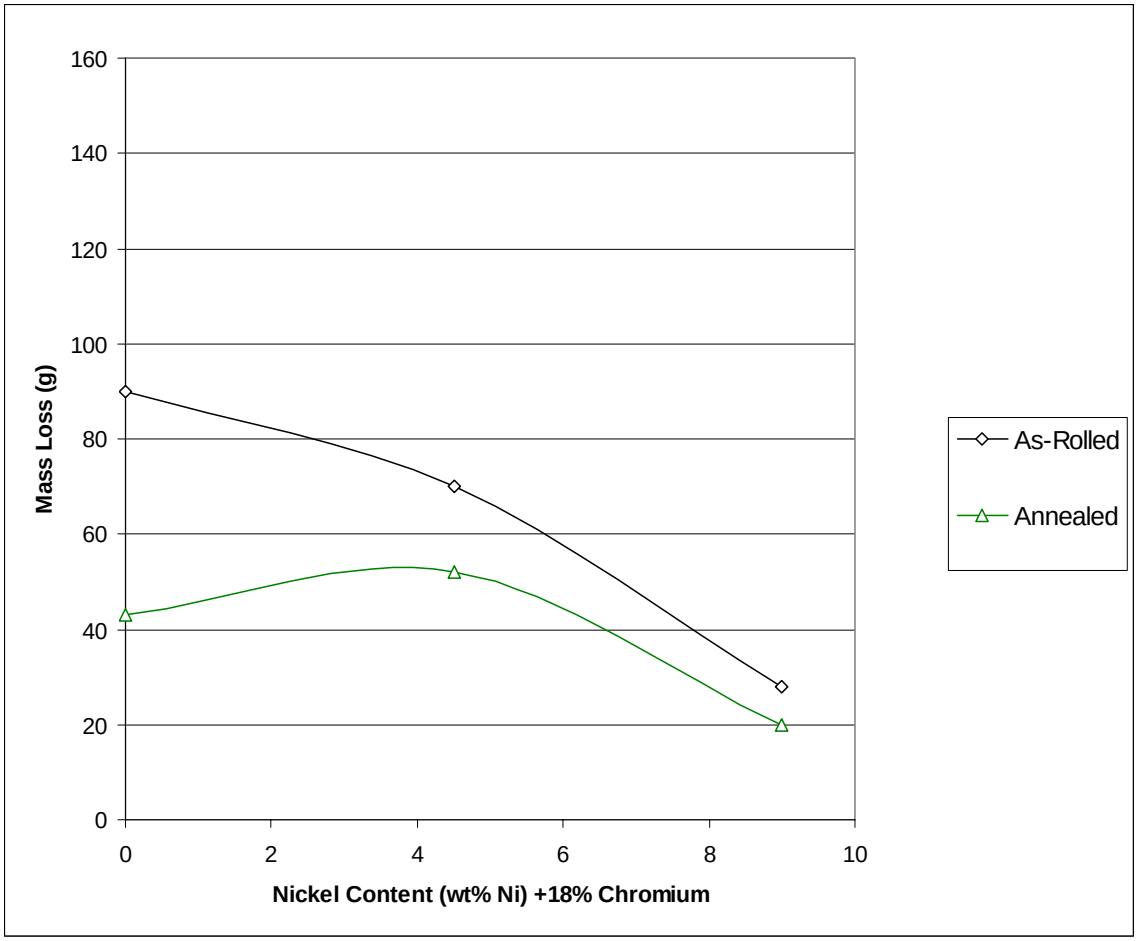

Figure 4-6: Static Corrosion Rates of Ni-Modified 316L Stainless after 120 hours in Zn-0.135%Al (0.03%Fe) Bath at 480°C [reproduced from Ref. 34]

Since 316L stainless steel is the standard material used in most continuous galvanizing lines, a full understanding of the behavior of 316L can begin to provide a foundation for extending the life of galvanizing hardware. The studies performed by Brunnock, et al. have formed the basis all subsequent investigations in the area of galvanizing pot hardware research.

With regards to the "sensitization" issue that was intimated from the Brunnock research, Mark Tackla of *Spartan Steel Coatings Company* proposed [Ref. 35] the possibility of a link between chromium carbide segregation (also known as "sensitization") in 316L stainless steel and an increased level of corrosion in the zinc

bath. In an actual production galvanizing line, Tackla observed a situation where two identical geometry components were immersed in the zinc bath at the same time, but one piece had over double the amount of degradation as the other upon removal. The two pieces of 316L stainless were in service for 22 days with 12 days being in Zn-0.165%Al at 449°C and continuing for 10 more days at Zn-0.130%Al at 466°C. The compositions of the two pieces are noted in Table 4-2.

Table 4-2: Compositions (wt%) of Field Trial Samples of 316L Stainless [Ref. 35]

element	Good Piece	Decayed Piece
C	0.020	0.029
Cr	19.4	18.0
Ni	12.5	11.8
Mo	2.0	2.0
Fe	66.1	68.2

Tackla noted that the decreased carbon content in the good sample could have promoted enhanced corrosion resistance. Reviewing the time-temperature sensitization curve for 316 stainless steel as a function of carbon content (Figure 4-7), the trend of chromium carbide formation can be understood. At lower carbon levels an insufficient amount of carbon is available for carbide formation, hence, minimizing sensitization.

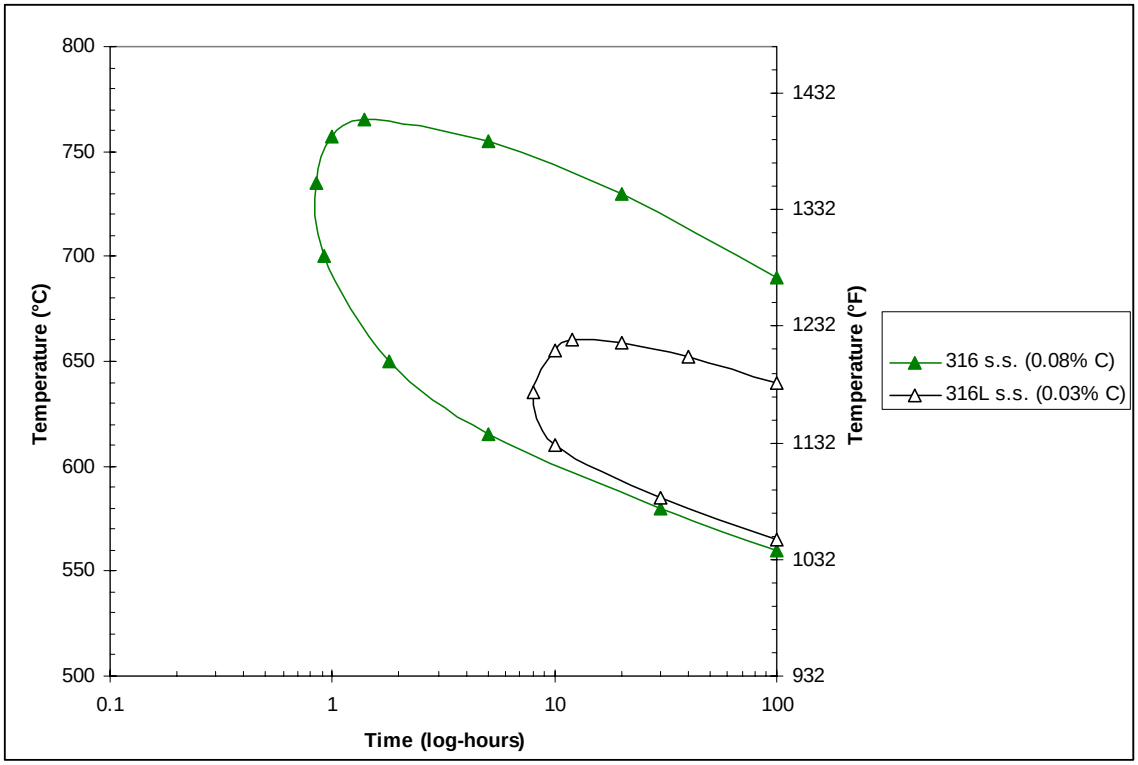

Figure 4-7: 316 Stainless Steel Time-Temperature Carbide Segregation Response Relative to Carbon Content [reproduced from Ref. 36]

Thus, it could be accurate to identify that a decreased level of carbon might provide enhancement to corrosive characteristics of 316L stainless steel in molten zinc. However, the decayed sample also possessed a reduced chromium level relative to the good sample, which would also contribute to its corrosion. Additionally, it is not fully understood what influence the change in process chemistry and temperature had on the corrosion of the samples. Further research needs to be done to fully investigate the impact of sensitization on the corrosive life of pot hardware in a continuous galvanizing line.

Concurrent with Brunnock in the 90's, Tomita, et al. [Refs. 37 & 38] investigated the reactions between Tungsten-Carbide-Cobalt (WC-Co) cermet coatings and molten zinc with varying levels of aluminum additions (from 0% to 3% aluminum). (As noted

previously, WC-Co plasma coatings are the typical means that industrial galvanizing operations utilize to increase the life of 316L stainless in molten Zn-Al baths.) The WC-12wt%Co coatings that Tomita, et al. employed were made from a crushed and sintered powder (<45μm) mainly consisting of η-phase (Co_3W_3C and Co_6W_6C). The powder was then applied to 15mm diameter rods of mild steel (JIS SS400) using a High Velocity Flame Spraying system to a thickness of approximately 200μm. The samples were then immersed in a bath of molten zinc with a specified aluminum concentration (and 0% Fe) at a given temperature. Upon removal, the samples were sectioned and the resulting reaction diffusion depth was measured.

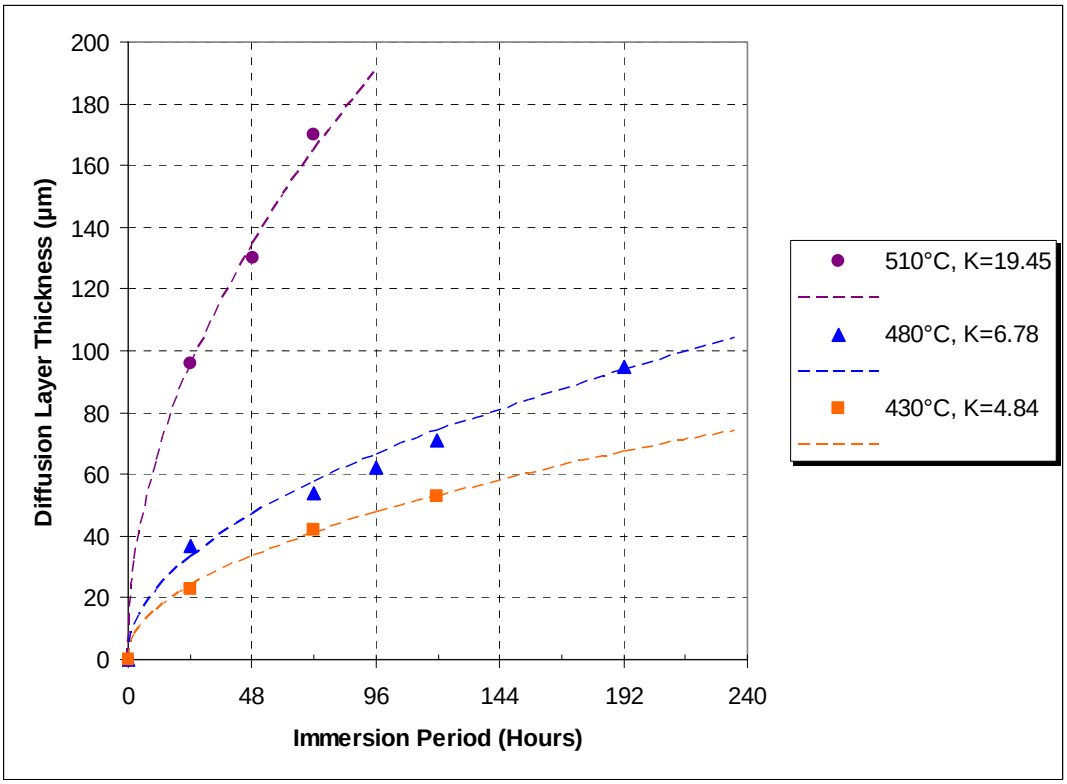

Figure 4-8: Diffusion Reactions between WC-Co Cermet Coatings (on Mild Steel) and Pure Molten Zinc [reproduced from Ref. 37]

First, the diffusion depths into the WC-12%Co coating in pure zinc (99.98%) at increasing temperatures (430°C, 480°C & 510°C) are displayed in Figure 4-8. Each reaction directly followed a standard diffusion response of $D = Kt^{½}$ with increasing K-constants for each higher temperature. Additionally, the diffusion layer penetration accelerated much more rapidly when the temperature exceeded 480°C, eventually to the point (at 510°C) where the entire coating thickness (200µm) was penetrated in under 100 hours.

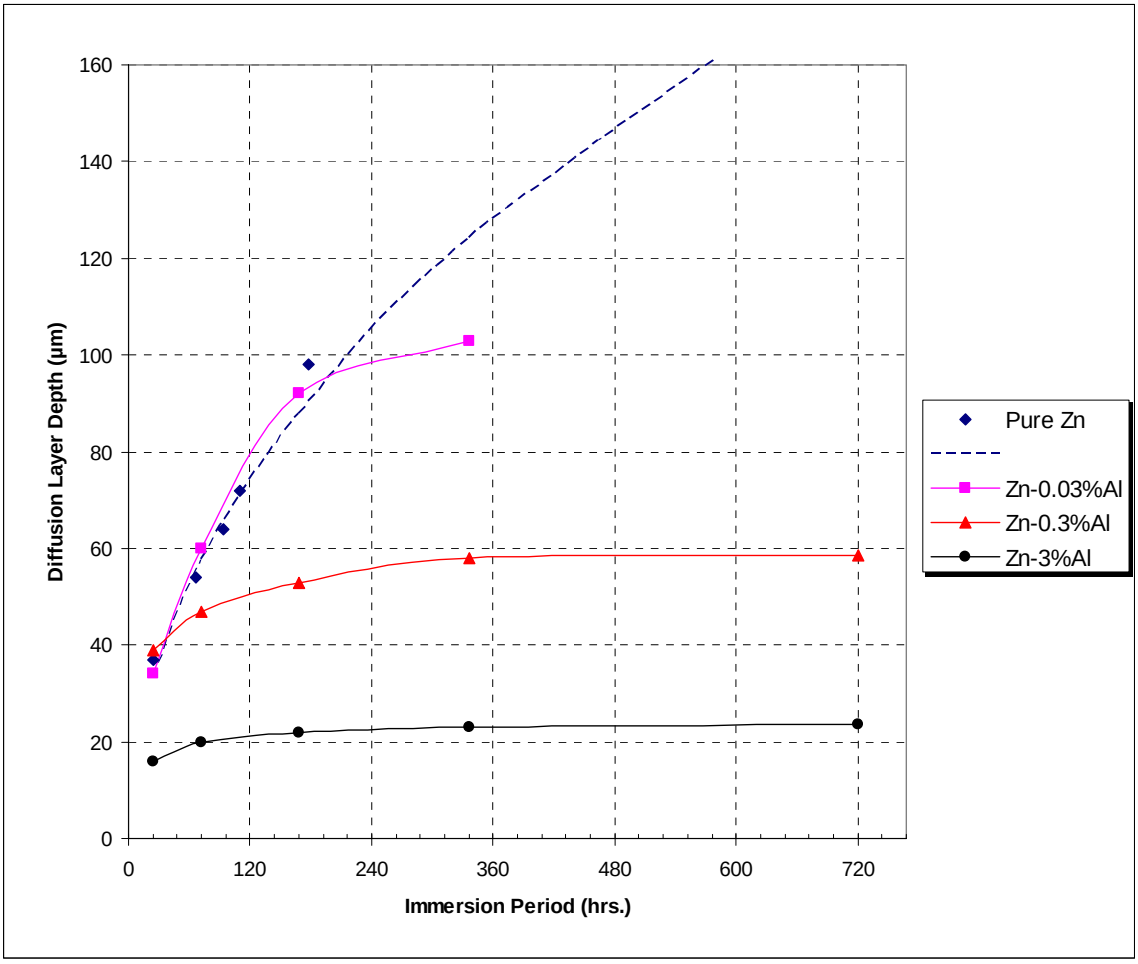

Figure 4-9: Diffusion Reactions between Molten Zn-Al Baths and WC-Co Cermet Coatings (on Mild Steel) [reproduced from Ref. 38]

Similarly, the response of the diffusion depth into the coating as a function of increasing aluminum content in the zinc bath (at 480°C) may be observed in Figure 4-9. Contrary to the tests in pure zinc, these results did not exactly follow a $D = Kt^{½}$ diffusion reaction. Each of the trials eventually reached a steady-state plateau with no further increase in diffusion depth. At higher aluminum levels, this passivation diffusion depth was not only lower in magnitude, but was also reached after a quicker time duration. The steady-state diffusion depths for each aluminum concentration were: Zn-0.03%Al = 102µm (at ~392 hrs.), Zn-0.3%Al = 58µm (at ~344hrs.) and Zn-3%Al = 23µm (at ~240hrs.). Hence, the research by Tomita, et al. indicates that higher aluminum levels in the zinc bath minimize diffusion attack into the WC-12%Co coating.

Now, looking at Figure 4-10, the compositional characteristics of the diffusion penetration may be reviewed, identifying the concentration of zinc as a ratio with the cobalt level (since the mass of stable WC particles is assumed to be constant). This figure shows that as the zinc diffusion front pushes into the coating and displaces cobalt almost completely (78% Zn), creating a consistent interaction zone (regardless of bath Al%) between the zinc front and undisturbed WC-12%Co coating. However, at the ends of the spectrum, pure zinc (0%Al) possessed a much deeper zinc diffusion front as a percentage of the total penetration layer, while higher aluminum (3%Al) created virtually no zinc diffusion front, only an interaction zone of diminishing Zn concentration. Surprisingly, Tomita, et al. found virtually no aluminum in the diffusion layer on the coating (except at high Al% after extended time).

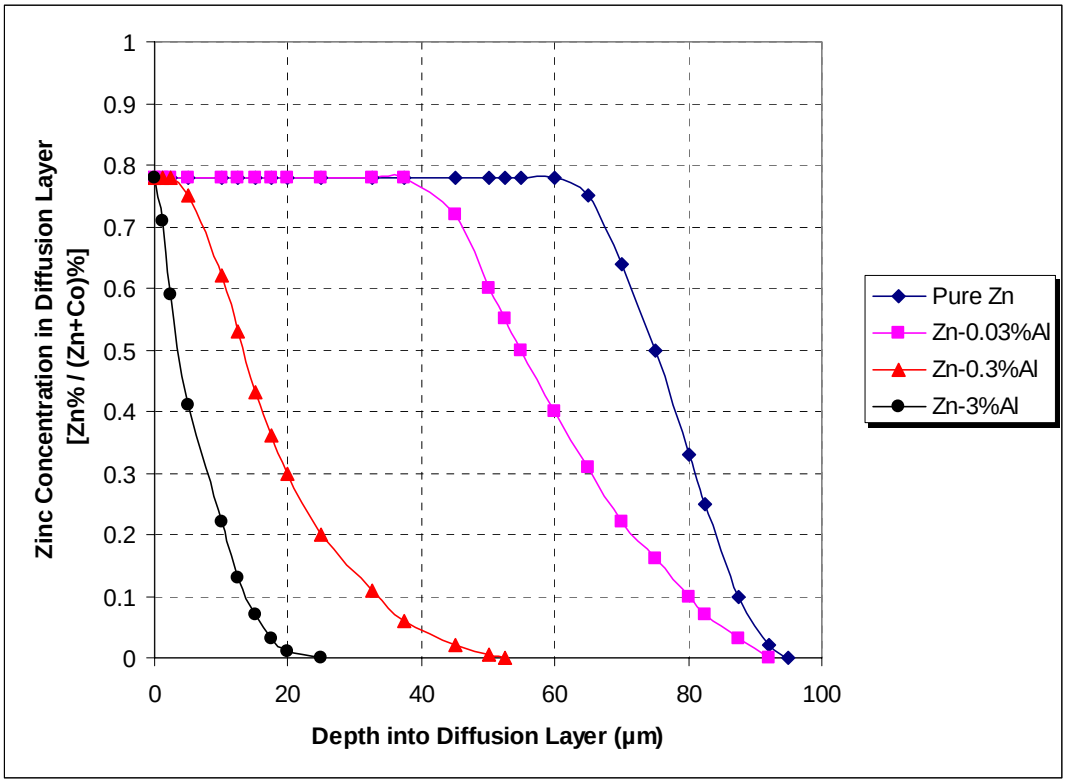

Figure 4-10: Diffusion Reaction Compositions in WC-Co Cermet Coatings (on Mild Steel) after 168 hours Immersion in Zn-Al Bath at 480°C [reproduced from Ref. 38]

Furthermore, the varying elemental concentrations at the coating surface are described in Figure 4-11 when the immersion time was extended to 336 hours. (The "As-sprayed" composition is noted for reference.) Hence, a high-Al concentration is now observed immediately on the coating surface (minimal diffusion), especially from the 3%Al bath. This accumulation of aluminum could potentially be due to the penetration of zinc depositing the residual aluminum at the surface as the zinc diffused into the coating.

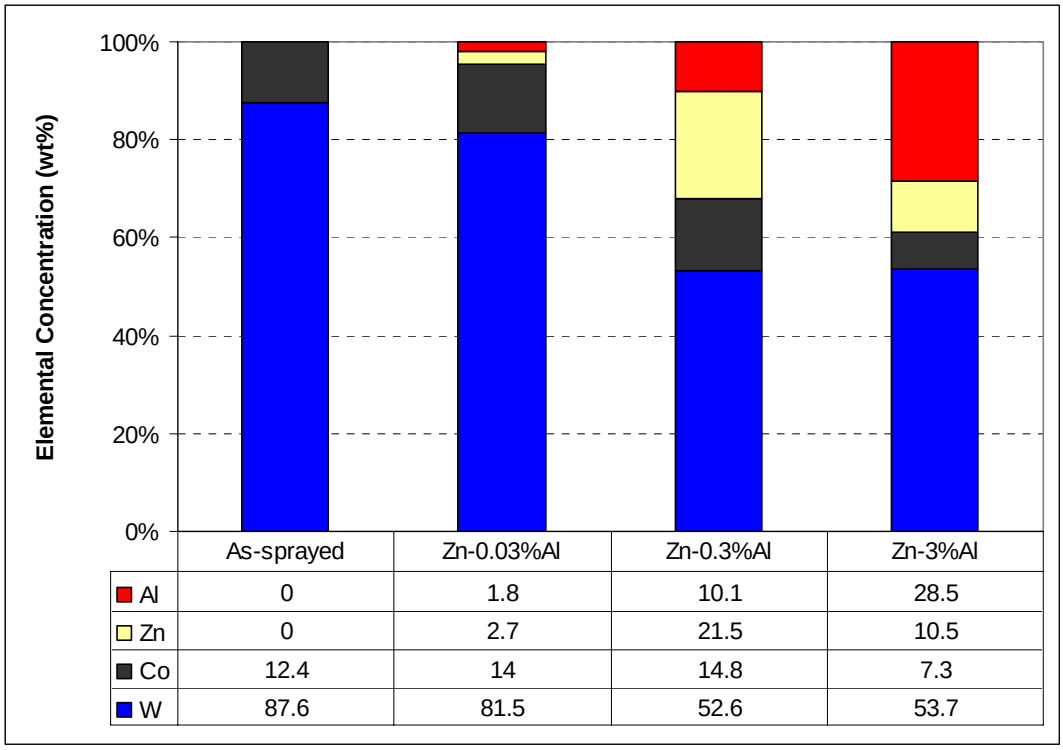

	As-sprayed	Zn-0.03%Al	Zn-0.3%Al	Zn-3%Al
Al	0	1.8	10.1	28.5
Zn	0	2.7	21.5	10.5
Co	12.4	14	14.8	7.3
W	87.6	81.5	52.6	53.7

Figure 4-11: Surface Composition of WC-Co Cermet Coatings (on Mild Steel) after Immersion for 336 Hours in Molten Zn-Al at 480°C [reproduced from Ref. 38]

Finally, using schematic representation, Tomita, et al. did an excellent job describing the diffusion reaction mechanism as they perceived it. "First, Al begins to concentrate immediately after the surface of the sprayed coating is immersed in the molten zinc bath (Figure 4-12(a)). Next, Zn diffuses into the Co phase of the sprayed coating (Figure 4-12(b)) while Co dissolved into the zinc. Though the reasons are not fully clarified at this point, Al hardly diffuses into the Co phase. On the other hand, Co dissolves into molten zinc with a high Al concentration from the coating side to produce an Al-rich solid phase containing Co and Zn by reacting with Al and Zn on the surface of the sprayed coating (Figure 4-12(c)).

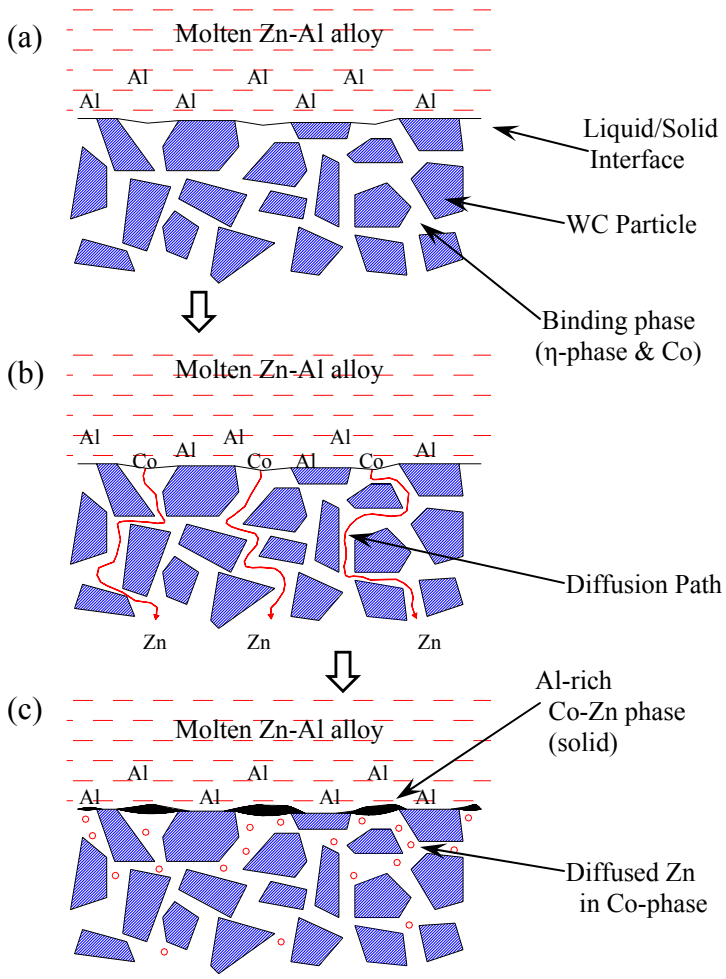

Figure 4-12: Representation of Diffusion Reactions on WC-Co Cermet Coatings in Zn-Al Baths [reproduced from Ref. 38]

From these studies, Tomita, et al. concluded several issues regarding tungsten-carbide coatings in molten zinc. First, as noted previously, "a diffusion layer is formed by the dissolution of Co and the penetration of Zn just under the surface of the sprayed coating", where the thickness of this diffusion layer is minimized at elevated bath aluminum concentrations. Also, an enriched aluminum phase develops on the surface of the coating, segregating from the zinc that diffuses into the coating. Consequently, "durability [of the coating] may be enhanced in response to an increase in the Al concentration of the molten zinc bath because this Al-rich phase acts as a diffusion

barrier against Zn and Co at the interface between the sprayed coating and the molten zinc bath, thereby suppressing the growth of the diffusion layer." (It would also be curious to see if these conclusions hold for alternate cobalt concentrations other than the WC-12%Co tested.) In general, this research by Tomita, et al. on the reactions of tungsten-carbide coatings in molten zinc is regarded as the cornerstone for all future research in the area of coatings for galvanizing hardware.

Meanwhile, it is interesting that the use of tungsten-carbide coatings in industrial galvanizing lines has propagated predominantly in lower aluminum applications such as those making "galvanneal" (0.13%Al) zinc coated products. It presents the question, *if the WC-Co coating is better than bare 316L stainless steel even at these lower aluminum levels, what is the reactivity of 316L stainless at varying aluminum concentrations?*

Subsequently building on this knowledge by Brunnock and Tomita (et al.), in 1997 one of the most extensive research projects to-date on galvanizing pot hardware was initiated and sponsored by the International Lead Zinc Research Organization (ILZRO) [Ref. 39]. The objective of that five-year project was to "reduce galvanizing line downtime by optimizing pot hardware bearing materials and designs using a full-sleeve bearing tester" and the research efforts were undertaken at the Product Technology Centre of Teck Cominco Metals Ltd. in Mississauga, Ontario. Being one of the largest producers of zinc and zinc alloys in the world and possessing possibly the deepest knowledge-base of expertise on zinc products and environments, Teck Cominco was ideally suited to undertake this important research endeavor.

The early efforts of this project focused on obtaining industrial information through operator questionnaires, understanding past research knowledge on galvanizing

materials as well as tribological theory with an intensive international literature review, and outlining theoretical modeling of dynamic bearing and wear configurations. From the literature review, a basic understanding was acquired by the researchers of the features that were necessary for galvanizing hardware materials. "In general, materials that can successfully survive submersion in the galvanizing bath for useful periods of time should be minimally wetted when in contact with the liquid alloy and produce minimal amounts of intermetallic particles on their surface." And similarly from a wear standpoint, "Dross [intermetallic particles], when present, can be expected to adversely impact bearing wear because the hardnesses of the dross particles in many cases exceeds those of the bearing materials".

With a detailed understanding of the industrial applications and a complete discernment of previous fundamental research on the topic, Teck Cominco progressed towards designing and constructing a large testing apparatus which could be utilized to rotate an actual (76mm diameter) bearing in a specified bath of molten zinc under various loading situations. When the bearing tester was completed (see Figures 4-13, 4-14 and 4-15), it had been outfitted with extensive instrumentation that allowed it to measure load, torque, displacement, bath temperature, bearing temperature, rotational speed, and friction coefficient. (As an example, the output graph of an actual bearing test for Stellite#6 against Stellite#6 bearings can be observed in Figure 4-16 with Figures 4-17 and 4-18 displaying the resultant wear components.).

Figure 4-13: Full-Scale Bearing Wear Tester at Teck Cominco Product Technology Centre [reprinted with permission from The International Lead Zinc Research Organization, Ref. 39]

Figure 4-14: Bearing Test Sample Attachment Apparatus [reprinted with permission from The International Lead Zinc Research Organization, Ref. 39]

Figure 4-15: Assembled Bearing Sample in Test Rig [reprinted with permission from The International Lead Zinc Research Organization, Ref. 39]

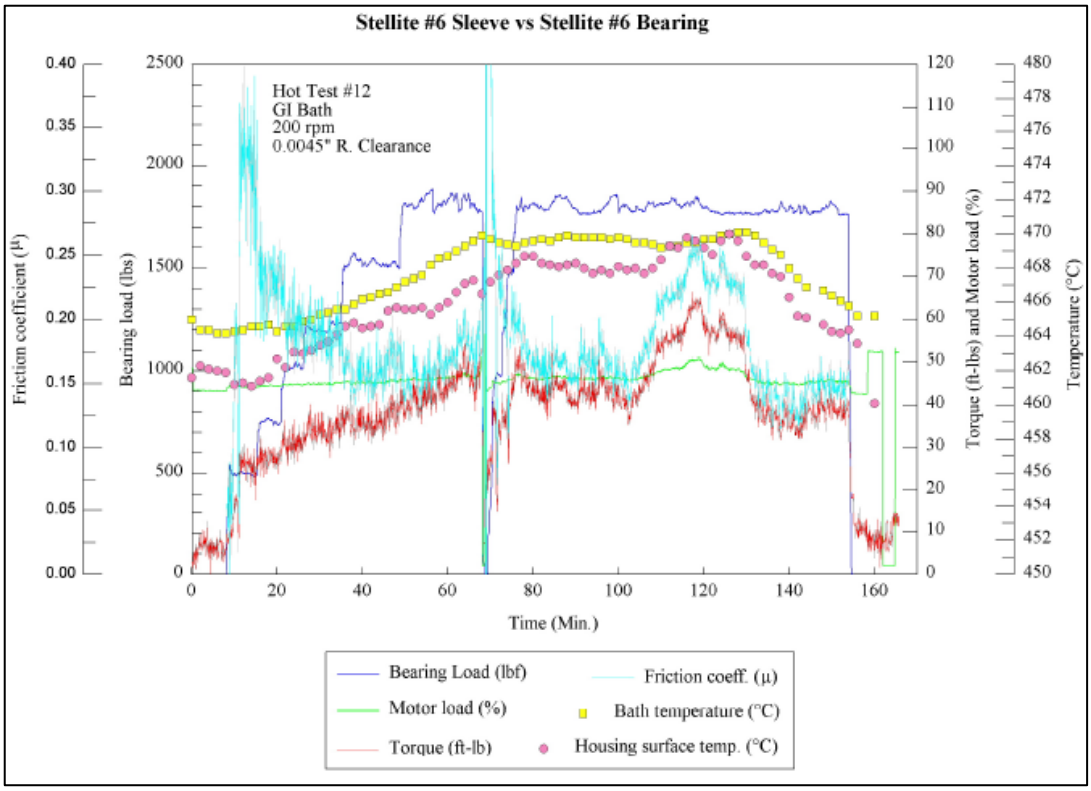

Figure 4-16: Example Output data from Teck Cominco Bearing Tester Showing Results of Stellite#6 on Stellite#6 Test Combination [reprinted with permission from The International Lead Zinc Research Organization, Ref. 39]

Figure 4-17: Stellite#6 Bearing (Rotating) Sleeve Following Wear Test (Data Shown above) [reprinted with permission from The International Lead Zinc Research Organization, Ref. 39]

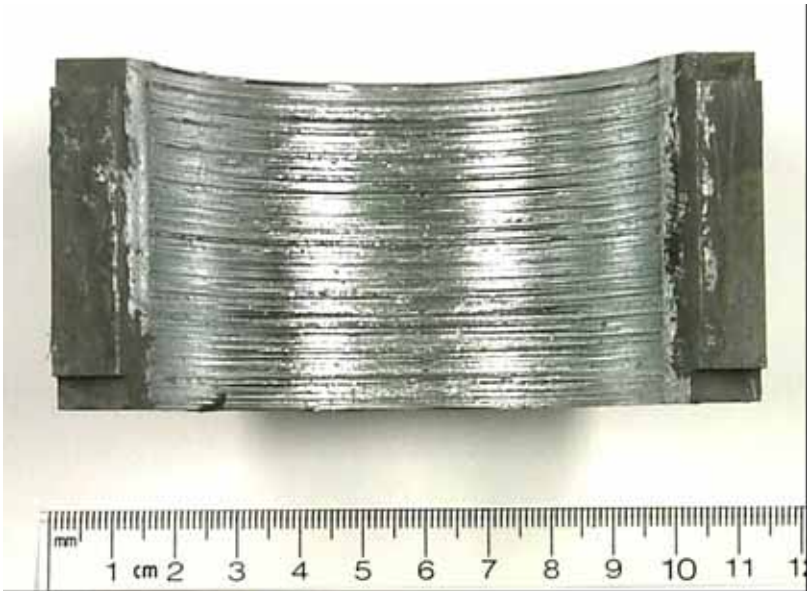

Figure 4-18: Stellite#6 Bushing (Static) Following Wear Test (Data Shown above) [reprinted with permission from The International Lead Zinc Research Organization, Ref. 39]

By employing this full-scale bearing tester, Teck Cominco was able to run tests using numerous different materials under a range of operating conditions. (The results of these tests have been widely published; Refs. 40 – 46, 48 – 49, 53) Moreover, subsequent analysis revealed a great deal about galvanizing bearings that had not been previously understood, especially with respect to the metallurgical response of the bearing materials in such an aggressive application. In general, "microstructural examination after testing revealed two principal wear mechanisms: abrasive wear and delamination wear, or surface fatigue. Zinc attack aggravated each of these mechanisms by creating intermetallics that accelerated abrasive wear, or creating brittle surface wear that increased delamination wear."

Furthermore, one of the most profound conclusions that Teck Cominco determined was that "the cobalt-based superalloys reacted with zinc and produced abrasive intermetallic particles." "Cobalt-based aluminides, transformed from wear debris and then attached and built up on the contact surfaces, are believed to be the main cause of the heavy wear grooves on the contact surfaces of the Stellite bearings, although dross particles could also play a role."

As a beneficial consequence of the thorough testing that was performed at Teck Cominco, the importance of the corrosion resistance of the hardware materials in industrial galvanizing applications was becoming enlightened. The researchers at Teck Cominco were beginning to recognize that the material corrosion attributes were one of the primary driving forces to pot hardware life. Hence, expanded focus was directed towards the understanding of reactions of iron- and cobalt-based alloys in Zn-Al baths,

especially with regards to how metallurgical modifications to the substrate surface contribute to accumulation of intermetallic dross particles on galvanizing pot hardware.

From the published research by Zhang, et al. at Teck Cominco [Refs. 47, 50 - 52], the diffusion characteristics of four different alloys (see Table 4-3) exposed to a Zn-0.22%Al bath at 470°C were observed. The change in reaction layer of Stellite 6 for up to one week immersion [Figure 4-19(a-d)] and the analogous change in 316L stainless steel [Figure 4-20(a-c)] were studied. Accordingly, further testing displayed the change in reaction layer for Norem 02 and Stellite 712PM, Figures 4-21 and 4-22 respectively, between one hour and one week exposure.

Table 4-3: Composition (wt%) of Corrosion Alloy Samples [Ref. 47]

element	316L (typ.)	Stellite 6	Stellite 712PM	Norem 02
C	0.03	1.2	2.0	1.2
Mn	1.5	0.8	1.0	4.5
Si	1.5	1.3	1.3	3.3
Cr	18.0	29.0	29.0	25.0
Mo	2.5	-	8.0	2.0
Co	-	59.3	53.3	4.0
Ni	10.0	1.8	2.7	-
Fe	66.47	1.8	2.7	60.0
W	-	4.8	-	-

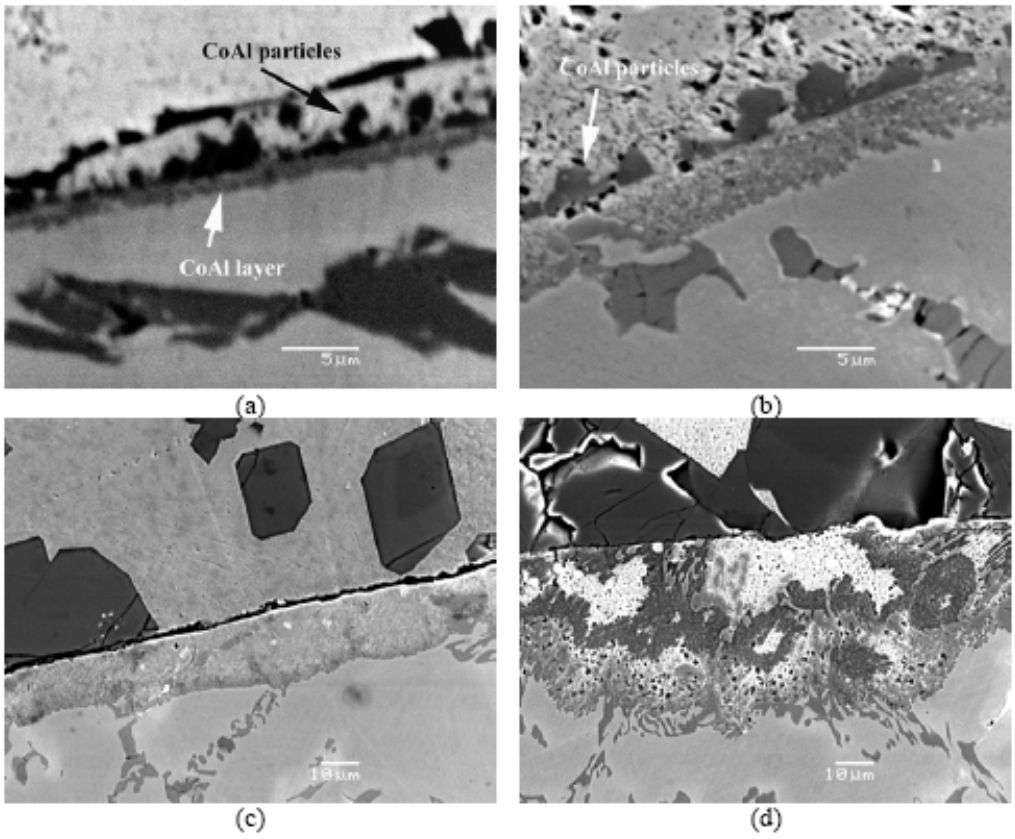

Figure 4-19: Cross-sectional views of Stellite 6 samples immersed in Zn-0.22%Al at 470°C for various lengths of time: (a) 1 hour; (b) 4 hours; (c) 24 hours; and (d) 168 hours [reprinted with permission from The Galvanizer's Association, Ref. 47]

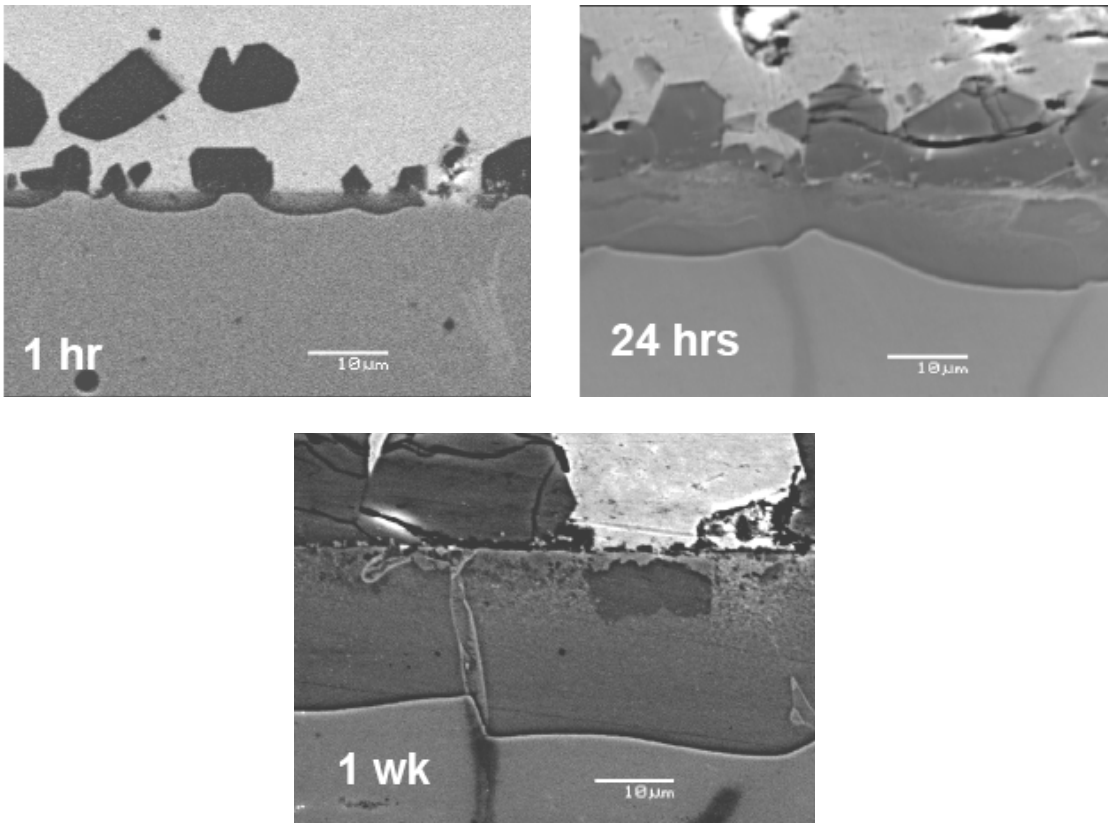

Figure 4-20: Cross-sectional views of 316L Stainless Steel samples immersed in Zn-0.22%Al at 470°C for various lengths of time: (a) 1 hour; (b) 24 hours; and (c) 168 hours [reprinted with permission from The International Lead Zinc Research Organization, Ref. 52]

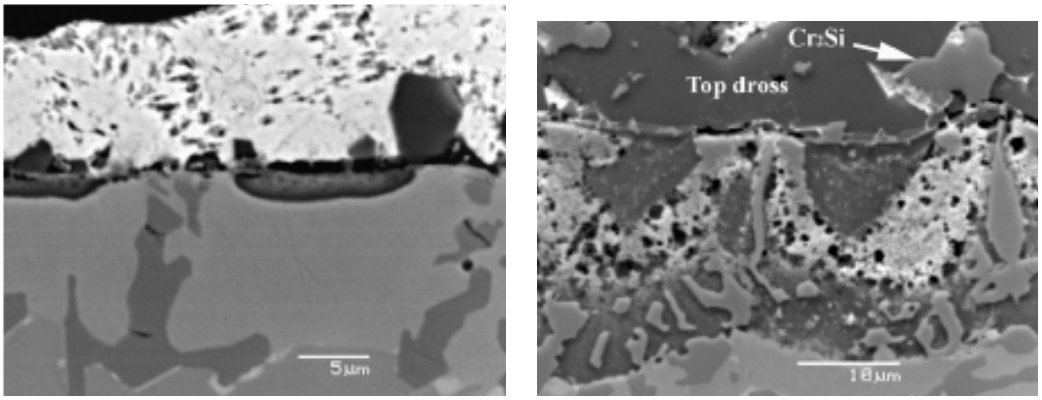

(a) (b)

Figure 4-21: Cross-sectional views of Norem 02 samples immersed in Zn-0.22%Al at 470°C for various lengths of time: (a) 1 hour; and (b) 168 hours [reprinted with permission from The Association for Iron and Steel Technology, Ref. 50]

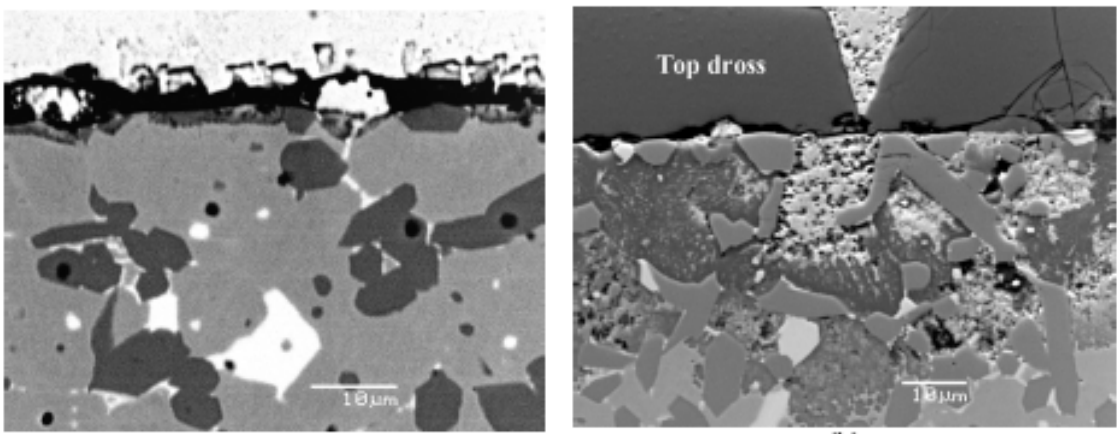

(a) (b)

Figure 4-22: Cross-sectional views of Stellite 712PM samples immersed in Zn-0.22%Al at 470°C for various lengths of time: (a) 1 hour; and (b) 168 hours [reprinted with permission from The Association for Iron and Steel Technology, Ref. 50]

Extracting the reaction depths from these micrographs, the diffusion rates of these four alloys after exposure to a Zn-0.22%Al bath at 470°C may be compared (Figure 4-23). The two cobalt-based alloys (Stellite 6 and Stellite 712PM) reacted similarly in the early stages of testing (< 1 day), but then the diffusion layer in the Stellite 712PM began to develop much more rapidly. On the other hand, the two iron-based alloys (316L stainless and Norem 02) maintained a proportional diffusion rate over the duration of the one-week test. Overall, the iron-based alloys displayed a lower diffusion rate than the cobalt alloys.

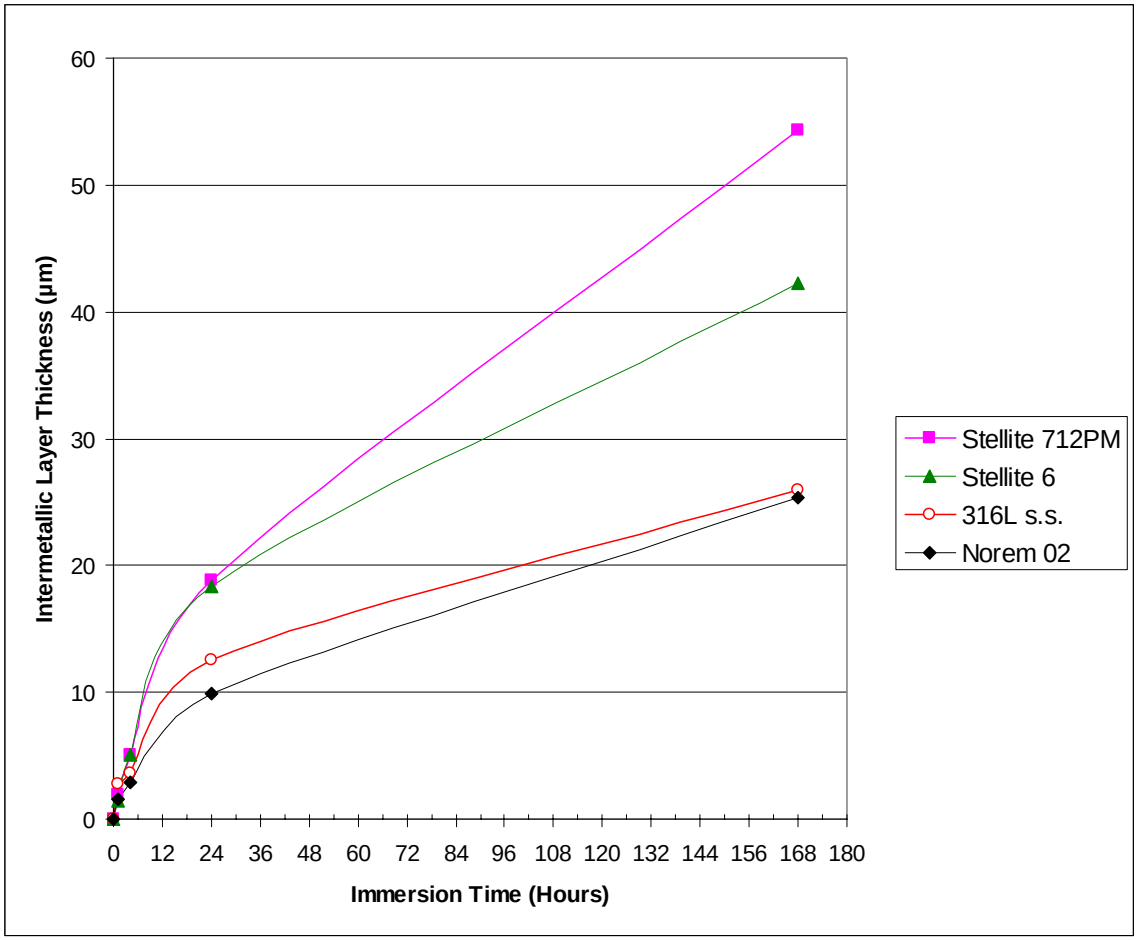

Figure 4-23: Reaction Layer Thickness of Several Samples after immersion in Zn-0.22%Al at 470°C [reproduced from Ref. 49]

Similarly, utilizing SEM/EDS analysis, the diffusion reactions may be observed (see Figures 4-24, 4-25 and 4-26) for 316L stainless steel at increasing concentrations of aluminum (0.129%, 0.152% and 0.226%) in the zinc bath (after 7 days immersion) [Ref. 52].

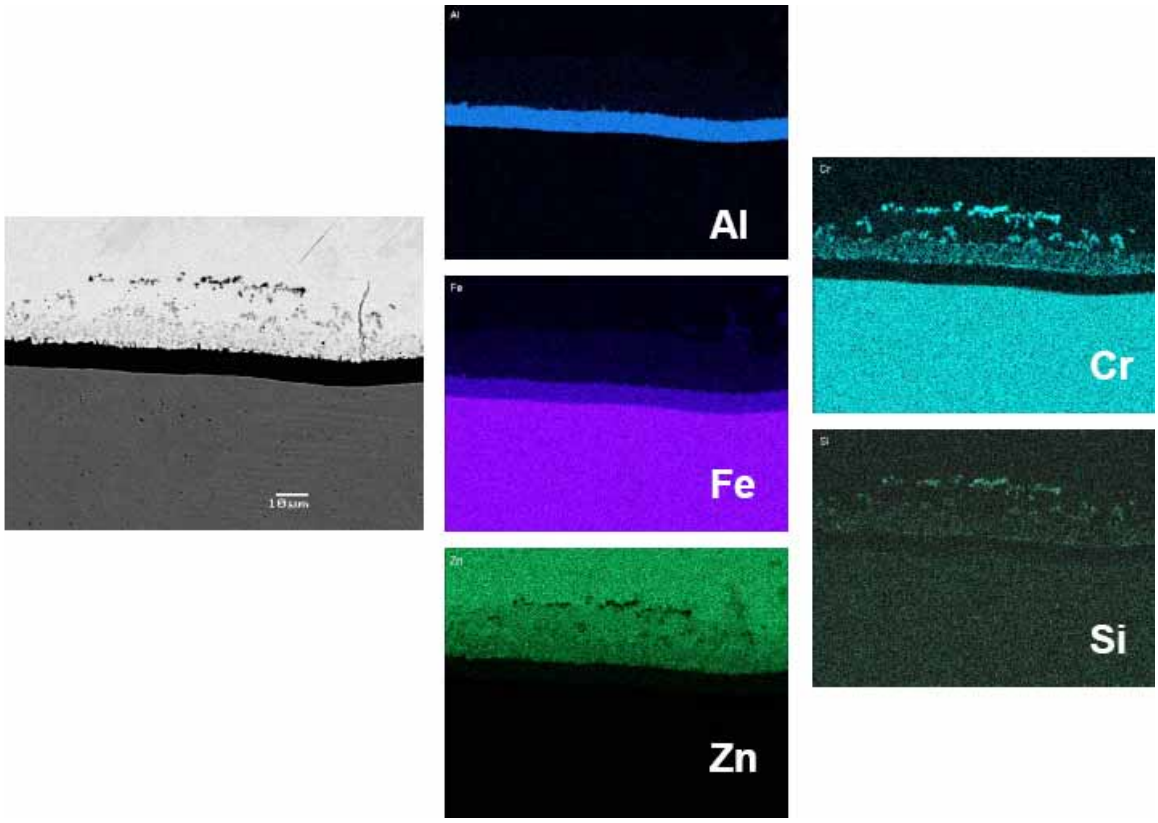

Figure 4-24: Cross-sectional views of 316L Stainless Steel samples immersed in Zn-0.129%Al at 465°C for 168 hours (SEM/EDS Mapping) [reprinted with permission from The International Lead Zinc Research Organization, Ref. 52]

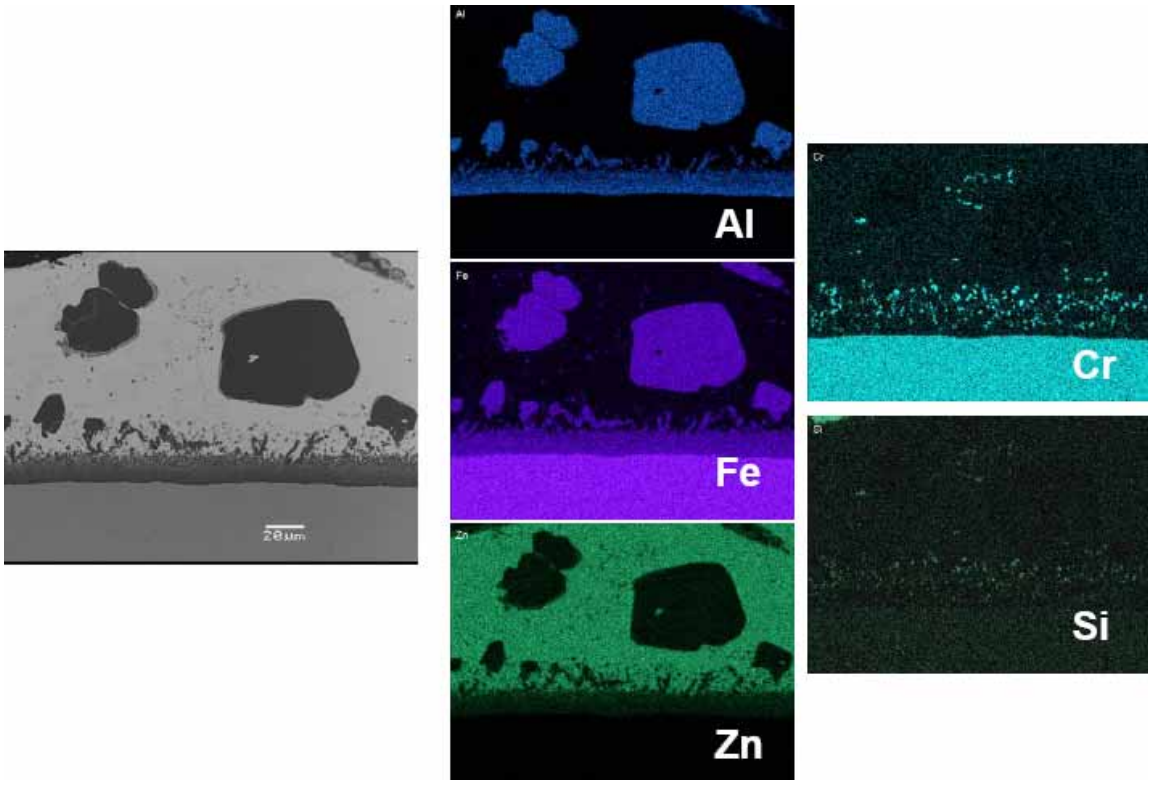

Figure 4-25: Cross-sectional views of 316L Stainless Steel samples immersed in Zn-0.152%Al at 490°C for 168 hours (SEM/EDS Mapping) [reprinted with permission from The International Lead Zinc Research Organization, Ref. 52]

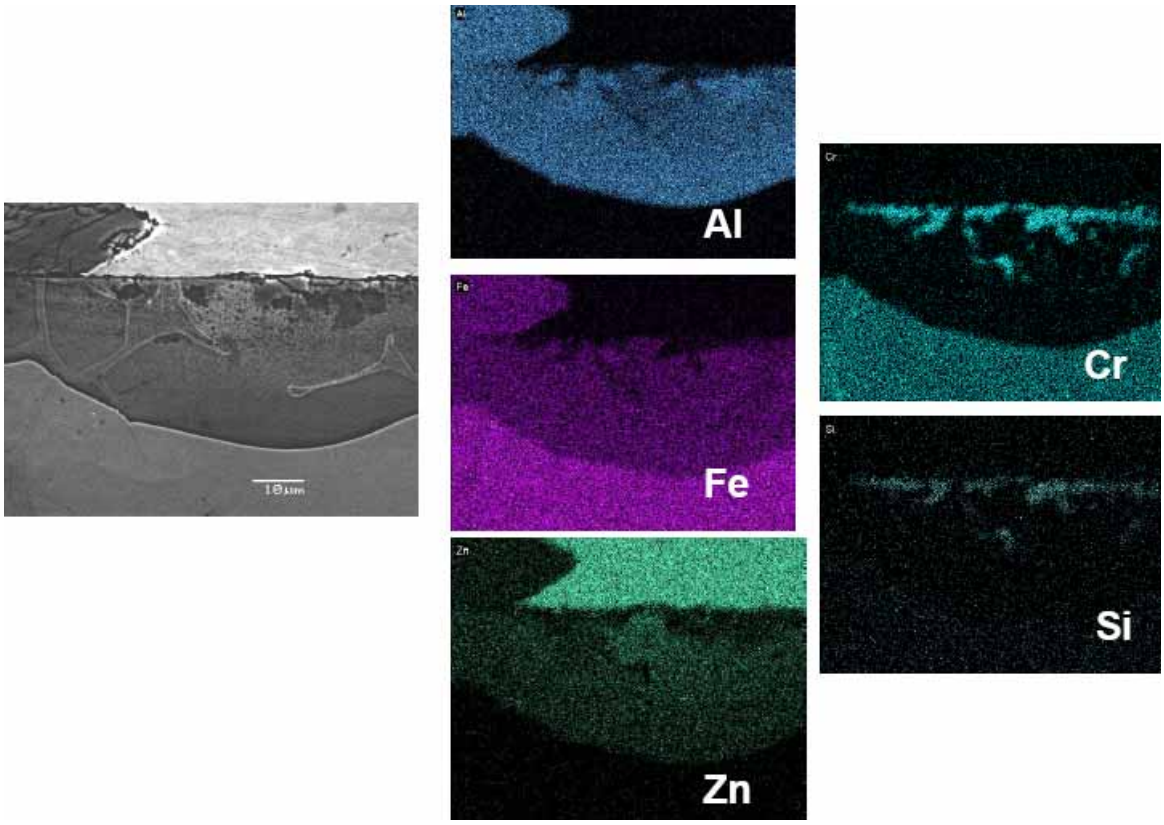

Figure 4-26: Cross-sectional views of 316L Stainless Steel samples immersed in Zn-0.226%Al at 470°C for 168 hours (SEM/EDS Mapping) [reprinted with permission from The International Lead Zinc Research Organization, Ref. 52]

Hence, from these micrographs the approximate change in reaction layer thickness may be measured (see Figure 4-27). With the limited data available, a linear dependence may be presumed with increasing aluminum levels providing advanced diffusion rates in the 316L stainless steel. In addition, the micrograph details of the elemental mapping show definitively that the aluminum penetrates into the surface of the stainless steel, reacting with the iron to (probably) form a Fe_2Al_5 structure and shedding chromium and nickel into the liquid zinc in the process.

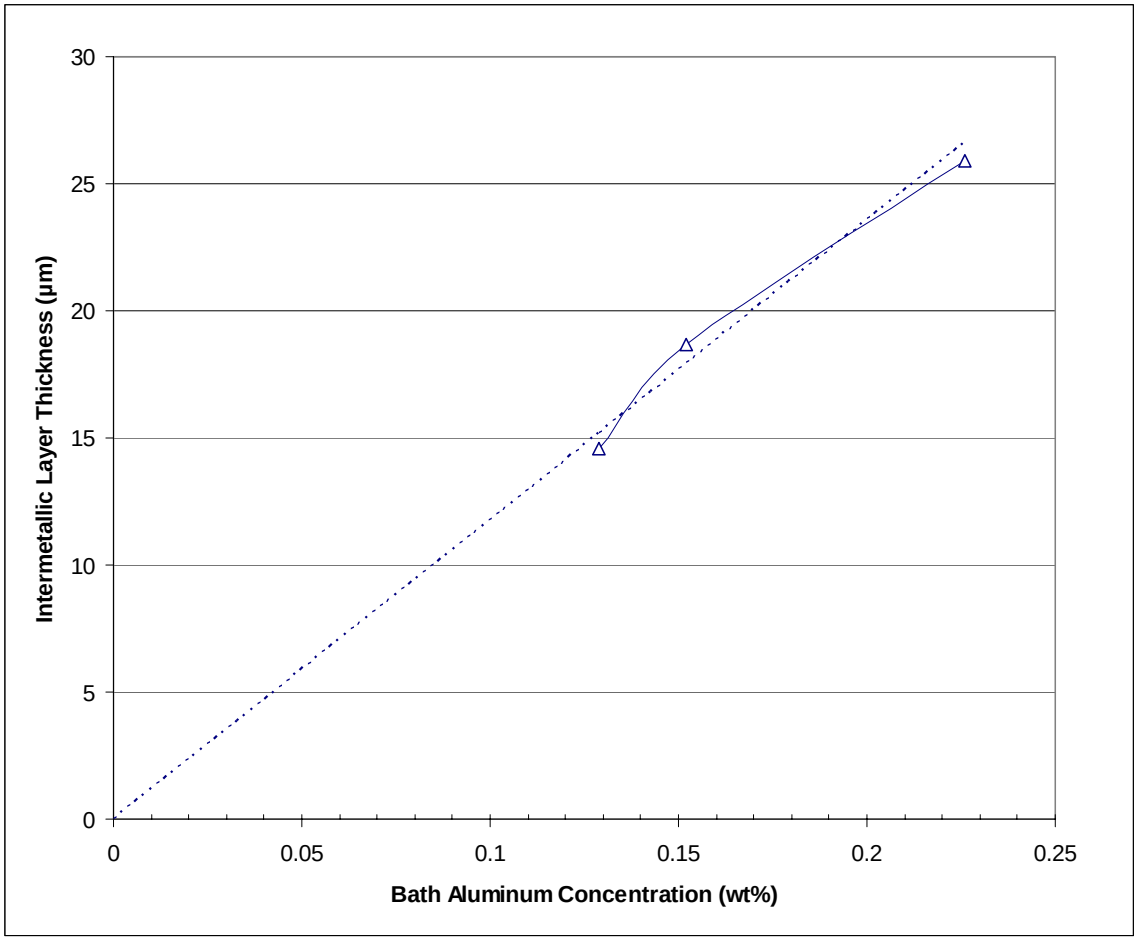

Figure 4-27: Reaction Layer Thickness on 316L Stainless Steel after 168 hours in Molten Zinc with increasing Aluminum Concentration [data extracted from Ref. 52]

Overall, this work by Zhang, et al. at Teck Cominco has been and continues to be the leading edge of knowledge acquisition in the area of understanding corrosion aspects of structural materials (standard materials, as well as iron- and cobalt-based superalloys) in industrial galvanizing baths.

Continuing, in the Spring of 2001, the U.S. Department of Energy – Office of Industrial Technologies awarded a development contract to an expansive collaboration of industry participants and research organizations to investigate ways of extending the life of pot hardware in steel mill continuous galvanizing lines. [Refs. 54 - 77] The goal of this project was "to result in extension of component life by a factor of 10 with estimated

savings of 2 trillion BTU/year and cost savings of up to $46 million/year for the 57 galvanizing lines operating in the U.S.". The research efforts for this project were carried out at West Virginia University (WVU) and Oak Ridge National Laboratory (ORNL) with technical (and financial) support from the International Lead Zinc Research Organization (ILZRO) and industrial sponsorship from at least 18 steel companies and component suppliers. The research goals for this project were "to develop new bulk materials and surface treatments/coatings for life improvement of molten metal bath hardware and bearings in continuous hot-dip process". "Development of such new materials would allow (1) energy savings, (2) reduction of line downtime and yield loss, (3) improvement in overall sheet quality, (4) reduced cost of repair and replacement cost of corroded components, (5) environmental improvements, and (6) improved economics. In general, "ORNL was focused on the long-term effects of static and dynamic corrosion on the hardware", while "WVU was tasked to study wear of the bearing materials along with mechanisms of dross build-up on the roll surface". The four primary activity areas for this project were:

a. Lab-scale Corrosion Testing (ORNL)
b. In-plant Corrosion Testing (WVU)
c. Lab-scale Wear Testing (small scale) (WVU)
d. Prototype-scale Wear Testing (WVU)

Hence, through this combination of corrosion and wear testing in conjunction with thermodynamic and material modeling, viable materials which would exceed the "magnitude improvement in material performance" could be determined. (Note: The results of the wear testing will not be discussed at this time but may reviewed in published literature. [Refs. 72-74, 76-77])

For the lab-scale static corrosion testing, ORNL devised a test procedure where a sample (12mm x 12mm x 6mm) of a selected material was immersed in a bath of Zn-Al alloy (Zn-0.16%Al-0.013%Fe) at 465°C and following intermittent time intervals the sample was removed, cleaned and weighed. The accumulated mass loss after 500 hours was then calculated. This test was repeated for a vast array of different iron- and cobalt-based alloys. (The chemical compositions of some of the materials used in this study are provided in Tables 4-4 and 4-5.)

Table 4-4: Compositions (wt%) of Corrosion Testing Alloys [Ref. 71]

element	A2	D2	316L (typ.)	Stellite 6	Tribaloy 800
C	0.95-1.05	1.40-1.60	0.03	1.2	0.1
Mn	0.75	1.00	1.50	1.0	-
P	0.03	0.03	0.04	-	-
S	0.03	0.03	0.04	-	-
Si	1.50	1.50	1.50	1.4	3.4
Cr	4.75-5.50	11.00-13.00	17.0-21.0	29.0	18.0
Mo	0.50-1.00	0.70-1.20	2.0-3.0	0.8	28.0
V	0.20-0.50	0.40-1.00	-	-	-
Co	-	0.70-1.00	-	58.1	49.5
Ni	-	-	9.0-13.0	2.0	1.0
Fe	-	-	-	2.0	-
W	-	-	-	4.5	-

Table 4-5: Compositions (wt%) of Alloys Developed at ORNL [Ref. 71]

	Alloy Designation (wt%)				
element	ORNL 4	ORNL 4-1	ORNL 4-2	ORNL 4-3	ORNL 4-4
Fe	74.78	74.58	72.58	70.68	62.68
Cr	20.00	20.00	20.00	20.00	30.00
Al	4.50	4.50	6.50	8.50	6.50
Ti	0.50	0.50	0.50	0.50	0.50
Si	0.10	0.10	0.10	0.10	0.10
Mn	0.10	0.10	0.10	0.10	0.10
Cr	0.02	0.02	0.02	0.02	0.02
Y	0.00	0.20	0.20	0.20	0.20

Since 316L stainless steel is generally regarded as the standard material for pot hardware in continuous galvanizing lines, ORNL initially performed extensive dissolution testing on 316L to determine a baseline of comparison for subsequent material tests [Ref. 61].

The results of some of the preliminary tests that were performed on 316L are indicated in Figure 4-28 with Table 4-6 providing a description of each of the samples.

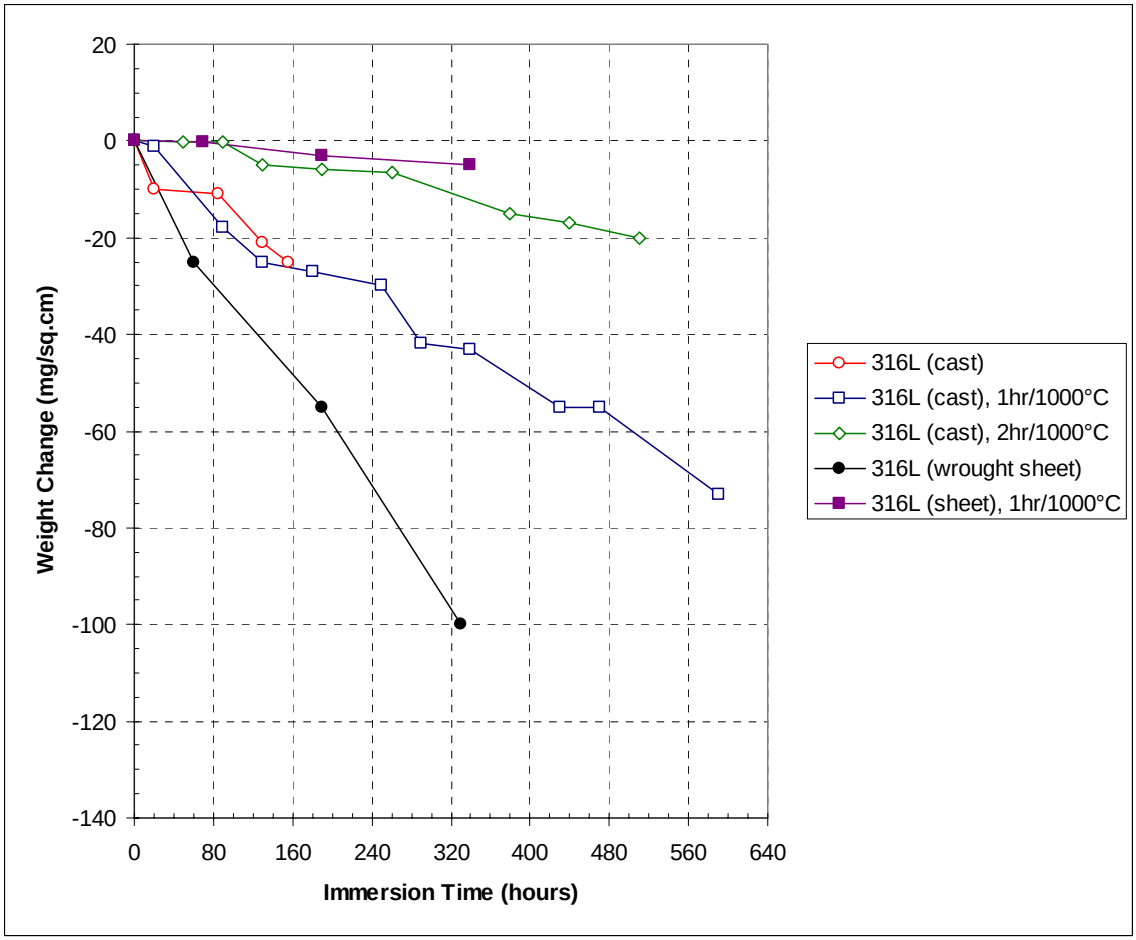

Figure 4-28: Static Corrosion Results of 316L Stainless Steel Samples immersed in Zn-0.16%Al at 465°C [reproduced from Ref. 61]

Table 4-6: Description of 316L Stainless steel static corrosion samples [Ref. 61]

Type	Material Condition
316L (cast)	section from a used cast stabilizer roll
316L (cast), 1hr/1000°C	same as above, but preoxidized in air at 1000°C for 1 hour
316L (cast), 2hr/1000°C	same as above, but preoxidized in air at 1000°C for 2 hours
316L (wrought sheet)	as-rolled sheet sample
316L (sheet), 1hr/1000°C	same as above, but preoxidized in air at 1000°C for 1 hour

From these results, it can be observed that oxidizing the surface does actually provide an increased resistance to zinc dissolution. However, from Figure 4-28 it is not entirely clear what baseline dissolution data should be used as the *standard* for 316L stainless. The 316L "cast" sample was harvested from an actual pot hardware component, but the dissolution testing was only run for 160 hours, making it difficult to extrapolate the data to 500 hours. Alternatively, the 316L "sheet" sample was run for much longer (330 hours), but the solubility rate was much higher than the "cast" sample. Meanwhile, although it was advertised [Ref. 61] that pre-oxidizing the 316L provided an increase in corrosion resistance, the level of improvement was different for the "cast" sample versus the "sheet" sample. Moreover, almost no background information was given for the 316L "cast" sample concerning chemical composition, historical thermal cycling and everything else (e.g. what was the carbon content in the 316L "cast" sample?). Thus, it is difficult to identify if this specific 316L sample is representative of typical galvanizing pot hardware materials. In other words, if 316L stainless was the baseline material for this research project, why was it not investigated more thoroughly?

Next, the dissolution rate of Stellite 6 was determined [Ref. 64] since Stellite 6 is the standard material employed for wear surfaces (i.e. bearings) in many continuous galvanizing pots. The time-rate of change of dissolution of the Stellite 6 compared to the aforementioned 316L stainless samples is shown in Figure 4-29. This data indicates that the corrosion rate of the Stellite 6 is quite similar to (but slightly less than) that of the baseline 316L "cast" sample.

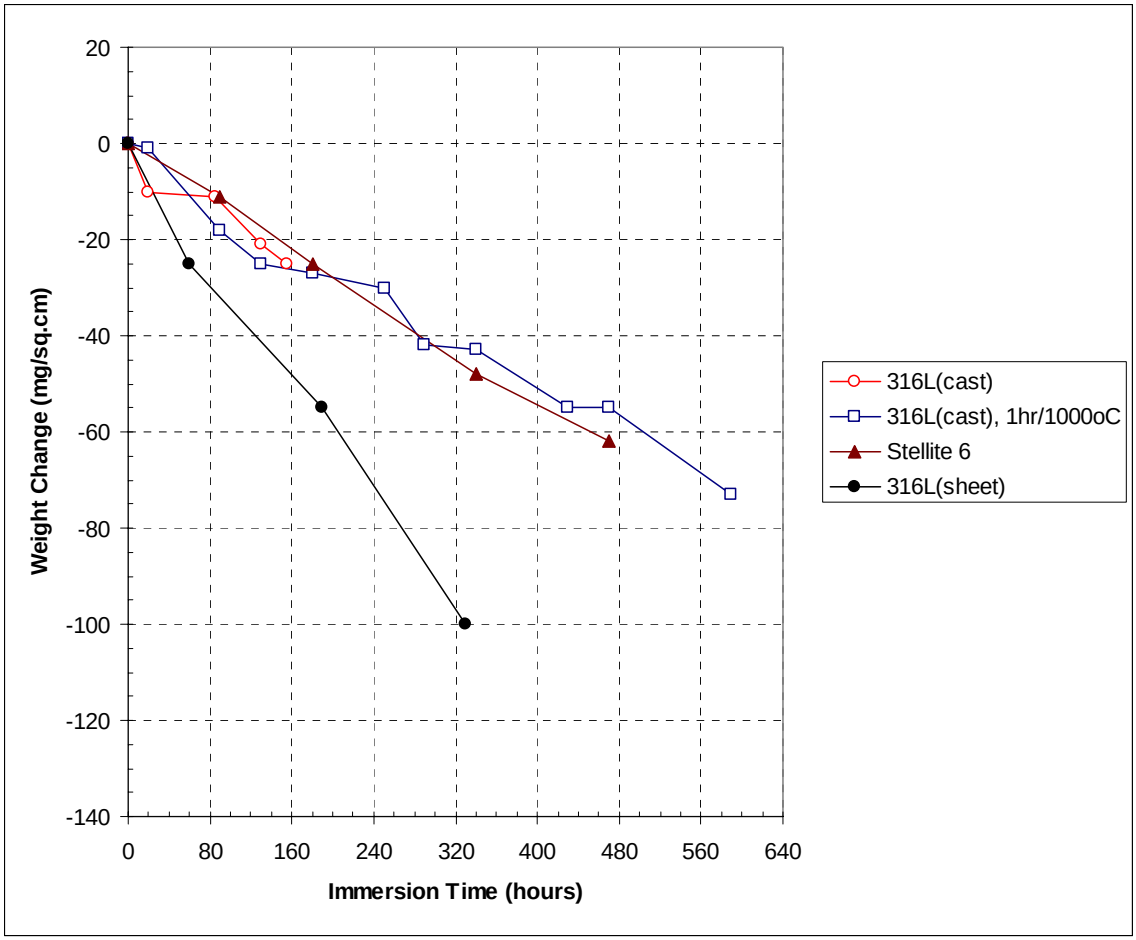

Figure 4-29: Static Corrosion Results of Stellite 6 samples immersed in Zn-0.16%Al at 465°C [reproduced from Ref. 64]

After performing analogous dissolution tests on numerous different metallic samples, the corrosion rate of each material was compared to determine the magnitude of improvement over the selected 316L stainless data. Since this project was looking for a ten times improvement in corrosion resistance compared with 316L, the results (Figure 4-30) provided only three bulk alloys meeting this criteria. MSA2012 and MSA2020 are carbide-rich ferrous alloys produced by Metaullics Systems of Solon, Ohio, while Tribaloy 800 is a cobalt-based superalloy manufactured by Deloro-Stellite. It should also be noted that several surface treatments and cladding materials (e.g. 80W-20Mo weld overlay) provided a significant life improvement over 316L stainless. At the same time it

is surprising that the Alloy 4-x series of alloys developed by ORNL did not provide much improvement over 316L unless these alloys were preoxidized (as described previously) prior to corrosion testing (see Figure 4-31). Nevertheless, this research performed at Oak Ridge National Laboratory offered a reasonable snapshot as to the supposed ranking of the corrosion resistance in molten Zn-0.16%Al at 465°C of a large matrix of materials.

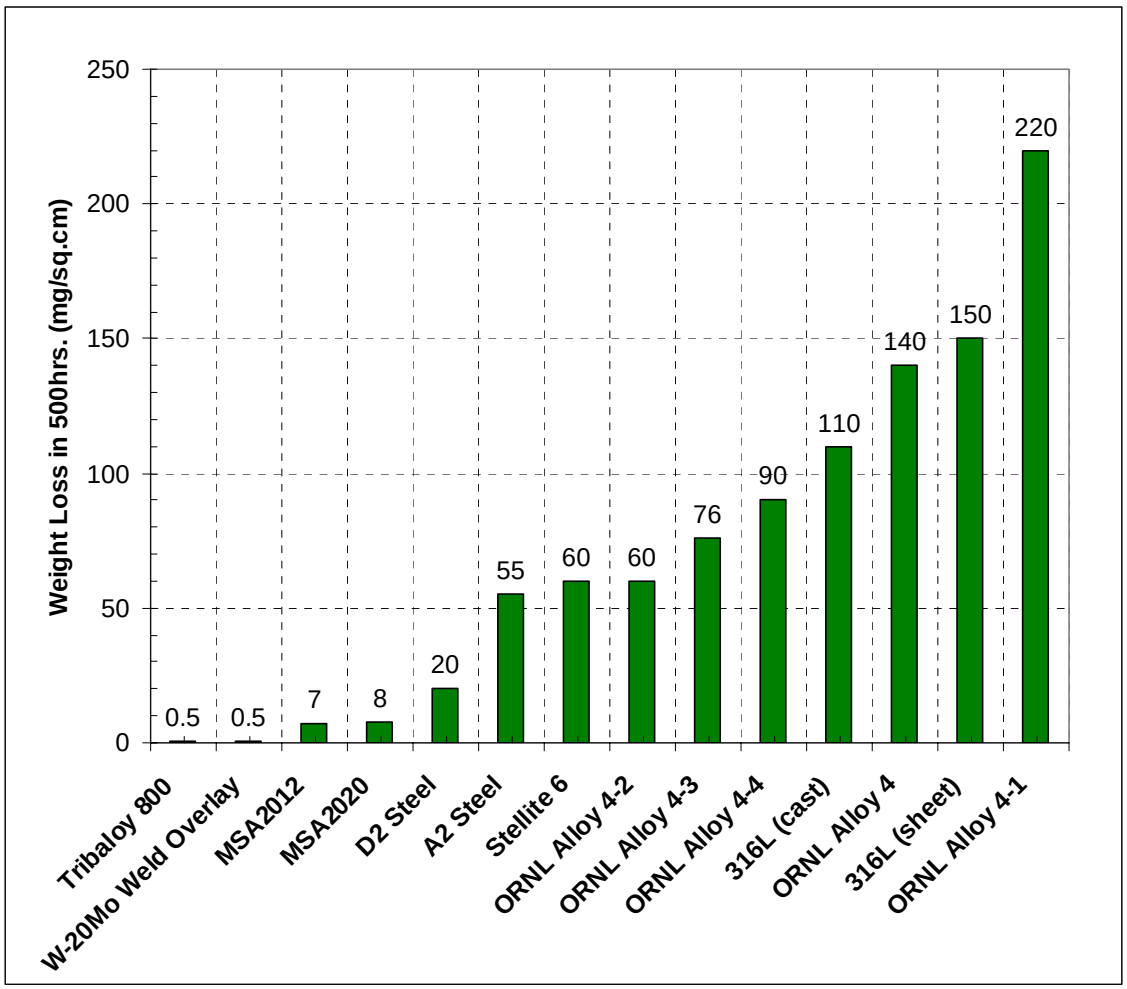

Figure 4-30: Metallic sample results of 500 Hour Static Corrosion in Zn-0.16%Al at 465°C [reproduced from Ref. 71]

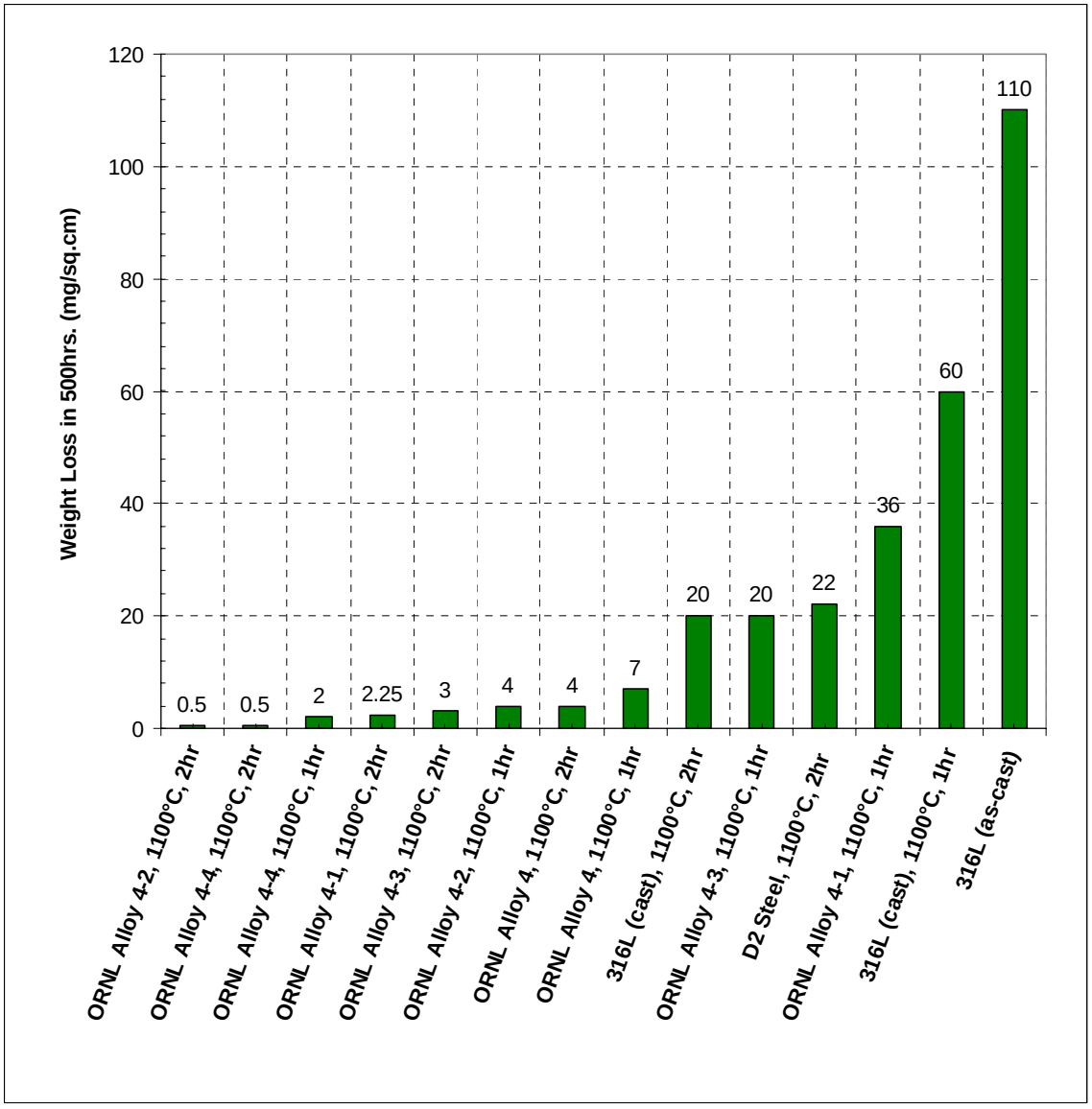

Figure 4-31: Pre-oxidized sample results of 500 Hour Static Corrosion in Zn-0.16%Al at 465°C [reproduced from Ref. 71]

Concurrently, in-plant testing was performed by suspending bar samples (304.8mm x 25.4mm x 6.4mm) of several materials in actual industrial galvanizing pots and then subsequently removing the samples at given time intervals for return to West Virginia University for analysis. An illustration of some of the results taken from these samples is presented in Figure 4-32. Note that the corrosion rate here indicates the average representative loss of a material from a given exposed surface of the sample.

The first data for 316L (cast) and Stellite 6 were taken from galvanizing pots (GI) with typical aluminum concentrations of 0.13% to 0.16% while the remainder of the data displayed in Figure 4-32 are for specimens immersed in Galvalume (55% Al) coating baths. Hence, it can easily be observed that a Zn-55%Al bath is appreciably more aggressive than a Zn-0.16%Al bath.

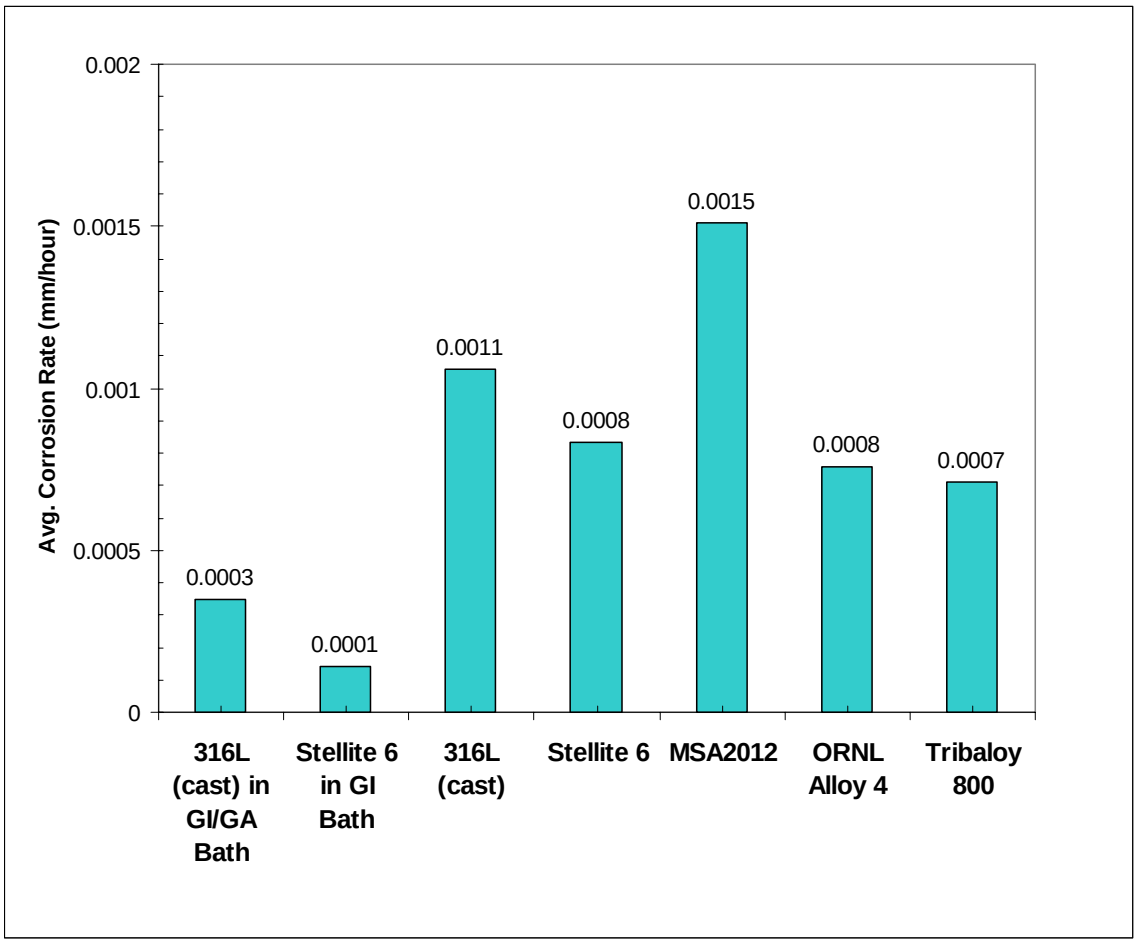

Figure 4-32: Average corrosion rate of metallic samples in industrial Galvalume (Zn-55%Al) baths [reproduced from Ref. 63]

In conjunction with this, Liu, et al. at WVU performed a series of SEM/EDS analyses on the corroded samples to observe the diffusion aspects of the reaction process. As observed in Figure 4-33(a-c), aluminum diffuses into the face of Stellite 6 more

rapidly at increasing aluminum concentrations in the zinc from 0.13%Al in Galvanneal (GA) and 0.16%Al in Galvanize (GI) to 55%Al in Galvalume (GL).

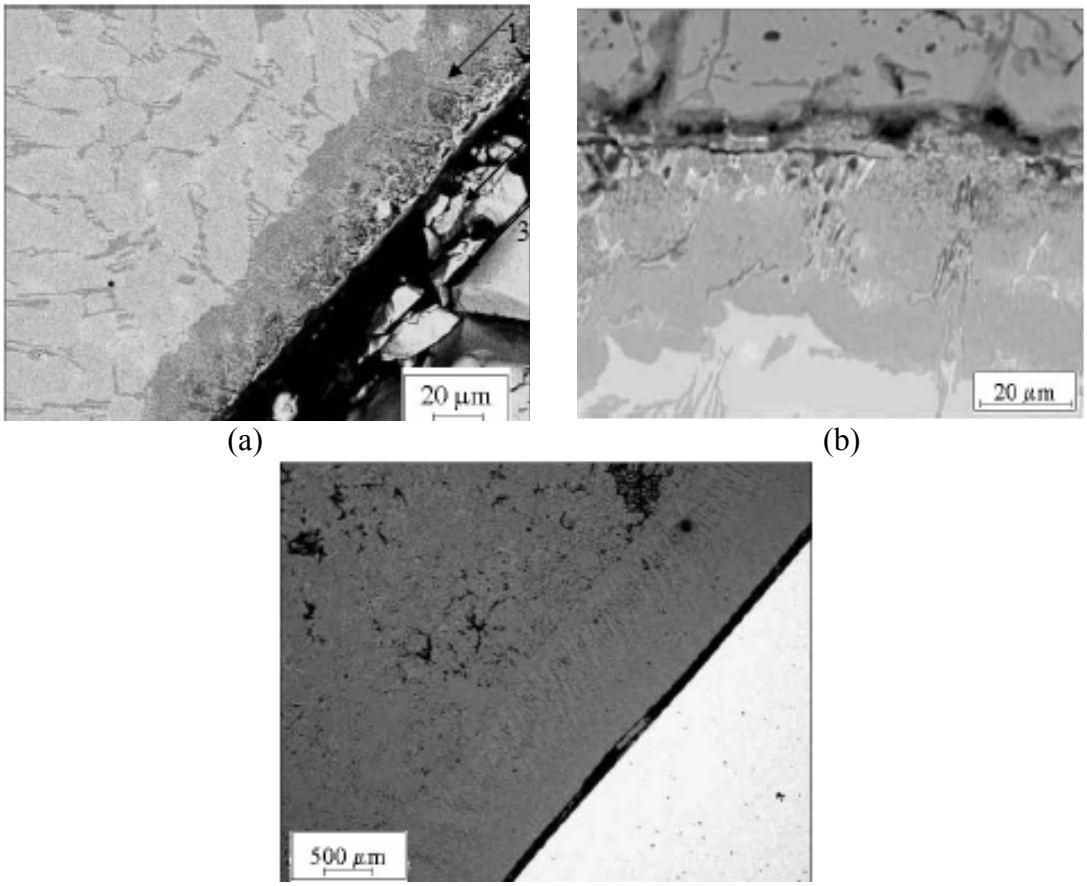

(a) (b)

(c)

Figure 4-33: Micrographs (SEM/BSI) of Stellite 6 samples after immersion in three different zinc baths: (a) GA bath for 6 weeks, (b) GI bath for 2 weeks, and (c) GL bath for 4 weeks [reprinted with permission from The Association for Iron and Steel Technology, Ref. 75]

The elemental analysis (Figure 4-34 (a and b)) confirms that the reaction layer is aluminum-based. As expected, the GL bath (Galvalume) with 55% aluminum penetrated at a much higher diffusion rate (~ 250µm diffusion per week) into the face of the substrate than the low aluminum melts (e.g. GA = ~5µm diffusion per week).

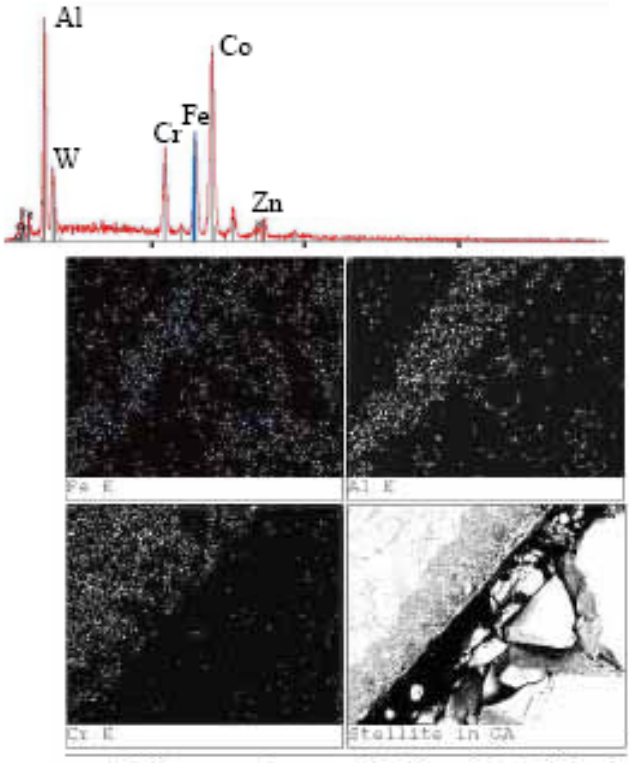

Figure 4-34: Elemental analysis and mapping of Stellite 6 sampleafter 6 weeks in GA bath [reprinted with permission from The Association for Iron and Steel Technology, Ref. 75]

As a result of this research, Liu, et al. at WVU have noted [Ref. 75] that dissolution of galvanizing bath hardware may not always occur at uniform degradation. Rather, non-homogeneous superalloys, such as Stellite 6, may develop selective corrosion where specific compounds and elements from the base material may disperse into a liquid Zn-Al bath at varying rates from the bulk of the material. Additionally, the composition of the molten Zn-Al (specifically the Al concentration) may accelerate this inconsistent metal solubility.

Hence, with this disclosure of selective corrosion, Liu, et al. question the validity of the typical method for evaluating galvanizing hardware materials, which is by comparing the weight loss of given materials after a designated time interval. They note

that the general assumption is that "the corrosion is a uniform dissolution process and that the lesser the material is lost, the better the corrosion resistance it offers". Therefore, it becomes obvious that just measuring the dissolution rate alone only provides half the picture. The diffusion reactions of pot hardware materials must also be considered in order to understand the full corrosion nature of the material in this aggressive liquid zinc environment.

In conjunction with this research of conventional pot hardware materials, West Virginia University and Oak Ridge National Laboratory also explored the possibility of utilizing iron-aluminide (Fe_3Al) intermetallic materials in galvanizing applications [Refs. 78-79].

First, a series of 24-hour static laboratory experiments were performed immersing Fe_3Al intermetallic samples (along with 316L stainless steel specimens, as a baseline) (Table 4-7) in four different molten metal baths of varying aluminum concentration (see Table 4-8) at temperatures from 460°C to 660°C.

Table 4-7: Compositions (wt%) of Corrosion Test Samples [Refs. 78-79]

element	316L	Fe_3Al
Fe	65.40	77.75
Al	-	15.83
Cr	17.00	5.45
Zr	-	0.96
C	0.03	0.01
Ni	12.00	-
Mo	2.50	-
Mn	2.00	-
Si	1.00	-
P	0.05	-
S	0.03	-

Table 4-8: Bath Composition (wt%) Utilized for Corrosion Testing [Refs. 78-79]

Bath	Zn%	Al%	Si%
Zinc	100	0	0
Zn-5Al	95	5	0
Zn-55Al	45	55	0
Al-8Si	0	92	8

Then, concurrently, 316L and Fe_3Al samples were placed in actual industrial galvanizing baths (with chemistries analogous to Table 4-8) for up to 240 hours. However, it should be noted that the bath composition for the static laboratory test did not define any iron concentration in the bath while in an active metallic coating bath iron is prevalent at levels exceeding the saturation limit of that bath composition. Thus, it is not clearly identified whether the lab tests identically mimicked the industrial environment. (But for the sake of similitude it will be assumed that both molten baths were nearly identical.)

A representation of the responses observed from the on-line and laboratory (static) corrosion tests is provided in Figure 4-35. As expected, the degradation rates increased substantially at very high aluminum levels. Conversely, at low aluminum levels the dissolution process diminished slightly with increasing aluminum contents before eventually rising again at very high aluminum. Additional detail is presented in Figure 4-36 which displays a close-up view of the zinc-rich corner of Figure 4-35. This graph shows how, for both laboratory and industrial baths, the dissolution rates of bath materials decreased significantly between ~0% and 5% aluminum, dropping to nearly inconsequential corrosion levels.

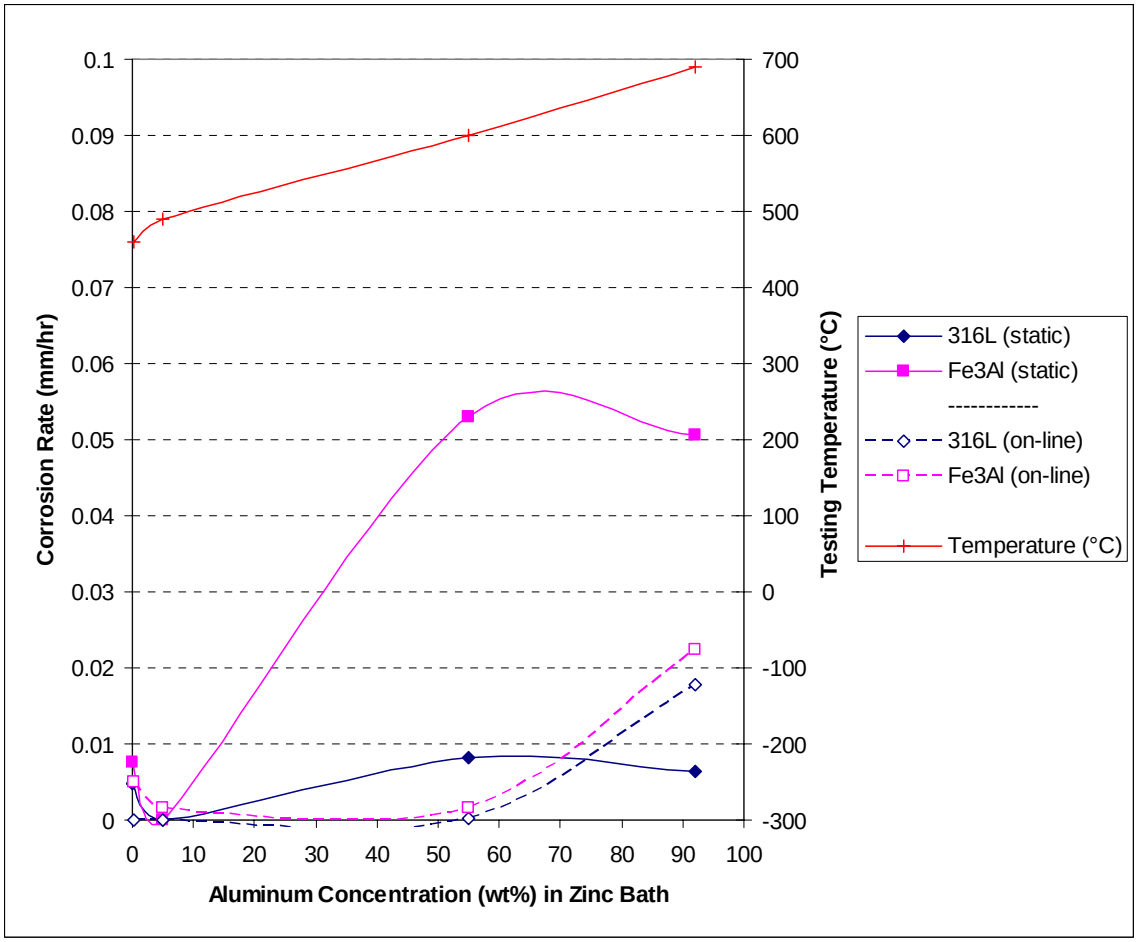

Figure 4-35: Comparison of static laboratory corrosion tests and industrial field tests (24 hours static tests; 240 hours on-line tests) [reproduced from Refs. 78-79]

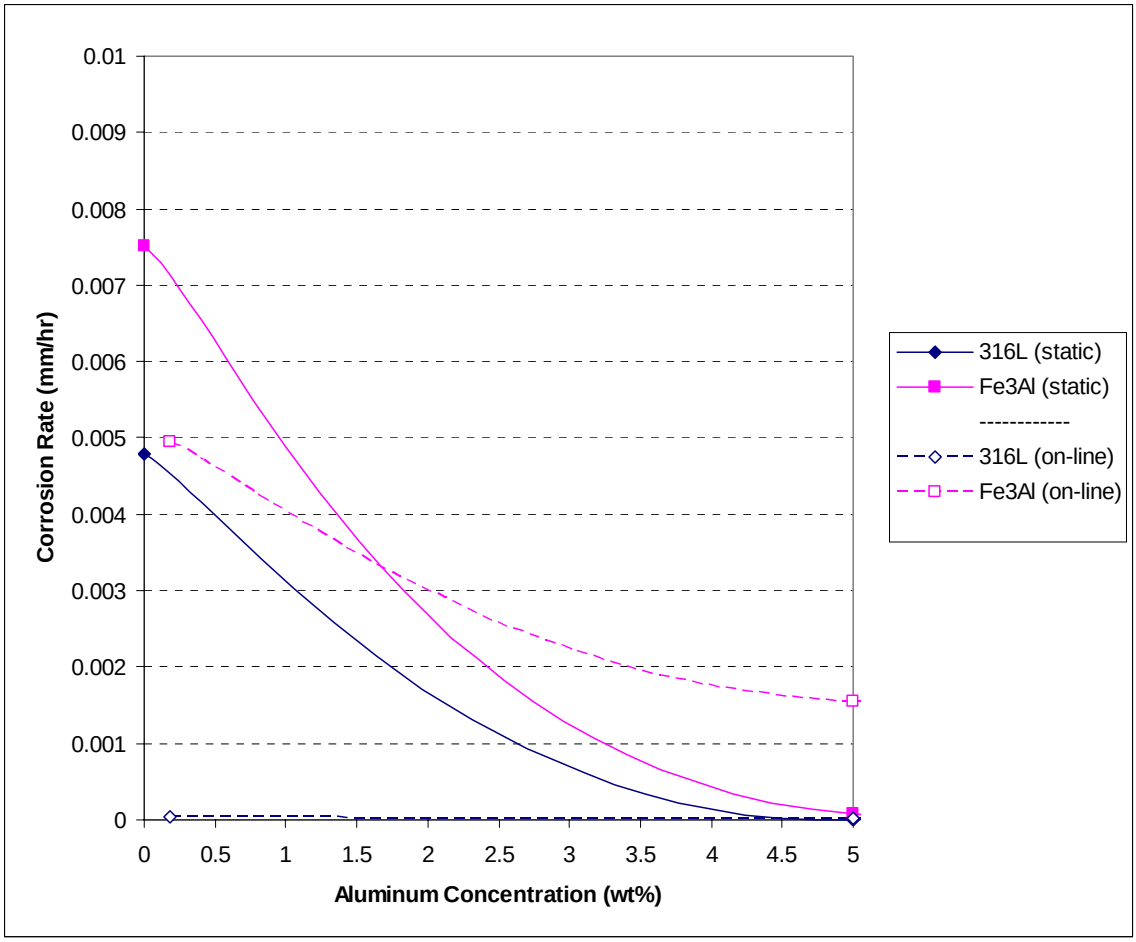

Figure 4-36: Enlarged view of lower Al% region of *Figure 4-35* [reproduced from Refs. 78-79]

In general the on-line industrial tests showed a considerable discrepancy from the corrosion rate in the static laboratory tests. This could possibly be due to the aforementioned issue of iron levels in the laboratory bath versus the industrial bath or it could be a result of variations in temperature between the two environments. Furthermore, if the bath composition (in the laboratory tests) is held constant for each sample the effect of increasing temperatures may be observed. As displayed in Figure 4-37, temperature did not play a significant role in changing the corrosion rate of 316L stainless at the 5% aluminum level and only had an impact in pure zinc at temperatures exceeding 560°C. Meanwhile, the reactions of Fe_3Al varied greatly with temperature and

did not react analogously when the aluminum content was increased from 0% to 5% either. (Based on these erratic results, industrial bath hardware constructed of Fe_3Al intermetallic material would probably not be advisable for use.)

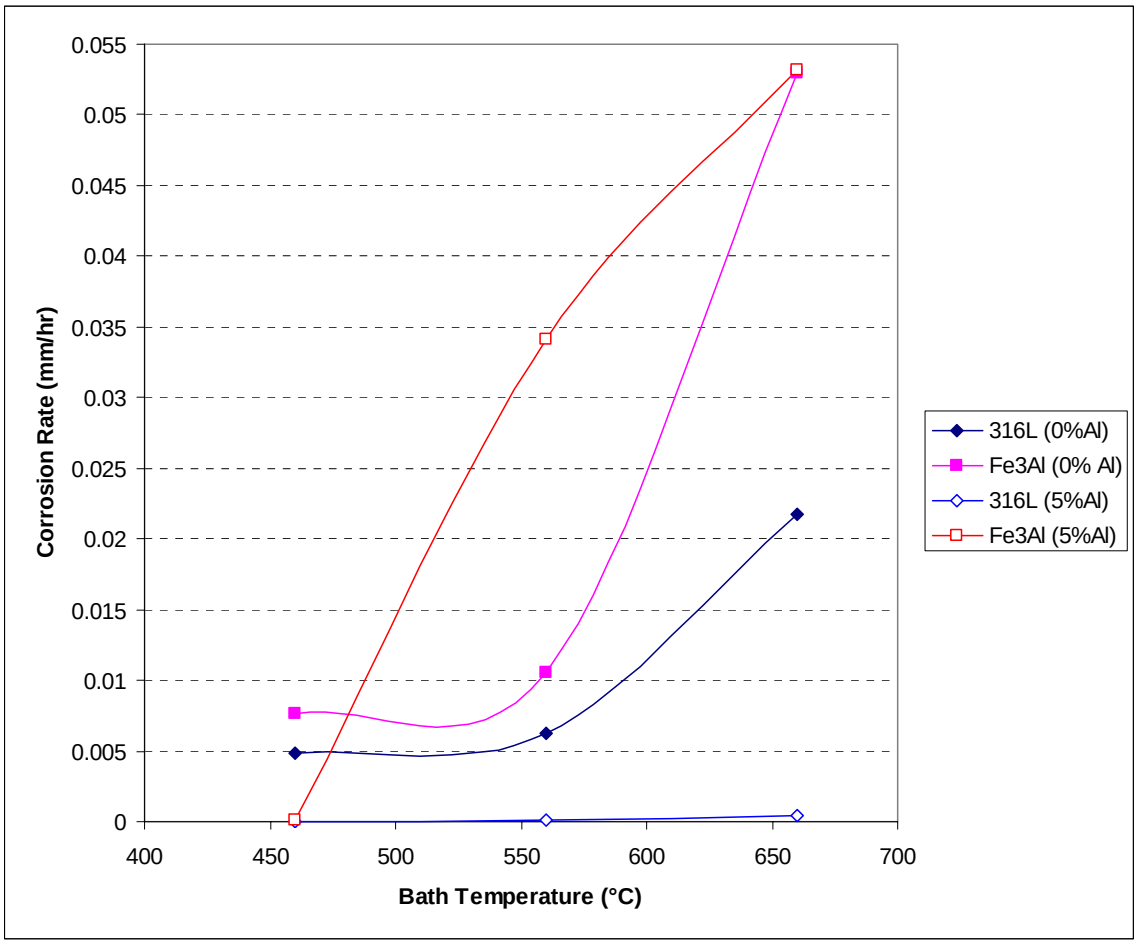

Figure 4-37: Results of 24 hour static corrosion test in zinc [reproduced from Refs. 78-79]

From these figures it is apparent that further research must be performed on corrosion of galvanizing hardware in molten zinc baths within the concentration range of 0% to 5% aluminum. Since this aluminum range encompasses the realm of most typical industrial zinc coating operations, a more complete understanding of the corrosion reaction mechanisms which occur in this typical galvanizing regime is needed.

Chapter 5: Methods and Materials

In the current project a series of experiments were undertaken to physically measure the dissolution rate of 316L stainless steel in molten zinc at increasing levels of aluminum starting with pure zinc. The composition of the 316L stainless samples used in this study is identified in Table 5-1.

Table 5-1: 316L Stainless Steel used in zinc corrosion testing

element	wt%
Fe	67.51
C	0.012
Si	0.40
Mn	1.39
S	0.029
P	0.024
Cr	17.55
Ni	10.74
Mo	2.05
Cu	0.257
N	0.0512

The experimental procedure for generating the 316L-zinc corrosion samples was as follows:

1) Corrosion samples (50.8mm long x 15.88mm dia.) and microscopy samples (15.88mm long x 15.88mm dia.) of 316L stainless steel were machined to precise dimensions (±0.04mm).
2) Clean, new, SHG-grade (99.99% pure) zinc (41kg) and the required amount of pure aluminum were weighed and melted in a silicon carbide crucible in an electric-resistance-heated kiln furnace. (Figures 5-1 and 5-2)

Figure 5-1: Electric-resistance-heated kiln furnace with silicon carbide crucible

Figure 5-2: Silicon carbide crucible containing molten zinc bath

3) Corrosion samples were weighed, measured and cleaned with acetone.
4) Zinc bath sample was taken at start of test.
5) Seven corrosion samples and three microscopy samples were immersed in the zinc bath.
6) At given time intervals, a corrosion sample and/or microscopy sample were removed from the zinc bath. In addition, a representative sample was taken from the molten bath. (Figure 5-3)

Figure 5-3: 316L stainless corrosion sample and microscopy sample after immersion in zinc

7) After all seven corrosion samples had been extracted, test specimens were prepared for analysis.
8) Zinc bath samples were subjected to Inductively Coupled Plasma (ICP) analysis to determine exact chemical composition.
9) Microscopy samples were preserved with the solidified zinc as-is then sectioned and polished for microstructural and elemental analysis by scanning electron microscope (SEM) with energy dispersive spectrometry (EDS).
10) Corrosion samples were pickled in a dilute (15%) HCl solution to remove the zinc coating. (Figure 5-4)
11) Corrosion samples were then weighed and measured to determine the weight loss and surface area reduction.

Figure 5-4: 316L stainless corrosion samples after pickling in a dilute (15%) HCl solution

Table 5-2: Zinc Corrosion Test Conditions

Test No.	Zinc Bath (starting) (wt%)			Set Temp. (°C)	Total Time (days)
	Al%	Fe%	Si%		
A1	0.002	0.090	0.036	500	6
A2	0.046	0.000	0.000	500	10
A3	0.117	0.004	0.172	500	10
A4	0.243	0.004	0.015	500	10
A5	0.492	0.003	0.000	500	10
A6	1.091	0.037	0.000	500	11
B1	0.025	0.003	0.000	520	12
B2	0.13	0.001	0.174	520	10
B3	0.26	0.005	0.172	520	10
B4	4.2	0.004	0.218	520	10

An array of corrosion tests (Table 5-2) were executed with 316L stainless steel in a zinc bath with varying concentrations of aluminum at two different temperatures (500°C and 520°C). Even though the typical temperature range for an industrial galvanizing bath is between 450°C and 480°C, these higher temperatures (500°C and 520°C) were utilized to accelerate the static testing.

Chapter 6: Dissolution

The utilization of 316L stainless steel in molten zinc galvanizing baths has become standard practice for structural hardware at most continuous coating facilities. Hence, a detailed understanding of the dissolution mechanisms of 316L in the molten zinc would provide the background for future solubility studies of more exotic hardware materials (such as cobalt- and nickel-based alloys).

Past investigations have indicated that a phenomenon exists where the dissolution rate of a metal substrate in liquid zinc is higher at extremely low aluminum concentrations (nearly 0% Al) and also at high aluminum concentrations while being reduced at aluminum concentrations in between. As noted previously in Figures 4-35 and 4-36, Liu, et al. identified a reduction in the dissolution rate of 316L stainless when the aluminum level in molten zinc was increased from 0 wt% to 5 wt% Al. The dissolution rate then increased for aluminum concentrations exceeding 50%. Similarly, Morando (in Figure 3-25) observed a rapidly increasing solubility once the aluminum level surpassed 50%. However, from both of these studies (and others), a minimum amount of detail exists describing the zinc corrosion reactions in the common galvanizing region of 0% to 5% aluminum.

6.1 Weight Loss Analysis

From the matrix of trials listed in Table 5-2, first, the bulk material loss of the iterative samples can be tracked. The 316L stainless steel reactions at 500°C in six different zinc baths with aluminum concentrations ranging from nearly zero percent to approximately 1wt% aluminum may be observed in Figure 6-1. Similarly, the analogous reactions at 520°C can be seen in Figure 6-2.

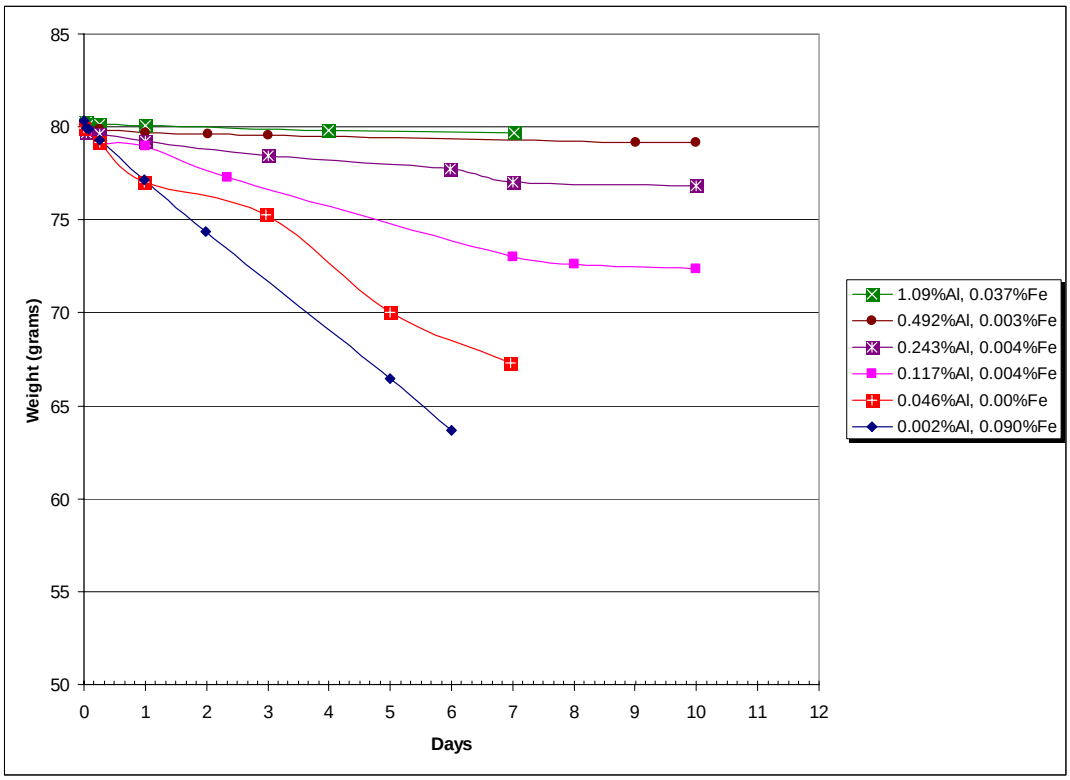

Figure 6-1: Weight Loss of 316L Stainless Steel Samples in Molten Zinc at 500°C

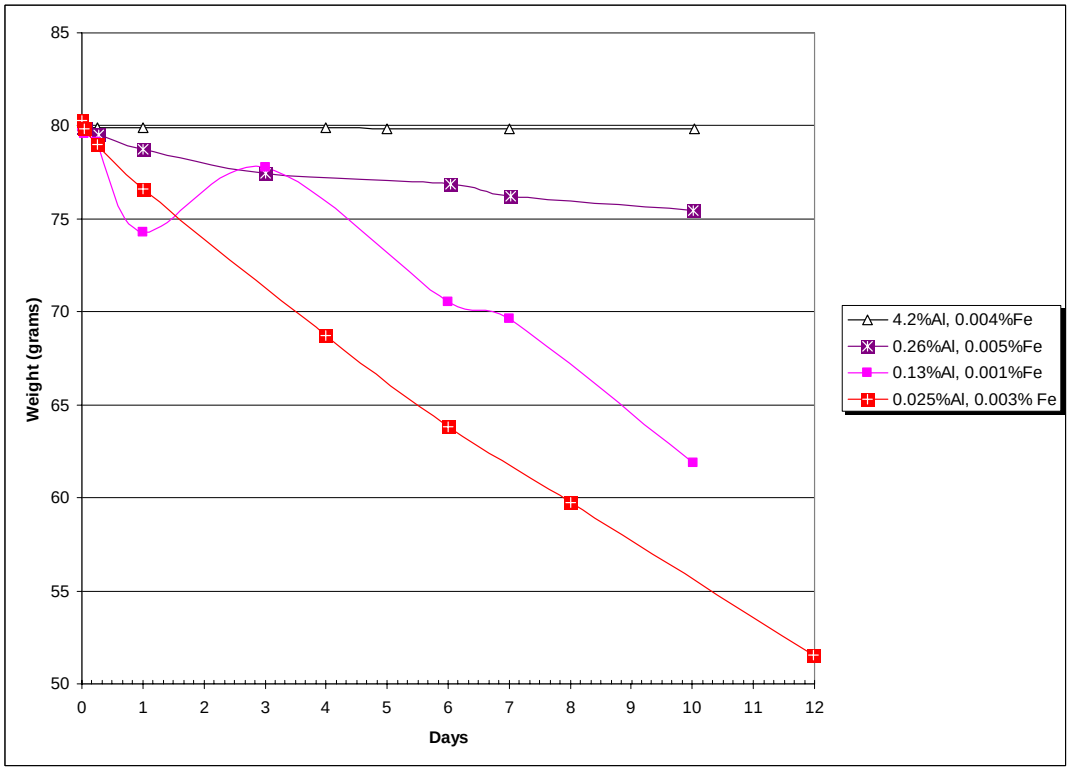

Figure 6-2: Weight Loss of 316L Stainless Steel Samples in Molten Zinc at 520°C

From the previous two figures, it is easily observed that by increasing the concentration of aluminum in the zinc bath the dissolution reactions decrease significantly. Furthermore, as exhibited in Figure 6-3, the approximate average dissolution rate (at both 500°C and 520°C) of the 316L stainless samples at increasing levels of aluminum in each specific zinc bath clearly identifies the suppression of molten metal degradation with the added concentrations of aluminum. Note: Two different temperatures were tested in order to verify the expected increase in activity at the elevated temperature (520°C), which was confirmed by these tests.

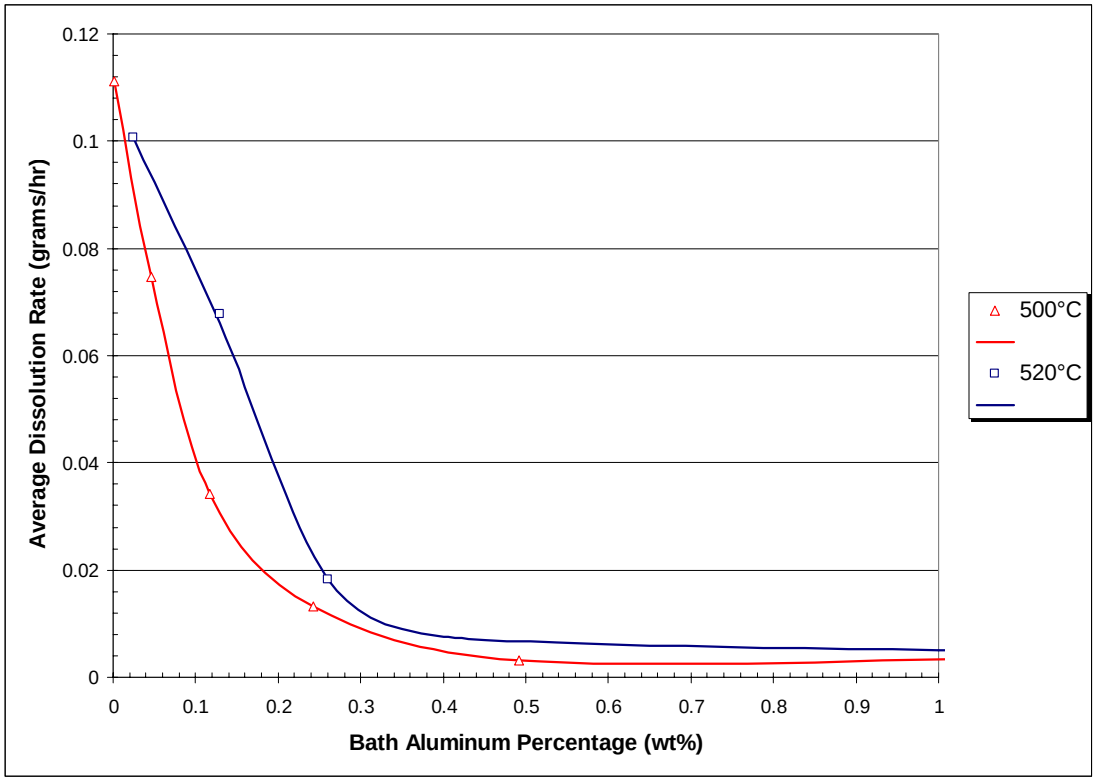

Figure 6-3: Average Dissolution Rate of 316L Stainless Steel Samples in Molten Zinc

6.2 Surface Area Corrosion Loss

It is generally accepted that corrosion loss is a function of the exposed surface area of the sample. Since several of these 316L samples are losing a significant quantity of material via dissolution over the duration of the trial, the instantaneous surface area of each specimen should also be considered by physically measuring the dimensions of each sample. Therefore, with the inclusion of weight loss as a function of surface area (in mg/cm^2), it can be seen in Figures 6-4 and 6-5 (for 500°C and 520°C, respectively) that the trend is not substantially different from the bulk weight loss figures (Figures 6-1 and 6-2).

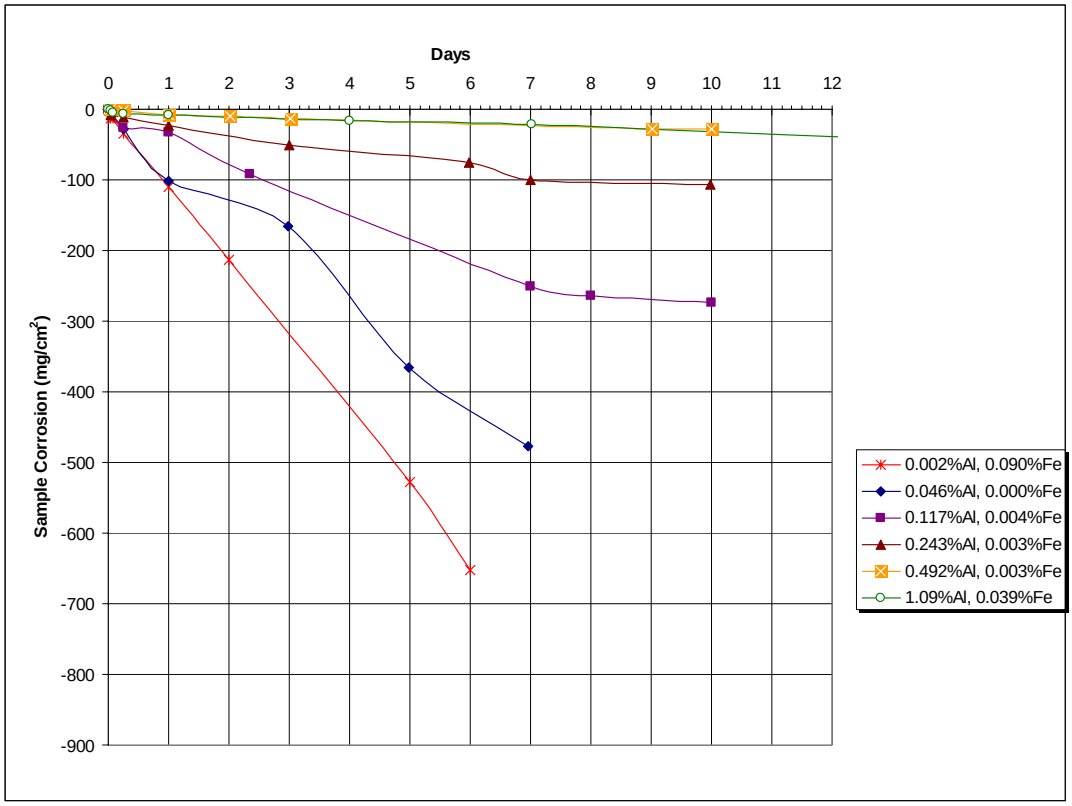

Figure 6-4: Molten Zinc (500°C) Corrosion of 316L Stainless Steel with respect to Instantaneous Surface Area of each Sample

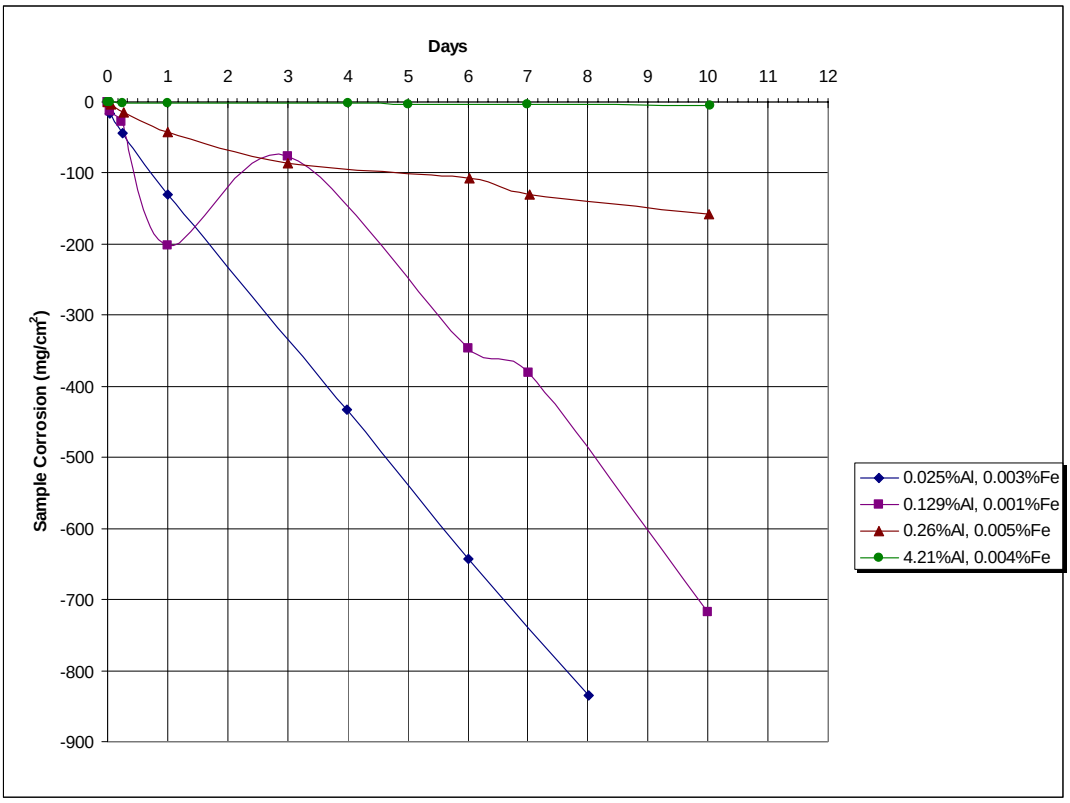

Figure 6-5: Molten Zinc (520°C) Corrosion of 316L Stainless Steel with respect to Instantaneous Surface Area of Each Sample

Next, to better understand the degradation mechanisms from these tests, the trends of the corrosion loss may be analyzed. Utilizing the data from the experiments at 500°C (i.e. Figure 6-4), trendlines for each series were interpolated and indicated a possible transition in the corrosion mechanism. Reviewing Figure 6-6, the corrosion data for samples where the aluminum content in the bath was below 0.12wt% aluminum displayed a linear relationship between degradation and time (which typically represents a dissolution-driven reaction) and lower aluminum concentrations corresponded to greater reaction rates (i.e. steeper slope).

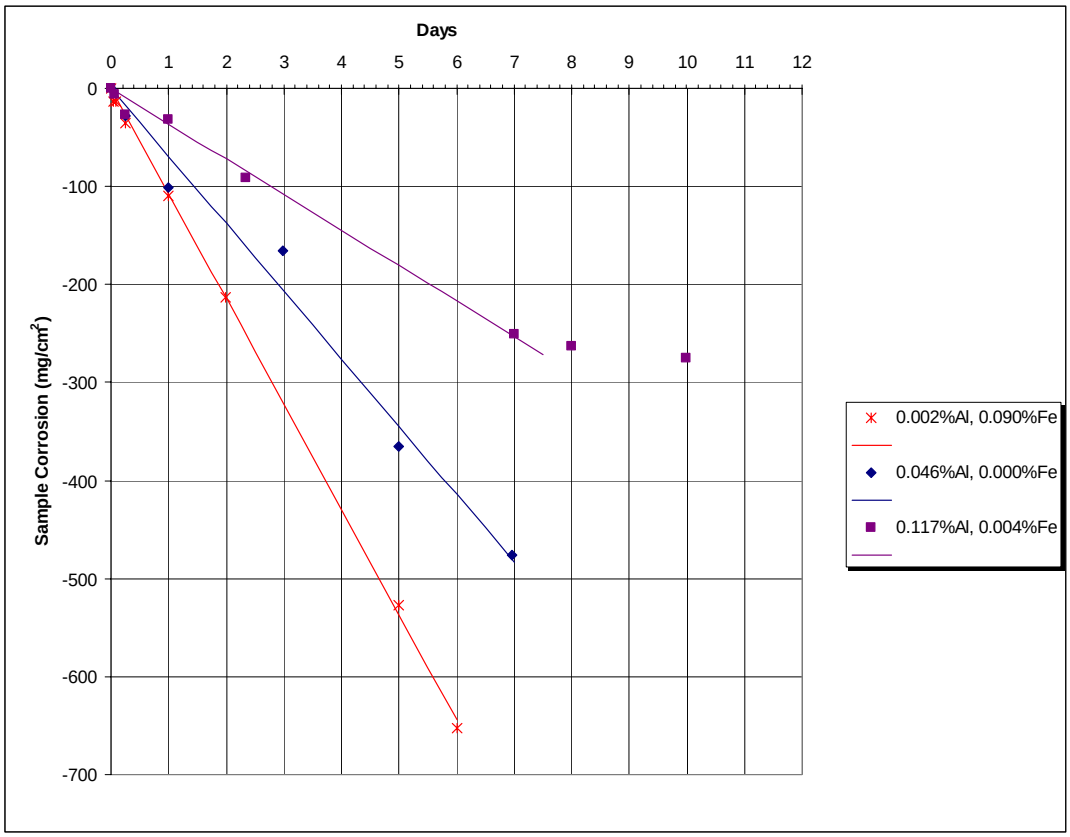

Figure 6-6: Linear Trend of Zinc Corrosion Rate for 316L Stainless Steel at Aluminum Concentrations less than 0.12wt%

Conversely, when the aluminum level in the bath was in excess of 0.24wt% (Figure 6-7), the data indicated an exponential response generally associated with a diffusion-controlled mechanism. Hence, once the aluminum level in the bath was increased beyond a transition point between 0.12wt% and 0.24wt% aluminum, the linear-to-exponential change in the degradation trend showed that the corrosion mechanism may be changing. Meanwhile, after a period of time many of the samples developed a steady-state corrosion status where the representative mechanism (i.e. linear or exponential) was no longer valid and the corrosion decay was significantly suppressed.

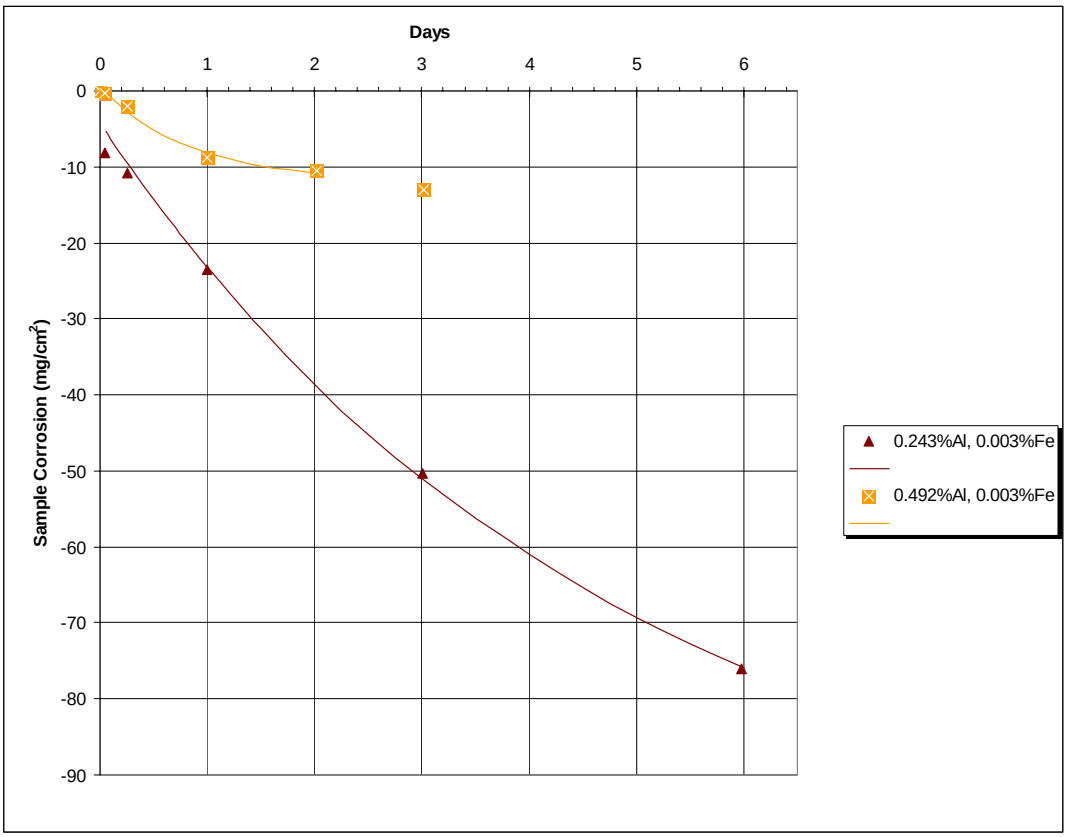

Figure 6-7: Exponential Trend of Zinc Corrosion Rate for 316L Stainless Steel at Aluminum Concentrations greater than 0.24wt%

Continuing, when the average corrosion rates for each set of data (from Figures 6-4 and 6-5) are plotted concurrently (Figure 6-8) the reflection of the importance of aluminum content in the zinc bath is obvious. The dissolution rates at 500°C began to stabilize at aluminum concentrations just below 0.2wt% (i.e. the rate of change of dissolution dropped below a relatively minimal 10 mg/cm^2/hr per wt%Al, which was less than half the rate of change at 0wt%Al). Similarly, the 520°C dissolution rates stabilized at just a slightly higher aluminum concentration.

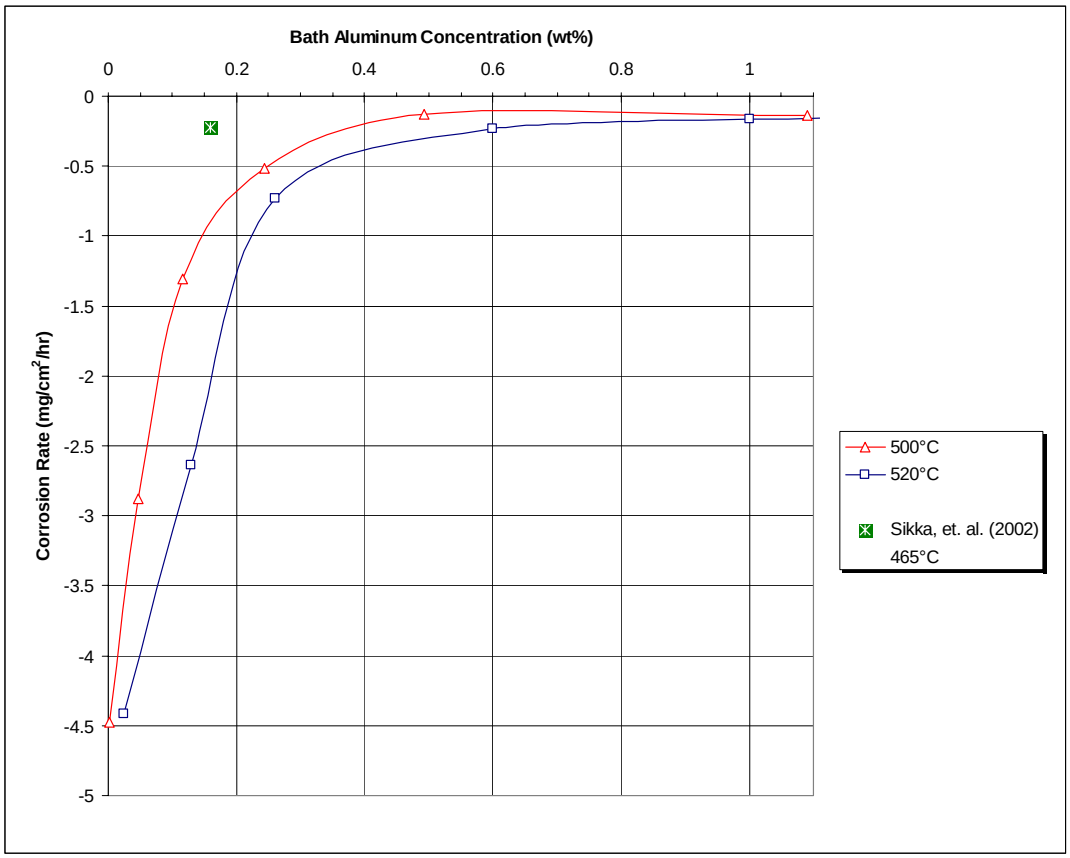

Figure 6-8: Zinc Corrosion Rate of 316L Stainless Steel as a Function of Aluminum Concentration

Furthermore, previous testing by Sikka, et al. [Ref. 64] identified an average dissolution rate of -0.22 mg/cm^2/hr for 316L stainless steel in a zinc bath with 0.16wt% aluminum at 465°C. Since the only change from the testing by Sikka, et al. to the current research is a variation in temperature (465°C vs. 500°/520°C), plotting this single point on Figure 6-8 provides an indication that the results of current study provide plausible output in that the data at 465°C is where it would be expected (relative to the data at 500°C and 520°C).

As a result of these tests, it can be shown that the aluminum concentration in a molten zinc bath has a pronounced effect on the corrosion (dissolution) resistance of 316L stainless steel. As an example, the dissolution rate of 316L in pure zinc

(99.99%Zn) is over ten times as great as the dissolution when the zinc bath contains 1.0wt% aluminum. Moreover, the enclosed data indicates that a rapid acceleration in the dissolution rate occurs when the aluminum concentration drops below 0.15wt% aluminum (at 500°C). Similarly, increased temperature provided a greater dissolution rate at lower aluminum concentrations but had a lesser effect at the low, steady-state dissolution rates observed in excess of 1.0wt% aluminum. Now that it has been shown that the aluminum level does, in fact, impact the dissolution of 316L stainless in molten zinc, further analysis can attempt to understand why this occurs.

6.3 Zinc Bath Saturation Limits

As with any liquid-solid system, the solubility limit of the solid solute material in the liquid environment can have a significant impact on the magnitude of material dissolved from the solid substrate and liquid zinc is no exception. Consequently, a large amount of research has explored the phase diagram regimes of zinc galvanizing baths containing additions of various elements with concentrations of iron and aluminum being the most important (and most widely studied). Although initial studies were performed over thirty years ago (Refs. 17, 80 and 81), the past 15 years or so have seen detailed and on-going investigations into understanding the Zn-Al-Fe system, especially with regards to interactions of molten zinc on carbon steel substrates and the solubility limits of iron in a Zn-Al bath (Refs. 82 – 111; in addition to others).

In 2000, Professor Arnold Marder of Lehigh University published a concise explanation of the metallurgy of galvanized steel (Ref. 93), where he summarized the solubility phase diagrams of the Zn-Fe-Al reactions. First, reviewing the binary reactions of zinc and iron, Marder reiterated the standard Fe-Zn binary phase diagram (Figure 6-9) and the associated phases that have been shown to occur in a zinc-rich galvanizing bath (Table 6-1).

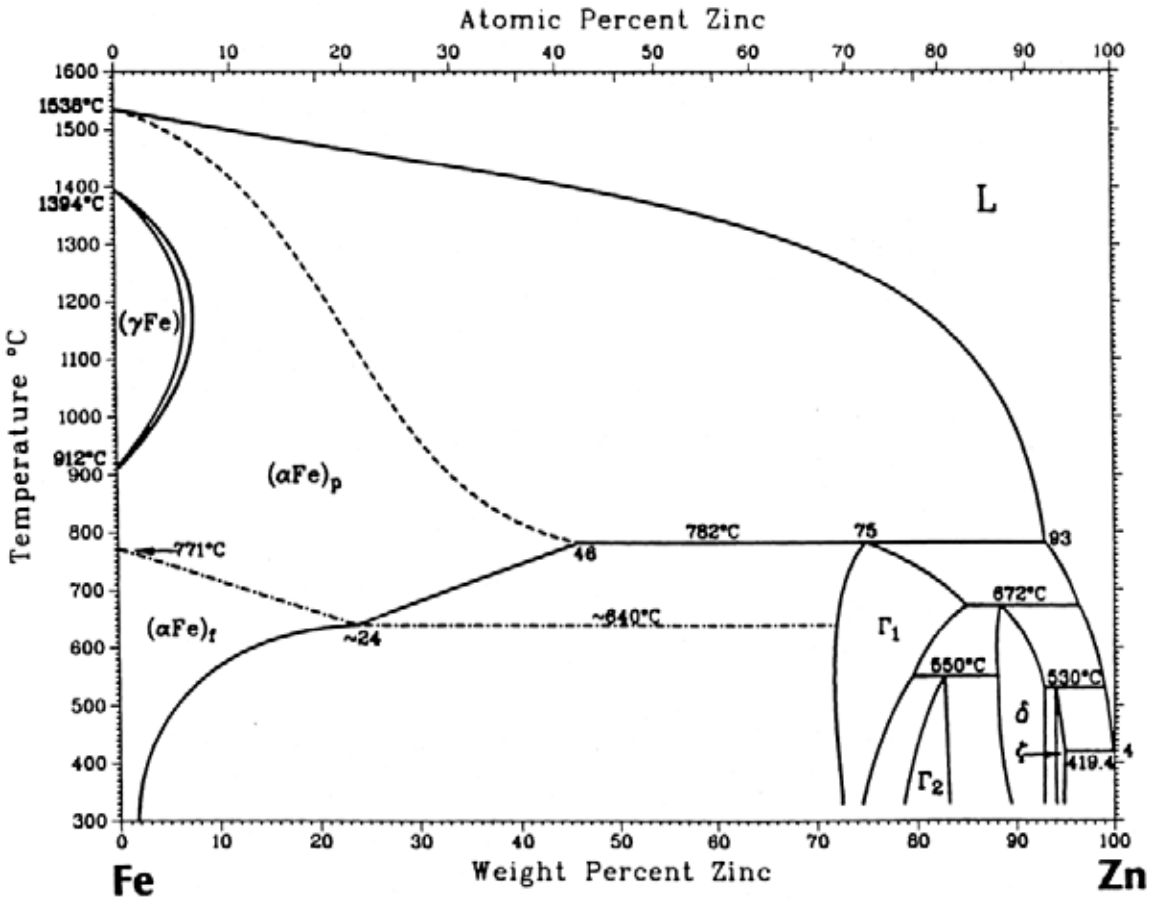

Figure 6-9: Fe-Zn Binary Alloy Phase Diagram
[Ref. 7, reprinted with permission from ASM International,
All rights reserved, www.asminternational.org]

Table 6-1: Fe-Zn Phase Characteristics (reproduced from Ref. 93)

Phases	Formula	Crystal Structure
αFe	Fe	BCC
Γ	Fe_3Zn_{10}	BCC
Γ_1	Fe_5Zn_{21}	FCC
δ	$FeZn_7$	Hexagonal
ξ	$FeZn_{13}$	Monoclinic
Zn	Zn	HCP

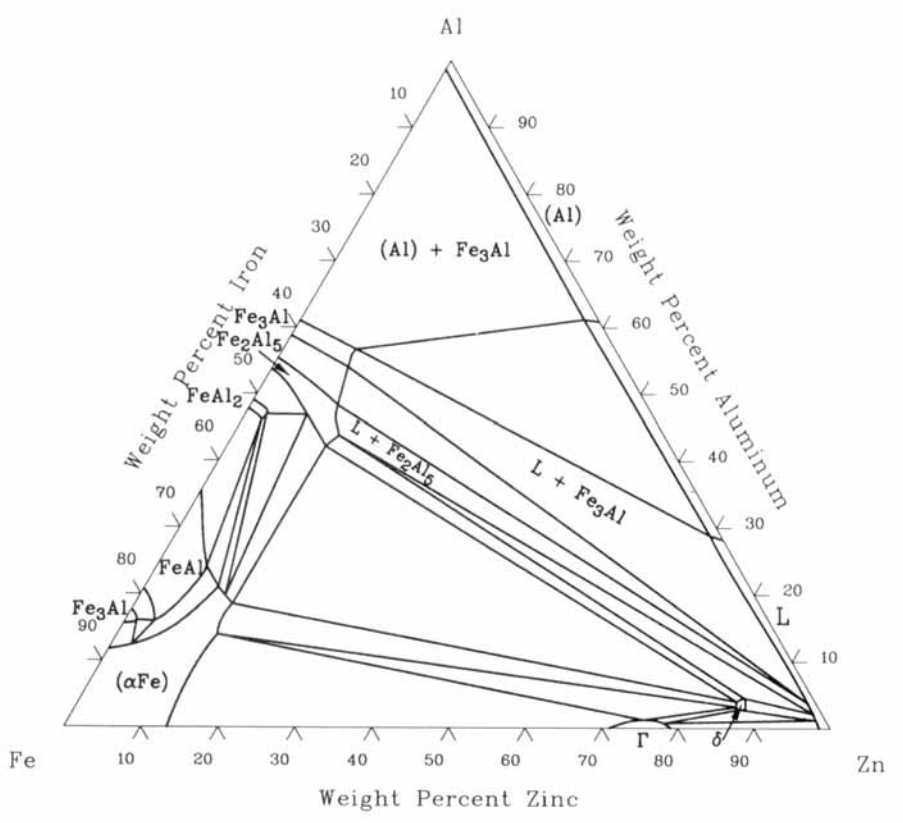

Figure 6-10: Zn-Fe-Al Isothermal (at 500°C) Ternary Phase Diagram
[Ref. 7, reprinted with permission from ASM International,
All rights reserved, www.asminternational.org]

Dr. Marder further discussed the response of aluminum with reference to the Zn-Fe-Al ternary phase diagram (Figure 6-10). However, as a result of finite compositional changes (in iron and aluminum) having a significant impact on the galvanizing

characteristics in a zinc pot, the wide scope of a full ternary phase diagram does not provide sufficient detail for functional use in industrial galvanizing applications.

As noted, numerous researchers have proposed variations of the zinc-rich corner of the Zn-Fe-Al phase diagram. However, the analysis by Dr. Nai-Yong Tang, et al. of Teck Cominco in Mississauga, Ontario (Refs. 99 – 104) has been recognized as the standard solubility explanation of the Zn-Fe-Al phase diagram. Previously (Refs. 7 & 93), it was established for a pure zinc bath (0%Al) that the iron solubility limit ([Fe] in wt%) was a function of temperature ([T] in Kelvin):

$$\ln[Fe] = 17.78 - 15388/[T]$$

Subsequently, Tang, et al. defined the iron solubility as a function of aluminum content relative to the temperature of the melt (for the popular galvanizing region greater than 0.13wt% aluminum). Upon precise refinement, the current relationship (Ref. 112) between iron ([Fe] in wt%) and aluminum ([Al] in wt%) solubility limits is accepted as (with [T] in Kelvin):

$$\ln[Fe]^2[Al]^5 = 28.1 - 33066/[T]$$

Moreover, the full phase diagram as determined by Tang, et al. may be descriptively observed in Figure 6-11, and, thus, with a complete understanding of the basic solubility phases present in an industrial galvanizing bath, broader analysis of the reactions between the zinc bath and 316L stainless steel pot hardware may be explored.

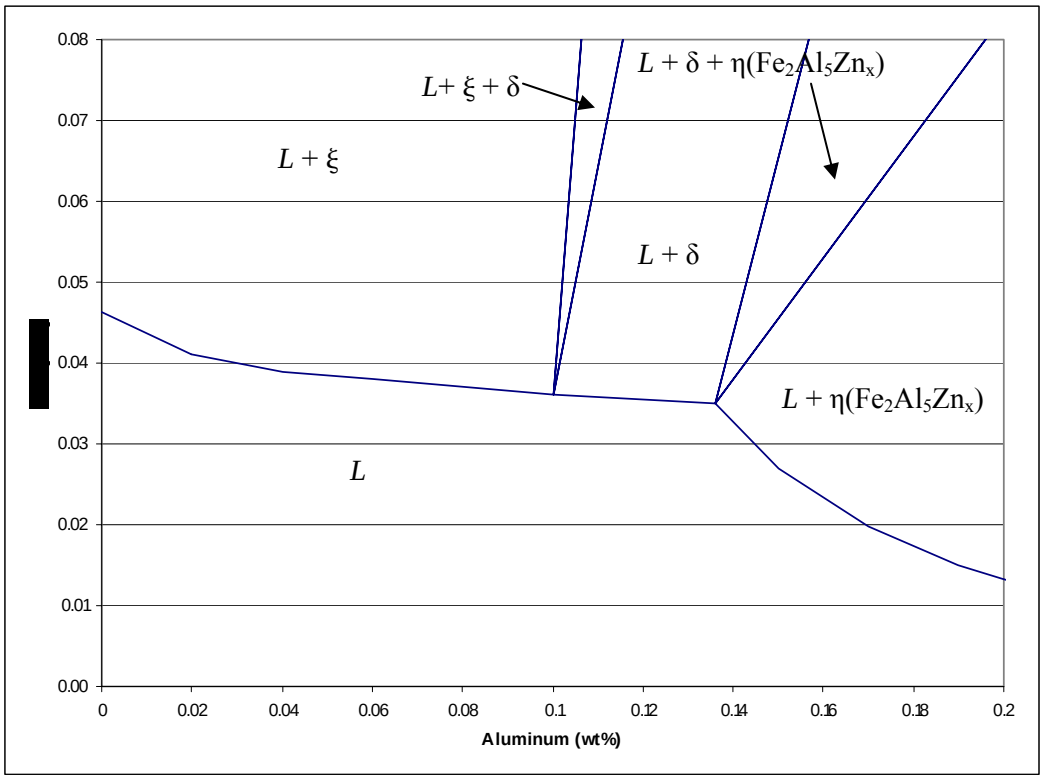

Figure 6-11: Zinc-Rich Corner of the Zn-Fe-Al Phase Diagram (at 465°C) (reproduced from Ref. 112)

Now, if reference is made again to the aforementioned zinc corrosion tests that were performed for the current study (Table 5-2), the actual iron concentration in the zinc bath for each data point may be plotted concurrently. As represented in Figure 6-12, the continual dissolution of iron from the immersed 316L stainless samples can be measured in the zinc bath. Analogous to the change in dissolution rate as a function of aluminum percentage, the iron content rapidly increases at lower aluminum concentrations in the liquid zinc.

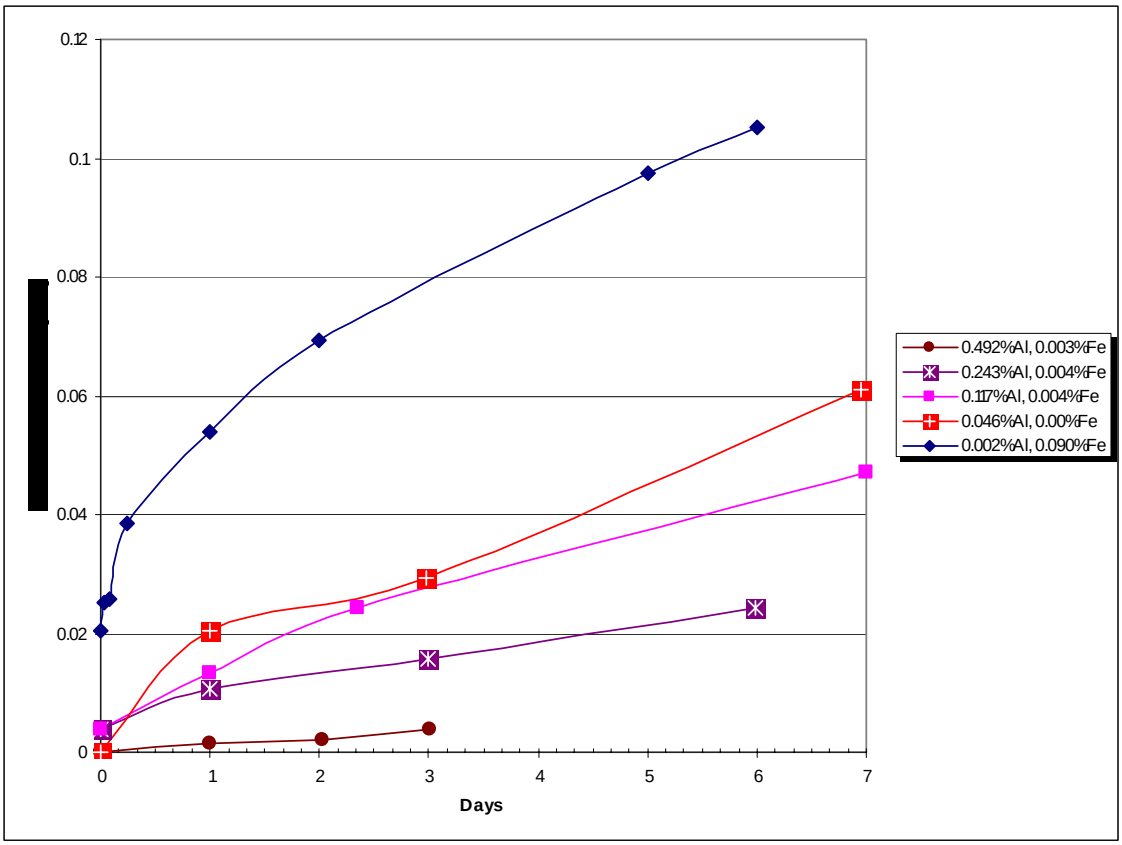

Figure 6-12: Total Iron Concentration in the Zinc Bath (at 500°C) during Dissolution Testing of 316L Stainless Steel Samples

Since these trials were run at 500°C, the phase diagram by Tang, et al. can be recalculated at the higher temperature (Figure 6-13) to provide a representation of the solubility limits experienced during the tests. From Figure 6-13, the iron saturation concentration may be determined for each of the testing conditions of the current trials (Table 6-2).

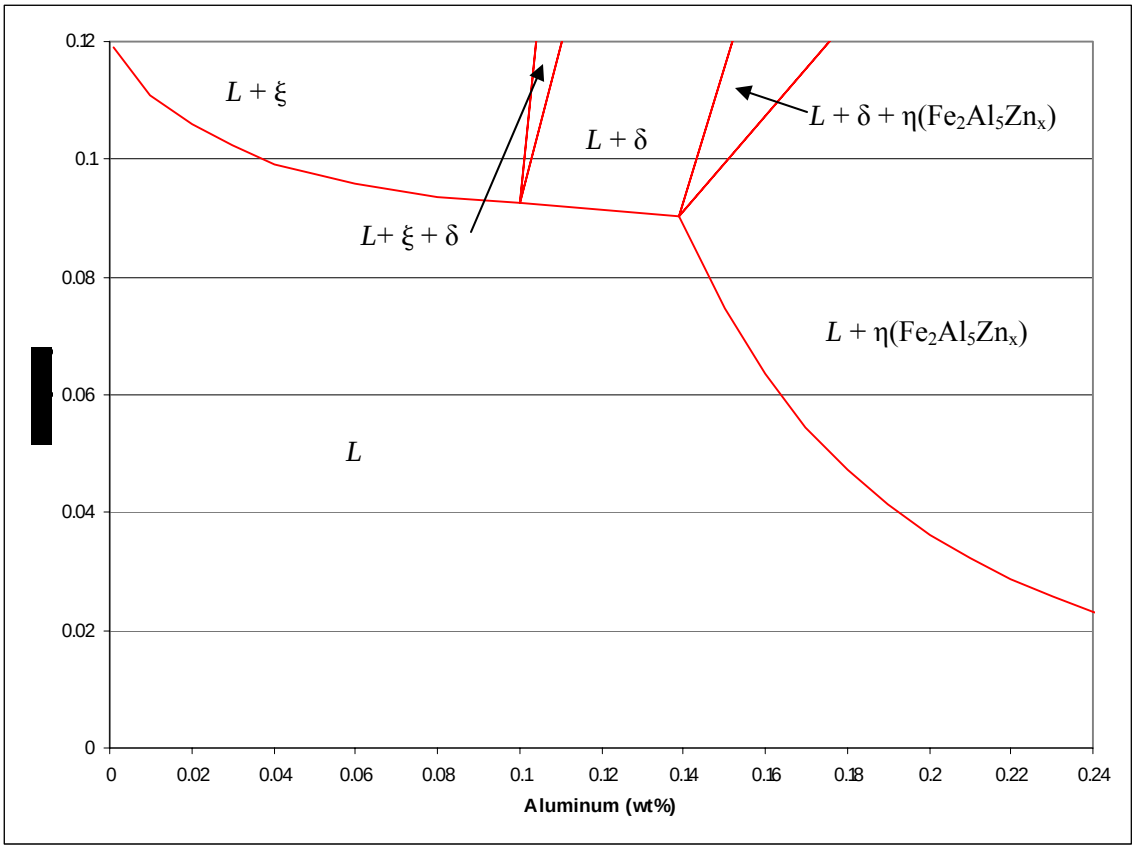

Figure 6-13: Zinc-Rich Corner of the Zn-Fe-Al Phase Diagram (at 500°C) (reproduced from Refs. 112 & 113)

Table 6-2: Iron Saturation Concentration (wt%) for Respective Zn-Al Baths (at 500°C)

Al%	Fe% Saturation
0.002	0.119
0.046	0.098
0.117	0.091
0.243	0.022
0.492	0.004

From Figure 6-10 it may be observed that the dissolved iron levels in the bath reached saturation levels at varying rates. Projecting the points from Table 6-2 onto Figure 6-10, saturation was achieved in less than 1 day for 0.492wt% aluminum bath; approximately 4 days for 0.243wt% aluminum bath; and in excess of 7 days for 0.117wt%, 0.046wt% and

0.002wt% aluminum baths. As a result, the corrosion results on Figure 6-4 suggest that the deceleration from rapid dissolution to steady-state decay (with reduced corrosion rate) may be triggered by saturation of iron in the zinc bath.

With this preliminary review of solubility limits of the Zn-Fe-Al system, a further investigation into the mechanisms of corrosion degradation of 316L stainless steel in typical galvanizing baths may be established.

6.4 Dissolution Theory

As discussed herewith, numerous projects have been undertaken to reveal the dissolution rates of various metallic specimens in molten zinc and molten aluminum and attempt to understand the reactions that correlate to these solvent environments. From literature (Refs. 20, 21, 22, 26-30, 78, 79; and others) it has been generally accepted that the defining rate characteristics of the dissolution of a solid metal in a liquid metal environment are governed by the Nernst-Shchukarev equation.

$$\ln[(C_s - C_o)/(C_s - C)] = K(A \cdot t/V)$$

where C is the instantaneous concentration of the dissolved metal in the melt (wt%), C_s is the saturation concentration (wt%), C_o is the initial concentration at t=0 (wt%), K is the dissolution rate constant (m/s), A is the surface area of the sample (m^2), and V is the volume of the melt (m^3).

As described earlier, Dybkov [Ref. 22] successfully verified that the Nernst-Shchukarev equation was applicable not only for pure iron in molten baths but also for highly alloyed stainless steel. Exhibited by Dybkov in Figure 6-14, the Nernst-Shchukarev equation is valid for predicting the linear relationship of dissolution for (in

this testing by Dybkov) 18-10 Stainless Steel in liquid aluminum, in spite of slight variations in the composition of the aluminum.

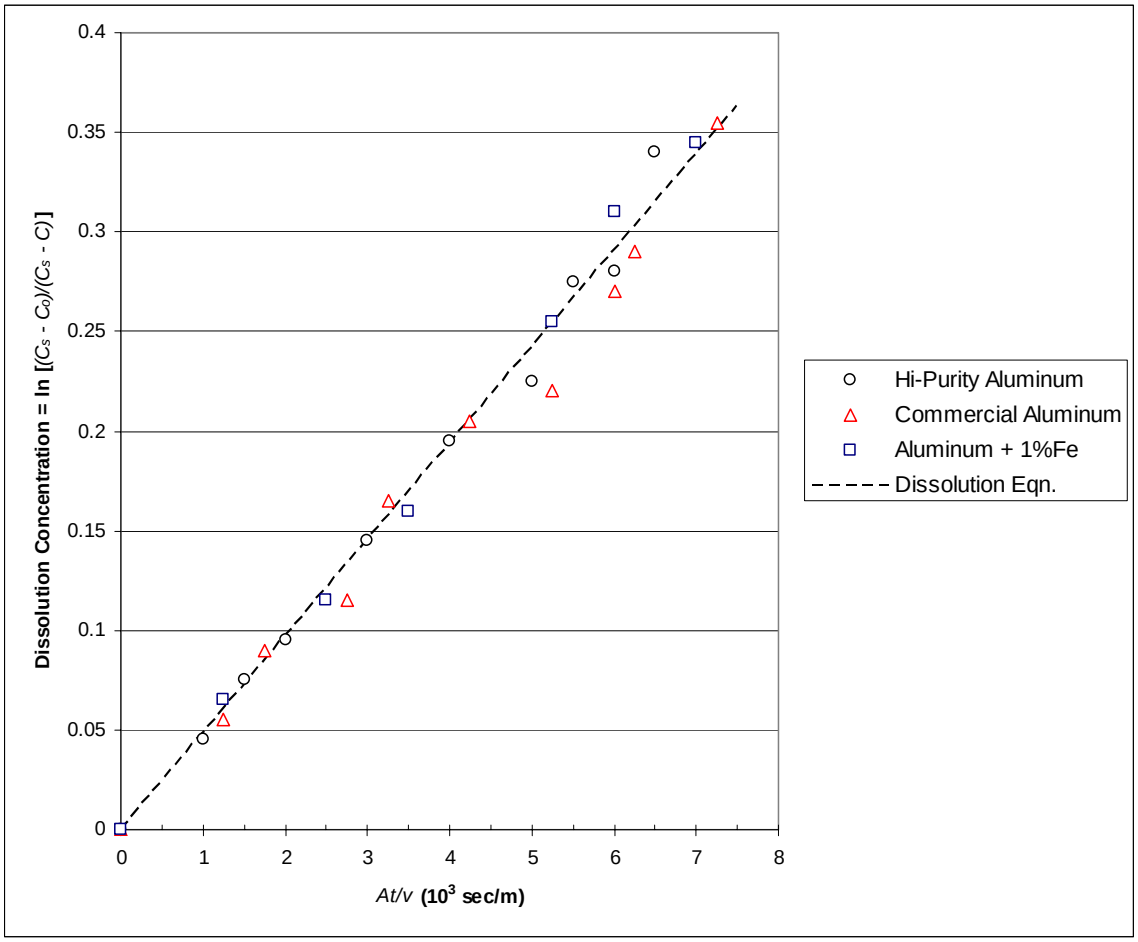

Figure 6-14: Comparison of Nernst-Shchukarev equation for dissolution and experimental corrosion data for 18-10 Stainless Steel in three liquid aluminum baths [figure reproduced from Ref. 22 by Dybkov] (See also Figure 3-8)

Accordingly, if once again the current array of tests investigating the reactions between 316L stainless steel and molten Zn-Al baths are considered, calculations may be made utilizing the Nernst-Shchukarev equation to plot the corresponding variables [Figure 6-15].

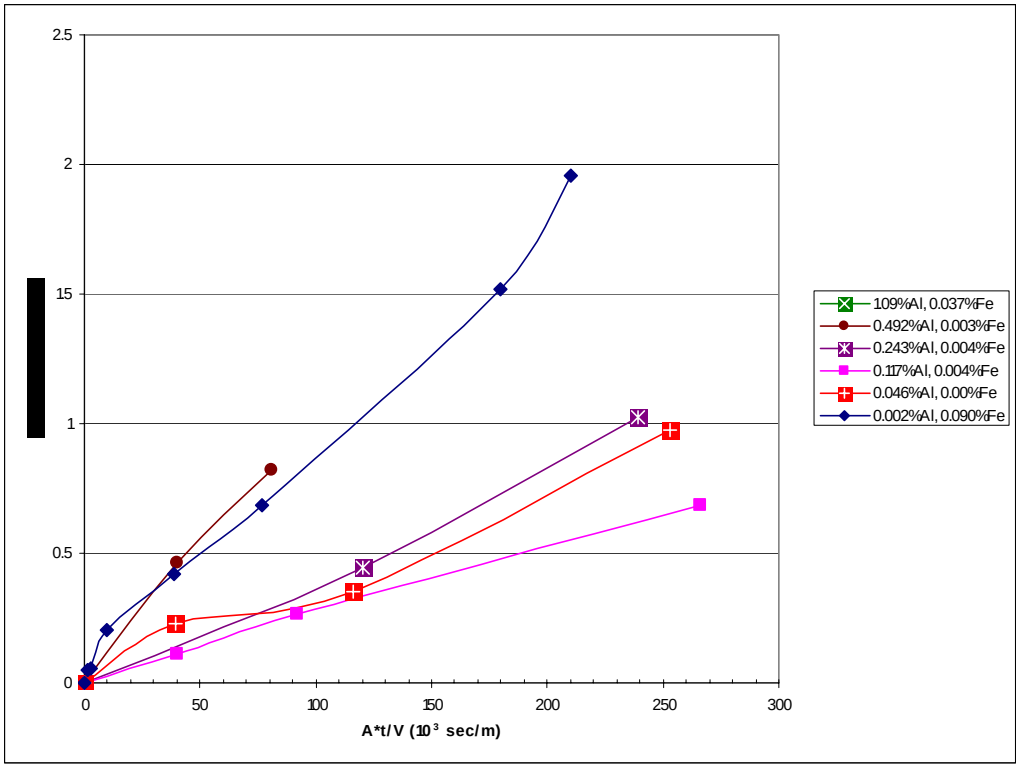

Figure 6-15: Correlation of Nernst-Shchukarev equation for dissolution to experimental corrosion data for 316L Stainless Steel in liquid Zn-Al at 500°C

However, since existing literature does not provide the saturation concentration of 316L stainless alloy composition in molten zinc, the saturation levels of iron (as described above) in Zn-Al were utilized as C_s for the Nernst-Shchukarev equation. From Figure 6-15 it is easily perceived that the experimental data does not agree with the linear function, such as the work performed by Dybkov (Figure 6-14).

As a continuation in the same body of research [Ref. 22], Dybkov recognized a phenomenon where the saturation levels of each individual constituent in the 18-10 stainless steel (specifically Fe, Cr, Ni) did not reach the saturation concentrations predicted by the binary phase diagrams of Al-Fe, Al-Cr and Al-Ni, respectively. As

Dybkov outlined (Figure 6-16), the saturation level of Fe nearly achieved the theoretical binary concentration, but the corresponding levels for Cr and Ni were far below expected. Furthermore, the Fe-Cr-Ni levels in the liquid bath maintained a similar ratio as that of the solid 18-10 stainless material.

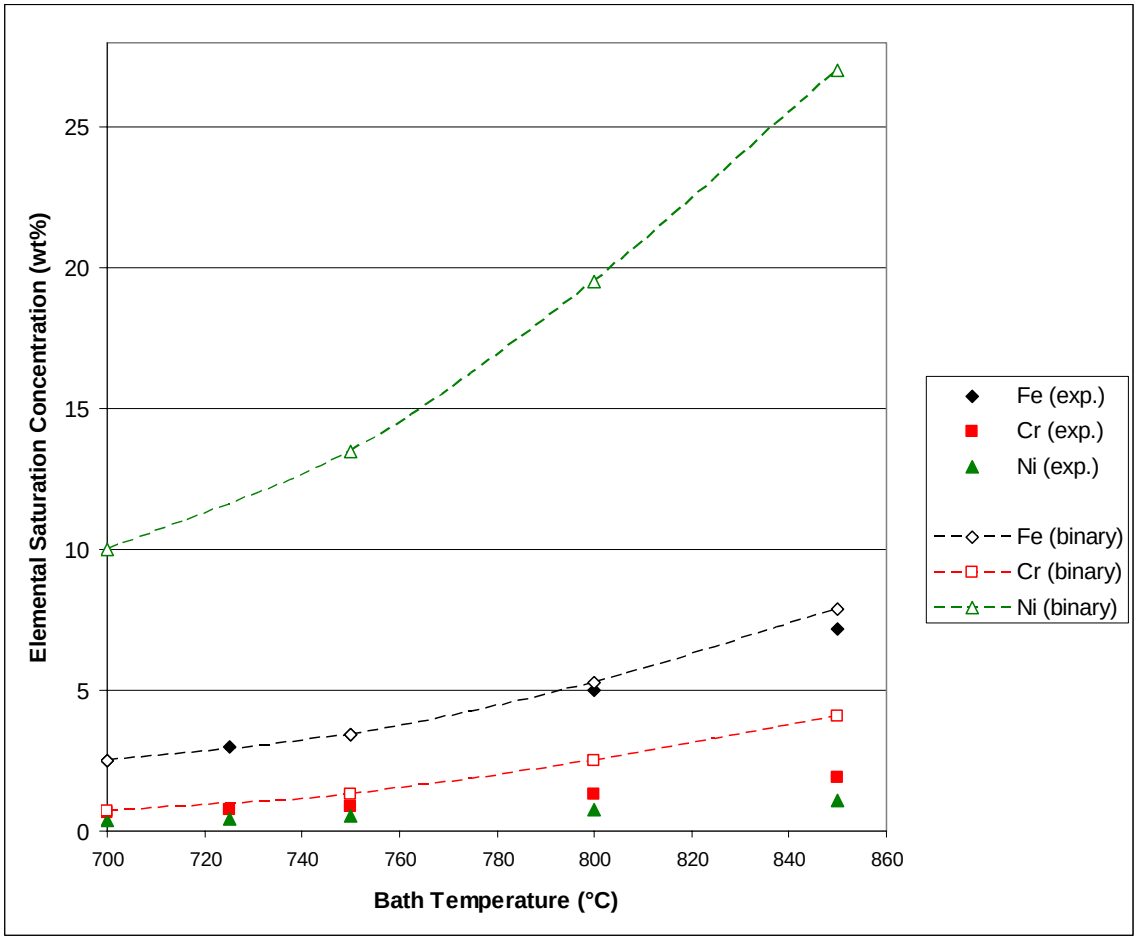

Figure 6-16: Comparison of Saturation Levels in Pure Aluminum for Experimental Corrosion Data from 18-10 Stainless Steel and the predicted saturations of the Binary Systems [figure reproduced from Ref. 22 by Dybkov] (See also Figure 3-15)

As a result, Dybkov postulated that the corrosion of 18-10 stainless steel by molten aluminum was "non-selective dissolution" and he illustrated the following: "In its lattice the iron, chromium and nickel atoms are connected together by metallic bonds of nearly

equal strength because those elements are neighbors in the Periodic Table. Therefore, it [is] supposed that the iron and chromium atoms, being major constituents of the steel, will not 'permit' the nickel atoms to leave its lattice at a rate which exceeds their own rates of transition into liquid aluminum. From this viewpoint all the elements should pass into the melt in those ratios in which they are present in the steel." [Ref. 22]

From this theory it can be assumed that dissolution of 316L stainless steel in a molten Zn-Al bath would follow a similar trend with the concentrations of the solute constituents maintaining a common weight percentage ratio to the substrate metal. Moreover, since 316L stainless possesses a higher concentration of Fe (67.5wt%) than Cr (17.5wt%) or Ni (10.75wt%), it would be presumed that iron would retain governing control of the solubility. As a consequence, it is proposed herein that the actual saturation level in the Zn-Al bath of the whole embodiment of 316L stainless closely agrees with 1/67.5% (i.e. 148%) of the reported saturation concentration of Fe for each specific bath Zn-Al composition.

Now, utilizing this revised ratio of the saturation concentration, the Nernst-Shchukarev data for the existing test results may be recalculated using the saturation concentration of 316L as 148% of the saturation concentration for Fe [or $1.48(C_{s,\,Fe})$]. Displayed in Figure 6-17, the effect of the adjusted C_s saturation concentration relative to previously calculated Figure 6-15 is immediately apparent. With this new C_s calculation, it appears that the leading trend of the data has now become quite linear as would be expected from the Nernst-Shchukarev equation.

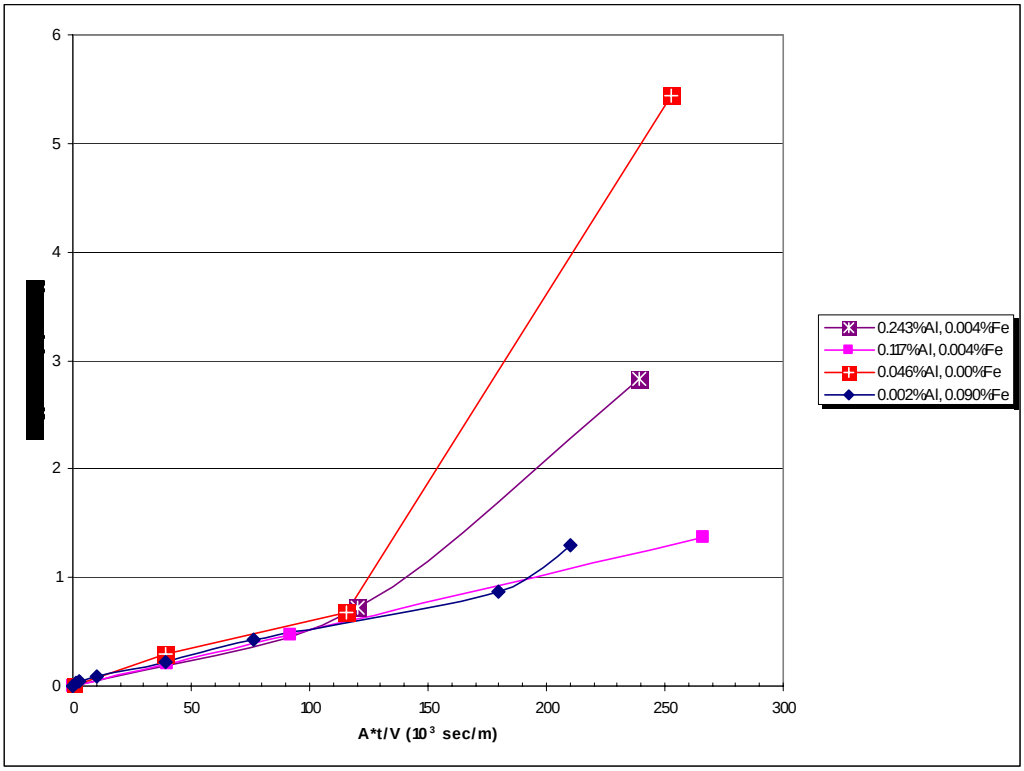

Figure 6-17: Correlation of Nernst-Shchukarev equation for dissolution to experimental corrosion data for 316L Stainless Steel in liquid Zn-Al at 500°C, utilizing an adjusted (148% Fe) saturation concentration to account for 316L solubility

Furthermore, if the data for each trendline is examined in the region where the Nernst-Shchukarev calculation deviates from the linear function, it is quickly discovered that divergence accelerates rapidly whenever the 316L concentration (C) in the bath exceeds 75% of the saturation level (C_s) for each specific Zn-Al bath composition. Hence, if the upper boundary condition for this application of the Nernst-Shchukarev equation is set at $C \leq 75\%C_s$, the revised data becomes almost entirely linear [Figure 6-18].

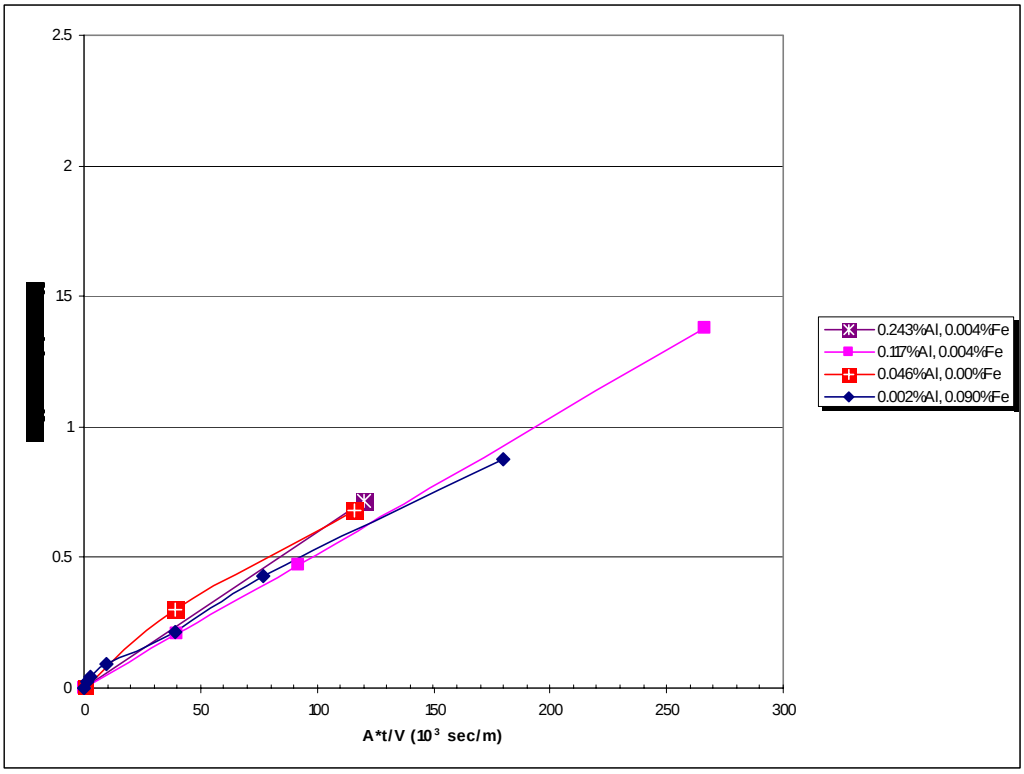

Figure 6-18: Correlation of Nernst-Shchukarev equation for dissolution to experimental corrosion data for 316L Stainless Steel in liquid Zn-Al at 500°C (with $C \leq 75\%C_s$)

Although all of the other data shown in Figure 6-18 reflected the "as-tested" measurements of the representative specimens, one simple correction factor was required in order for the data trend of the Zn-0.002%Al bath to meet the regime of the other linear gradients. When the [148% ($C_{s,Fe}$)] calculation of the saturation concentration for 316L was performed utilizing the reported $C_{s,Fe}$ = 0.119wt% Fe for nearly pure zinc at 500°C, the data did not fall within the trends of the other data. However, if the theoretical saturation concentration of Fe in this bath was to be increased to $C_{s,Fe}$ = 0.19wt% Fe, the subsequent calculation of the 316L saturation level [by 148% ($C_{s,Fe}$)] results in the linearity shown in Figure 6-18. Thus, it is necessary to attempt to identify this increased saturation level at extremely low aluminum concentrations in the zinc bath.

Recently, Dr. Tang and his team of researchers at Teck Cominco have begun investigating the responses of increased levels of chromium in Zn-Fe-Al galvanizing baths due to dissolution of 316L stainless steel submerged hardware materials [Ref. 111]. As reflected in Figure 6-19, the liquid phase solubility concentrations have been determined for the zinc-rich quaternary system of Zn-Fe-Al-Cr (at 450°C). From this plot, the magnitude of the chromium saturation levels is very high (0.4wt%) at low aluminum points, but, remarkably, the Cr solubility drops rapidly to below 0.1wt% saturation when the aluminum level is above 0.12wt%.

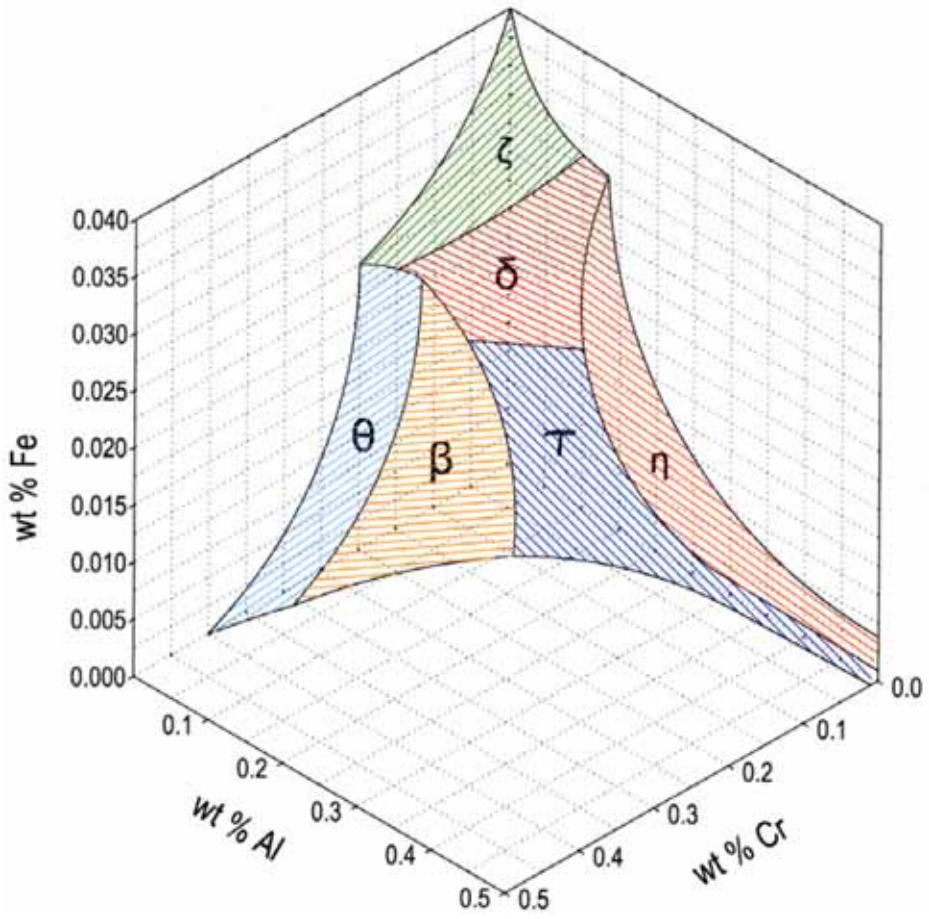

Figure 6-19: Liquid phase domain for Zn-Fe-Al-Cr Quaternary System at Isothermal 460°C [reprinted with permission from The International Lead Zinc Research Organization, Ref. 111]

In conjunction, if the details of the Zn-Fe-Al-Cr quaternary system are evaluated under a condition of nearly 0% aluminum, the resultant ternary phase diagram (at 450°C) becomes Figure 6-20. From this figure the elevated solubility of chromium may be further observed. Thus, as mentioned earlier, the saturation level of 316L stainless dissolved in pure zinc (0% Al) was calculated to be about 0.28% (or [1/67.5% x 0.19wt% Fe]). (In other words, due to the high solubility of Cr at 0wt% Al, the saturation level of 316L must take into account the solubility of Cr and not just Fe.) Hence, in order to accurately validate this solubility calculation for low aluminum concentrations, further testing of the Zn-Fe-Cr system would need to be performed so that the 450°C isothermal ternary section shown in Figure 6-20 may be extrapolated to encompass the analogous results at 500°C.

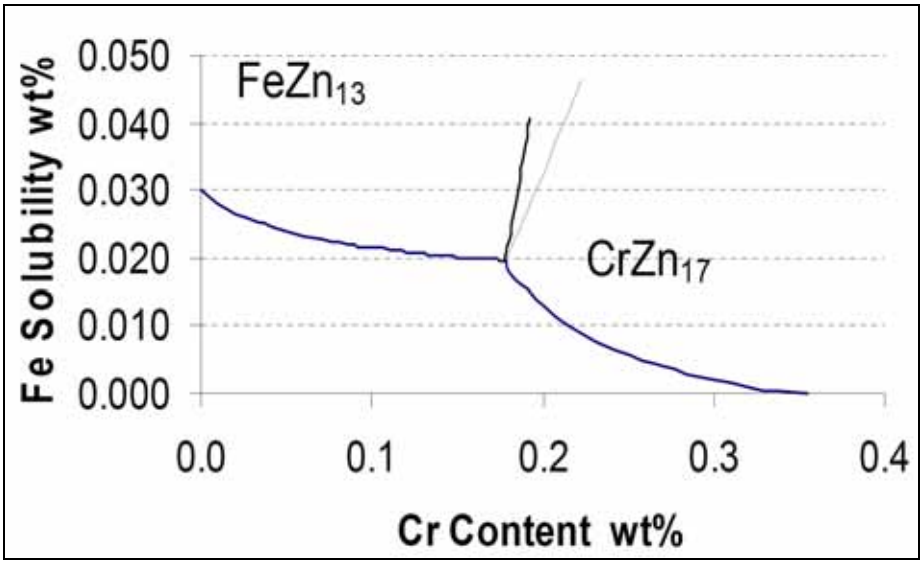

Figure 6-20: Zn-Rich Corner of Zn-Fe-Cr Phase Diagram at 450°C [reprinted with permission from The International Lead Zinc Research Organization, Ref. 111]

Meanwhile, since 316L stainless steel is an alloy of iron, chromium and nickel, evaluating the Zn-Fe-Ni phase diagram (Figure 6-21) indicates that the solubility of nickel in molten zinc may be as much as 0.5wt% Ni when the iron content is very low. Hence, the accelerated nickel solubility may further contribute to the skewed saturation concentration (C_s) discussed previously.

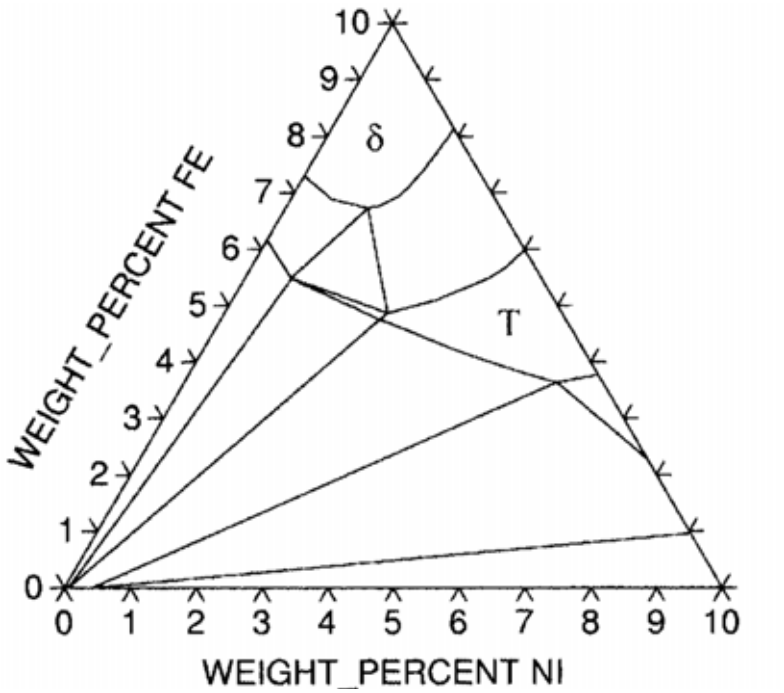

Figure 6-21: Zn-Rich Corner of Zn-Fe-Ni Phase Diagram at 450°C
[Ref. 109, reprinted with permission from ASM International,
All rights reserved, www.asminternational.org]

As a result, by utilizing proven phase diagrams in conjunction with the Nernst-Shchukarev equation for dissolution in liquid metal, this theoretical analysis of the experimental data for 316L stainless steel corrosion in molten Zn-Al provides an initial path for subsequent prediction of corrosion rates of 316L submerged hardware in industrial galvanizing applications in addition to creating a fundamental platform for future calculation of molten metal corrosion rates of other structural metals.

Chapter 7: Diffusion

Up to this point, discussions have been made as to the measurable changes in bulk dissolution characteristics of 316L stainless steel in a bath of liquid zinc with variable concentrations of aluminum. However, little has been mentioned as to the purpose of aluminum additions in an industrial galvanizing bath. As noted by Marder [Ref. 93], "Low aluminum additions (0.1 – 0.3 wt%) to the Zn bath are deliberately added to form Zn coated galvanized sheet. These additions have been made to (1) improve the luster or reflectivity of the coating, (2) reduce oxidation of the zinc bath, and (3) to obtain a ductile coating by suppressing the formation of brittle Fe-Zn phases." It is widely accepted that small amounts of aluminum are added to the zinc galvanizing bath to promote an inhibition mechanism which controls the growth of Fe-Zn intermetallic compounds on the delicate steel substrate. Thirty-five years ago, Ghuman and Goldstein [Ref. 17] reiterated previous research that found that "small additions of aluminum to the bath delay the reaction between iron and zinc". Furthermore, suppression of Zn-Fe intermetallics by the inhibition mechanism (also referred to as "incubation period") is variable for fluctuating Zn bath and substrate conditions. Inhibition may be promoted by [Refs. 93, 114]:

1. Increased aluminum content in the bath
2. Lower bath temperatures
3. Reduced bath iron content
4. Enhanced agitation of the bath
5. Increased silicon presence in the steel
6. Decrease surface roughness of the steel substrate

However, in an actual industrial environment, the aluminum content is the most easily adjusted, yet phase diagrams indicate that it is possibly the most critical variable affecting inhibition. As Marder summarized based on the work by Tang, et al. [Ref. 93, 115], "The origin of the potential inhibition layer compound will depend upon the Al concentration in the bath, thus it can be seen from [the Zn-Al-Fe phase diagram at 465°C (Fig. 6-11)] that the minimum Al content necessary for the full inhibition effect of $Fe_2Al_5Zn_x$ (η) is approximately 0.15 wt% Al, that is slightly higher than the concentration corresponding to the changeover from delta (δ) phase to $Fe_2Al_5Zn_x$ (η) being the thermodynamically stable phase." In conjunction, Tang summarized [Ref. 93, 116] the coating microstructures found on galvanized steel based on the bath aluminum concentration (Table 7-1) and revealed that only the $Fe_2Al_5Zn_x$ (η) phase is capable of providing a full inhibition from Fe-Zn intermetallic compounds forming.

Table 7-1: Summary of Coating Microstructures in Continuous Galvanizing (with Al Content Relative to 460°C Bath Temperature) [reproduced from Refs. 93, 116]

Al content (wt%)	Equilibrium Compound	Intermetallics in coating	Alloy Layer Characteristics
< 0.100	ξ	ξ/δ/Γ'/Γ	Continuous
0.100-0.135	δ	ξ/δ/Γ'/Γ	Gaps exist
0.135-0.140	η	Mostly ξ	Discontinuous
0.140-0.145	η	ξ plus η	ξ dissolution
0.145-0.150	η	Mostly η	ξ dissolution
> 0.150	η	η	Full inhibition

Continuing, Marder [Ref. 93] commented on the work by Nakayama, et al. [Ref. 119], where it was observed that "the [inhibition] incubation period (i.e. the time for Fe-Zn phases to form) increases with an increase in Al content in the bath and decreasing bath temperature". Moreover, from Figure 7-1 it is recognized that the rate of incubation

accelerated dramatically (at typical galvanizing bath temperatures of 450 to 480°C) when the aluminum content was increased from 0.12wt% to only 0.14wt%.

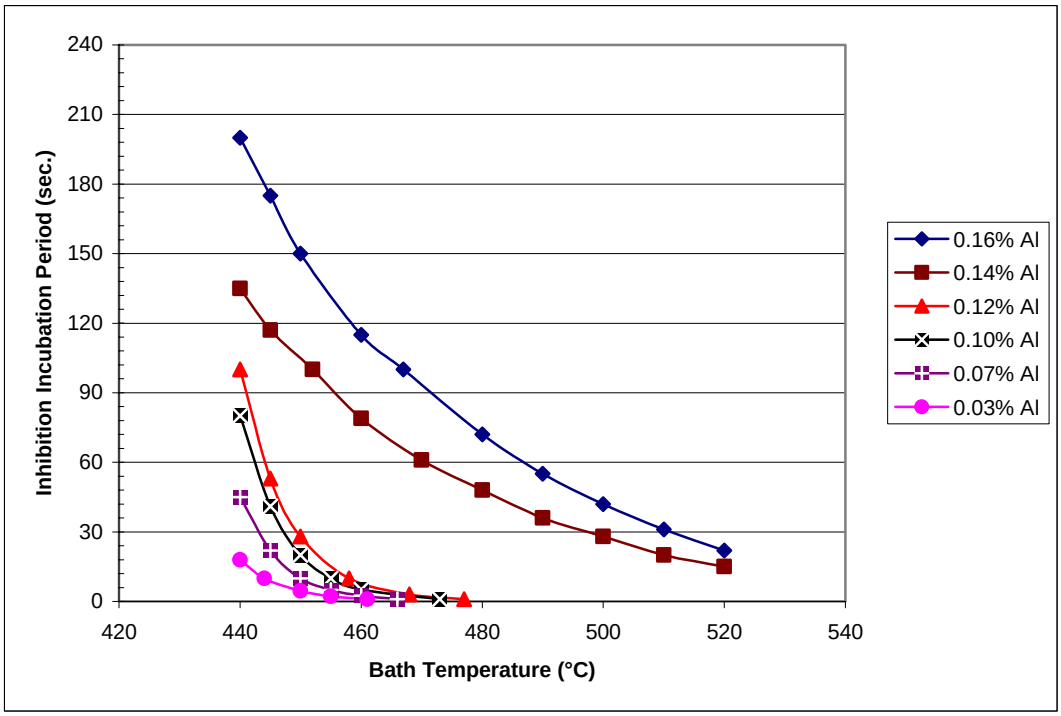

Figure 7-1: Effects of Bath Aluminum Content and Alloying Temperature on Fe-Zn Inhibition Incubation Period
[figure reproduced from Refs. 93, 117 by Nakayama, et al.]

Thus, based on previous literature, a considerable quantity of evidence exists identifying a major shift in the reactivity of a carbon steel substrate in a molten zinc bath whenever the aluminum concentration in the bath transitions from less than 0.12% to greater than 0.14% aluminum. It was within this same aluminum regime where it has been discovered that the dissolution reactivity of 316L stainless in molten Zn-Al changes significantly also [Figures 6-3 and 6-8].

In order to obtain a deeper understanding of the reaction products on the 316L stainless steel samples explored in the current investigation, advanced analysis techniques were employed utilizing a Hitachi S-4700 Scanning Electron Microscope (SEM) with

integral EDAX Genesis Energy Dispersive Spectrometer (EDS). From this analysis structural changes in the surface reactions relative to variations in the bath aluminum concentration can be traced [Figures 7-2 to 7-6]. The reaction differences on 316L after immersion for both 1 day and 7 days in a zinc bath with 0.046wt% Al at 500°C were identified (Figure 7-2). Keeping the sample in the bath for 168 hours, no appreciable diffusion of zinc or aluminum was recognized in the stainless substrate. Furthermore, EDS analysis identified that the coating composition for both samples were nearly identical in spite of the immersion time differential. An iron concentration of about 7wt% was noted near the undisturbed 316L surface with Fe levels diminishing to about 2wt% at the outer coating surface for both time duration samples. Similar to these 0.046%Al corrosion samples, the zinc bath containing 0.117wt% Al (Figure 7-3) created no aluminum diffusion into the 316L after 7 days and both samples (after 1 day and 7 days) exhibited about 8wt% Fe accumulation immediately above the substrate and approximately 5wt% Fe at the outer coating surface.

Now, as the aluminum content of the trial zinc bath is increased above the inhibition point (~0.14wt% Al) described earlier, the 316L stainless samples immediately begin to reflect formations of $Fe_2Al_5Zn_x$ particles and reactions similar to the transformation depicted by Marder [Ref. 93] and subsequently supported by Zhang, et al. [Refs. 118 & 119] and DuBois [Ref. 120]. The reaction on 316L following immersion in liquid zinc with 0.243wt% Al at 500°C showed distinct particles of $Fe_2Al_5Zn_x$ forming at the surface of the 316L substrate in less than 24 hours [Figure 7-4(a)]. Concurrently, aluminum is reacting into the surface of the 316L creating a $Fe_2Al_5Zn_x$ composition containing high concentrations of molybdenum (4wt% Mo) and chromium (~1wt% Cr).

As the dipping time of the sample is continued for 168 hours (Figure 7-4(b)), the surface reaction begins to manifest a laminar structure. Through EDS analysis it is determined that the composition of the dark and light layers of the laminar zone are somewhat similar with a basic $Fe_2Al_5Zn_x$ constitution, but with the dark phase possessing significantly higher molybdenum content (6.9wt% Mo) relative to the lighter phase (2.1wt% Mo). This type of reaction has also been observed by Zhang, et al. [Refs. 118 & 119]. Meanwhile, the composition of the reaction "front" into the substrate (i.e. deepest point of the reaction) after 7 days ($Fe_2Al_5Zn_x$ + 3.2wt% Mo + ~1wt% Cr) is still quite similar to the reaction "front" after only 1 day ($Fe_2Al_5Zn_x$ + 4wt% Mo + ~1wt% Cr). Furthermore, the reduced dissolution due to the creation of the inhibition layer by the elevated bath aluminum content has propagated a residual coating that is significantly lower in iron and other alloying components (such as Cr, Ni and Mo) than the samples from the lower (<0.12wt%) aluminum content baths.

Continuing, it can be generally observed in subsequent SEM/EDS samples that, as the aluminum content is increased from 0.243wt% to 0.492wt% to 1.091wt% Al (Figures 7-4, 7-5, 7-6, respectively), the reaction structure forms in a similar manner with $Fe_2Al_5Zn_x$ particles nucleating on the surface at the same time as the bath constituents penetrate into the 316L substrate. Moreover, the dark and light laminar structure described above continues to develop after long immersion times.

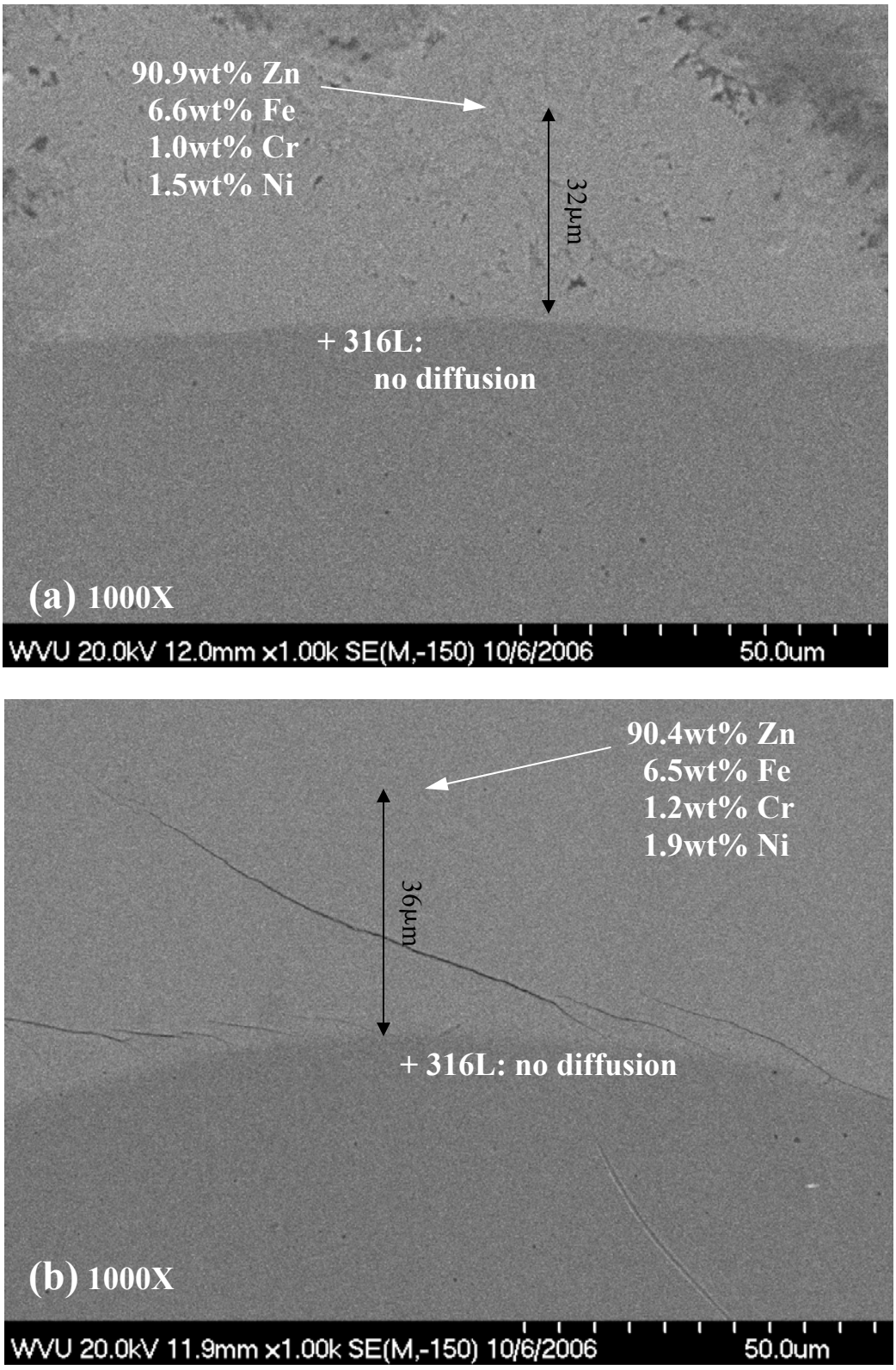

Figure 7-2: 316L Stainless Samples after Immersion in Zn–0.046%Al Bath at 500°C for: (a) 1 Day, (b) 7 Days [SE/BSI]

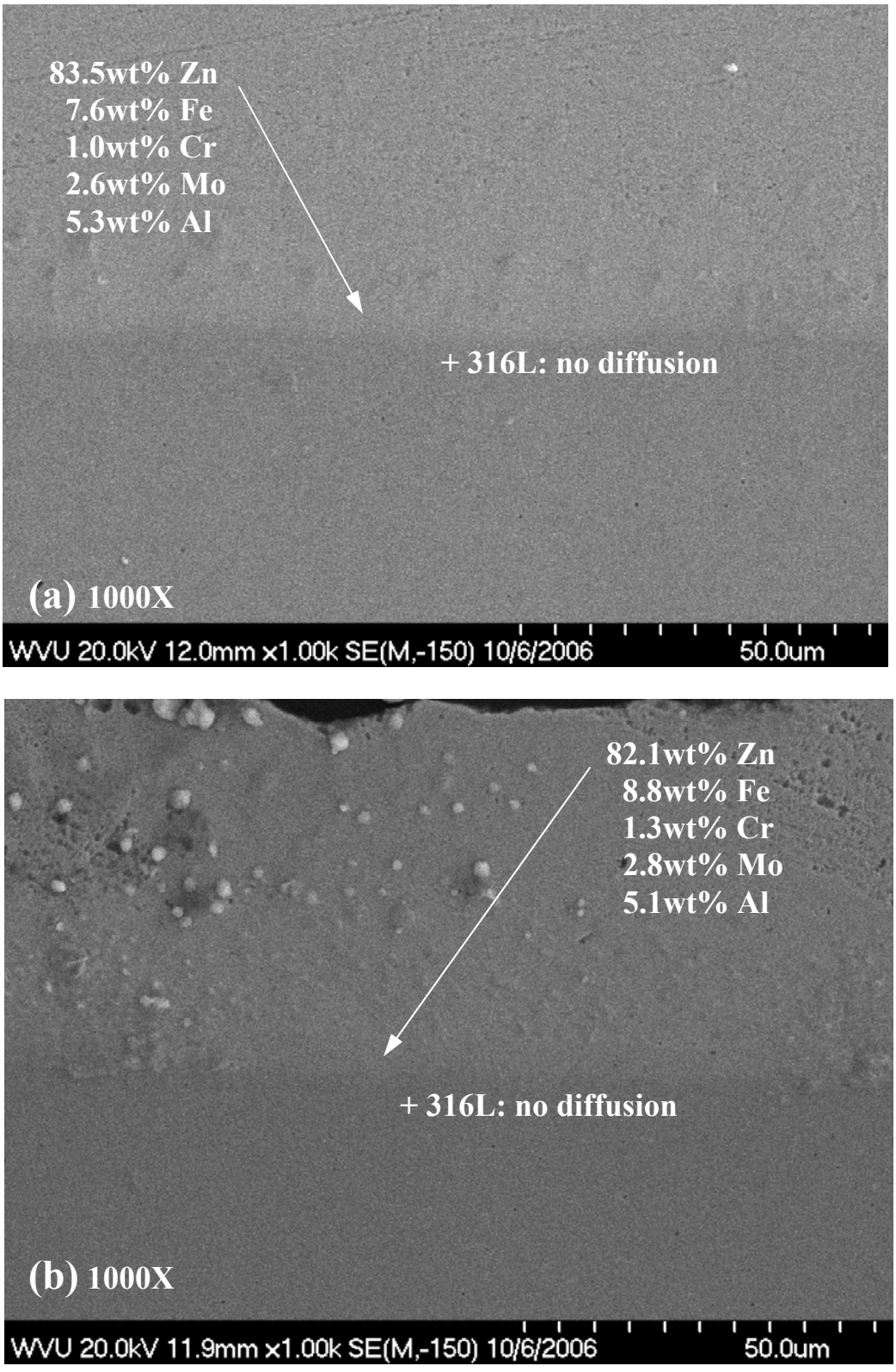

Figure 7-3: 316L Stainless Samples after Immersion in Zn–0.117%Al Bath at 500°C for: (a) 1 Day, (b) 7 Days [SE/BSI]

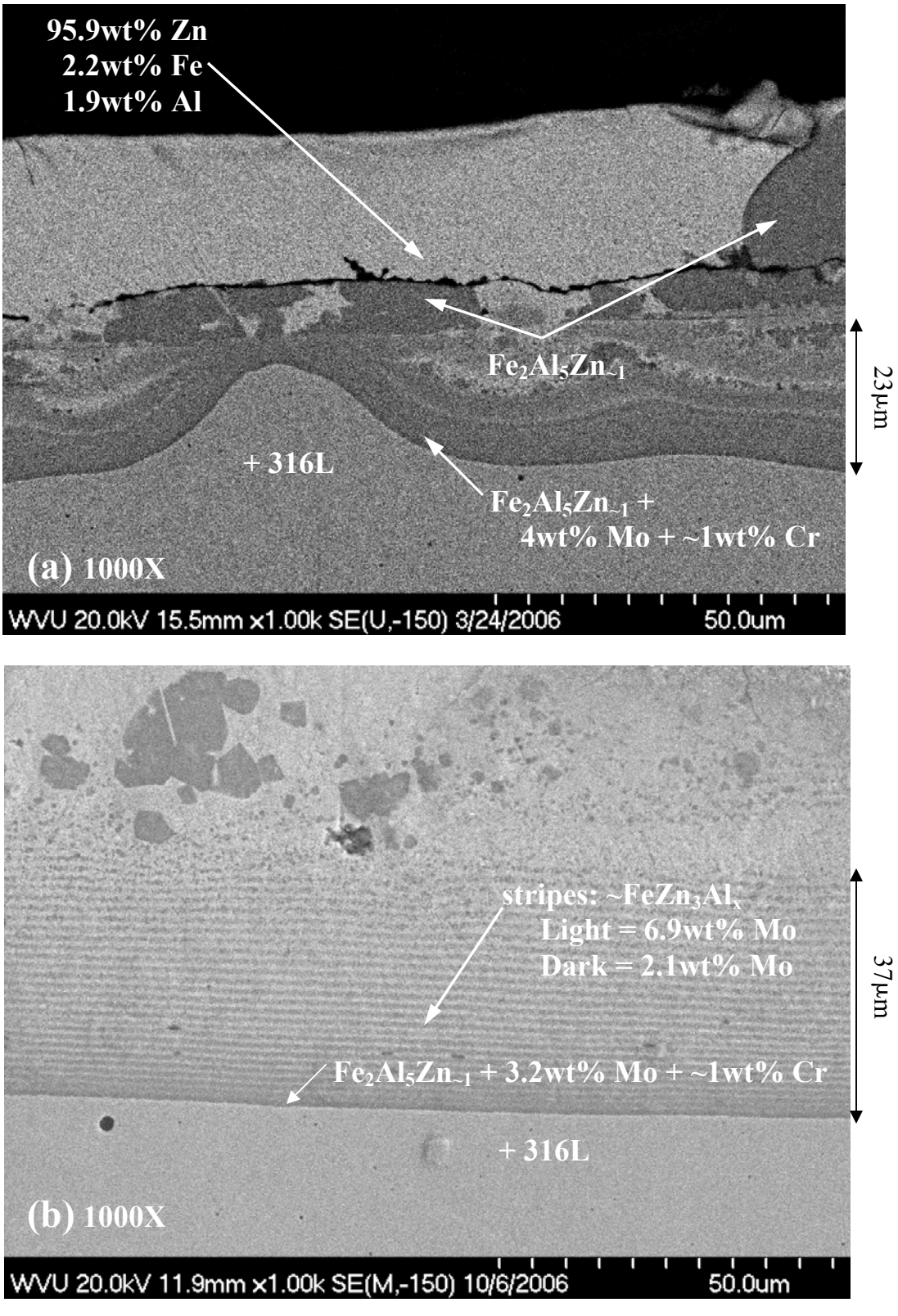

Figure 7-4: 316L Stainless Samples after Immersion in Zn–0.243%Al Bath at 500°C for: (a) 1 Day, (b) 7 Days [SE/BSI]

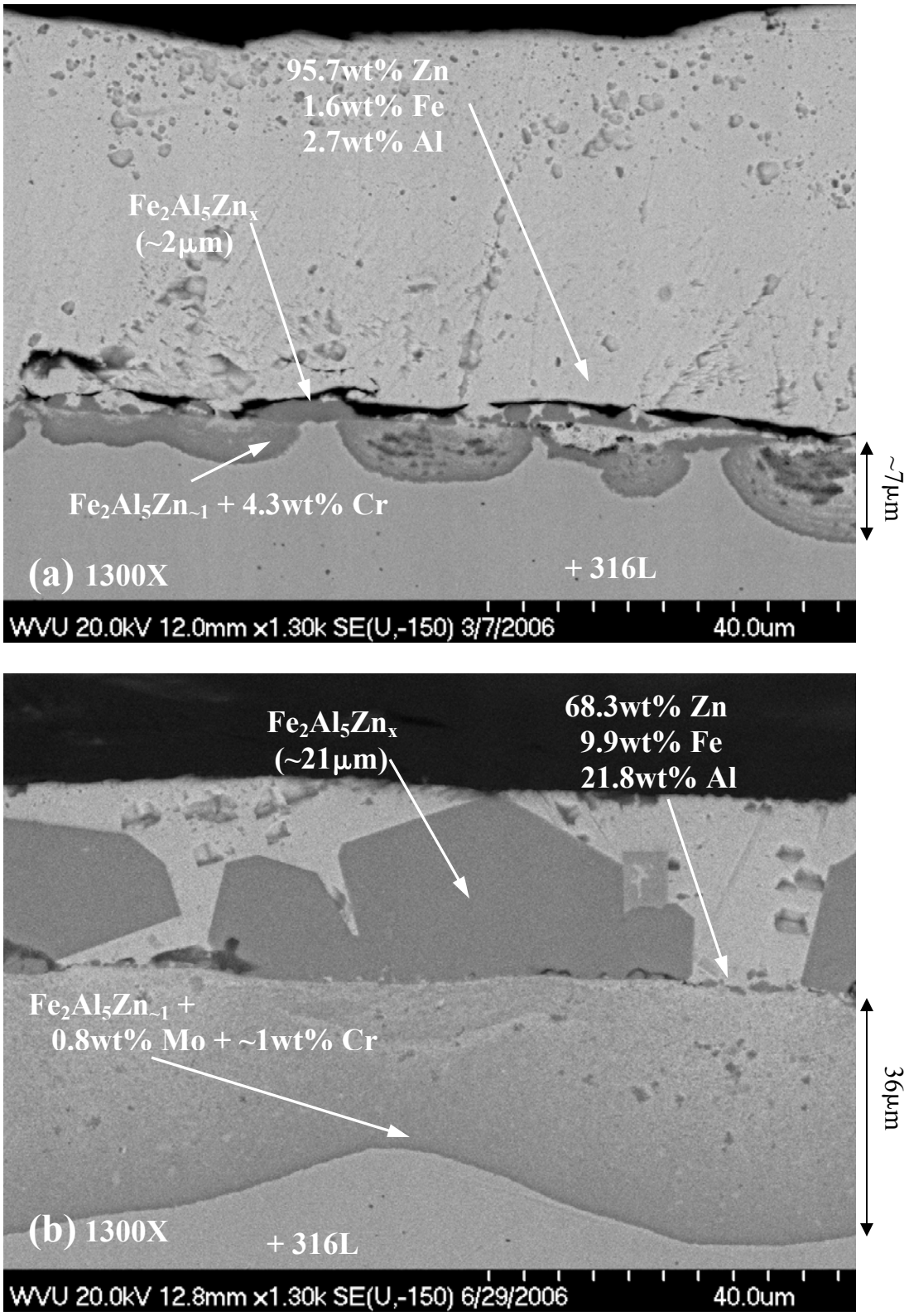

Figure 7-5: 316L Stainless Samples after Immersion in Zn–0.492%Al Bath at 500°C for: (a) 1 Day, (b) **3** Days [SE/BSI]

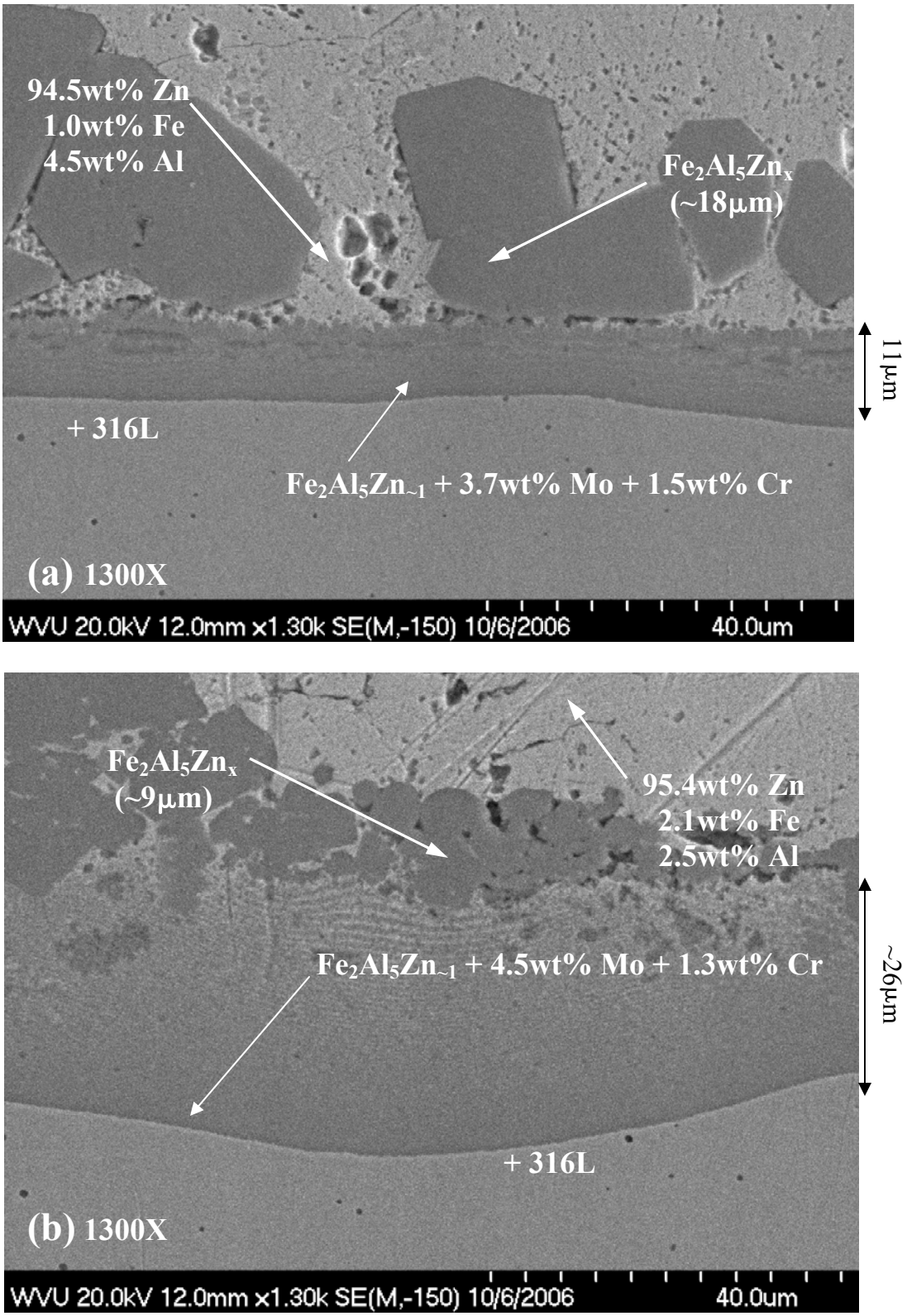

Figure 7-6: 316L Stainless Samples after Immersion in Zn–1.091%Al Bath at 500°C for: (a) 1 Day, (b) 7 Days [SE/BSI]

As a result of this microanalysis, several points can be made to enhance our understanding of Zn-Al bath reactions on 316L stainless. First, as predicted by Marder and others, the aforementioned inhibition mechanism in carbon steel at aluminum concentrations in excess of 0.14wt% also responds to 316L by creating a $Fe_2Al_5Zn_x$ surface phase that changes the fundamental reaction driving force from predominantly dissolution of the substrate constituents into the molten bath to a diffusion-controlled situation whereby the highly-active aluminum in the zinc bath penetrates into the surface of the 316L substrate. Additionally, in spite of gradual increases in the aluminum content (well beyond the initial inhibition at 0.14wt% Al), the resultant reaction structures did not change substantially. The samples at 0.243wt%, 0.492wt% and 1.091wt% aluminum each displayed an accumulation of Fe_2Al_5 particles at the surface and a penetrating formation of a Fe_2Al_5 phase into the 316L surface. It is difficult to exactly quantify the rate of diffusion into the 316L substrate since dissolution was still removing layers of the sample surface, albeit at a significantly reduced rate relative to the low aluminum samples.

In general, the results of the microanalysis support the concept that dissolution rates of 316L stainless in molten zinc increase at lower aluminum concentrations, especially below the transition point at 0.14wt% aluminum. In order to obtain a detailed understanding of the reaction compounds which form as a result of Zn-Al diffusion into the 316L substrate surface, a precise array of controlled experiments should be undertaken. The testing contained herein provides insight as to the initial baseline diffusion reactions that would be expected.

Chapter 8: Conclusions

An array of tests were performed to measure the actual corrosion loss of 316L stainless steel samples after immersion in molten zinc with aluminum concentrations ranging from about 0% to 1wt% Al. The data indicate that the corrosion rate of 316L is quite high for pure zinc (0% Al) then decreases dramatically for increasing aluminum levels between 0% and about 0.14wt% to a rather minimal corrosion rate beyond 0.14% aluminum.

Next, numerous researchers have accepted the fundamental Zn-Fe-Al phase diagram which indicates that (among other things) a definite phase change ($\delta \rightarrow \eta$) occurs in the region of Zn-0.14wt% Al. Additionally, the phase diagram surmises that the iron solubility decreases swiftly at aluminum levels exceeding 0.14wt%. In support of these theoretical solubility limits, the iron concentrations from the zinc baths of the 316L corrosion tests surveyed herein correlate very well with Fe concentrations estimated through the published phase maps.

Previous literature has recognized the Nernst-Shchukarev equation as the standard theoretical definition for estimating the dissolution rate of solid metals in a bath of molten metal. However, in order for this equation to work effectively, the saturation concentration of the solute material in the molten solvent bath must be known. Through the application of the Nernst-Shchukarev equation to the enclosed 316L-zinc dissolution tests it was determined that the Fe-solubility limits outlined by the published phase diagrams would not be sufficient for the dissolution rate calculation. It requires the as yet undefined solubility threshold of actual 316L metal for each specific test condition (temperature, Al%, etc.).

On the other hand, prior research has also revealed that, in a high alloy compound such as 316L stainless steel, the constituents (in this case Fe, Cr and Ni) must dissolve in a ratio representative of the weight percentages contained in the solid material (67.5wt% Fe, 17.5wt% Cr and 10.75wt% Ni). As an example, a typical molten solvent bath will not be able to selectively dissolve the nickel components from the substrate and leave behind the iron undisturbed. Therefore, this uniform dissolution provides evidence that the solubility concentration of 316L stainless might be approximated by utilizing the defined solubility of Fe and adjusting it by the concentration of Fe in 316L. This estimated solubility of 316L can be further justified by examining the preliminary Zn-Fe-Al-Cr quaternary phase diagrams that have been recently published, but do not yet fully define the dissolution characteristics of 316L stainless steel (which also contains Ni and Mo in addition to Fe and Cr).

Thus, it has been shown that when the Nernst-Shchukarev equation is recalculated utilizing the estimated 316L saturation concentrations, then the equation represents the data very well. However, the results also indicate that when the 316L concentration in the bath exceeds 75% of the maximum theoretical 316L saturation limit, then the Nernst-Shchukarev equation is invalid. Thus, the upper bound for 316L concentration in the bath is $C \leq 75\% C_s$.

Finally, a study into the microstructure and compositional characteristics at the interface between the 316L stainless substrate and the Zn-Al bath utilizing SEM and EDS techniques help explain the variable corrosion rate at increasing bath aluminum concentrations. Previous literature had defined an inhibition mechanism in Zn-Fe-Al baths where elevated aluminum levels suppressed the formation of hard, brittle Fe-Zn

intermetallic particles, whereby steel that had been galvanized in a zinc pot with greater than 0.14wt% Al resulted in a more lustrous and ductile coating. Those investigations indicated that formation of $Fe_2Al_5Zn_x$ compounds on the surface of the carbon steel substrate inhibited the alternative formation of potentially detrimental high Fe-Zn intermetallics. Predictably, the microanalysis of the 316L corrosion trials performed herewith also identified the formation of $Fe_2Al_5Zn_x$ inhibition compounds on the stainless steel substrate in the region above 0.14wt% aluminum contained in the zinc bath. This is a diffusion-controlled mechanism.

As a result of the testing and analyses performed, it has been definitively ascertained that the corrosion rate of 316L stainless steel in molten zinc accelerates considerably whenever the aluminum content is diminished below 0.14wt%. The significance of 0.14wt% Al has been defined by not only the microanalysis of the reaction mechanisms on test samples but also industry-accepted phase diagrams.

Based on the results of this research, it may be possible to further understand the reaction mechanisms and detailed corrosion features of other alloys utilized in industrial galvanizing operations, such as cobalt-based and iron-based corrosion resistant superalloys. Moreover, recognizing the significance of the phase transformations in the region of 0.14wt% aluminum on these advanced alloys may promote more focused research in this economically important aluminum regime. In continuation of the investigations described herein, further work may be done to not only refine the exact aluminum transition point of decreased reactivity but also to formulate mathematical simulations which could predict theoretical dissolution rates of different alloy systems as a function of aluminum concentration and temperature.

References

1) Davies, J., Galvanized Iron: its manufacture and uses, Spon and Chamberlain, 1914
2) Hodge, W., Evans, R. M., Haskins, A. F., "Metallic materials resistant to molten zinc", Journal of Metals, July 1955, pp. 824-832
3) Burman, R. W., Litchfield, G., "Severe molten zinc corrosion is reduced by improved molybdenum-tungsten alloy", Engineering and Mining Journal, April 1963, pp. 88-90
4) Archer, R.S., Briggs, J. Z., Loeb, Jr., C. M., Molybdenum Steels, Irons and Alloys, Climax Molybdenum Company, The Hudson Press, 1948
5) Burman, R. W., Gilbert, Jr., R. W., Barr, R. Q., "Molybdenum-30% Tungsten alloy handles liquid zinc", Climax Molybdenum Company of Michigan, Inc., Technical Notes, June 1970
6) Schwarzkopf Technologies Corporation, Franklin, MA, "Molybdenum-Tungsten Alloys Technical Bulletin", 1996
7) ASM Handbook, Volume 3, Alloy Phase Diagrams, ASM International, 1992
8) Wakita, S., Sakonooka, A., U.S. Patent no. 4,363,660, "Iron-base Alloy Having High Resistance to Molten Zinc Attack", December 14, 1982
9) Handa, T., Nakajima, T., Arikata, K., U.S. Patent no. 5,783,143, "Alloy Steel Resistant to Molten Zinc", July 21, 1998
10) Konstal, C., "New Application for AL-6XN", Rolled Alloys Incorporated: internal report, February 1993
11) Haynes International Inc. company website: www.haynesintl.com

12) Antony, C. M., Srivastava, S. K., “Haynes 556: An Fe-Ni-Cr-Co Alloy for Hot-Dip Galvanizing Hardware”, Haynes International Technical Bulletin, 1993

13) Wang, X., Liang, Y., “Corrosive wear of the Co-Cr-W alloy in liquid zinc”, Journal of Material Research, 2001, vol. 16, no. 6, pp. 1585-1592

14) Wang, X., “Corrosion of Co-Cr-W alloy in liquid zinc”, Metallurgical and Materials Transactions B, December 2003, vol. 34B, pp. 881-886

15) Yao, M. X., Wu, J. B. C., Liu, R., “Microstructural characteristics and corrosion resistance in molten Zn-Al bath of Co-Mo-Cr-Si alloys”, Materials Science and Engineering, 2005, vol. 407, pp. 299-305

16) Leighty, J., “Galvanizing hardware: Stellite experience”, DOE-OIT Project: Development of Improved Materials for Pot Hardware, Kickoff Meeting, Pittsburgh, PA, May, 2001

17) Ghuman, A. R., Goldstein, J. I., “Reaction mechanisms for the coatings formed during the hot dipping of iron in 0 to 10 pct. Al-Zn baths at 450° to 700°C, Metallurgical Transactions, October 1971, vol. 3, pp. 2903-2914

18) Uchiyama, Y., Koga, H., Inokuchi, H., “Reaction between Fe-Si alloys and liquid zinc”, Transactions of the Japan Institute of Metals, 1983, vol. 24, no. 5, pp. 272-280

19) Selverian, J. H., Marder, A. R., Notis, M. R., “The reaction between solid iron and liquid Al-Zn baths”, Metallurgical Transactions A, May 1988, vol. 19A, pp. 1193-1202

20) Tunca, N., Smith, R. W., "Intermetallic Compound Layer Growth at the Interface of Solid Refractory Metals Molybdenum and Niobium with Molten Aluminum", Metallurgical Transactions A, May 1989, vol. 20A, pp. 825-836

21) Tunca, N., Delamore, G. W., Smith, R. W., "Corrosion of Mo, Nb, Cr, and Y in Molten Aluminum", Metallurgical Transactions A, November 1990, vol. 21A, pp. 2919-2928

22) Dybkov, V. I., "Interaction of 18Cr-10Ni stainless steel with liquid aluminum", Journal of Material Science, 1990, vol. 25, pp. 3615-3633

23) Sundqvist, M., Hogmark, S., "Effects of Liquid Aluminum on Hot-Work Tool Steel", Tribology International, 1993, vol. 26, no. 2, pp. 129-134

24) Batchelor, A.W., Hung, N. P., Lee, T. K., "Wear of stirring rods in molten aluminum and suspensions of alumina particles in molten aluminum", Tribology International, 1996, vol. 29, no. 1, pp. 41-50

25) Tsipas, D. N., Triantafyllidis, G. K., Kiplagat, J. K., Psillaki, P., "Degradation behavior of boronized carbon and high alloy steels in molten aluminum and zinc", Materials Letters, 1998, vol. 37, pp. 128-131

26) Morando, J. A., U.S. Patent no. 6,004,507, "Material Formulation for Galvanizing Equipment Submerged in Molten Zinc and Aluminum Melts", December 21, 1999

27) Morando, J. A., U.S. Patent no. 6,168,757, "Material Formulation for Galvanizing Equipment Submerged in Molten Aluminum and Aluminum/Zinc Melts", January 2, 2001

28) Morando, J. A., U.S. Patent no. 6,562,293, “Material Formulation for Galvanizing Equipment Submerged in Molten Aluminum and Aluminum/Zinc Melts”, May 13, 2003

29) Morando, J. A., personal conversations, January 1997 – May 2006

30) Morando, J. A., U.S. Patent no. 6,899,772, “Alloy Composition Suitable for Molten Magnesium Environments”, May 31, 2005

31) Brunnock, M. S., Jones, R. D., Jenkins, G. A., Llewellyn, D. T., “Interactions between liquid zinc and bath hardware materials in continuous galvanizing lines”, Ironmaking and Steelmaking, 1996, vol. 23, no. 2, pp. 171-176

32) Brunnock, M. S., Jones, R. D., Jenkins, G. A., Llewellyn, D. T., “Durability of bath hardware materials in continuous galvanizing”, 1996 Galvanizer’s Association Proceedings, Chicago, IL

33) Brunnock, M. S., Jones, R. D., Jenkins, G. A., Llewellyn, D. T., “Supermeniscus interactions between molten zinc and bath hardware materials in galvanizing”, Ironmaking and Steelmaking, 1997, vol. 24, no. 1, pp. 40-46

34) Brunnock, M. S., Jones, R. D., Jenkins, G. A., Llewellyn, D. T., “Investigation of the interactions between liquid zinc and stainless steels for use in continuous galvanizing hardware”, Zinc-Based Steel Coating Systems: Production and Performance (TMS Symposium), 1998, pp. 51-61

35) Tackla, M., “Accelerated corrosion of 316L stainless steel in a galvanizing-galvannealing zinc bath”, 2003 Galvanizer’s Association Proceedings (closed session), Monterrey, Mexico

36) Technical Product Literature: 304L, 316L Stainless Steels, Sandvik Materials Technology, www.smt.sandvik.com, November 2003

37) Tomita, T., Takatani, Y., Kobayashi, Y., Harada, Y., Nakahira, H., "Durability of WC/Co sprayed coatings in molten pure zinc", ISIJ International, 1993, vol. 33, no. 9, pp. 982-988

38) Tani, K., Tomita, T., Kobayashi, Y., Takatani, Y., Harada, Y., "Durability of sprayed WC/Co coatings in Al-added zinc bath", ISIJ International, 1994, vol. 34, no. 10, pp. 822-828

39) Zhang, K., Battiston, L., "ILZRO ZCO-15-1: Improving Performance of Pot Hardware", Reports 1-9, 1997-2002

40) Goodwin, F. E., Adams, G. R., Battiston, L., "Design and performance of pot hardware bearings", 1998 Galvanizer's Association Proceedings, Indianapolis, IN

41) Zhang, K., Battiston, L., Goodwin, F., Friction and wear characteristics of materials in molten zinc", Galvatech 2001 Conference Proceedings, Brussels, Belgium, pp. 247-254

42) Dmochowski, W., Brockwell, K., Battiston, L., "Feasibility study of hydrodynamic lubrication in supporting rotating elements of galvanizing hardware submerged in molten zinc", Lubrication Engineering, September 2002, pp. 36-42

43) Zhang, K., Battiston, L., "Friction and wear characterization of some cobalt- and iron-based superalloys in zinc alloy baths", Wear, 2002, vol. 252, pp. 332-344

44) Zhang, K., Tang, N.-Y., Goodwin, F. E., "Effects of bearing design on the wear of a journal bearing sliding in molten zinc", 44th Mechanical Working and Steel

Processing Conference Proceedings (Iron and Steel Society), 2002, vol. 40, pp. 1285-1297

45) Zhang, K., Tang, N.-Y., Filc, A. B., "A practical approach to enhance wear resistance of bearings in molten zinc", 2002 Galvanizer's Association Proceedings, Dearborn, MI

46) Zhang, K., "Wear of cobalt-based alloys sliding in molten zinc", Wear, 2003, vol. 255, pp. 545-555

47) Zhang, K., Tang, N.-Y., "Reactions of various materials with galvanizing bath", 2003 Galvanizer's Association Proceedings, Monterrey, Mexico

48) Zhang, K., Tang, N.-Y., "On the wear of a cobalt-based superalloy in zinc baths", Metallurgical and Materials Transactions A, October 2003, vol. 23A, pp. 2387-2396

49) Zhang, K., Tang, N.-Y., Goodwin, F. E., "Research and development of pot bearings in continuous galvanizing", Galvatech 2004 Conference Proceedings, Chicago, IL, pp. 605-615

50) Zhang, K., Tang, N.-Y., Yao, M. X., "On the reaction of superalloys with a Zn-Al bath", Galvatech 2004 Conference Proceedings, Chicago, IL, pp. 617-628

51) Zhang, K., Tang, N.-Y., "Reactions of Co based and Fe based superalloys with a molten Zn-Al alloy", Materials Science and Technology, June 2004, vol. 20, pp. 739-746

52) Zhang, K, "ZCO-15-4: Dross Buildup – Influences on the Hardware Materials and Line Operating Conditions", ILZRO Progress Report, April/May 2005

53) Zhang, K., “On the Selection of Materials for Improved Performance of Pot Bearings”, AISTech 2005 Conference Proceedings, Charlotte, NC, May 2005, pp. 475 - 482

54) Chang, K.-M., “Project Overview”, DOE-OIT Project: Development of Improved Materials for Pot Hardware, Kickoff Meeting, Pittsburgh, PA, May, 2001

55) Long, H., “Industry View”, DOE-OIT Project: Development of Improved Materials for Pot Hardware, Kickoff Meeting, Pittsburgh, PA, May, 2001

56) Gast-Bray, A., “Materials in hot dip zinc pots”, DOE-OIT Project: Development of Improved Materials for Pot Hardware, Kickoff Meeting, Pittsburgh, PA, May, 2001

57) Chang, K.-M., “Dross in hot-dipping bath”, DOE-OIT Project: Development of Improved Materials for Pot Hardware, Progress Meeting, Mississauga, Ont., August, 2001

58) Liu, X., “Corrosion testing overview”, DOE-OIT Project: Development of Improved Materials for Pot Hardware, Progress Meeting, Mississauga, Ont., August, 2001

59) Sikka, V., “ORNL Progress report”, DOE-OIT Project: Development of Improved Materials for Pot Hardware, Progress Meeting, Mississauga, Ont., August, 2001

60) Chang, K.-M., “Dross in hot-dipping bath”, DOE-OIT Project: Development of Improved Materials for Pot Hardware, Progress Meeting, Charleston, WV, December, 2001

61) Sikka, V., McElroy, S., Santella, M., Babu, S., Howell, R., “Material selection”, DOE-OIT Project: Development of Improved Materials for Pot Hardware, Progress Meeting, Charleston, WV, December, 2001

62) Chang, K.-M., “WVU Progress report on liquid metal corrosion testing”, DOE-OIT Project: Development of Improved Materials for Pot Hardware, Progress Meeting, Oak Ridge, TN, June, 2002

63) Liu, X., “WVU Progress report on liquid metal corrosion testing”, DOE-OIT Project: Development of Improved Materials for Pot Hardware, Progress Meeting, Charleston, WV, December, 2002

64) Sikka, V., McElroy, S., Ott, R., “Long-term corrosion tests and second generation of materials for corrosion and wear testing”, DOE-OIT Project: Development of Improved Materials for Pot Hardware, Progress Meeting, Charleston, WV, December, 2002

65) Liu, X., “WVU Progress report on liquid metal corrosion testing”, DOE-OIT Project: Development of Improved Materials for Pot Hardware, Progress Meeting, Morgantown, WV, May, 2003

66) Sikka, V., McElroy, S., Ott, R., “ORNL Progress report on development of materials for pot hardware”, DOE-OIT Project: Development of Improved Materials for Pot Hardware, Progress Meeting, Morgantown, WV, May, 2003

67) Liu, X., “WVU Progress report on liquid metal corrosion testing”, DOE-OIT Project: Development of Improved Materials for Pot Hardware, Progress Meeting, Roanoke, WV, October, 2003

68) Sikka, V., McElroy, S., "ORNL Progress report on development of materials for pot hardware", DOE-OIT Project: Development of Improved Materials for Pot Hardware, Progress Meeting, Roanoke, WV, October, 2003

69) Sikka, V., McElroy, S., "Microstructural analysis of wear tested specimens", DOE-OIT Project: Development of Improved Materials for Pot Hardware, Progress Meeting, Roanoke, WV, October, 2003

70) Liu, X., Barbero, E., Loth, J., Kang, B., Damiani, T., Gopalakrishnan, B., Irwin, C., Sikka, V., Goodwin, F. E., "WVU Progress Report", DOE-OIT Project: Development of Improved Materials for Pot Hardware, Progress Meeting, Morgantown, WV, October, 2004

71) Irwin, C., Barbero, E., Sikka, V., Goodwin, F. E., Final Project Report, DOE-OIT Project: Development of Improved Materials for Pot Hardware, June, 2005

72) Goodwin, F. E., Chang, K.-M., Sikka, V., "Development of a new generation of bath hardware materials", 2002 Galvanizer's Association Proceedings, Dearborn, MI

73) Barbero, E., Liu, X., Kang, B., Loth, J., Snider, J., Sikka, V., Goodwin, F. E., "Performance Evaluation of Current Hot-Dip Pot Hardware Materials", 2003 Galvanizer's Association Proceedings, Monterrey, Mexico

74) Snider, J., Loth, J., "Empirical Wear Rate Modeling of Zinc Pot Bearing Materials Using the WVU Small Scale Tester", Galvatech 2004 Conference Proceedings, Chicago, IL, pp. 595-604

75) Liu, X., Barbero, E., Sikka, V., "Corrosion of Several Alloys in Industrial Hot Dipping Baths", Galvatech 2004 Conference Proceedings, Chicago, IL, pp. 629-636

76) Parthasarathy, V., Kang, B., Krishnaswamy, A., Barbero, E., Chang, K.-M., Irwin, C., Goodwin, F. E., "Long Time Performance of Pot hardware in Continuous Galvanizing Line", Galvatech 2004 Conference Proceedings, Chicago, IL, pp. 637-656

77) Loth, J., "Zinc Pot Bearing Design Modification for Increased Life", Galvatech 2004 Conference Proceedings, Chicago, IL, pp. 657-666

78) Chang, K.-M., Burris, M., Yang, W., Sikka, V., "Evaluation of Fe_3Al intermetallic alloys for hot-dip pot-hardware applications", Galvatech 2001 Conference Proceedings, Brussels, Belgium, pp. 270-277

79) Liu, X., Barbero, E., Xu, J., Burris, M., Chang, K.-M., Sikka, V., "Liquid metal corrosion of 316L, Fe_3Al and FeCrSi in molten Zn-Al baths", Metallurgical Transactions A, vol. 36A, August 2005, pp. 2050-2058

80) Urednicek, M., Kirkaldy, J. S., "An investigation of the phase constitution of iron-zinc-aluminum at 450°C", Z. Metallkde., 1973, vol. 64, H.6, pp. 419-427

81) Urednicek, M., Kirkaldy, J. S., "Mechanism of iron attack inhibition arising from additions of aluminum to liquid Zn(Fe) during galvanizing at 450°C", Z. Metallkde., 1973, vol. 64, H.12, pp. 899-910

82) Belisle, S., Lezon, V., Gagne, M., "The solubility of iron in continuous hot dip galvanizing baths", 1989 Galvanizer's Association Proceedings, Hermitage, PA

83) Chen, Z. W., Sharp, R. M., Gregory, J. T., “Fe-Al-Zn ternary diagram at 450°C”, Materials Science and Technology, December 1990, vol. 6, pp. 1173-1176

84) Belisle, S., Lezon, V., Gagne, M., “The solubility of iron in continuous hot-dip galvanizing baths”, Journal of Phase Equilibria, 1991, vol. 12, no. 3, pp. 259-265

85) Chen, Z. W., Gregory, J. T., Sharp, R. M., “Intermetallic phases formed during hot dipping of low carbon steel in a Zn-5%Al melt at 450°C”, Metallurgical Transactions A, September 1992, vol. 23A, pp. 2393-2400

86) Shimozaki, T., Wakamatsu, Y., Onishi, M., “Beginning time formation of new phase in Fe-Zn diffusion couple during non-isothermal diffusion and numerical analysis for the phase growth behavior”, ISIJ International, 1993, vol. 33, no. 9, pp. 1003-1008

87) Toussaint, P., Segers, L., Winand, R., Dubois, M., “Intermetallic particles in continuous hot dip galvanizing baths at aluminium concentrations between 0.1 and 4.5 wt%”, Ironmaking and Steelmaking, 1995, vol. 22, no. 6, pp. 498-501

88) Perrot, P., Reumont, G., Tissier, J. C., Foct, J., “Dross Formation by Reaction Between the Tank Surface and the Zn-Al Bath”, Galvatech 1995 Conference Proceedings, Chicago, Illinois, pp. 763-767

89) Reumont, G., Gloriant, T., Perrot, P., “Experimental influence of kinetics on galvanized coatings when saturating a zinc bath with alloying elements”, Journal of Materials Science Letters, 1996, vol. 15, pp. 445-449

90) Uwakweh, O. N., Liu, Z., “Kinetics and phase transformation evaluation of Fe-Zn-Al mechanically alloyed phases”, Metallurgical and Materials Transactions A, March 1997, vol. 28A, pp. 517-525

91) Adachi, Y., Arai, M., “Transformation of Fe-Al phases to Fe-Zn phase on pure iron during galvanizing”, Materials Science and Engineering, 1998, vol. 254, pp. 305-310

92) Reumont, G., Perrot, P., Fiorani, J. M., Hertz, J., Thermodynamic assessment of the Fe-Zn system”, Journal of Phase Equilibria, 2000, vol. 21, no. 4, pp. 371-378

93) Marder, A. R., “The Metallurgy of Zinc-Coated Steel”, Progress in Materials Science, 2000, vol. 45, pp. 191-271

94) Giorgi, M.-L., Guillot, J.-B., Nicolle, R., Biausser, H., “Assessment of the zinc-aluminium-iron phase diagram in the zinc-rich corner”, Galvatech 2001 Conference Proceedings, Brussels, Belgium, pp. 179-186

95) Maniez, S., Reumont, G., Perrot, P., Foct, J., Gay, B., Piccinin, A., Claessens, S., “Thermodynamical investigation of the chromium influence during galvanizing and galvannealing reaction”, Galvatech 2001 Conference Proceedings, Brussels, Belgium, pp. 98-104

96) Zermout, Z., Drillet, P., Houziel, J., “Reaction mechanisms during immersion of low-carbon steel in a Zn-5wt%Al bath”, Galvatech 2001 Conference Proceedings, Brussels, Belgium, pp. 345-351

97) Shim, J.-H., Chung, S. H., Cho, Y. W., “Prediction of aluminum concentration in molten zinc pot of continuous hot dip galvanizing line”, Ironmaking and Steelmaking, 2002, vol. 29, no. 29, pp. 454-458

98) Giorgi, M.-L., Durighello, P., Nicolle, R., Guillot, J.-B., “Dissolution kinetics of iron in liquid zinc”, Journal of Materials Science, 2004, vol. 39, pp. 5803-5808

99) Tang, N.-Y., Anderson, G. N., “Aluminum-antimony interaction in molten galvanizing alloys”, 1993 Galvanizer’s Association Proceedings, Baltimore, MD

100) Tang, N.-Y., “Comment on Fe-Al-Zn (iron-aluminum-zinc)”, Journal of Phase Equilibria, 1994, vol. 15, no. 3, pp. 237-238

101) Tang, N.-Y., “Modeling Al enrichment in galvanized coatings”, Metallurgical and Materials Transactions A, July 1995, vol. 26A, pp. 1699-1704

102) Tang, N.-Y., “Refined 450°C isotherm of Zn-Fe-Al phase diagram”, Materials Science and Technology, September 1995, vol. 11, pp. 870-873

103) Tang, N.-Y., “450°C isotherm of Zn-Fe-Al phase diagram update”, Journal of Phase Equilibria, 1996, vol. 17, no. 5, pp. 396-398

104) Tang, N.-Y., “Discussion of ‘Kinetics and phase transformation evaluation of Fe-Zn-Al mechanically alloyed phases’”, Metallurgical and Materials Transactions A, November 1997, vol. 28A, pp. 2433-2435

105) Shastry, C. R., Galka, J. J., “Analysis of zinc melt for aluminum, iron and dross intermetallics”, 1998 Galvanizer’s Association Proceedings, Indianapolis, IN

106) Gauthier, M., Ajersch, F., McDermid, J. R., “Phase transformation mechanisms of intermetallic particles suspended in hot-dip galvanizing and galvannealing baths”, Galvatech 2001 Conference Proceedings, Brussels, Belgium, pp. 352-358

107) Arioka, T., Hori, M., Toki, T., “Growth mechanism of dross particles in molten Zn baths”, Galvatech 2001 Conference Proceedings, Brussels, Belgium, pp. 393-400

108) Su, X., Tang, N.-Y., Toguri, J. M., "Thermodynamic assessment of the Ni-Zn system", Journal of Phase Equilibria, 2002, vol. 23, no. 2, pp. 140-147

109) Tang, N.-Y., Liu, Y. H., Zhang, K., "Development of high order phase diagrams for practical applications in galvanizing", 44th Mechanical Working and Steel Processing Conference Proceedings (Iron and Steel Society), 2002, vol. 40, pp. 815-821

110) Tang, N.-Y., "Practical applications of phase diagrams in continuous galvanizing", 2005 Galvanizer's Association Proceedings, Lexington, KY

111) Tang, N.-Y., "ZCO-15-4: Dross Buildup – Influences on the Hardware Materials and Line Operating Conditions", ILZRO Progress Report, October 2005

112) Tang, N.-Y., "Determination of liquid-phase boundaries in Zn-Fe-Mx systems", Journal of Phase Equilibria, 2000, vol. 21, no. 1, pp. 70-77

113) Tang, N.-Y., personal conversations, May - June 2006

114) Mackowiak, J., Short, N., "Metallurgy of Galvanized Coatings", Int. Met. Reviews, 1979, No. 1

115) Tang, N.-Y., Adams, G. R., "Studies on the inhibition of alloy formation in hot-dip galvanized coatings", The Physical Metallurgy of Zinc Coated Steel (TMS Conference), 1994

116) Tang, N.-Y., "Thermodynamics and kinetics of alloy formation in galvanized coatings", Zinc-Based Steel Coating Systems: Production and Performance (TMS Symposium), 1998, pp. 3-12

117) Nakayama, M., Kanamaru, T., Numakura, Y., “Effect of alloying conditions and phase structure on alloying behavior and formability of galvannealed steel sheet”, CAMP-ISIJ, 1992, vol. 5

118) Zhang, K, “ZCO-15-4: Dross Buildup – Influences on the Hardware Materials and Line Operating Conditions”, ILZRO Progress Report, October 2006

119) Zhang, K., Tang, N.-Y., Goodwin, F., Sexton, S., “On-line Testing of 316L Stainless Steel”, 2006 Galvanizer’s Association Proceedings, Columbus, OH

120) DuBois, M., ILZRO Galvanized Autobody Partnership Meeting, October 2005